

Environmental Stability Studies of an Organic Semiconductor

**A thesis submitted to The University of Manchester for the
degree of Doctor of Philosophy
in the Faculty of Engineering and Physical Sciences.**

2013

Laila Mohamed Abusen

School of Chemistry

Contents

List of figures	5
List of Table	16
Declaration	18
Copyright Statement.....	19
Acknowledgements	20
Motivation	21
Abstract	22
1 Introduction	24
1.1 Organic semiconductors	24
1.1.1 The chemical structures of organic semiconductors	25
1.1.2 Physics of organic semiconductor	26
1.1.3 Electronic transitions in organic semiconductors	28
1.1.4 Applications of organic semiconductor	30
1.2 Organic Thin film Transistors (OTFTs).....	31
1.2.1 Physical parameters of OTFTs.....	32
1.2.2 Working principle of OTFTs	32
1.2.3 Deposition techniques for organic semiconductor thin film.....	34
1.2.4 Passivation of OTFTs	36
1.2.5 Environmental Stability of Functionalized Acenes	37
1.2.6 Soluble pentacene precursors.....	40
1.2.7 Substituted soluble pentacene derivatives	41
1.3 Optical properties and electronic properties of acenes organic semiconductors.....	54
1.4 Aggregation of π -conjugated systems in solution.....	57
1.5 Aims and Objectives	59
2 Experimental.....	60
2.1 Materials Used.....	60
2.2 Ultraviolet and visible (UV-vis) spectroscopy.....	64
2.2.1 Absorption process.....	64
2.2.2 Solution preparation.....	66
2.2.3 Photostability study in solution.....	66
2.3 Fluorescence spectroscopy	67

2.3.1	Emission process.....	67
2.4	Nuclear magnetic resonance NMR	69
2.5	Atmospheric pressure chemical ionization (APCI) mass spectrometry	69
2.6	Isothermal titration calorimetry (ITC).....	69
2.7	Small-Angle X-ray scattering (SAXS).....	72
2.8	Thermal stability	74
2.8.1	Thin film formation.....	74
2.8.2	Thermal gravimetric analysis (TGA).....	74
2.8.3	Differential scanning calorimetry (DSC).....	74
3	Solvent-dependent photochemical instability of TIPS-pentacene at low concentration 1×10^{-5} M at 26 °C	75
3.1	Photooxidative stability of TIPS-pentacene	75
3.2	Effect the solvent on the photooxidative degradation of TIPS-pentacene	76
3.3	Literature reports on the photooxidative degradation of TIPS-pentacene in different solvents at low concentration	76
3.4	Experimental conditions.....	78
3.5	Photooxidative degradation of TIPS-pentacene at a concentration of 1×10^{-5} M at 26 °C.	78
3.6	Photooxidation mechanism of TIPS-pentacene	84
3.6.1	Analysis of the photooxidation products of TIPS-pentacene	86
3.7	Kinetics of the photodegradation of TIPS-pentacene in solution	93
3.8	TIPS-Pentacene solubility	98
3.8.1	Solubility parameters: theory	98
3.8.2	Solvent effect	101
3.9	Conclusion.....	105
4	Concentration dependent photostability of TIPS-pentacene	106
4.1	The effect of concentration on the photooxidative degradation kinetics of TIPS-pentacene in toluene solution.....	106
4.2	The effect of concentration on the photo-oxidative degradation kinetics of TIPS-pentacene at different solvents.....	108
4.3	Experimental observations of TIPS-pentacene in solution as a function of concentration	111
4.3.1	Fluorescence spectra of TIPS-pentacene in solution	111

4.3.2	ITC of TIPS-pentacene	115
4.3.3	Small-Angle X-ray scattering (SAXS)	122
4.4	Models and mechanisms for TIPS-pentacene photodegradation	123
4.4.1	Interaction distance and oxygen solubility	123
4.4.2	Aggregation of TIPS-pentacene in solution.....	126
4.4.3	Isodesmic aggregation model	127
4.4.4	Cooperative aggregation model	129
4.4.5	Nearest Neighbour Interactions.	130
4.4.6	Concluding remarks on concentration effects.....	131
4.5	Conclusion.....	132
5	Photochemical instability of other substituted pentacene derivatives	133
5.1	Effect the solvent on rate of photo-oxidative degradation of pentacene derivatives at low concentration.....	133
5.1.1	Effect the solvent on rate of photochemical instability of α - mono-Fluoro-TIPS-pentacene.....	133
5.1.2	Effect the solvent on rate of photochemical instability of β -mono-Fluoro-TIPS-pentacene.....	135
5.1.3	Effect the solvent on rate of photochemical instability of α -di-Fluoro-TIPS-pentacene.....	137
5.1.4	Effect the solvent on rate of photochemical instability of β -di-Fluoro-TIPS-pentacene.....	139
5.1.5	Effect the solvent on rate of photochemical instability of TMTES-pentacene	141
5.2	Photostability kinetics of pentacene derivatives	146
5.3	Effect the concentration on rate of photo-oxidative degradation of pentacene derivatives in toluene solution.....	149
5.4	Comparison with TIPS pentacene	152
5.5	Conclusions	153
6	Effect of solvent mixtures and additive aromatic solvent and polymer on rate of photooxidative degradation of TIPS-pentacene.....	154
6.1	Effect of solvent mixtures on rate of photooxidative degradation of TIPS-pentacene.....	155

6.2	Effect additive aromatic solvent on rate of photo-oxidative degradation of TIPS-pentacene in THF (2×10^{-4} M) at different light conditions.....	159
6.3	Effect of added polymer on rate of photo-oxidative degradation of TIPS-pentacene in THF (2×10^{-4} M).....	160
6.3.1	Effect of added amorphous polystyrene on rate of photo-oxidative degradation of TIPS-pentacene in THF (2×10^{-4} M)	161
6.3.2	Effect of added isotactic polystyrene on rate of photo-oxidative degradation of TIPS-pentacene at concentration (2×10^{-4} M) in THF.....	162
6.3.3	Effect of added isotactic poly (methylmethacrlate) i-PMMA and poly(triaylamine) (PTAA) on rate of photo-oxidative degradation of TIPS-pentacene at concentration (2×10^{-4} M) in THF	164
6.4	Conclusion.....	167
7	Conclusion and Further work	168
7.1	Conclusion.....	168
7.2	Further work.....	169
8	References	170
9	Appendix	178

List of figures

Figure 1.1: Scheme of the P_z orbitals and σ -, π -bonds for two sp_2 - hybridized carbon atoms [1].	24
Figure 1.2: Examples of p-type organic semiconductors [3-7].....	25
Figure 1.3: Examples of n-type organic semiconductor [3, 4, 6, 7].	26
Figure 1.4: The energy levels of a π -conjugated molecule. The lowest electronic excitation is between the bonding π -orbital (HOMO) and the antibonding π^* -orbital (LUMO) [1].	27
Figure 1.5: The energy structure of small molecule organics (top) and the energy structure of polymer organics (bottom) [9].....	28
Figure 1.6 :The unpaired electrons of an excited molecule can either have their spins antiparallel or parallel are known as singlet and triplet state [10].	29
Figure 1.7: A selection of commercially available and future products, in which Semiconducting organic moieties are employed.	30
Figure 1.8 :Two types of organic thin film transistor device configuration [7].	31
Figure 1.9: Formation of conducting channel in OTFT [21].	33
Figure 1.10: Output characteristics and transfer characteristics of TIPS-pentacene TFTs [24].	34
Figure 1.11 : Vacuum Thermal evaporation deposition organic semiconductors.	35
Figure 1.12: Schematically depiction of the various methods for obtaining thin film by solution processing [28].	36
Figure 1.13: The structure and the tradition herring-bone of pentacene molecule [36].	37
Figure 1.14: Chemical structure of side products produced during train –sublimation [37].	38
Figure 1.15: Chemical structure of (a) photo-dimerization and (b) endo-peroxide of pentacene [38].	38
Figure 1.16: Photooxidation of pentacene in the Diels-Alder reaction with calculated reaction energies (kcal/mol) [40].	39
Figure 1.17: Chemical structure of some common oxidation products of pentacene [41].	40

Figure 1.18: Schematic showing the Diels-Alder reaction making pentacene soluble in organic solvents [42].	41
Figure 1.19 : Chemical structure of Aryl pentacenes [45].	42
Figure 1.20: Schematic showing Photo-oxidation of 2-thienyl pentacene [48].	42
Figure 1.21: Chemical structure of silyl-functionalized pentacenes [50].	43
Figure 1.22: Face-to-face packing of TIPS-pentacene [51].	44
Figure 1.23: HOMO and LUMO orbitals and energy of pentacene and TIPS-pentacene [39].	44
Figure 1.24: Chemical structures of dimerisation of TIPS-pentacene induced by UV-light [54].	45
Figure 1.25: Structures of halogenated (a), thiolated (b, c) and phenylated (d) pentacene derivatives with their associated half-lives (min) [59].	46
Figure 1.26: Proposed mechanism for the oxidation of 6, 13-bis (phenylthio) pentacene and 6, 13-bis (decylthio) pentacene to afford pentacene-6,13-dione and the corresponding disulfides [59].	47
Figure 1.27 : Chemical structure pentacene with substitution of the 2, 3, 6, 9, 10 and 13 position [60].	48
Figure 1.28: Chemical structure of Anthradithiophenes [52].	49
Figure 1.29: Chemical structures of soluble pentacene and anthradithiophene derivatives [65].	49
Figure 1.30: Chemical structure of perfluorination [66].	50
Figure 1.31: Chemical structures of silyethynylated N-heteropentacene [67].	51
Figure 1.32: Chemical structures of stable radical pentacene hybrids, (a) pentacene-phenyl, oxo-verdazyl radical and (b) pentacene-phenyl,-nitronyl nitroxide radical moieties [69].	52
Figure 1.33: Chemical structures of silyethyne substituted hexacene derivatives [72].	52
Figure 1.34: Schematic showing photooxidation of heptacene derivative [73].	53
Figure 1.35: Normalized absorption spectra of polyacenes (spectra of anthracene to pentacene recorded in toluene, spectra of hexacene and heptacene recorded in a polymer matrix) [75].	54
Figure 1.36: Calculated HOMO, LUMO and band gaps for acenes [76].	55
Figure 1.37: Absorption spectra of functionalized acenes [83].	56

Figure 1.38: The schematic structures of H and J aggregate [87].	58
Figure 2.1: Molecular structures of substituted 6, 13- pentacenes derivatives.	62
Figure 2.2: Molecular structures of polymers used in this study.	63
Figure 2.3: Light of intensity I_0 incident upon a sample of thickness t undergoes a loss in intensity upon passing through the sample. The intensity measured after passing through the sample is I [92].	64
Figure 2.4: Interband optical absorption between an initial state of energy E_i in an occupied lower band and a final state at an energy E_f in an empty upper band. The energy difference between the two bands is the band gap (ΔE) [92].	65
Figure 2.5: Jablonski diagram.	68
Figure 2.6: Schematic diagram of (A) the Isothermal Titration Calorimetry instrument, and (B) the example of binding profile [94].	71
Figure 2.7: Schematic diagram of general scattering experiment measuring the variation in intensity as a function of Θ (scattering angle).	72
Figure 3.1: UV-visible absorption spectra of TIPS-pentacene in toluene solution at a concentration of 1×10^{-5} M at 26°C .	79
Figure 3.2: HOMO and LUMO of TIPS-pentacene [112].	80
Figure 3.3: UV-visible absorption of TIPS-pentacene in different solvents at a concentration of 1×10^{-5} M at 26°C .	80
Figure 3.4: Plot of λ_{max} of the absorption spectra versus the solvent dipole moment for a solution of TIPS-pentacene at a concentration of 1×10^{-5} M at 26°C .	81
Figure 3.5: UV-visible absorption spectra for the photooxidation of TIPS-pentacene in chloroform at 1×10^{-5} M in a 10 mm pathlength at 26°C .	82
Figure 3.6: Normalised absorbance/ time profiles at λ_{max} of TIPS-pentacene in different solvents at a concentration 1×10^{-5} M at 26°C .	83
Figure 3.7: Schematic showing two mechanistic pathways to photooxidation of oligoacenes: electron transfer (Type-I) and energy transfer (Type-II) [98].	85
Figure 3.8: Mass spectroscopy (AP^-) of TIPS-pentacene at 1×10^{-5} M in toluene, (a) before and (b) after photooxidation.	87
Figure 3.9: Mass spectroscopy (AP^+) of TIPS-pentacene at 1×10^{-5} M in toluene, (a) before and (b) after photooxidation.	87
Figure 3.10: Mass spectroscopy (AP^-) of TIPS-pentacene at 1×10^{-5} M in chloroform, (a) before and (b) after photooxidation.	88

Figure 3.11: Mass spectroscopy (AP^+) of TIPS-pentacene 1×10^{-5} M in chloroform, (a) before and (b) after photo-oxidation.....	88
Figure 3.12: 1H NMR spectra TIPS-pentacene 1×10^{-5} M in toluene, (a) before and (b) after photooxidation.	90
Figure 3.13: 1H NMR spectra TIPS-pentacene at 1×10^{-5} M in chloroform, (a) before and (b) after photooxidation.....	91
Figure 3.14: Schematic showing photooxidation of TIPS-pentacene.....	92
Figure 3.15: UV-visible absorption spectra for the photooxidation of TIPS-pentacene in toluene at 1×10^{-5} M in a 10 mm pathlength at $26^\circ C$	92
Figure 3.16: Plot of $\ln(A_t/A_0)$ versus time for TIPS-pentacene in a variety of solvents at a concentration of 1×10^{-5} M at $26^\circ C$	95
Figure 3.17: Plot of (A_t/A_0) versus time for TIPS-pentacene in a variety of solvents at a concentration of 1×10^{-5} M at $26^\circ C$	96
Figure 3.18: Plot of $1/(A_t/A_0)$ versus time for TIPS-pentacene in a variety of solvents at a concentration of 1×10^{-5} M at $26^\circ C$	96
Figure 3.19: schematic of the Hansen solubility sphere.	99
Figure 3.20: Plot of interaction distance (R_a) versus half-life of TIPS-pentacene in different solvents at a concentration of 1×10^{-5} M at $26^\circ C$	103
Figure 3.21: Plot of oxygen solubility (mole fraction $\times 10^4$) versus half-life of TIPS-pentacene in different solvents at a concentration of 1×10^{-5} M.....	104
Figure 3.22: Comparison of interaction distance (R_a) \times oxygen solubility (mole fraction $\times 10^4$) versus half-life of TIPS-pentacene in different solvents at a concentration of 1×10^{-5} M.	105
Figure 4.1 :UV-visible absorption spectra of TIPS-pentacene in toluene solution at concentrations ranging from 2.5×10^{-6} M to 5×10^{-4} M in 1mm pathlength at $26^\circ C$.	107
Figure 4.2: Normalised absorbance/time profiles for photooxidation of TIPS-pentacene in toluene solutions for a range of concentration at $26^\circ C$	107
Figure 4.3: Variation of half-life ($t_{1/2}$ min) as function of concentration (M) of TIPS-pentacene in a variety of solvents between 2.5×10^{-6} M to 2×10^{-2} M at $26^\circ C$	108
Figure 4.4: Plot of $\ln(A_t/A_0)$ versus time for TIPS-pentacene in toluene solution at different concentrations at $26^\circ C$	110

Figure 4.5: Fluorescence emission intensity of TIPS-pentacene in toluene at concentrations ranging from 2.5×10^{-6} M to 1×10^{-3} M in 10mm pathlength cuvette (excitation at 643nm).	112
Figure 4.6: Fluorescence emission intensity of TIPS-pentacene in toluene at concentrations ranging from 2.5×10^{-6} M to 1×10^{-3} M in 10mm pathlength cuvette (excitation at 550nm).	112
Figure 4.7 : Variation of the wavelength of the maximum fluorescence intensity of TIPS-pentacene in toluene at concentrations ranging from 2.5×10^{-6} M to 1×10^{-3} M for the ~ 650 nm emission band for excitation at 643 and 550 nm.	113
Figure 4.8: Variation of the fluorescence intensity of TIPS-pentacene in toluene between 2.5×10^{-6} M to 1×10^{-3} M for the ~ 650 nm emission band for excitation at 643 and 550 nm.....	114
Figure 4.9 : Variation of the fluorescence intensity of TIPS-pentacene in toluene between	114
Figure 4.10: The chemical structure of sodium dodecyl sulphate (SDS), and Titration of 30g/l of sodium dodecyl sulphate (SDS) in water at 30°C [125].	117
Figure 4.11 : ITC raw heats (a) and the ITC thermogram (b) of TIPS-pentacene in toluene solution at concentration 1×10^{-5} M in 25°C.	119
Figure 4.12: ITC raw heats (a) and the ITC thermogram (b) of 5×10^{-4} M TIPS-pentacene in toluene at 25°C.....	120
Figure 4.13: ITC raw heats (a) and the ITC thermogram (b) of 2×10^{-3} M TIPS-pentacene in toluene at 25°C.....	121
Figure 4.14: A 2-Dimensional scattering detector image, and experimental SAXS data from TIPS-pentacene in DCM solution at concentration 1×10^{-3} M at 25 °C.....	122
Figure 4.15: Plot of interaction distance (R_a) versus half-life of TIPS-pentacene in different solvents at a concentration of 1×10^{-4} M at 26°C.	124
Figure 4.16: Plot of oxygen solubility (mole fraction $\times 10^4$) versus half-life of TIPS-pentacene in different solvents at a concentration of 1×10^{-4} M.	124
Figure 4.17: Comparison of interaction distance(R_a) \times oxygen solubility (mole fraction $\times 10^4$) versus half-life of TIPS-pentacene in different solvents at a concentration of 1×10^{-4} M.	125

Figure 4.18: Comparison of interaction distance (R_a) \times oxygen solubility (mole fraction $\times 10^4$) versus half-life of TIPS-pentacene in different solvents at a concentration of 1×10^{-3} M.....	125
Figure 4.19: Schematic representation of the degree of aggregation versus concentration, (b) schematic molecular weight distribution for an isodesmic and cooperative aggregation mechanism [128].	127
Figure 4.20: Plot of half-life versus time for TIPS-Pentacene in toluene at concentrations ranging from 2.5×10^{-6} M to 5×10^{-2} M using $K = 1000 \text{ M}^{-1}$	129
Figure 4.21: Variation of half-life versus average intermolecular distance between 2.5×10^{-6} M to 2.0×10^{-2} M at 25 °C.	131
Figure 5.1: V-visible absorption of 1×10^{-5} M solutions of α -mono-Fluoro-TIPS-pentacene in different solvents at 26°C.....	134
Figure 5.2: UV-visible absorption spectra of for the photodegradation of α -mono-Fluoro-TIPS-pentacene in toluene solution at 1×10^{-5} M in a 10mm pathlength at 26°C.	134
Figure 5.3: Normalised absorbance/ time profiles for α -mono-Fluoro-TIPS-pentacene 1×10^{-5} M at different solvent at 26°C.	135
Figure 5.4: UV-visible absorption spectra of 1×10^{-5} M solutions of β –mono-Fluoro-TIPS-pentacene in different solvents at 26°C.....	136
Figure 5.5: UV-visible absorption spectra for the photodegradation of β -mono-Fluoro-TIPS-pentacene in toluene solution at 1×10^{-5} M in a 10mm pathlength at 26°C.	136
Figure 5.6: Normalised absorbance/ time profiles for β -mono-Fluoro-TIPS-pentacene 1×10^{-5} M at different solvents at 26°C.....	137
Figure 5.7: UV-visible absorption spectra of 1×10^{-5} M solutions of α -di-Fluoro-TIPS-pentacene in different solvent at 26°C.....	138
Figure 5.8: UV-visible absorption spectra for the photodegradation of α -di-Fluoro-TIPS-pentacene in toluene solution at 1×10^{-5} M in a 10mm pathlength at 26°C.	138
Figure 5.9: Normalised absorbance /time profiles for α -di-Fluoro-TIPS-pentacene 1×10^{-5} M at different solvents at 26°C.....	139
Figure 5.10: UV-visible absorption spectra of 1×10^{-5} M solutions of β -di-Fluoro-TIPS-pentacene in different solvents at 26°C.	140

Figure 5.11: UV-visible absorption spectra for the photodegradation of β -di-Fluoro-TIPS-pentacene in toluene at 1×10^{-5} M in a 10mm pathlength at 26°C	140
Figure 5.12: Normalised absorbance/ time profiles for β -di-Fluoro-TIPS -pentacene 1×10^{-5} M at different solvents at 26°C	141
Figure 5.13: UV-visible absorption spectra of 1×10^{-5} M solutions of TMTES-pentacene in different solvent at 26°C	142
Figure 5.14: UV-visible absorption spectra for the photodegradation of TMTES-pentacene in toluene solution at 1×10^{-5} M in a 10mm pathlength at 26°C	142
Figure 5.15: Normalised absorbance/ time profiles for TMTES-pentacene 1×10^{-5} M at different solvents at 26°C	143
Figure 5.16: Normalised absorbance/time profile of pentacene derivatives (1×10^{-5} M) at λ_{max} in toluene at 26°C	144
Figure 5.17: Normalised absorbance/time profile of pentacene derivatives (1×10^{-5} M) at λ_{max} in chloroform at 26°C	144
Figure 5.18: Normalised absorbance/time profile of pentacene derivatives (1×10^{-5} M) at λ_{max} in THF at 26°C	145
Figure 5.19: Normalised absorbance/time profile of pentacene derivatives (1×10^{-5} M) at λ_{max} in DCM at 26°C	145
Figure 5.20: Plot of $\ln(A_t/A_0)$ versus time for pentacene derivatives in toluene at a concentration of 1×10^{-5} M at 26°C	147
Figure 5.21: Plot of $\ln(A_t/A_0)$ versus time for pentacene derivatives in chloroform at a concentration of 1×10^{-5} M at 26°C	147
Figure 5.22: Plot of $\ln(A/A_0)$ versus time for pentacene derivatives in THF at a concentration of 1×10^{-5} M at 26°C	148
Figure 5.23: Plot of $\ln(A/A_0)$ versus time for pentacene derivatives in DCM at a concentration of 1×10^{-5} M at 26°C	148
Figure 5.24: Normalised absorbance/time profiles for photooxidation of β -di-Fluoro-TIPS-pentacene in toluene solutions for a range of concentration at 26°C	150
Figure 5.25: plot of half-life ($t_{1/2}$ min) vs concentration (M) of pentacene derivatives in toluene solution between 2.5×10^{-6} M to 5×10^{-3} M at 26°C	150
Figure 5.26: Variation of half-life versus average intermolecular distance between 2.5×10^{-6} M to 5.0×10^{-3} M for pentacene derivatives in toluene solution.	153

Figure 6.1: Variation of half-lives as a function of volume (v%) of toluene in solvent mixtures for TIPS-pentacene at concentration 5×10^{-5} M at 26°C.	156
Figure 6.2: Variation of half-lives as a function of volume (v %) of THF in solvent mixtures (THF/anisole) for TIPS-pentacene at concentration 5×10^{-5} M at 26°C.	157
Figure 6.3: Variation of half-lives as a function of volume (v %) of anisole in solvent mixtures (anisole/decane) for TIPS-pentacene at concentration 2×10^{-4} M at 26°C...	158
Figure 6.4: The $t_{1/2}$ vs mole ratio of toluene/TIPS-pentacene in THF (2×10^{-4} M) under different conditions at 26°C.	159
Figure 6.5: The $t_{1/2}$ vs mole ratio amorphous polystyrene (aPS) polystyrene/ TIPS-pentacene in THF (2×10^{-4} M) under different conditions at 26°C.	162
Figure 6.6: The $t_{1/2}$ vs mole ratio isotactic polystyrene/ TIPS-pentacene in THF (2×10^{-4} M) under different conditions at 26°C.	163
Figure 6.7: The $t_{1/2}$ vs mole ratio TIPS-pentacene/ i-PMMA and TIPS-pentacene/ PTAA in THF (2×10^{-4} M) under light conditions at 26°C.	164
Figure 6.8: Effect of added toluene and polymer to half-life of photo-oxidation of TIPS-pentacene in THF (2×10^{-4} M) under light conditions at 26°C.	166
Figure 9.1: UV-visible absorption spectra for the photooxidation of TIPS-pentacene in dodecane at 5×10^{-5} M in a 10 mm pathlength at 26°C.....	178
Figure 9.2: UV-visible absorption spectra for the photooxidation of TIPS-pentacene in decane at 5×10^{-5} M in a 10 mm pathlength at 26°C.....	178
Figure 9.3: UV-visible absorption spectra for the photooxidation of TIPS-pentacene in DCM at 1×10^{-5} M in a 10 mm pathlength at 26°C.....	179
Figure 9.4: UV-visible absorption spectra for the photooxidation of TIPS-pentacene in THF at 1×10^{-5} M in a 10 mm pathlength at 26°C.	179
Figure 9.5: UV-visible absorption spectra for the photooxidation of TIPS-pentacene in THF at 1×10^{-4} M in a 10 mm pathlength at 26°C.	180
Figure 9.6: UV-visible absorption spectra for the photooxidation of TIPS-pentacene in IPA at 1×10^{-4} M in a 10 mm pathlength at 26°C.	180
Figure 9.7: ^1H NMR spectra of TIPS-pentacene 1×10^{-5} M in THF, (a) before and (b) after photooxidation.	181
Figure 9.8: Mass spectroscopy (APCI) (AP^+) of TIPS-pentacene 1×10^{-5} M in THF, (a) before and (b) after photooxidation.	182

Figure 9.9: Mass spectroscopy (APCI) (AP^+) of TIPS-pentacene 1×10^{-5} M in THF, (a) before and (b) after photooxidation.	182
Figure 9.10: UV-vis absorption spectra of TIPS-pentacene in DCM at concentrations ranging from 2.5×10^{-6} M to 5×10^{-4} M in 1mm pathlength cuvette.....	183
Figure 9.11: UV-vis absorption spectra of TIPS-pentacene in THF at concentrations ranging from 2.5×10^{-6} M to 5×10^{-4} M in 1mm pathlength cuvette.....	183
Figure 9.12: UV-vis absorption spectra of TIPS-pentacene in chloroform at concentrations ranging from 2.5×10^{-6} M to 5×10^{-4} M in 1mm pathlength cuvette.	184
Figure 9.13: UV-vis absorption spectra of TIPS-pentacene in dodecane at concentrations ranging from 2.5×10^{-6} M to 5×10^{-4} M in 1mm pathlength cuvette.	184
Figure 9.14: UV-vis absorption spectra of TIPS-pentacene in decane at concentrations ranging from 2.5×10^{-6} M to 5×10^{-4} M in 1mm pathlength cuvette.....	185
Figure 9.15: UV-vis absorption spectra of TIPS-pentacene in IPA at concentrations ranging from 2.5×10^{-6} M to 5×10^{-4} M in 1mm pathlength cuvette.....	185
Figure 9.16: Fluorescence emission intensity of TIPS-pentacene in chloroform at concentrations ranging from 2.5×10^{-6} M to 1×10^{-3} M in 10mm pathlength cuvette at an excitation wavelength of 643nm.	186
Figure 9.17: Fluorescence emission intensity of TIPS-pentacene in chloroform at concentrations ranging from 2.5×10^{-6} M to 1×10^{-3} M in 1mm pathlength cuvette at an excitation wavelength of 643nm.	186
Figure 9.18: Fluorescence emission intensity of TIPS-pentacene in chloroform at concentrations ranging from 2.5×10^{-6} M to 1×10^{-3} M in 10mm pathlength cuvette at an excitation wavelength of 550nm.	187
Figure 9.19: Fluorescence emission intensity of TIPS-pentacene in chloroform at concentrations ranging from 2.5×10^{-6} M to 1×10^{-3} M in 1mm pathlength cuvette at an excitation wavelength of 550nm.	187
Figure 9.20: Fluorescence emission intensity of TIPS-pentacene in THF at concentrations ranging from 2.5×10^{-6} M to 1×10^{-3} M in 10mm pathlength cuvette at an excitation wavelength of 643nm.	188
Figure 9.21: Fluorescence emission intensity of TIPS-pentacene in THF at concentrations ranging from 2.5×10^{-6} M to 1×10^{-3} M in 1mm pathlength cuvette at an excitation wavelength of 643nm.	188

Figure 9.22: Fluorescence emission intensity of TIPS-pentacene in THF at concentrations ranging from 2.5×10^{-6} M to 1×10^{-3} M in 10mm pathlength cuvette at an excitation wavelength of 550nm.	189
Figure 9.23: Fluorescence emission intensity of TIPS-pentacene in THF at concentrations ranging from 2.5×10^{-6} M to 1×10^{-3} M in 1mm pathlength cuvette at an excitation wavelength of 550nm.	189
Figure 9.24: Fluorescence emission intensity of TIPS-pentacene in DCM at concentrations ranging from 2.5×10^{-6} M to 1×10^{-3} M in 10mm pathlength cuvette at an excitation wavelength of 643nm.	190
Figure 9.25: Fluorescence emission intensity of TIPS-pentacene in DCM at concentrations ranging from 2.5×10^{-6} M to 1×10^{-3} M in 1mm pathlength cuvette at an excitation wavelength of 643nm.	190
Figure 9.26: Fluorescence emission intensity of TIPS-pentacene in DCM at concentrations ranging from 2.5×10^{-6} M to 1×10^{-3} M in 10mm pathlength cuvette at an excitation wavelength of 550nm.	191
Figure 9.27: Fluorescence emission intensity of TIPS-pentacene in DCM at concentrations ranging from 2.5×10^{-6} M to 1×10^{-3} M in 1mm pathlength cuvette at an excitation wavelength of 550nm.	191
Figure 9.28: Fluorescence emission intensity of TIPS-pentacene in decane at concentrations ranging from 2.5×10^{-6} M to 1×10^{-3} M in 10mm pathlength cuvette at an excitation wavelength of 643nm.	192
Figure 9.29: Fluorescence emission intensity of TIPS-pentacene in decane at concentrations ranging from 2.5×10^{-6} M to 1×10^{-3} M in 1mm pathlength cuvette at an excitation wavelength of 643nm.	192
Figure 9.30: Fluorescence emission intensity of TIPS-pentacene in decane at concentrations ranging from 2.5×10^{-6} M to 1×10^{-3} M in 10mm pathlength cuvette at an excitation wavelength of 550nm.	193
Figure 9.31: Fluorescence emission intensity of TIPS-pentacene in decane at concentrations ranging from 2.5×10^{-6} M to 1×10^{-3} M in 1mm pathlength cuvette at an excitation wavelength of 550nm.	193
Figure 9.32: Fluorescence emission intensity of TIPS-pentacene in dodecane at concentrations ranging from 2.5×10^{-6} M to 1×10^{-3} M in 10mm pathlength cuvette at an excitation wavelength of 643nm.	194

Figure 9.33: Fluorescence emission intensity of TIPS-pentacene in dodecane at concentrations ranging from 2.5×10^{-6} M to 1×10^{-3} M in 1mm pathlength cuvette at an excitation wavelength of 643nm.	194
Figure 9.34: Fluorescence emission intensity of TIPS-pentacene in dodecane at concentrations ranging from 2.5×10^{-6} M to 1×10^{-3} M in 10mm pathlength cuvette at an excitation wavelength of 550nm.	195
Figure 9.35: Fluorescence emission intensity of TIPS-pentacene in dodecane at concentrations ranging from 2.5×10^{-6} M to 1×10^{-3} M in 10mm pathlength cuvette at an excitation wavelength of 550nm.	195
Figure 9.36: Fluorescence emission intensity of TIPS-pentacene in IPA at concentrations ranging from 2.5×10^{-6} M to 2×10^{-4} M in 10mm pathlength cuvette at an excitation wavelength of 643nm.	196
Figure 9.37: Fluorescence emission intensity of TIPS-pentacene in IPA at concentrations ranging from 2.5×10^{-6} M to 2×10^{-4} M in 1mm pathlength cuvette at an excitation wavelength of 643nm.	196
Figure 9.38: Fluorescence emission intensity of TIPS-pentacene in IPA at concentrations ranging from 2.5×10^{-6} M to 2×10^{-4} M in 10mm pathlength cuvette at an excitation wavelength of 550nm.	197
Figure 9.39: Fluorescence emission intensity of TIPS-pentacene in IPA at concentrations ranging from 2.5×10^{-6} M to 2×10^{-4} M in 1mm pathlength cuvette at an excitation wavelength of 550nm.	197
Figure 9.40: UV-visible absorption spectra for the photooxidation of β –mono-FTIPS-pentacene in DCM 1×10^{-5} M in a 10 mm pathlength at 26°C.	198
Figure 9.41: UV-visible absorption spectra for the photooxidation of α -di-FTIPS-pentacene.	198
Figure 9.42: UV-visible absorption spectra for the photooxidation of TMTE-pentacene 5×10^{-5} M in toluene solution in a 10 mm pathlength at 26°C.	199
Figure 9.43: UV-visible absorption spectra for the photooxidation of β –di-FTIPS-pentacene 2×10^{-4} M in THF solution in a 10 mm pathlength at 26°C.	199
Figure 9.44: TGA plots of TIPS-pentacene thin film drop casting when exposed to UV light.	200
Figure 9.45: Differential scanning calorimetry of TIPS-pentacene thin film drop casting when exposed to UV light.	201

Figure 9.46: TGA plots of thin film drop casting for β -di-Flouro-TIPS-pentacene when exposed to UV light.....	202
Figure 9.47: The DSC traces of β -di-Flouro-TIPS-pentacene thin film drop casting when exposed to UV light.....	202

List of Table

Table 2.1: Chemical structure and physical properties of the solvents used in this study.....	61
Table 2.2: Fluorescence set up parameters.	69
Table 3.1: Review of literature of photo- oxidation stability of TIPS-pentacene.....	77
Table 3.2: The photochemical conversion of TIPS-pentacene at concentration 1.8×10^{-5} M in different solvents upon irradiation with 15 W lamp at 300nm in the absence of oxygen [53].	77
Table 3.3: The λ_{\max} of TIPS-pentacene at concentration 1×10^{-5} M in different solvents at 26°C	81
Table 3.4: The half-life ($t_{1/2}$) of TIPS-pentacene in different solvents at concentration (1×10^{-5} M) at 26°C	83
Table 3.5: Effective reaction rate constants, $k'(\text{min}^{-1})$ determined and R^2 for TIPS-pentacene in different solvents at a concentration of 1×10^{-5} M 26°C	97
Table 3.6: Hansen parameters Fractional solubility parameters, solubility limits and oxygen solubility at different solvents.	102
Table 4.1: Comparison of experimental $t_{1/2}$ (min) of TIPS-pentacene in toluene, THF, chloroform, DCM, IPA, dodecane and decane at different concentration at 25°C , the (*) solubility limit.	109
Table 5.1: The λ_{\max} and $t_{1/2}$ (min) of pentacene derivatives in toluene, THF, Chloroform and DCM solutions at concentration 1×10^{-5} M at 26°C	146
Table 5.2: The kinetic data of pentacene derivatives in toluene, THF, Chloroform and DCM solutions at concentration 1×10^{-5} M at 26°C	149
Table 5.3: The $t_{1/2}$ min of pentacene derivatives in toluene solutions at different concentrations at 26°C	151
Table 5.4: the λ_{\max} and $t_{1/2}$ min of pentacene derivatives at concentration (1×10^{-4} M and 2×10^{-4} M) in THF solutions.	152

Table 6.1: The half-lives for TIPS-pentacene in mixed solvent at concentration 5×10^{-5} M.....	156
Table 6.2: The half-lives for TIPS-pentacene at concentration 5×10^{-5} M in mixed solvent THF/anisole.	157
Table 6.3: The half-lives for TIPS-pentacene 2×10^{-4} M in mixed solvent anisole/decane	158
Table 6.4: The half-lives for TIPS-pentacene / toluene at concentration (2×10^{-4} M) in THF solutions at different ratio (w/w) under different irradiation conditions at 26°C.	159
Table 6.5: The half-lives for TIPS-pentacene/amorphous polystyrene (aPS) at concentration (2×10^{-4} M) in THF solution at different ratio (w/w) under different irradiation conditions at 26°C.	161
Table 6.6 : The half-lives for TIPS-pentacene / isotactic polystyrene at concentration (2×10^{-4} M) in THF solution at different ratio (w/w) under different irradiation conditions at 26°C.	163
Table 6.7: The half-lives for TIPS-pentacene/ i-PMMA and TIPS-pentacene/ PTAA at concentration (2×10^{-4} M) in THF solution at different ratio (w/w) under light conditions at 26°C.	165

Declaration

I declare that this is my own work and has not been submitted in any form for another degree or qualification of The University of Manchester or any other university or any other institute of learning. Information derived from the published work of others has been acknowledged in the text and list of references is given.

Laila Abusen

Copyright Statement

- i. The author of this thesis agrees any copy right in it and she has given the University of Manchester the permission to utilize such copy right for any institute of learning, and educational aims.
- ii. Copies of this thesis, either in full or extracts, may be made only in accordance with the regulations of the John Ryland's University Library of Manchester. Details of these regulations may be obtained from the Librarian. This page must from part of any such copies made.
- iii. The ownership of any patents, designs, trade marks and any and all other intellectual property rights except for Copyright (the intellectual Property Rights) and any reproductions of copyright works, for instanced graphs and tables (Reproductions),which may be described in this thesis, may not be owned by the author and may be owned by third parties. Such intellectual Property Rights and Reproductions can not and must not be made available for utilize without the prior written permission of the owner(s) of the relevant intellectual Property Rights and/or Reproductions.
- iv. Further information on conditions under which disclosure, publication and exploitation of this thesis, the Copyright and any intellectual Property Rights and /or Reproductions described in it may take place is available from the Head of the School of Chemistry and the Dean of the Faculty of Life Sciences, for Faculty of Life Sciences candidate

Acknowledgements

Put God in the centre and everything will come together

To Him I give thanks for making all things possible!

I am grateful to my thesis supervisors, Professor S. G. Yeates, and Dr Andrew B. Horn, who are knowledgeable, enthusiastic and helpful and for their excellent and invaluable guidance throughout my PhD. They have given me passion for science and guided me to understand this project from start to finish. Without their continuous encouragement for improving my dissertation, I can hardly finish it. The professional training and the style I learned from them will benefit me in my future career.

Many thanks especially go to Professor S. G. Yeates and Dr Andrew B. Horn for proofreading and I wish them good luck in their future. As well I would like to thank Dr Gonzalo Rincon, Dr Jaroslaw Wasikiewicz and Dr John Morrison who were synthesized and characterized pentacene derivatives which were used as our samples. My next thanks go to Ministry of Higher Education, Libyan government and Merck Chemicals Limited for their financial support throughout my PhD study.

I also thank to great people past and present who worked in the Organic Materials Innovation Centre (OMIC), for their time, help, advice and inspiring discussions, especially the people in my office, namely Dr John Morrison, Dr Mark McCairn, Abdebasset Chakin and Fatima Alzaharni.

Thank you all. Last but not least, to my family, your love is the greatest gift of all, my husband, Elmabrouk. He came to UK to stay with me and quit his job in Libya. His arrival eased my upset and worries. He has supported me in multiple capacities over the last four years and he encouraged me to pursue and finish a Ph.D. For such a sacrifice, I know I cannot say thank you enough. My sweet kids Mohamed, Fatema and Farah their smile removed all my tiredness from the whole day work in the lab. My father who is in Libya, always encourage me when we talked by phone. Thanks to my siblings, my brothers and sisters, and all the family for their love and support. I have also been blessed with a handful of true friends Sadia Muminovic and her family for helping me during my time in Manchester.

Motivation

The potential advantage of solution processed organic semiconductors, high operating speed, low cost, and large area flexible circuit, has motivated many studies in this field. Applications on organic semiconductors include organic light emitting diodes (OLEDs), organic field effect transistors (OFETs) and organic photovoltaic cells (OPVs). Candidate molecules however contain intense chromophores and a quality-limiting factor in device fabrication is photochemical degradation in the solution phase. This instability can be substantially reduced for many species by chemical derivatisation. For example, pentacene shows a strong tendency to dimerise in solution under the influence of light, which can be attenuated by derivatisation at the 6, 13 positions. As a consequence, materials such 6, 13 trialkylsilylethyl-pentacene and its derivatives are becoming popular replacements for pentacene in electronic devices because of both their excellent semiconducting properties coupled with relatively stable solution processability. However, these derivatives are themselves still prone to photochemical degradation during processing, which potentially perturbs both the optical absorption and electronic properties of films cast from solution. The half-life for photo-oxidation in solution is very short when it exposed to air and light and it is clear that photochemical instability merits further work is in order to establish a fundamental understanding of the photophysical and photochemical processes in solution.

Abstract

The University of Manchester

Abstract of thesis submitted by Laila Mohamed Abusen for the Degree of Doctor of Philosophy and entitled “Environmental Stability Studies of an Organic Semiconductor”

Month and year of submission: November 2013

The formulation induced photooxidative stability of substituted 6, 13 trialkylsilylethynylpentacene derivatives is reported for the first time. It is known that 6,13 trialkylsilylethynylpentacene derivatives undergo rapid oxidation through singlet oxidation and is believed to be primarily to the 6,13 endoperoxide. The effect of solvent, organic semiconductor concentration and the presence of polymeric binder on the rate of photooxidative degradation in oxygen saturated solutions on degradation kinetics have been investigated.

The photochemical stability of 6,13 trialkylsilylethynylpentacene has been studied in toluene, THF, dichloromethane, chloroform, decane and dodecane at concentrations ranging from 2.5×10^{-6} M to 5×10^{-2} M by measurement of the half-life by UV-visible spectroscopy. The predominant degradation products of TIPS-Pentacene are the same regardless of solvent and concentration, being predominantly an endo-peroxide resulting from O_2 addition across the 6, 13 position of the pentacene. At low concentration ($< 1 \times 10^{-3}$ M), the half-life of TIPS-Pentacene is observed to vary with solvent and the amount of dissolved oxygen, with half-life showing a strong, positive correlation between the product of the Hansen Solubility Parameter (HSP) and the mole-fraction oxygen solubility. In this range, the half-life is observed to increase markedly with increasing solution concentration, showing a linear correlation with mean intermolecular distance within the solution. From intermediate to high concentration, the half-lives increase more rapidly with increasing concentration, which is attributed to aggregation. In most solvents, this behaviour shows a specific onset point, suggesting a cooperative rather thanisodesmic aggregation mechanism.

Photooxidative half-lives of TMTES-pentacene and fluorinated soluble pentacene derivatives were determined from 2.5×10^{-6} M to 5.0×10^{-3} M solutions in THF, toluene, chloroform and CH_2Cl_2 . Independent of solvent and at constant concentration the relative ordering of photo-oxidative resistance was: α -di-FTIPS-pentacene > β -di-FTIPS-pentacene, α -mono -FTIPS-pentacene, β -mono-FTIPS-pentacene > TIPS-pentacene \geq TMTES-pentacene. The same rank order for a particular derivative was generally maintained over the concentration range 2.5×10^{-6} M to 5×10^{-3} M. The stability to photooxidation for all derivatives increased with increasing concentration. All derivatives showed a mixture of endoxidation products as shown by APCI mass spectrometry, and ^1H NMR.

Added polystyrene and isotactic polystyrene were found to accelerate photooxidative degradation whilst isotactic polymethylmethacrylate (i-PMMA) and poly (triethylamine) (PTAA) had no effect adding weight to the argument that anything which can act as an acceptor to the solution slows down the degradation and anything which impairs pair-wise energy transfer speeds up the degradation. Understanding of these phenomena is therefore essential for the further application of solution processing of organic materials.

Chapter 1

1 Introduction

1.1 Organic semiconductors

Organic semiconductors are classified into three main groups; small molecular, low weight (oligomers) and polymers with high molecular weight. All types have in common extended π -electron systems of sp^2 -hybridized orbitals in which carbon is bonded to its neighbours with three strong σ bonds and a P_z orbital. The intra-molecular interaction between two carbon atoms leads to the overlapping of sp^2 orbitals that form directional σ bond, while the two remaining P_z orbitals usually form π -bond figure 1.1. For larger molecules the bonding (overlap) of P_z orbitals are delocalized along the backbone of the molecule, oligomer or polymer and form π -conjugate systems which extend over the whole molecule. Conjugation allows for electrons to move beyond its π -bond and move over longer distances giving rise to resonance stabilisation.

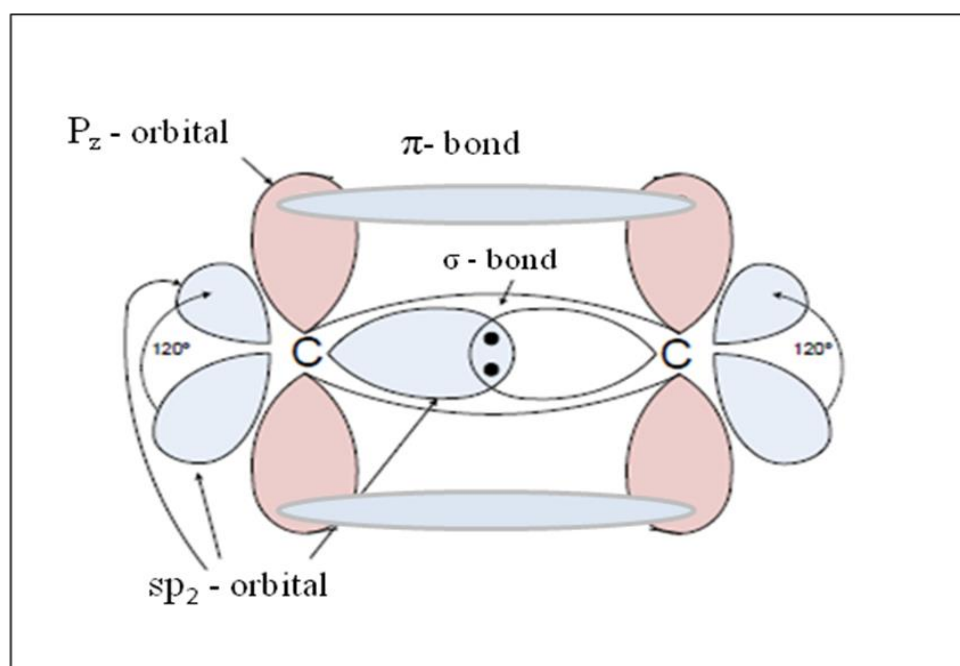


Figure 1.1: Scheme of the P_z orbitals and σ -, π -bonds for two sp^2 - hybridized carbon atoms [1].

1.1.1 The chemical structures of organic semiconductors

Organic semiconductors can be divided into two main types of semiconductors, p-type and n-type (hole- or electron-transport) according to charge carrier [2]: positive charge and high dispersion in the valence band for p-type compounds and negative charge and high dispersion in the conduction band for n-type materials. Hole-transporting materials have low ionization potentials together with low electron affinities, whereas electron-transporting materials have high electron affinities together with high ionization potential [3, 4]. Figures 1.2 and 1.3 display some examples of p-type and n-type organic semiconductors. The most widely used and studied semiconductors for organic transistors are p-type due to the higher mobility and higher stability in air in contrast to n-type that are highly sensitive to oxygen and water under operating conditions.

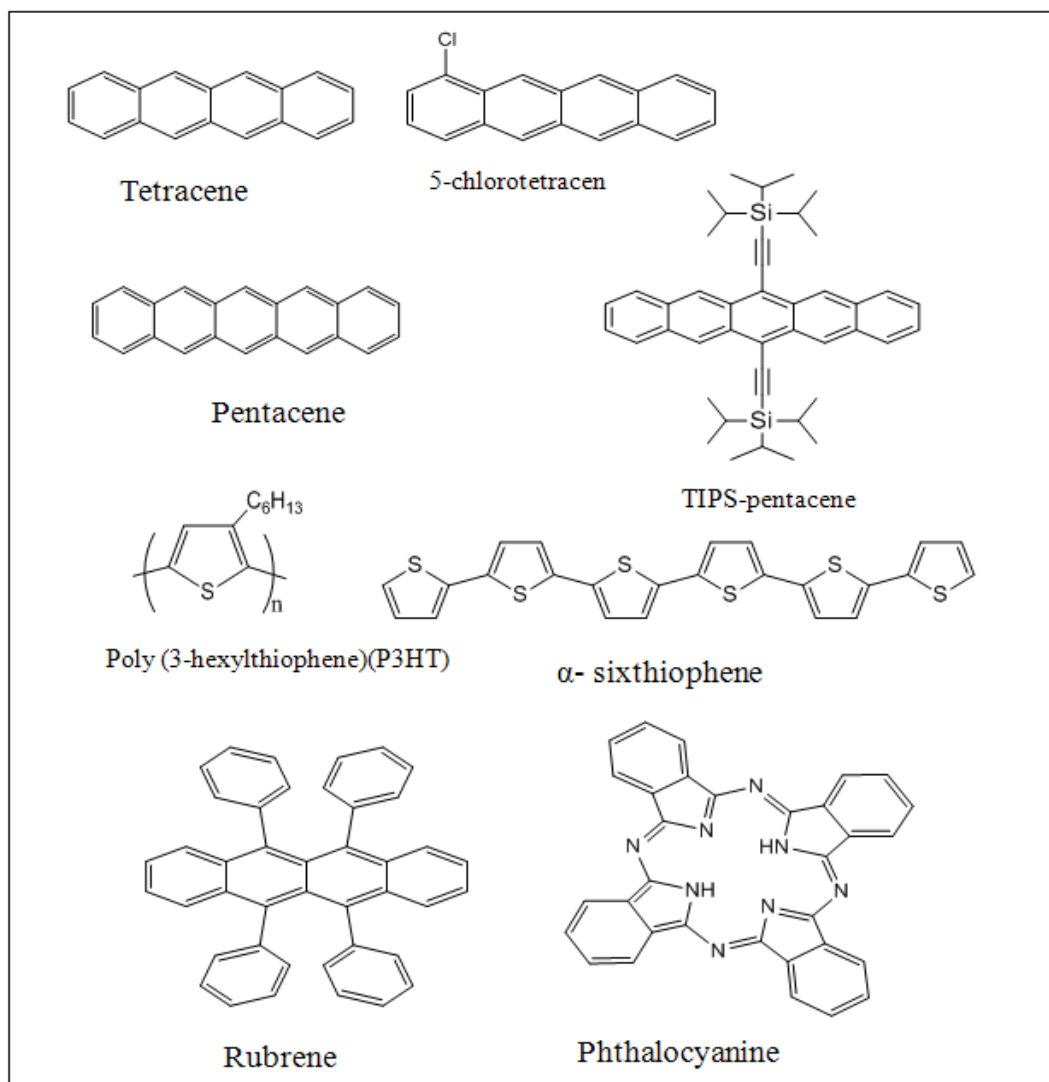


Figure 1.2: Examples of p-type organic semiconductors [3-7].

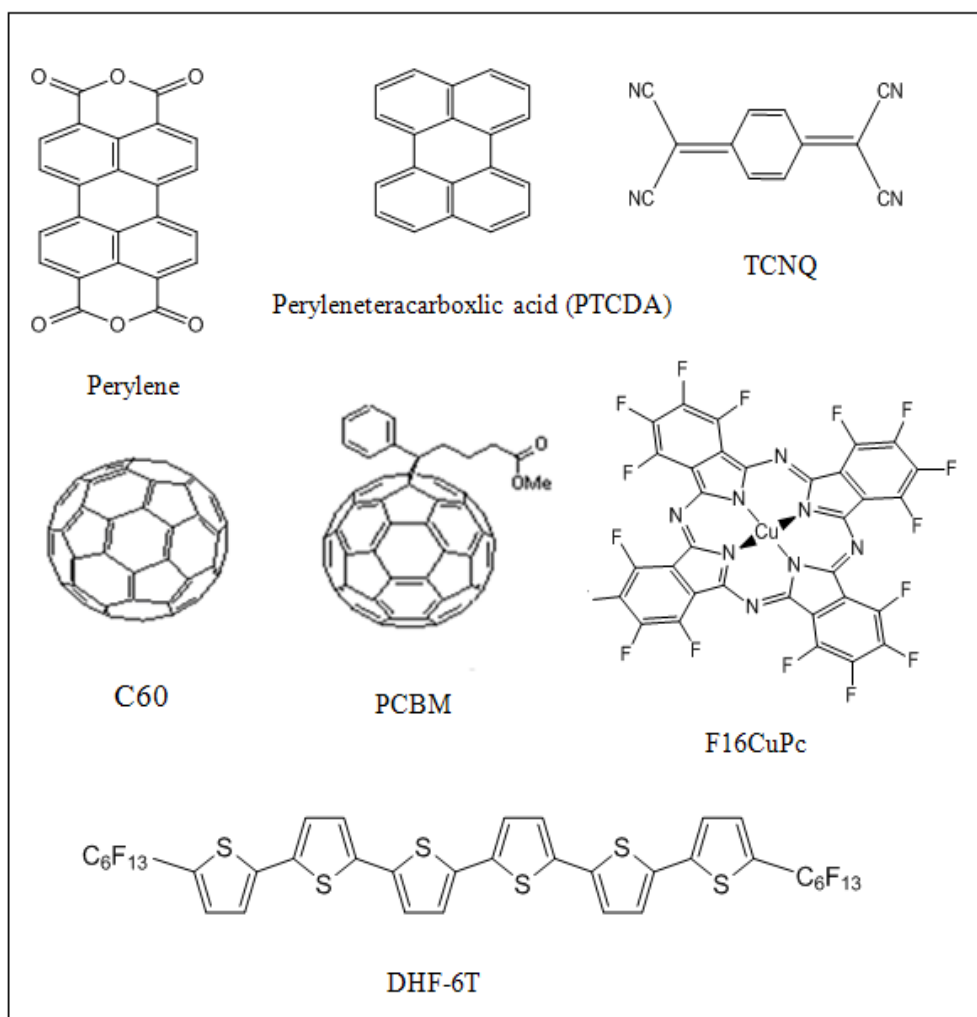


Figure 1.3: Examples of n-type organic semiconductor [3, 4, 6, 7].

1.1.2 Physics of organic semiconductor

In conjugated molecules the π -bonding molecular orbitals and π^* -antibonding molecular orbitals are the highest occupied state (HOMO) and the lowest unoccupied state (LUMO), respectively. The π -bonding is much weaker due to lower overlap of the two parallel P_z atomic orbitals compared with sp^2 orbitals forming σ bonding. Therefore, the energy level of the bonding σ is lower than that of bonding π while the antibonding π^* is lower than antibonding σ^* as shown in figure 1.4. The energy for π - π^* transition corresponds to the lowest energy needed to generate electronic excitation. When the molecule contains a conjugated π system the energy difference or band gap between the HOMO and LUMO is reduced, and can lead to strong absorption in the visible spectral range and to semiconducting properties.

As the molecules exist in a bulk phase, the union of all the molecular orbitals of the individual molecules lead to a formation of quasi-bands, forming a system that is similar to their inorganic counterparts. The band gap of organic semiconductor is typically between 1 to 4 eV [8].

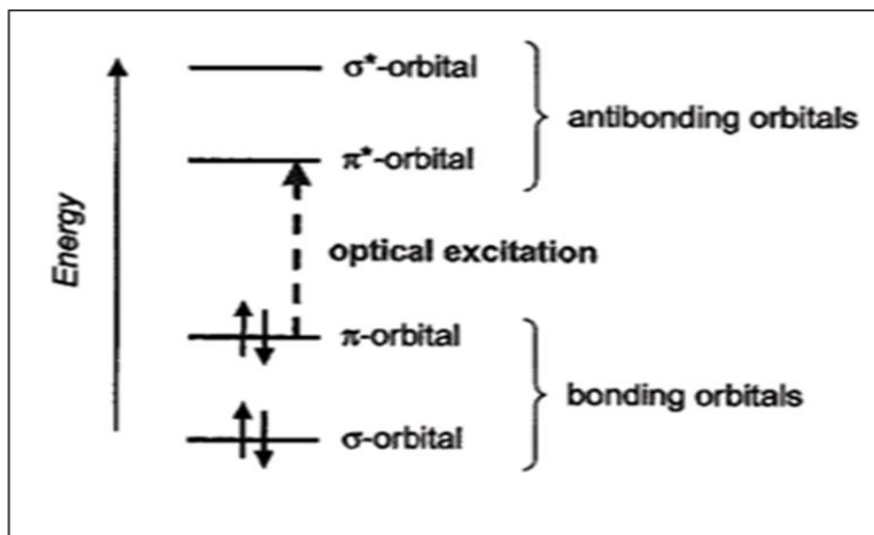


Figure 1.4: The energy levels of a π -conjugated molecule. The lowest electronic excitation is between the bonding π -orbital (HOMO) and the antibonding π^* -orbital (LUMO) [1].

In organic semiconductors, molecules are linked to each other by comparatively weak van der Waals interactions. Therefore, electrons are largely localized to individual molecules except electrons in the π orbital, and the weak intermolecular interactions cause a narrow electronic bandwidth in molecular solids. As the interaction between π orbitals increases the degree of π - π overlap increases.

Small molecule organic semiconductors such as pentacene, anthracene and rubrene are usually formed by a series of fused benzene rings as the basic unit in which the π bonds become delocalized to form a π system. The gap between occupied and empty states in these π systems becomes smaller with increasing delocalization, leading to absorption and fluorescence in the visible (smaller band gap) as shown in figure 1.5. Polymers semiconductors like poly (3-hexylthiophene) and poly (p-phenylene vinylene) have π bonds that are delocalized along the chain and form a one-dimensional electronic system resulting in a 1D-band which has considerable band width on the scale of an eV. The transport properties of such polymers are usually limited by defects in the 1D-chains or by hopping from chain to chain [9].

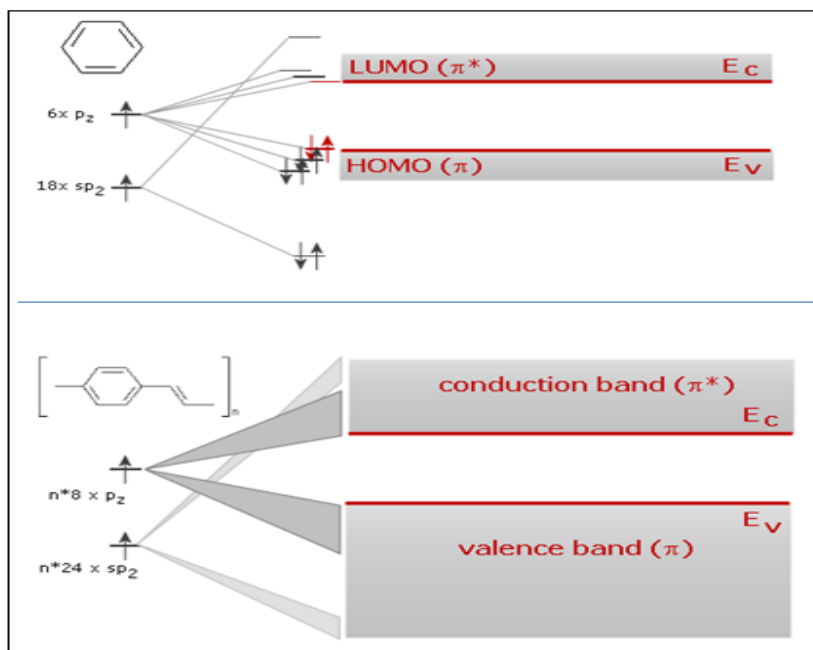


Figure 1.5: The energy structure of small molecule organics (top) and the energy structure of polymer organics (bottom) [9].

1.1.3 Electronic transitions in organic semiconductors

The optical properties of organic semiconductors can be derived the highest occupied molecular orbital (HOMO) and the lowest unoccupied molecular orbital (LUMO) that are π and π^* orbitals and delocalize over the molecule. Absorption of light (optical excitation) promotes an electron from the HOMO to the LUMO, thus creating an excited state. The excitons in organic materials are an electron and hole pair. In organic materials, the exciton is localised on a single polymer unit or a small molecule. According to the rules of addition of angular momentum, two spin $\frac{1}{2}$ electrons can combine to give a total spin of either 0 or 1 as shown in figure 1.6(a). The multiplicity of the spin states is equal to $(2S+1)$, because there are $(2S+1)$ degenerate m_s levels in each state. Hence the electron and hole are orientated with spin anti-parallel and the total angular momentum equals to zero ($S=0$) with combination $1/\sqrt{2}(\downarrow\uparrow-\uparrow\downarrow)$ and opposite (spin momentum $m_s=0$) are known as singlet states as shown in figure 1.6(b). While the $S=1$ states are called triplets. The triplet states contain three possible spin orientations.

First, both the electron and hole are spin down ($m_s=-1$, $S=1$). Secondly, both of them are spin opposite but with a non-zero resultant spin component ($m_s=0$, $S=1$). Thirdly, both electron and hole are spin up ($m_s=1$ and $S=1$) as shown in figure 1.6 (b). The separations of the electronic levels into singlet and triplet states have very important consequences on the optical spectra. Each molecule will have a series of singlet excited states labeled S_1 , S_2 , S_3 ..., in addition to its singlet ground state which is labelled S_0 . There will be a similar series of triplet excited states labeled T_1 , T_2 , T_3 ... Since photons carry no spin, they can excite only transitions between electronic states of the same spin. Therefore, transitions from the S_0 ground state to the triplet excited state are not allowed. The main optical absorption edge therefore corresponds to the $S_0 \rightarrow S_1$ singlet-singlet transition. The emission spectrum is likewise dominated by the $S_1 \rightarrow S_0$ transition [10, 11].

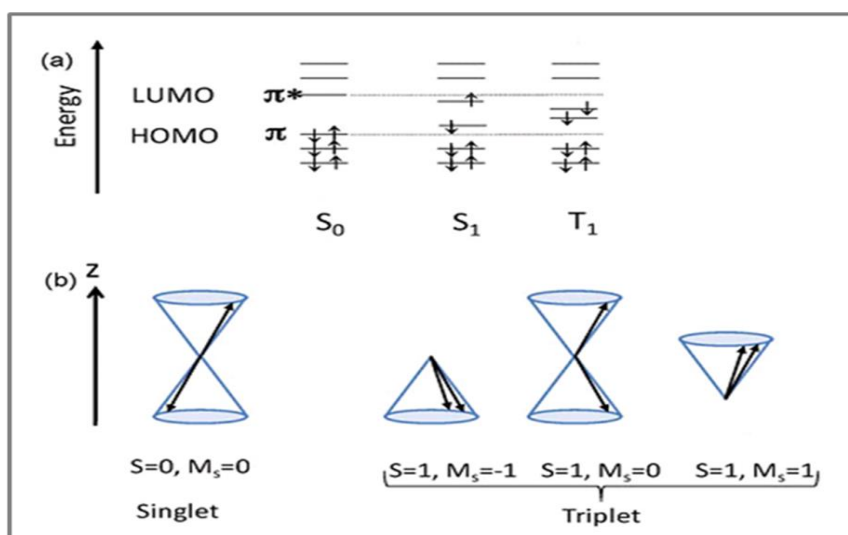


Figure 1.6 :The unpaired electrons of an excited molecule can either have their spins antiparallel or parallel are known as singlet and triplet state [10].

The singlet excited states have short lifetimes of order 1-100 picosec due to the dipole allowed transitions to the S_0 ground state. The lowest triplet state on the other hand, has a long radiative lifetime because of the low probability for the $T_1 \rightarrow S_0$ transition. The different time scales for the singlet-singlet and triplet-singlet transitions are conveniently distinguished by describing the emission process as fluorescence and phosphorescence, respectively [10]. In organic semiconductors the molecules, exciton fission refers to the spin- allowed conversion of one photo-generated singlet excitation into two triplet excitons residing on different chromophores [12, 13].

1.1.4 Applications of organic semiconductor

Organic semiconductors have attracted lot of attention in technological community due to their potential application in electronic devices such as organic field effect transistors (OFETs), light emitting diodes (LEDs) [7, 14] and solar cells (OPV). The main advantage of organic materials is their solubility in a range of solvents with the potential for low cost device fabrication by a range of coating and printing techniques. Secondly the ability to tune properties by chemical modification of the structure, doping or combination with other materials. OTFTs can be used in integrated circuits which lead to electronic product identification such as RFID-tage (Radio-frequency identification tage), intelligent cards, electronic noses, flexible displays, sensors, and portable electronics. OLED have so far had the largest impact in the field of organic electronics. These devices have already entered the market and are presently being used mainly for commercial display applications, e.g. in car radios, mobile phone displays, TV screens, computer laptop displays and DVD-player monitors. OPV is still in its infancy but is receiving a substantial and strongly increasing amount of attention. Despite their lower efficiency compared with silicon based devices, organic solar cells offer the advantage of low cost large area production, which might lead to a cost-effective use. Some examples are shown in figure 1.7.

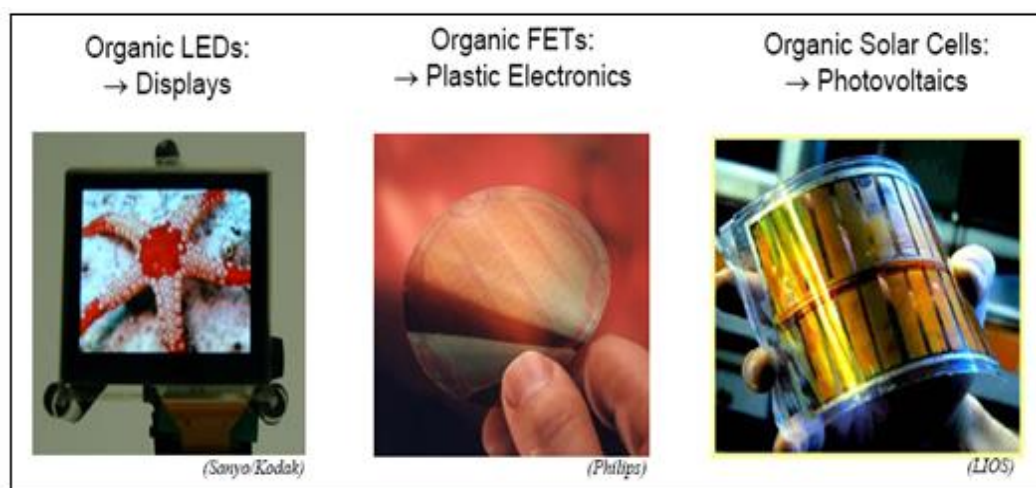


Figure 1.7: A selection of commercially available and future products, in which Semiconducting organic moieties are employed.

1.2 Organic Thin film Transistors (OTFTs)

Small molecules as a class can show high crystallinity, high field effect mobility, and high stability, but often have poor solution processability [3, 4, 15, 16]. Polymer semiconductor compared with small molecules generally show lower crystallinity and low field effect mobility. However they exhibit excellent solution processability enabling simple fabrication processes such as inkjet patterning [17]. An organic thin film transistor (OTFTs) contains four types of material: electrical conducting material for use as gate (G), source (S) and drain (D) electrodes, electrical insulating material as the medium between gate electrode and semiconductor (dielectric layer), the substrate typically glass and SiO₂/Si, and organic semiconductor as active layer. They can be assembled in either top-contact or bottom-contact geometry, figure 1.8. In the bottom-contact device, the source and drain electrodes are pre-fabricated on the dielectric, and then the organic materials layer is deposited directly on the top of the electrodes. In the top-contact configuration, an active organic semiconductor layer is first deposited on the dielectric, and then the two electrodes (source and drain) are evaporated through a shadow mask. The advantage of this device is the larger contact area between the electrodes and the organic semiconductor, as compared with bottom-contact devices [18].

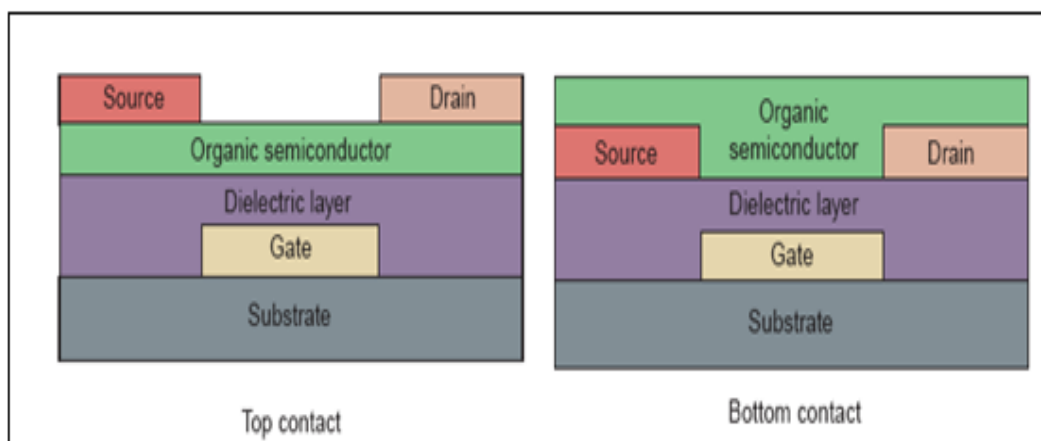


Figure 1.8 :Two types of organic thin film transistor device configuration [7].

1.2.1 Physical parameters of OTFTs

The nature and quality of the organic semiconductors is crucial for achieving high OFET performance due to four important parameters: (1) Charge carrier mobility or the field-effect mobility (μ) that represents a measure of the charge carrier drift velocity per unit of electric field (measured in cm^2/Vs). The mobility μ is also directly related to the switching time of the device. For practical application this value should be greater than $0.5 \text{ cm}^2/\text{Vs}$, the value for amorphous silicon. (2) The on/off current ratio ($I_{\text{on/off}}$), the ratio of current flow between the current in the accumulation mode and the current in the depletion mode. An on/off ratio of greater than 10^5 is required for any practical device application. (3) The threshold voltage ($-V_T$) which is the gate voltage corresponding to the opening of the conduction channel. (4) The sub-threshold swing or slope (S), determines how fast the device can switch back to the on state in the region of exponential current increase from the off state [19, 20].

1.2.2 Working principle of OTFTs

The working principle of OFET is similar to the first metal-oxide-semiconductor field-effect transistor (MOSFET). The theory developed for MOSFET is used as starting point in modelling the OFET behaviour, although the electrical transport in organic semiconductors is different than the covalently bonded inorganic semiconductors. The sketch of OFET is shown in figure 1.9, two electrodes (drain and source) with the width (W), namely channel width, are connected by the organic semiconducting material with the distance of (L) called channel length. Application of a potential (V_G) between the source and gate electrode polarizes the semiconductor - insulator interface resulting in the accumulation of charge carriers between the source and drain electrode. The transistor channel is active only when the gate voltage (V_G) value exceeds the value of the threshold voltage (V_T). Below this point, the transistor is turned *off*, and there is no conduction between drain and source. In the *on* state of the device application of potential (V_D) between the source and drain electrodes results in the conduction of charge carriers in the accumulation layer [21].

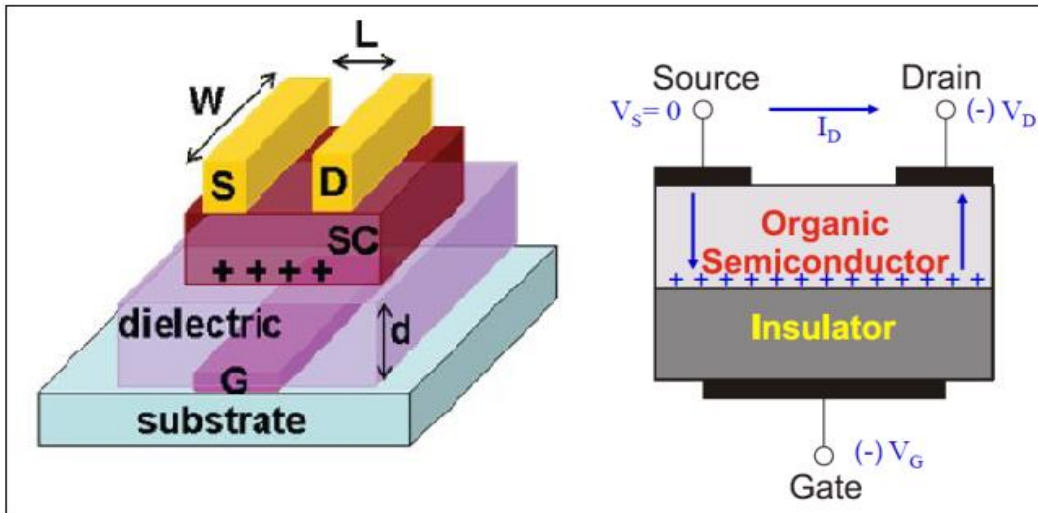


Figure 1.9: Formation of conducting channel in OTFT [21].

The transistor performance is generally characterized by the current voltage plots that are output characteristics, figure 1.10 (a), and transfer curves figure 1.10 (b). The output curve shows the relation between the drain current I_D and the drain source voltage ($-V_D$) with different gate voltage ($-V_G$) applied. As the applied potential is increased the device deviates from Ohmic behavior and with further increase in potential the current flowing through the device reaches a constant value.

The source-drain current (I_D) generated in the linear and saturation regions can be calculated by the following equations.

For the linear regime ($V_D \gg V_G$):

$$I_D = (W/L) \mu C_i (V_G - V_T) V_D \quad 1.1$$

For the saturated regime ($V_D < V_G$):

$$I_D = (W/2L) \mu C_i (V_G - V_T)^2 \quad 1.2$$

where C_i is the capacitance per unit area of the gate insulator. The charge carrier mobility in the linear and saturation regime can be calculated from equations (1.1) and (1.2) respectively. The transfer curve, which is in log scale, shows the relation between the drain current I_D and the gate voltage V_G with different drain source voltage applied [21-23].

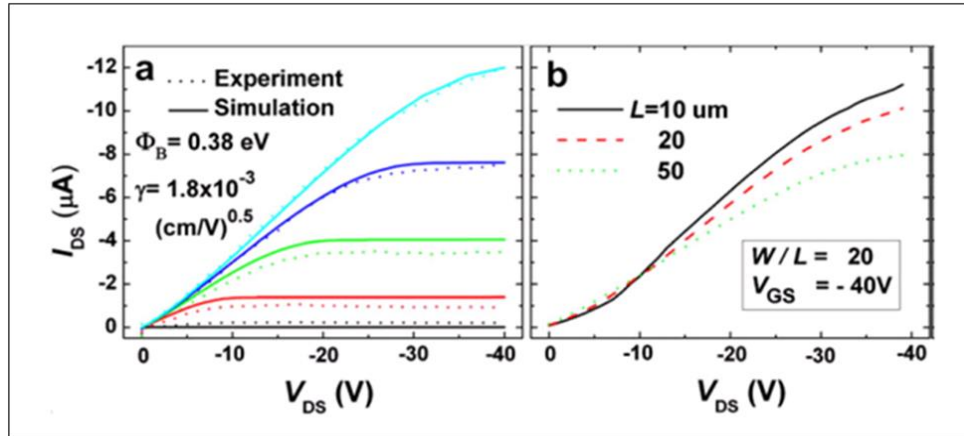


Figure 1.10: Output characteristics and transfer characteristics of TIPS-pentacene TFTs [24].

1.2.3 Deposition techniques for organic semiconductor thin film

For practical applications, the active layer of most organic semiconductor devices is composed of a thin film with thickness ranging between 25-150 nm. Therefore, deposition of high quality organic thin film with desired structure is the key to achieving certain electrical and optical properties in the devices.

There are many methods available that can be used for depositing organic thin films on a substrate which depend on the properties of the organic material: which can be split into vacuum evaporation techniques such as in figure 1.11, and solution processing techniques such as in figure 1.12 [7, 25-27]. Small molecules can be deposited by physical vapour deposition (PVD), organic molecular beam deposition (OMBD) and organic vapour phase deposition (OVPD). In the OMBD the material is evaporated under high to ultra-high vacuum (10^{-8} - 10^{-12} Torr). An organic material is heated and a beam of evaporated molecules is ejected onto a substrate. These molecules will then form (crystal) nuclei on the surface which will grow as more molecules are deposited typically resulting in a polycrystalline thin film. The disadvantage of this technique is the use of high vacuum and the difficulties to process large areas. The OVPD is used at low vacuum a gas carrying organic semiconductor molecules flows through a showerhead and the molecules deposits onto the substrates. Using this technique is possible to combine low vacuum with good growth control and yielding well-ordered films.

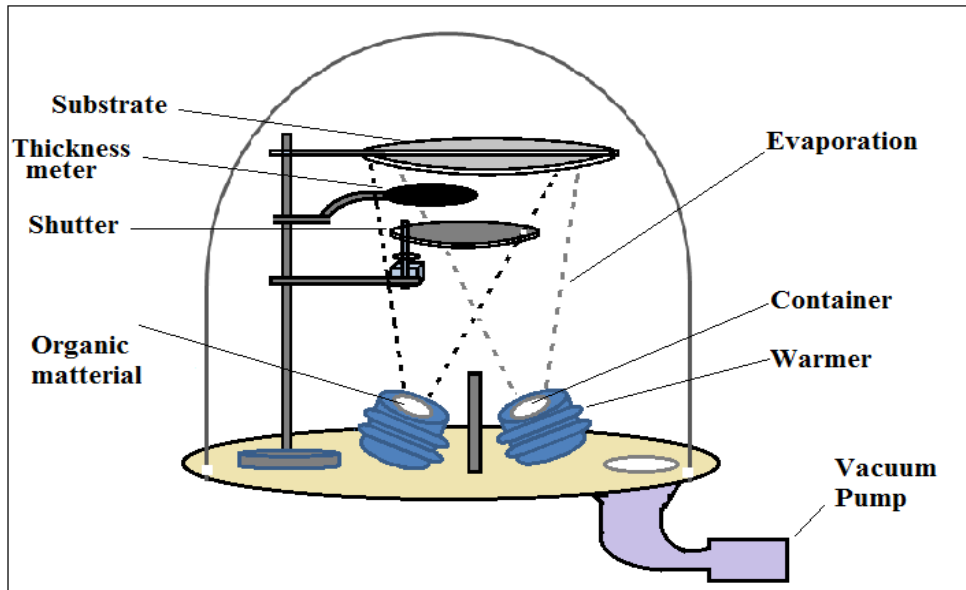


Figure 1.11 : Vacuum Thermal evaporation deposition organic semiconductors.

Small molecules and polymer thin films can be prepared through solution processing techniques. These methods avoid the use of vacuum, have comparatively lower processing temperatures and are compatible with large areas. The resulting polymer film is amorphous or semi-crystalline depending on the processing conditions. Examples of different solution processing techniques are depicted in figure 1.12:

- a- Drop casting: a solution is poured onto the substrate figure 1.11(a).
- b- Inkjet printing: small droplets of a solution are ejected in a patterned way on a substrate figure 1.12(b).
- c- Aerosol spray: a “mist” of droplets is homogeneously sprayed on a substrate figure 1.12(c).
- d- Doctor Blading: a blade is spreading the solution over a substrate figure 1.12(d).
- e- Screen printing: a solution is pressed through a screen on a substrate figure 1.12 (e).
- f- Dip coating: a substrate is dipped into a solution figure 1.12(f).
- g- Spin coating: a solution is spread out over the substrate by rotating it figure 1.12(g).

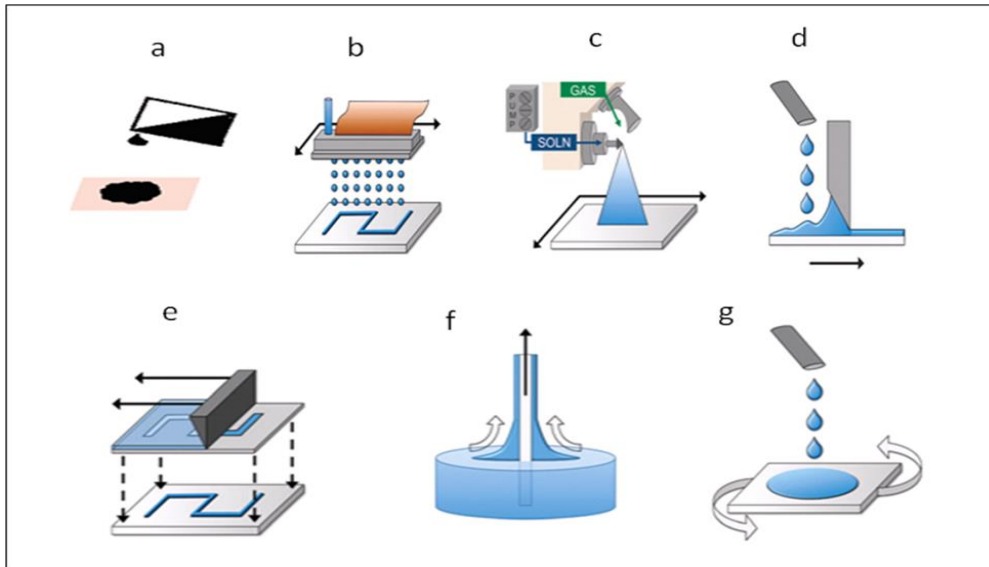


Figure 1.12: Schematically depiction of the various methods for obtaining thin film by solution processing [28].

1.2.4 Passivation of OTFTs

Organic thin film transistors need to be environmental stable in air for low processing cost and to avoid expensive encapsulation or passivation in-use. The lifetime of the OTFTs having no passivation layer is usually short when they are exposed to ambient air due to the interaction of organic semiconductor with oxygen and moisture [29]. Therefore, in order to achieve OTFTs with long lifetime, the OTFTs should be protected from the environmental moisture and oxygen [30]. Organic transistors still have the significant shortcoming of performance degradation due to environmental and operational stability of the organic active layer [31]. Extensive research efforts have been focused on synthesizing organic semiconductor materials with environmental and operation stability, high mobility, and good current modulation to improve OTFTs performance [32]. For pentacene OTFT's the long term stability of transfer characteristics is related to interaction with oxygen that induces appreciable degradation of field-effect mobility [33].

1.2.5 Environmental Stability of Functionalized Acenes

Pentacene belongs to the family of polyaromatic hydrocarbon that consists of five linear fused benzene rings, figure 1.13 (a). Pentacene is a conjugated molecule and as already mentioned it is the most promising organic semiconductor because of its excellent transistor characteristics. It shows mobilities higher than $1 \text{ cm}^2 \text{ V}^{-1}\text{s}^{-1}$ and on/off current ratio greater than 10^8 [34, 35].

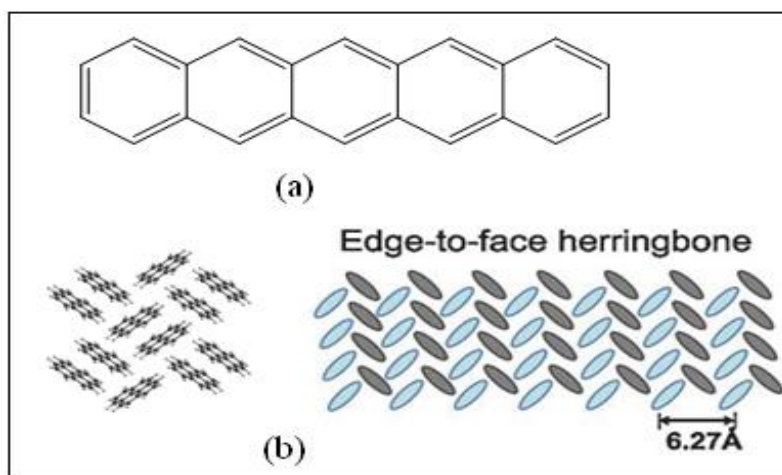


Figure 1.13: The structure and the tradition herring-bone of pentacene molecule [36].

Pentacene forms a film when grown by evaporation in high vacuum with a favourable crystal geometry and orientation. Due to the morphology of the films, there is good intermolecular overlap which leads to the high mobility and on/off ratio that are measured. The molecules arrange themselves into the so-called herringbone structure, “edge to face,” figure 1.13 (b) with their molecular axes perpendicular to the substrate [36]. However, pentacene has two main drawbacks. First, the low solubility in commonly used organic solvents, and as such pentacene-based devices are fabricated using ultra-high vacuum techniques which are costly because of expensive equipment, sophisticated instrumentation, low deposition throughput and limited upscalability. Additionally, commercially available pentacene is not pure enough for use in OTFTs requiring intensive purification by train sublimation. Due to the high temperature needed for vacuum sublimation, $> 250^\circ\text{C}$, a fraction of the pentacene will be degraded. For example, during the purification, dihydropentacene (a) and a series of polycondensed aromatic hydrocarbons like peripentacene (b) have been identified figure 1.14 [37].

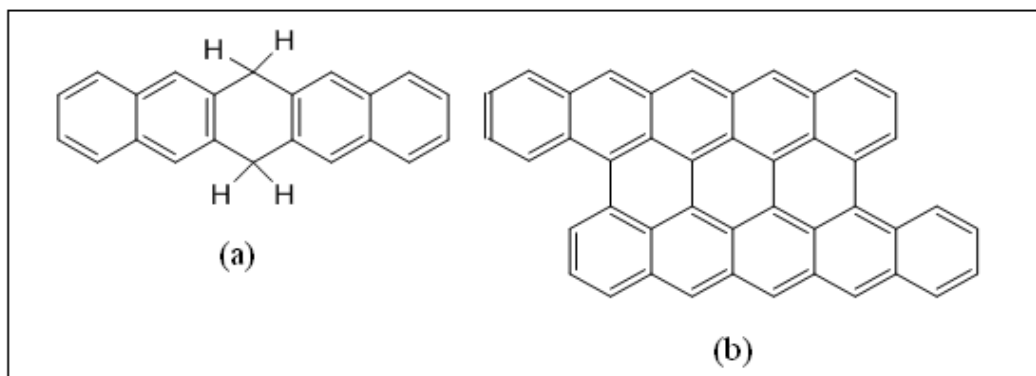


Figure 1.14: Chemical structure of side products produced during train –sublimation [37].

Secondly, the poor oxidative stability of pentacene when it is exposed to light and oxygen resulting in linked dimer as shown in figure 1.15(a) [38], or oxidized (endoperoxide formation), figure 1.15(b) [39] by radical reaction and [4+2]-cycloadditions (Diels -Alder reaction with oxygen) taking place between the aromatic rings in the molecules as shown in figure 1.16 [40]. The oxidation of the pentacene molecule based OFETs, in ambient condition, may lead to the formation of alcohols or quinines as shown in figure 1.17 [41].

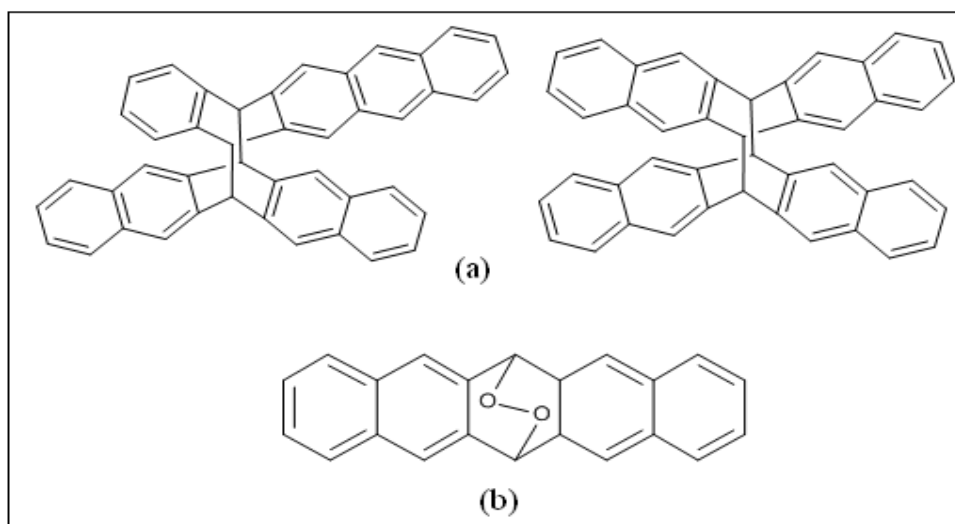


Figure 1.15: Chemical structure of (a) photo-dimerization and (b) endo-peroxide of pentacene [38].

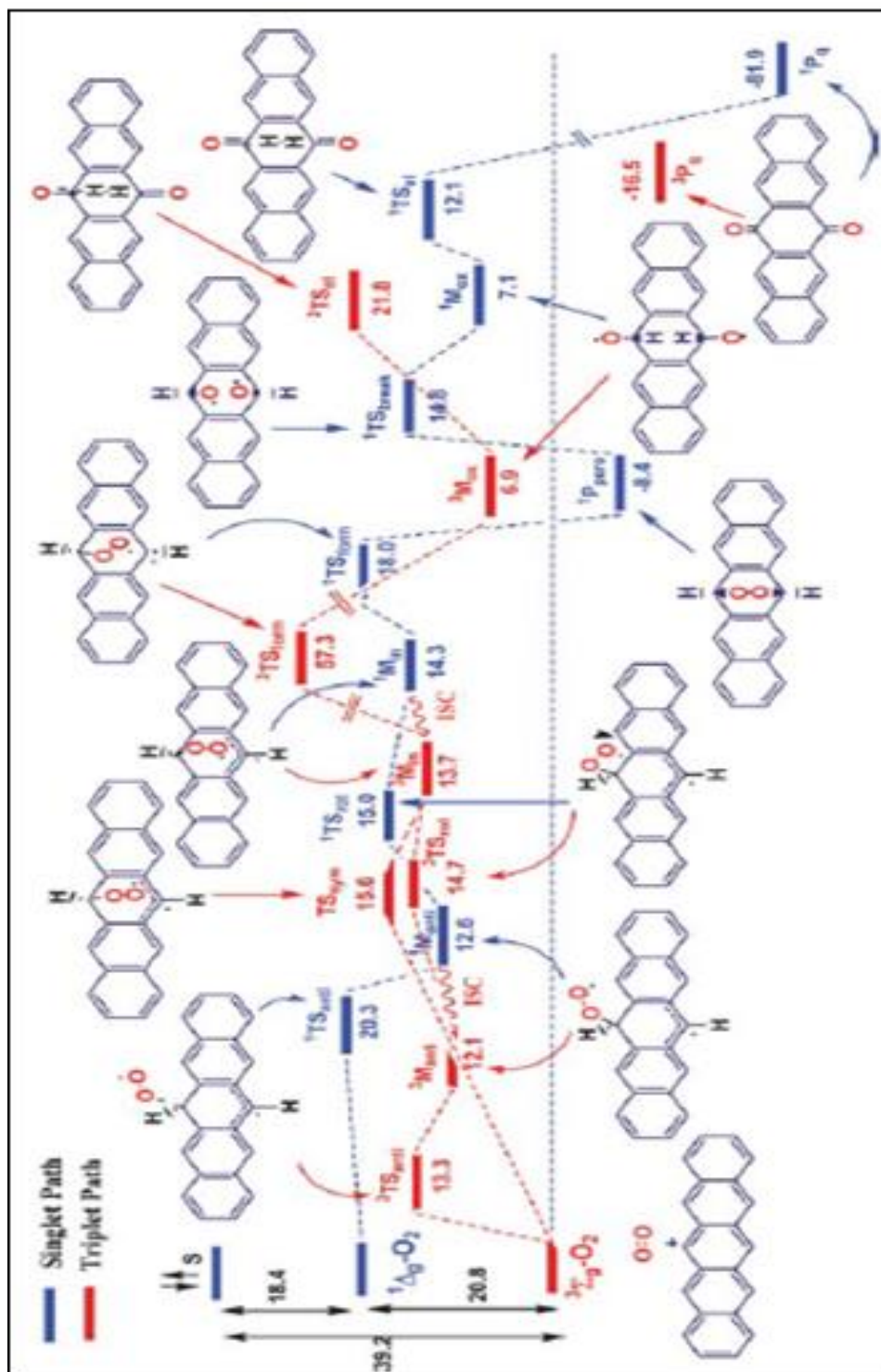


Figure 1.16: Photooxidation of pentacene in the Diels-Alder reaction with calculated reaction energies (kcal/mol) [40].

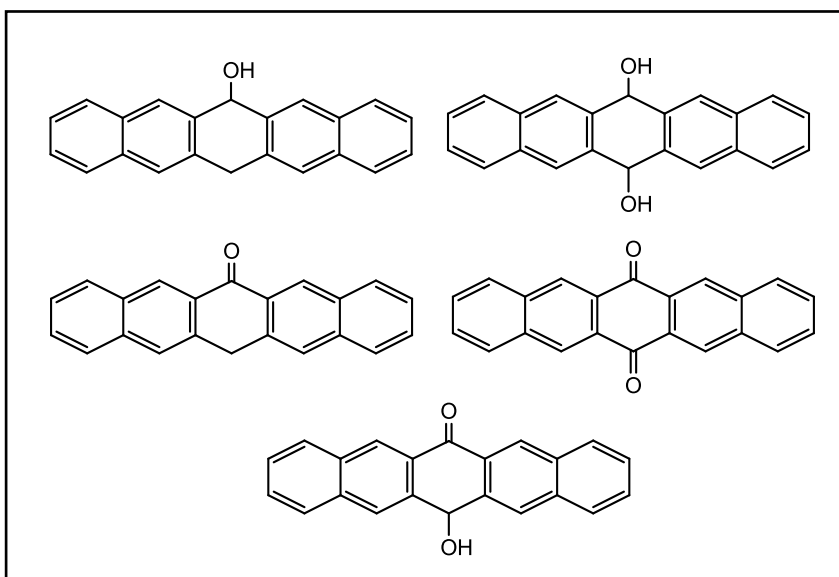


Figure 1.17: Chemical structure of some common oxidation products of pentacene [41].

Two methods can overcome these problems which will increase both solubility and stability. Solubility can be overcome by synthesis of a soluble pentacene Diels-Alder precursors [42] which after integration into transistor structures, pentacene is regenerated. The second method by introducing substituents on the aromatic core which will increase both solubility and stability [43].

1.2.6 Soluble pentacene precursors

Pentacene precursors are Diels-Alder adducts which because of their butterfly-like structure; they are more soluble than the planar pentacene and thus can be purified in a straightforward manner. A second advantage of the improved solubility is the possibility of depositing the precursor from solution which makes them competitive with polymers. After deposition the precursor can be reconverted to the semiconducting pentacene by a simple retro-Diels-Alder reaction. Depending on the precursor, this reaction can be induced by heat or light. The need of converting the precursor back to pentacene demands some requirements of the precursor. It has to be relatively easy to break the bridge and one has to be sure to remove the formed products, both in a quantitative way. For example, a pentacene precursor was synthesized by Diels-Alder chemistry using N-sulfinylamide as the heterodienophile (figure 1.18).

This product is highly soluble in chlorinated organic solvents, as well as tetrahydrofuran and dioxane. On annealing at 120 - 200 °C, the precursor reverts back to pentacene, yielding thin film transistors with mobilities in the range of 0.1- 0.8 cm²/Vs [42, 44] .

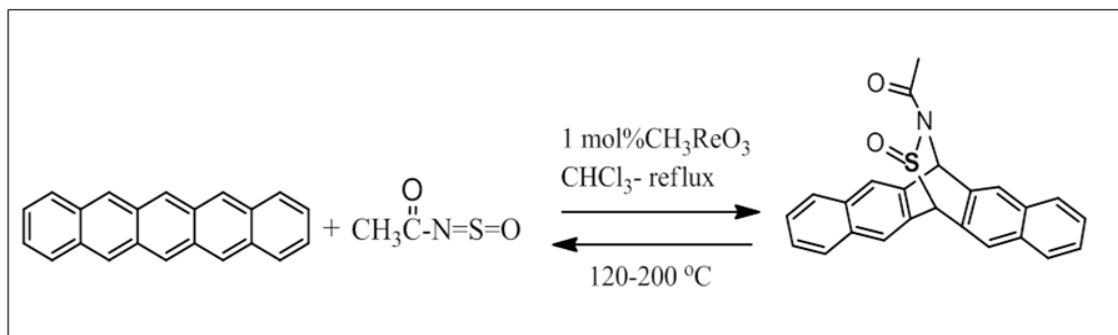


Figure 1.18: Schematic showing the Diels-Alder reaction making pentacene soluble in organic solvents [42].

1.2.7 Substituted soluble pentacene derivatives

Incorporation of substituent in the central 6, 13 position of pentacene can strongly improve the solubility without excessive perturbation of the π -orbital overlap. Pentacene derivatives substituted by aromatic groups at the 6, 13 sites, figure 1.19 were amongst one of the earliest attempts at obtaining solution processed pentacene materials. The 6, 13-diaryl pentacenes are in general both more stable and more soluble than the parent compound because of substitution on the most reactive position of the acene. Moreover, the substituents can affect the self-assembly of pentacene moieties resulting in a closer packing that leading to better intermolecular overlap between pentacene moieties and in this way improve the electric properties [45]. In 2005, Dehaen and co-workers described the synthesis of 6,13-di(2'-thienyl) pentacene, figure 1.19 (c), and its benzothiophene analogue figure 1.19 (d) [46], but neither electronic properties nor device characterization were reported. However a very interesting series of pentacene derivatives was synthesized and tested by Miao et al [47], where they substituted pentacene with a phenyl group on different position.

Transistors made by evaporation showed that substitution in the 5, 7, 12 and 14 position were most successful. The mobility increased in spectacular way to $10^{-1} \text{ cm}^2 \text{ V}^{-1} \text{ s}^{-1}$ when Miao et al. replaced the phenyl group in the 6, 13 position by 2-thienyl group, figure 1.19 (c) [47].

The photo-oxidation of pentacene derivative with 2-thienyl groups, figure 1.19 (c) was investigated in solution under light and afforded endoperoxides formation when it reacted with oxygen, figure 1.20 [48, 49].

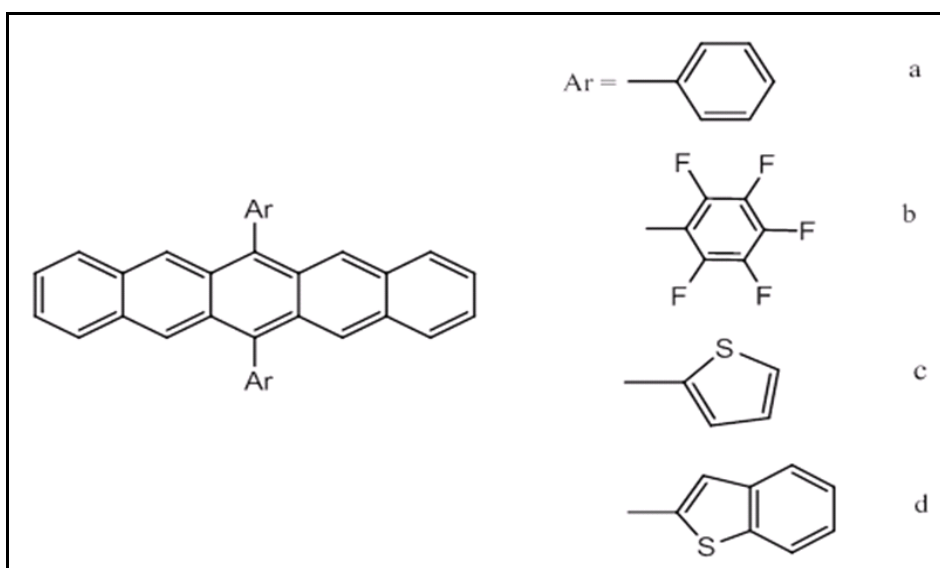


Figure 1.19 : Chemical structure of Aryl pentacenes [45].

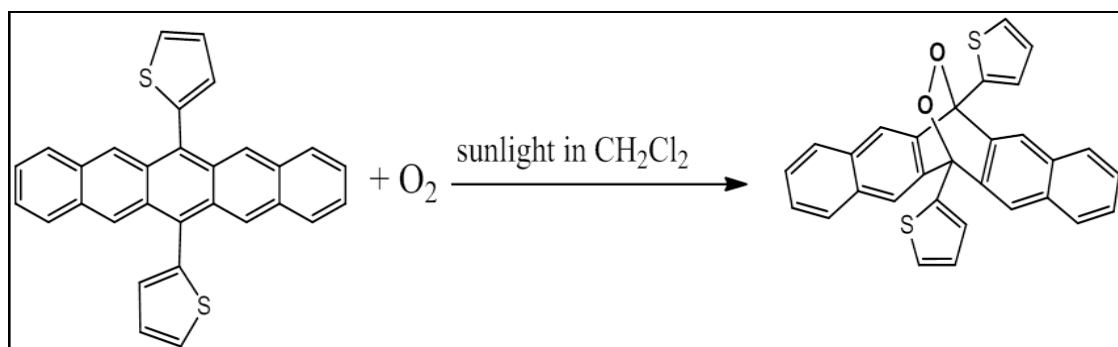


Figure 1.20: Schematic showing Photo-oxidation of 2-thienyl pentacene [48].

The substitution at the 6 and 13 positions of the pentacene with a relatively bulky group (trialkylsilyl group), figure 1.21, was employed to avoid complete disruption of π -stacking between the neighbouring molecules due to the large silyl groups by the intermolecular “face to face” interaction, figure 1.22. These substituted pentacene showed an increase in solubility in common organic solvents, stability and molecular packing [50, 51]. Substitution with appropriate solubilising trialkysilylethynyl at the C-6/C-13 position of pentacene was reported to give a mobility of $0.17 \text{ cm}^2 \text{ V}^{-1} \text{ s}^{-1}$ in OTFTS [52]. The C-6/C-13 positions of pentacene as in TIPS-pentacene has proven to be effective for photooxidative stability when exposed to visible light in air and it is longer lived than pentacene. Recent efforts found that the alkynyl group cause a decrease of the LUMO energy, TIPS-pentacene have lower LUMO energy than pentacene, figure 1.23 [39]. TIPS-pentacene alters the intermolecular and, intramolecular electronic effects interactions and HOMO-LUMO energy gaps. These have been obtained from the combination of closely related high-resolution gas phase and solid phase ultraviolet photoelectron spectroscopy (UPS) measurements along with solution electrochemical measurements. The results showed that the intermolecular effects have a greater influence on the electronic interactions of the TIPS-pentacene [53].

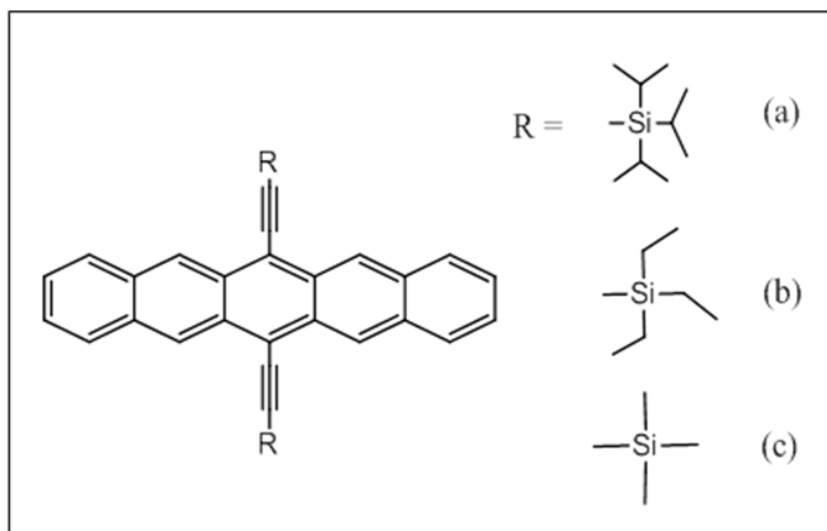


Figure 1.21: Chemical structure of silyl-functionalized pentacenes [50].

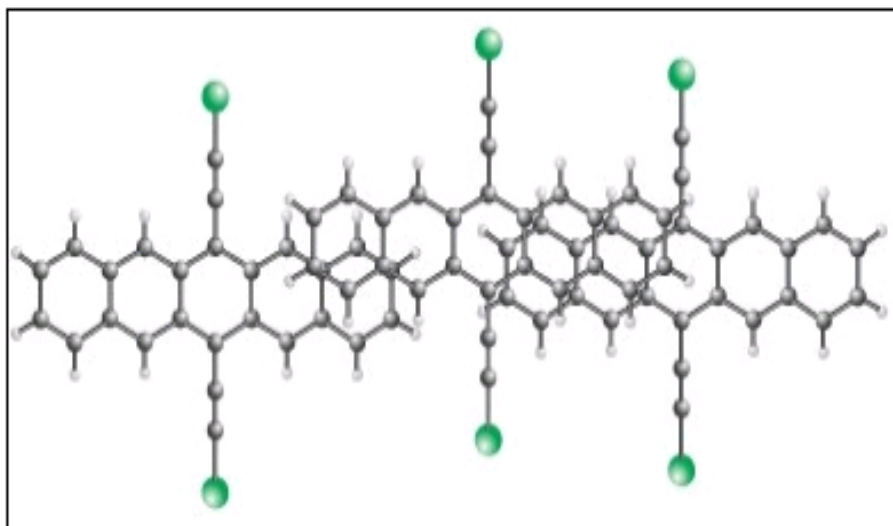


Figure 1.22: Face-to-face packing of TIPS-pentacene [51].

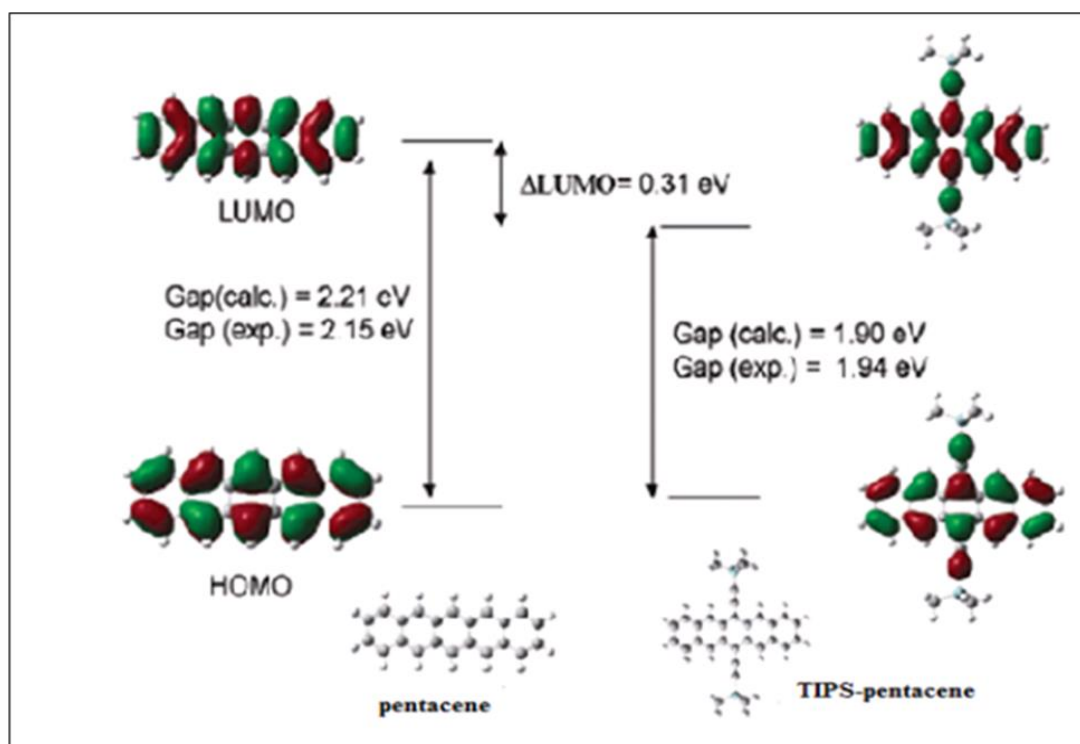


Figure 1.23: HOMO and LUMO orbitals and energy of pentacene and TIPS-pentacene [39].

Recently it has been shown that UV-light is leading to a degradation of the product also without the presence of oxygen by promotion of dimerization on the 5 and 14 positions, figure 1.24 [54], as previously observed for pentacene. It is therefore important to protect the substituted pentacenes against UV-light.

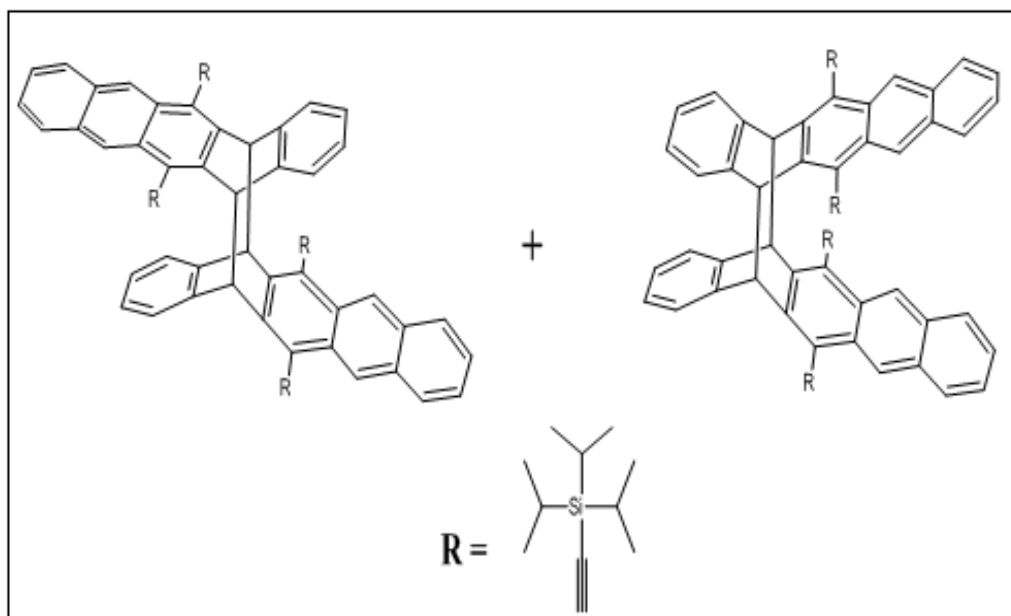


Figure 1.24: Chemical structures of dimerisation of TIPS-pentacene induced by UV-light [54].

The triisopropylsilylethynyl group was also introduced at the positions of 5 and 14 because it was believed that this unsymmetrical derivative would have a nearly perfect stacking, but this was only partly true [55]. The molecule formed pairs that had a nearly perfect stacking but the pairs were then arranged in a herringbone pattern. Moreover the compound seemed extremely sensitive to oxygen and the films decomposed rapidly upon exposure to air. However, the photooxidative stability of pentacene structure can be achieved through appropriate pentacene at the position 6, 13 to promote extended π -electron delocalization without the use bulky trialkylsilyl group. The series of 6,13-diethynyl-substituted pentacenes showed good photooxidative stability as well as high OFET properties in solution processed thin film semiconductor under ambient condition, with 6,13-bis(4-pentylphenylethynyl) pentacene showing a hole mobility of as $0.5\text{cm}^2\text{ V}^{-1}\text{ s}^{-1}$ [56].

The photooxidative stability of pentacene that are functionalized at the 5,14 and 6,13 positions with methoxy, alkylethynyl and phenylethynyl groups was studied by monitoring change in their absorption in air saturated toluene showed improved solubility and higher stability than pentacene [57]. Another approach considered for improving the stability of acene molecules is by selective LUMO orbital stabilization in series of 6, 13-bis (arylkynyl)-substituted pentacene in the presence of oxygen. These studies indicate that photo stabilization can be increased by having low singlet energies and low excited state oxidation potentials (low LUMO orbital energy) [58].

Irvinder and co-workers reported the kinetics of photooxidation for halogenated phenylated, silylethylated, and thiolated of pentacene derivatives under identical photo-oxidative conditions [59]. 2, 3, 9, 10-tetrachloro-6,13-bis(2,6-dimethylphenyl) pentacene, figure 1.25 (a) I was found to be more stable than TIPS-pentacene, with thiopentacene derivatives, figure 1.25 (b, c), showing high photo-stability with small HOMO-LUMO gaps. Resultant oxidization of these to afford pentacene -6, 13-dione and either diphenyl disulfide or didecyl disulfide, respectively as shown in figure 1.26. While the phenylated pentacene derivatives, figure 1.25(d) is substantially short lived than TIPS-pentacene, figure 1.21 (a).

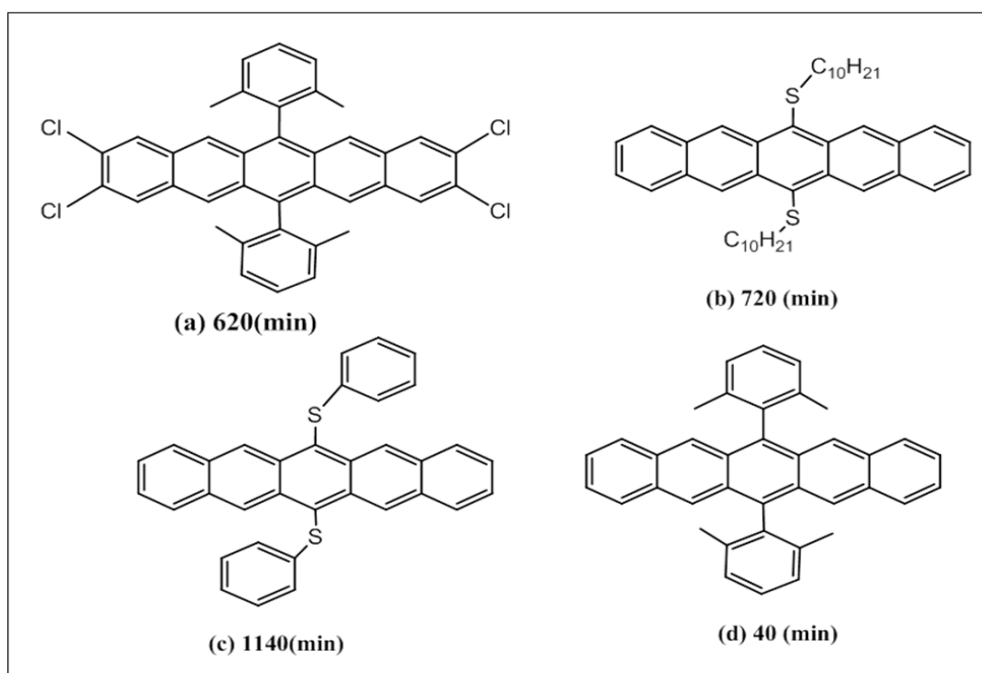


Figure 1.25: Structures of halogenated (a), thiolated (b, c) and phenylated (d) pentacene derivatives with their associated half-lives (min) [59].

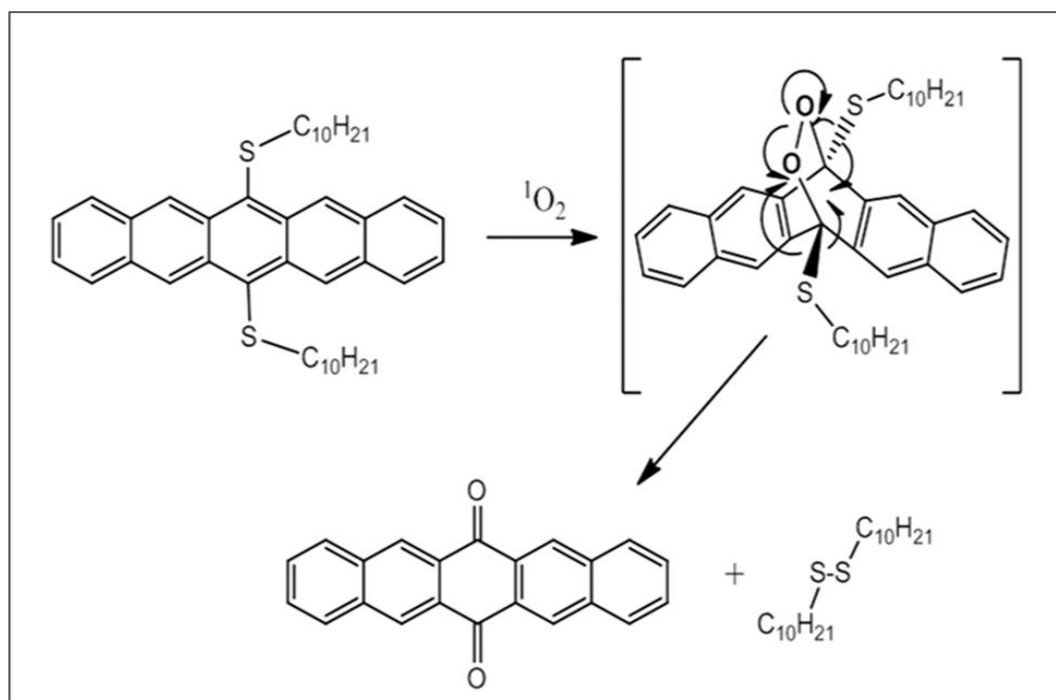


Figure 1.26: Proposed mechanism for the oxidation of 6, 13-bis (phenylthio pentacene and 6, 13-bis (decylthio) pentacene to afford pentacene-6,13-dione and the corresponding disulfides [59].

Another method for modifying the structure of pentacene is to introduce substituents on the 2, 3, 9, and 10 positions of the terminal rings in order to affect the arrangement of pentacene molecules [60], substitution at these positions would also be less disruptive compared to the previous efforts. Through facile synthesis methods 2, 3,9,10 tetramethyl pentacene was prepared and characterized. This material showed higher transport charge mobility due to its altered morphology. The tetra-bromo functional groups on the 2, 3, 9, and 10 positions of pentacene also showed high stability both in solution and in the solid state, when exposed to air and laboratory lighting [61].

A recent attempt to produce stable, soluble derivatives of pentacene, figure 1.27 that demonstrated, modified π stacking and rationally modifiable electronic properties, has given rise to highly substituted systems. These materials showed strong intermolecular interaction that gives rise to improvement in the hole transport mobility. These thin films are also quite stable when exposed to the ambient conditions [62].

The physical properties such as molecular spectroscopy and electronic properties were studied of series soluble 6,13-disubstituted 2,3,9,10-tetrakis(trimethylsilyl) pentacene by virtue of their solubility in organic solvents and these pentacene derivatives found good solubility and stability, which might elucidate the influence of substituents on HOMO-LUMO gaps [63].

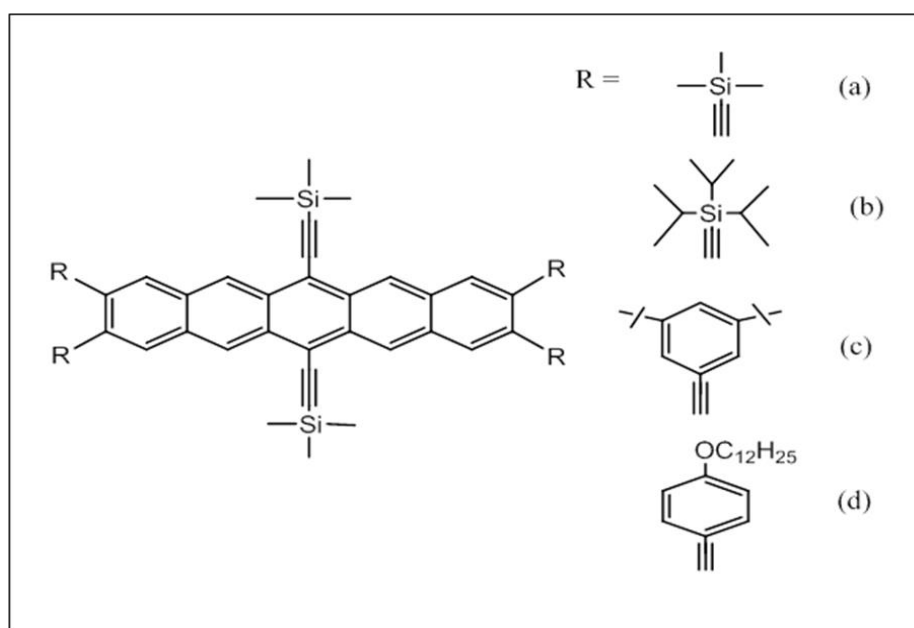


Figure 1.27 : Chemical structure pentacene with substitution of the 2, 3, 6, 9, 10 and 13 position [60].

Similar to the approach of improving solubility and π -stacking of pentacenes, the Antony group used the peri-functionalization approach on anthradithiophene that is a pentacene analogue where the two terminal benzene rings are replaced by two thiophene units, on the central ring the same silylethynyl groups were introduced figure 1.28 [52]. In the case of anthradithiophenes, the shorter acene length requires a smaller triethylsilyl substituent to achieve 2D π -stacking. TES Anthradithiophene (TES ADT, figure 1.28 (b)) exhibits 2D π -stacking with a reduced carbon- carbon distance of 3.23 Å compared to TIPS-pentacene. Field effect transistor made from drop-cast thin film of these molecules yielded mobility of 1 cm²/Vs and the molecules showed greater stability over pentacene because of high energy barrier to oxidation. However spin coated thin film of TES ADT were amorphous and exhibited poor device performance [52]. In order improve the crystallinity of spin coated films of ADT the difluoro derivative was synthesized [64].

TES difluoro Anthradithiophene derivative pecks in a 2D fashion with smaller co-facial distance. Devices made by spin casting gave uniform, crystalline films with mobility as high as $5 \text{ cm}^2/\text{Vs}$, large current on/off ratios ($I_{\text{on}}/I_{\text{off}} = 1 \times 10^8$) [64].

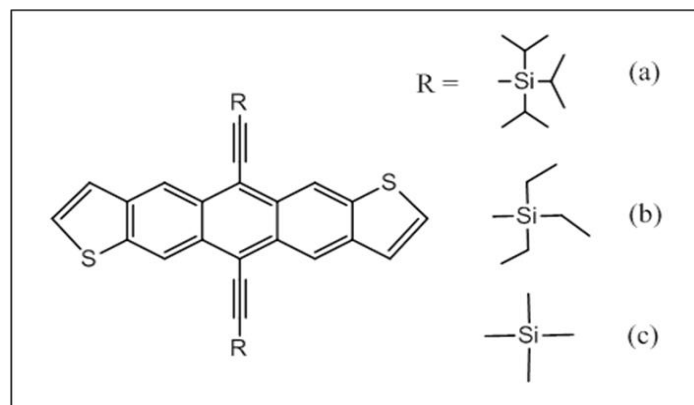


Figure 1.28: Chemical structure of Anthradithiophenes [52].

Anthradithiophene (ADT) based phenylethynyl or triethylsilylphenylethynyl substituents, given in figure 1.29, have been found to exhibit OTFT p-channel transport with hole mobilities as high as $\sim 0.01 \text{ cm}^2/\text{Vs}$ with the ADT-derivatives exhibiting improved photo-oxidative stability in aerated $\text{C}_6\text{H}_5\text{Cl}$ solutions (0.00005M) while exposing to white light (fluorescent lamp) at room temperature compared to the equivalent pentacene derivatives [65].

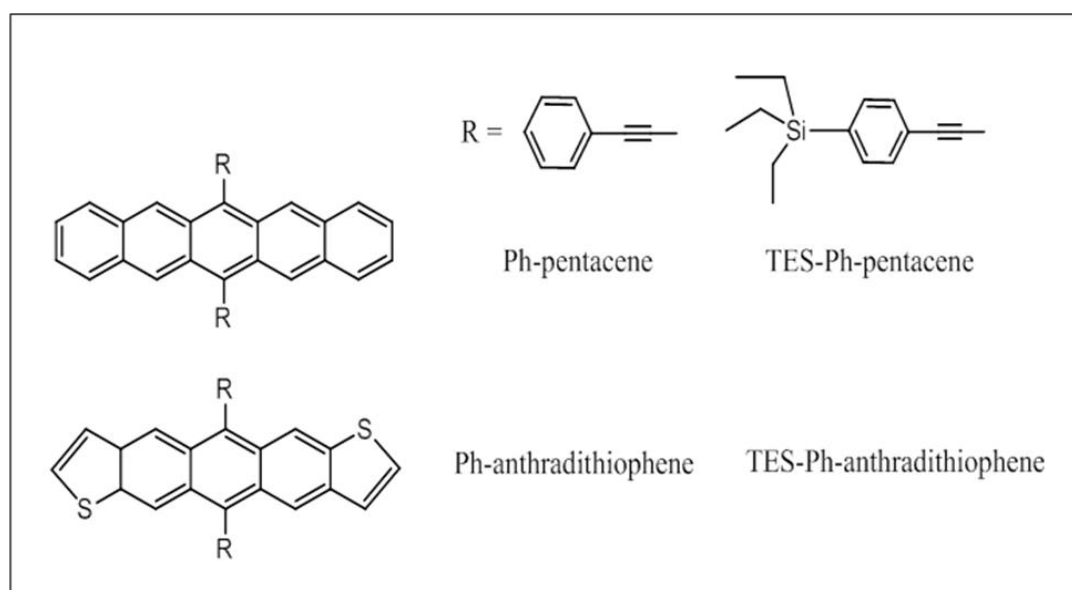


Figure 1.29: Chemical structures of soluble pentacene and anthradithiophene derivatives [65].

When producing bipolar transistors and complementary circuits with pentacene, the n-type organic semiconductor should have similar physical and electrical properties except for the type of carriers [66]. As fluorine is the most electronegative of all the elements and relatively small (hydrogen > fluorine > carbon), perfluorination is an effective way to convert a p-type organic semiconductor to an n-type one without changing the molecular size greatly, figure 1.30. Hence, perfluoropentacene has been designed as a potential n-type semiconductor for OFETs. When perfluoropentacene is deposited on the first layer of pentacene, the device works also well as a bipolar OFET.

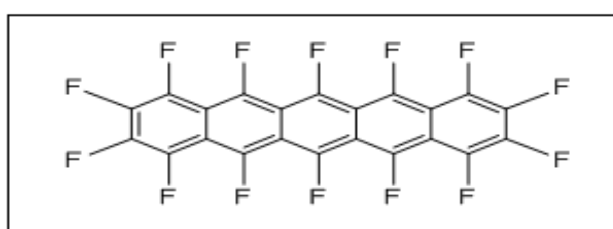


Figure 1.30: Chemical structure of perfluorination [66].

The silylethynylated N-heteroacenes as shown in figure 1.31, are stable and solution processable and can be p-type, n-type, or ambipolar depending on the structure of its π -backbone. Semiconductor properties of tetraazapentacene n-type organic semiconductors exhibited electron mobility of up to $3.3 \text{ cm}^2 \text{ Vs}^{-1}$, because its low LUMO energy level and close packing of molecules in a 2D brickwork arrangement [67]. The environmental stability of substituting N-heteropentacene in solution was studied in $0.05\text{mM CH}_2\text{Cl}_2$ when exposed to ambient light, and were shown to be more stable than TIPS-pentacene [68].

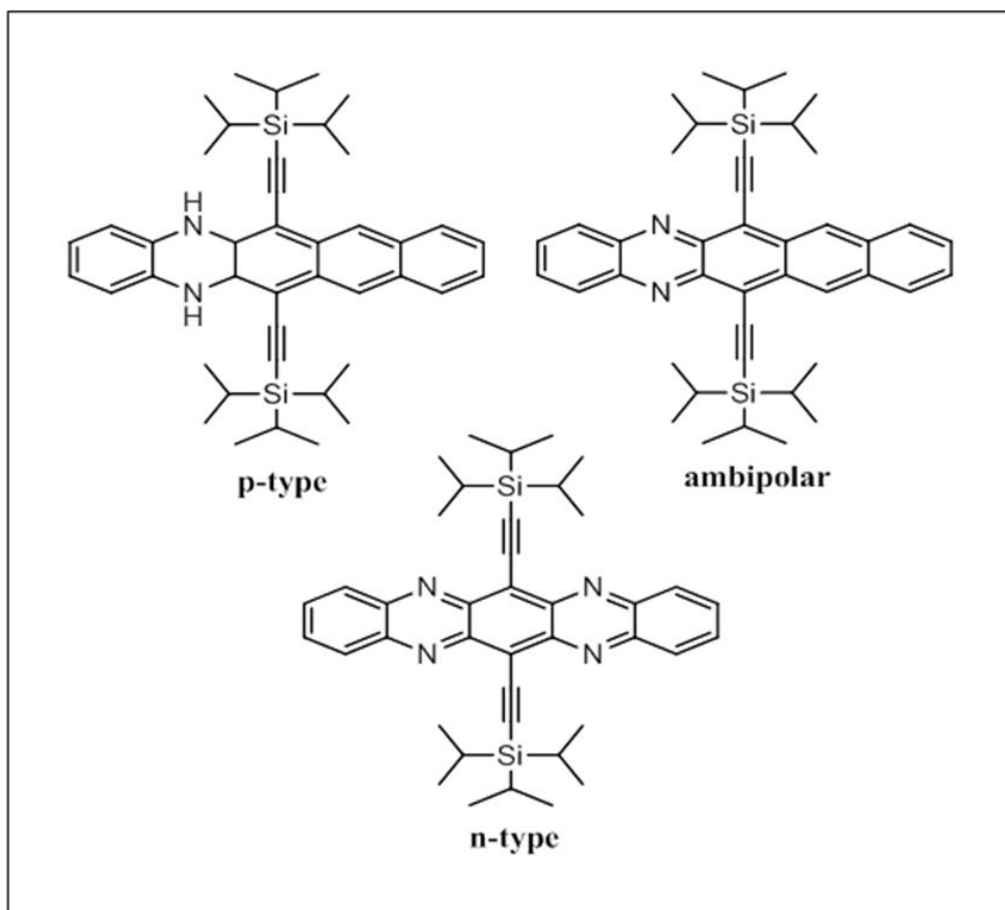


Figure 1.31: Chemical structures of silyethynylated N-heteropentacene [67].

More recently it has been shown that the photochemical stability of pentacene derivatives can be considerably improved using stable radical pentacene hybrids, pentacene-phenyl, oxo-verdazyl radical figure 1.32 (a) and pentacene-phenyl,-nitronyl nitroxide radical moieties figure 1.32 (b). The photochemical stability was reported by UV-vis absorption in THF and CH_2Cl_2 under ambient light in saturated air conditions. The lifetime of pentacene-phenyl-oxo-verdazyl and pentacene-phenyl,-nitronyl nitroxide is approximately 202 and 380 times longer than of their precursors respectively in THF. In addition, the photochemical instability of pentacene-phenyl,-nitronyl nitroxide was 500 times better than that of pentacene in THF solution and it is more stable in CH_2Cl_2 with the half-life being more than 2000 min. The photochemical instability in CH_2Cl_2 solution of pentacene could not be obtained because pentacene is not soluble in CH_2Cl_2 [69].

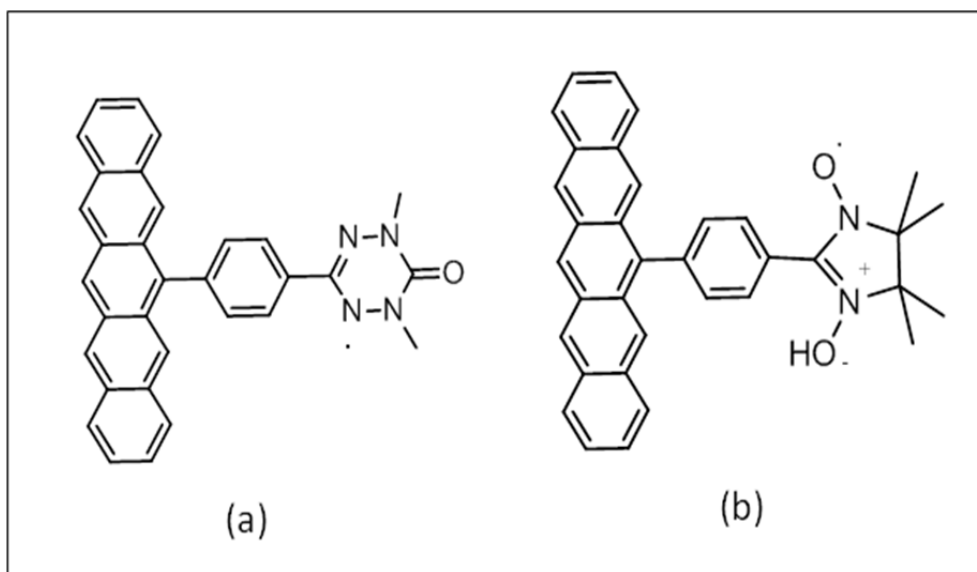


Figure 1.32: Chemical structures of stable radical pentacene hybrids, (a) pentacene-phenyl, oxo-verdazyl radical and (b) pentacene-phenyl,-nitronyl nitroxide radical moieties [69].

Functionalization strategies to improve the process ability of pentacene have also been applied to the synthesis of larger acenes such as hexacene [70]. However, the low solubility and stability requires the use of functional groups to stabilize and solubilize these materials if they are to be used in electronic devices [71]. Balaji and coworkers have reported the synthesis of new silylethyne substituted hexacene derivatives, figure 1.33. Their solubility and stability in both solution and the solid state were studied. These materials showed dimerization rather than oxidation for the decomposition pathways [72].

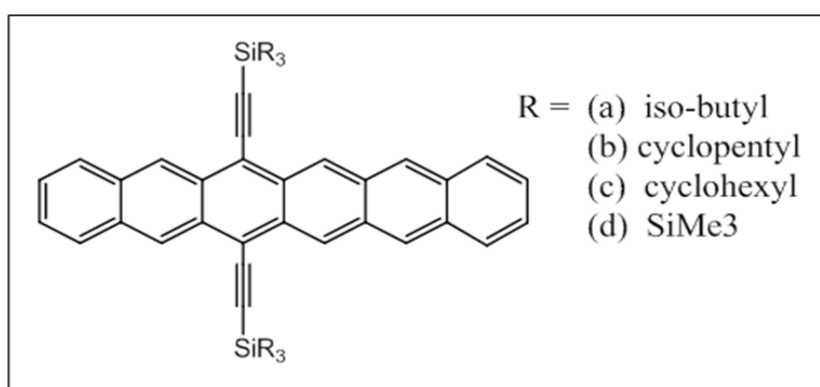


Figure 1.33: Chemical structures of silylethyne substituted hexacene derivatives [72].

Functionalized acenes larger than hexacene have proven elusive. Wudl and co-workers have reported the synthesis of a stable tetraphenyl heptacene derivative (figure 1.34) [73] using a tri-iso-propylsilyl ethynyl substituent. The phenyl groups are effective in preventing the aromatic cores from reacting with each other or with the alkyne, and as a result the smaller alkyne substituent could be used. Photooxidation of the aromatic core was reported to be the major decomposition process for this heptacene derivative, figure 1.34 [73]. A heptacene derivative with two triisopropylsilyl ethynyl (TIPS) groups at the 7 and 16 positions and four trifluoromethylphenyl groups at the 5, 9, 14 and 18 positions was synthesized by a new synthetic strategy [74]. The photostability of this compound was investigated in toluene under different irradiation conditions. The compound was reported as the most stable heptacene derivative. Its presence was still detectable by UV/Vis/NIR spectroscopy in degassed toluene after 47 hours of exposure to air and ambient light irradiation.

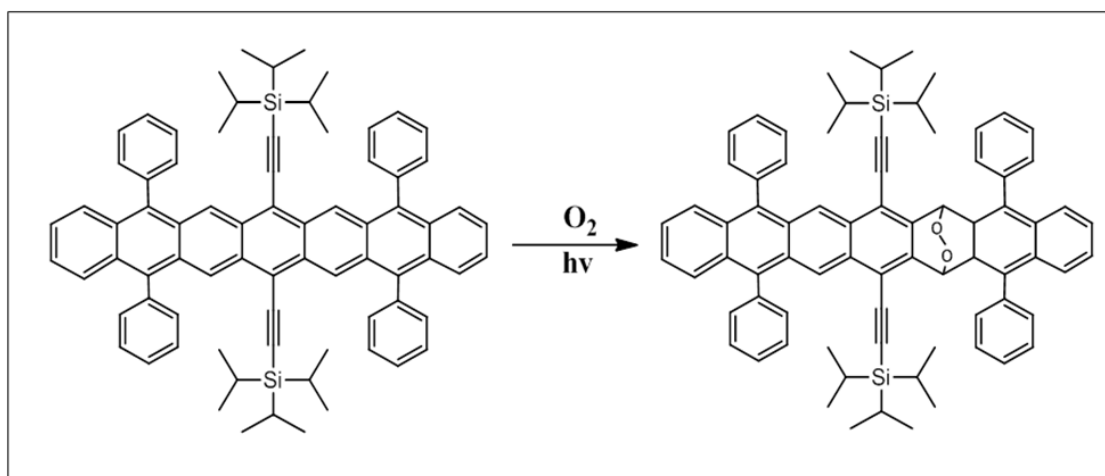


Figure 1.34: Schematic showing photooxidation of heptacene derivative [73].

1.3 Optical properties and electronic properties of acenes organic semiconductors

The electronic structure of acenes determines their optical properties. The electronic π - π^* transitions are responsible for the absorption of photons of a resonant frequency that matches the energy gap between the π and π^* states. Chemical engineering of the molecular structure allows the optoelectronic properties of acenes organic semiconductors to be fine-tuned. Normalized UV-visible absorption spectra for anthracene through heptacene are shown in figure 1.35. The spectra of anthracene to pentacene were recorded in toluene, whereas the spectra of hexacene and heptacene were recorded after they were generated photochemically in a polymer matrix. The wavelength of absorption maximum for the family of polyacenes from anthracene to heptacene (λ_{max}) are respectively 374, 472, 585, 665, and 760 nm. It can be seen that as the degree of conjugation increases (more benzene rings) the absorption and maxima show a systematic red shift (~ 100 nm), indicating a band gap.

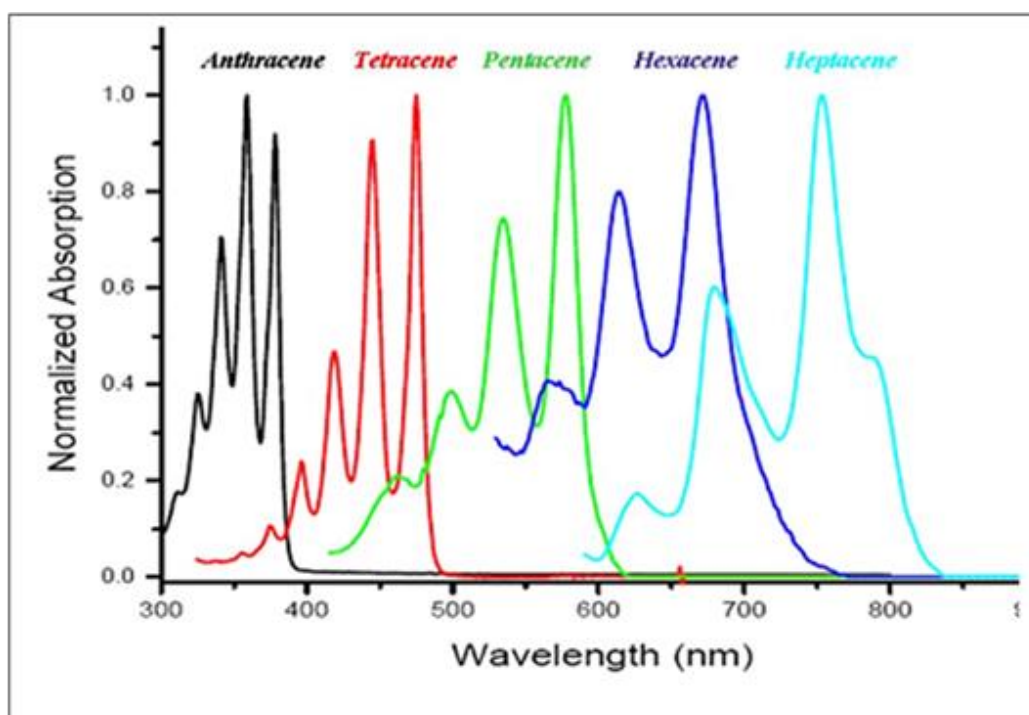


Figure 1.35: Normalized absorption spectra of polyacenes (spectra of anthracene to pentacene recorded in toluene, spectra of hexacene and heptacene recorded in a polymer matrix) [75].

Figure 1.36 shows how the energy gap changes with the conjugation length in the family of polyacenes. It is obvious that when the size of the acene increases, the HOMO level becomes higher and the band gap between HOMO and LUMO becomes narrower as shown in figure 1.36. Higher polyacenes have a higher lying HOMO level and smaller band gap which makes the movement of electrons from HOMO to LUMO easier, this also leads to a greater susceptibility to air oxidation and chemical reactions under ambient conditions [76].

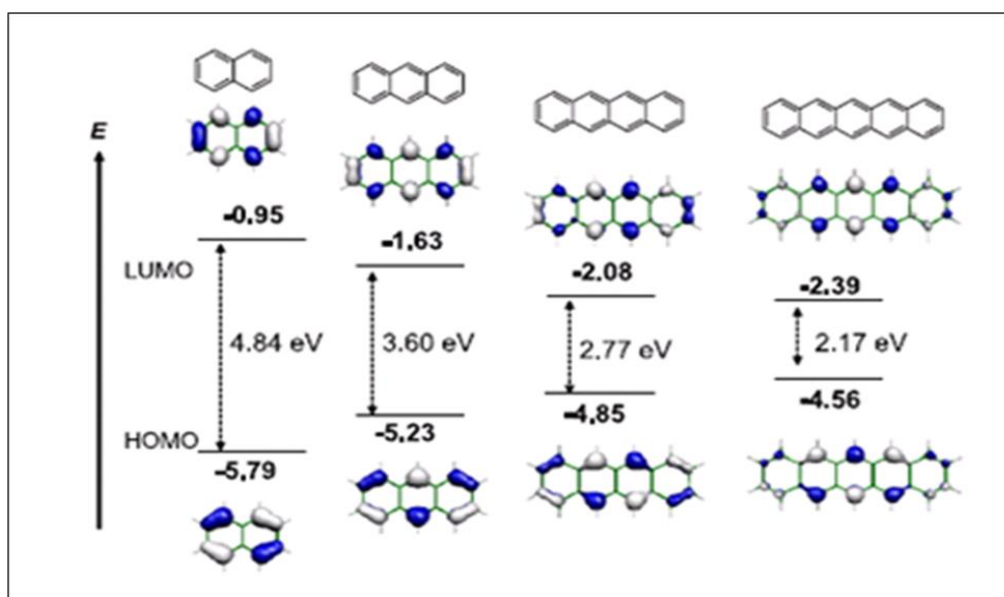


Figure 1.36: Calculated HOMO, LUMO and band gaps for acenes [76].

Precise control of the electronic properties and molecular ordering of tetracene is achieved by substitution with different functional groups. Functionalization of these tetracenes not only can increase the solubility and processibility of the potential devices, but also controls the general type of interaction occurring in the solid, such as herringbone arrangement vs. π -stacking (face-to-face) and allows tuning the oxidation potential for charge carriers (p-type vs. n-type behavior) [77, 78].

Additionally, the substituents increase the stability against oxidation of tetracenes derivatives and the derivatives react with $^1\text{O}_2$ to afford form endoperoxide in high yield [79] different endoperoxide products in solution and in crystals [80], and mixtures endoperoxide [81]. There have been a variety of 6,13-bis (triisopropylsilyl) acenes strategies to increase the stability of TIPS-oligoacenes.

TIPS- groups have been critical in stabilization large acenes, such as hexacene and heptacene. TIPS-heptacene is reported to be the most stable such derivatives [73, 74]. The absorption spectra of TIPS-oligoacenes characteristic acene fine structure are shown in figure 1.37, with the λ_{max} from anthracene to heptacene 438, 535, 635, 733, and 835 nm respectively, showing a red shift of approximately 60 nm relative to the parent hydrocarbons anthracene to hexacene [82, 83].

In addition, the effects of intermolecular interactions on the electronic properties of TIPS-anthracene, tetracene, and pentacene was studied and the measurements showed that the HOMO-LUMO energy gaps are strongly dependent on the acene core size [84-86].

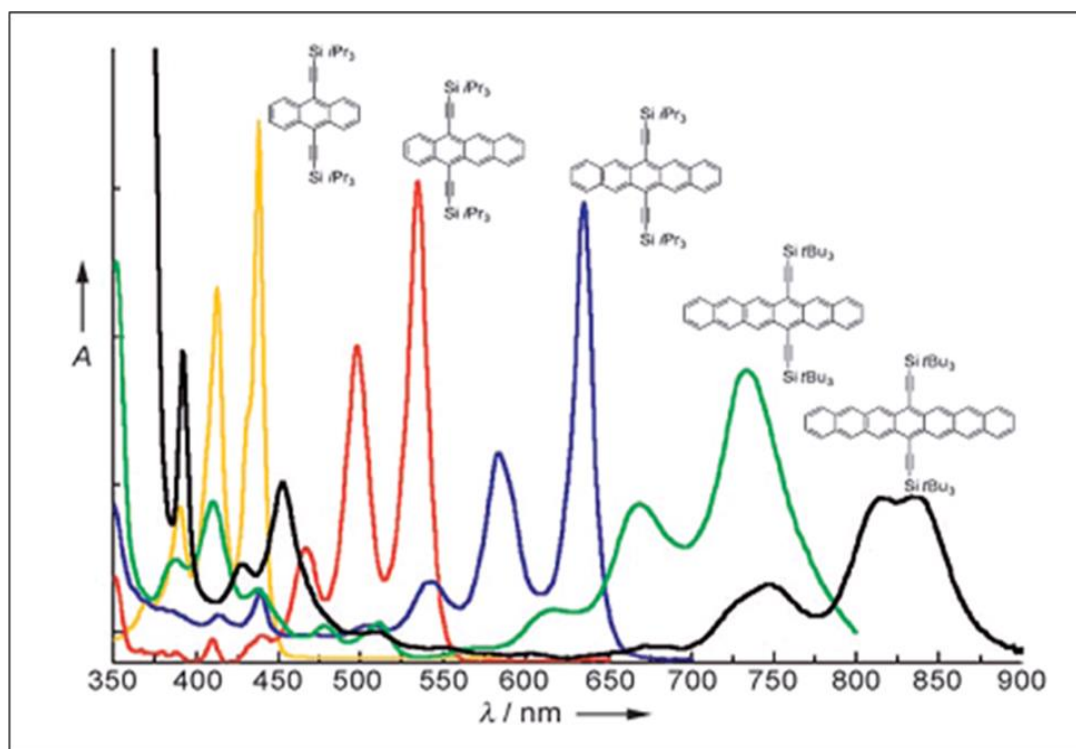


Figure 1.37: Absorption spectra of functionalized acenes [83].

1.4 Aggregation of π -conjugated systems in solution

Aggregates generated by self-assembly of functional π -systems have captured the attention from the traditional field toward novel technologies. Examples include organic photoconductors, organic semiconductors, and solar cells for the optimization of the optical or electronic properties of these devices, it is necessary to understand the aggregation process to optimize specific functions.

The aggregation of functional conjugated molecules in solution is a frequently encountered phenomenon in π -system chemistry owing to strong intermolecular van der Waals-like attractive forces between the molecules. The aggregation in solution can be divided into categories based on different electronic and spectroscopic properties: J-aggregates and H-aggregates as shown in figure 1.38. The formation of H and J aggregates has been explained by considering the electronic states of the aggregate molecules using exacton theory. The H-aggregate is a face-to-face arrangement in which the transition moments of individual molecules are aligned parallel to each other. J-aggregation occurs when molecules assume a head-to-tail arrangement. The optical difference of these two aggregates is: H-aggregate consists of a blue-shifted band in the absorption spectrum with respect to the unaggregated molecule absorption. However, the absorption spectra of the J-aggregate exhibit a narrow peak red-shifted with respect to unaggregated molecule absorption. The transition energy difference of aggregate and monomer is dependent on the electronic coupling. The splitting of the ground state S_0 is negligible, the excited state S_1 for aggregate is split into energy levels, E_1 and E_2 , the transition is not allowed from S_0 to E_1 (E_2) in H (J) aggregates. The energy difference between E_1 and E_2 depends on the orientation of the transition dipole moment of the molecules.

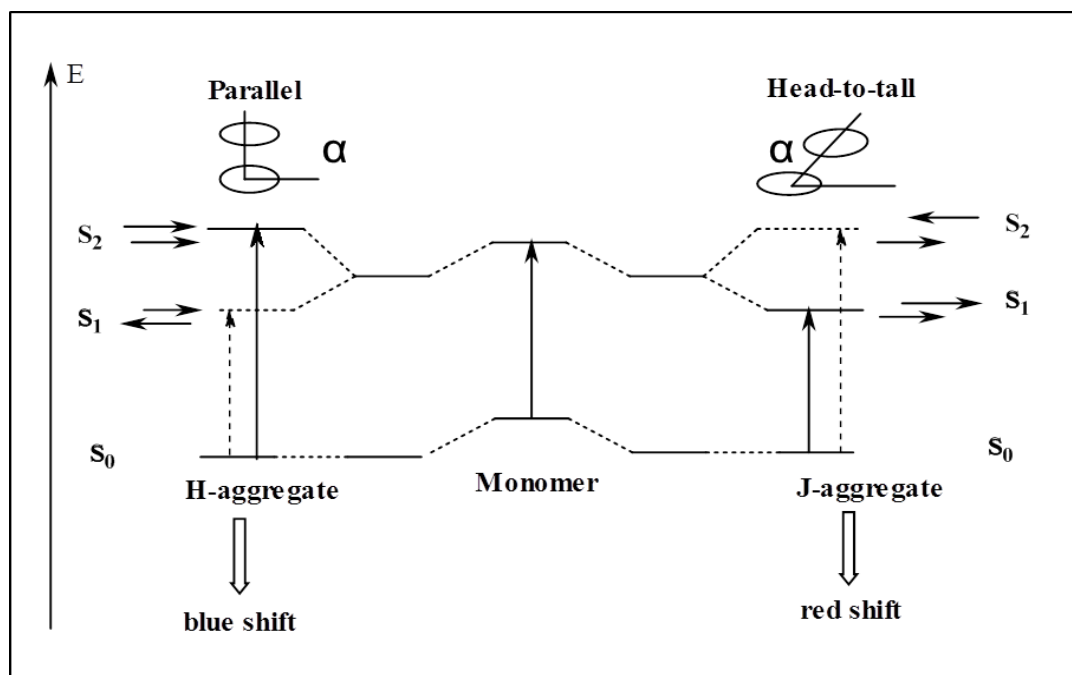


Figure 1.38: The schematic structures of H and J aggregate [87].

The present studies were previously reported for organic semiconductors which aggregate with various aggregation patterns by combination of H- and J-types aggregation. J-aggregation occurs when molecules assume with head-to-tail molecular stacking. In J-aggregation, couplings are negative, and the UV absorption peak of the film is red-shifted compared to the absorption peak in solution. The UV absorption peak for an H-aggregated film is blue-shifted compared to the absorption peak in solution because of cancellation of the transition dipole moments of the lower-lying state. H-aggregation can improve the performance of organic semiconductors in OFETs by large area π -stacking between adjacent molecules, which occur when molecules stack side by side [87-90].

1.5 Aims and Objectives

Whilst there have been many reports on the photooxidation of substituted acenes in solution and the effects of chemical structure, to date there has been no consideration of the role of formulation.

This project therefore has three main aims:

1. To study the stability of TIPS-pentacene in solution with respect to oxidative degradation by variation of solvent, concentration, solvent mixtures, blends, and light.
2. The extension of 1 to a range of 6, 13- substituted pentacene derivatives to confirm universality of results.
3. To develop models to interpret observations with respect to possible mechanisms and check using spectroscopic and calorimetric methods.

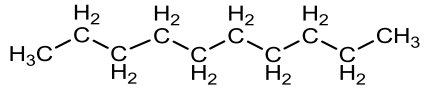
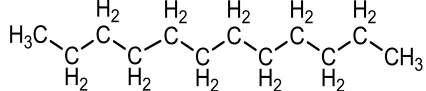
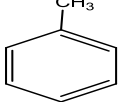
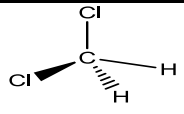
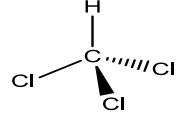
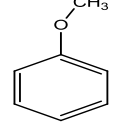
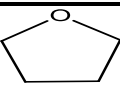
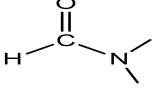
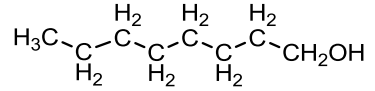
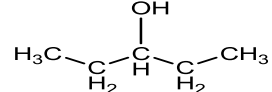
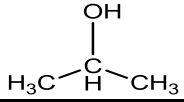
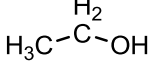
Chapter 2

2 Experimental

2.1 Materials Used

All solvents were obtained from Sigma-Aldrich UK and used without further purification unless otherwise noted. In table (2.1) are the chemical structures and physical properties of toluene, tetrahydrofuran (THF), chloroform, anisole, dichloromethane (DCM), dimethylformamide (DMF), 1-octanol, 3-pentanol, isopropanol (IPA) and ethanol which were used as solvent for the samples used here. TIPS-pentacene samples were provided by Dr John Morrison, synthesised using the Swager modification of Anthony's synthesis [50]. TMTES-pentacene was synthesized by Dr Gonzalo Rincon according to the procedure reported in [91]. The family of mono- and di- fluorinated TIPS-pentacenes were synthesized by Dr Jaroslaw Wasikiewicz. Purified pentacene derivatives (figure 2.1) were characterized by a combination of ^1H and ^{13}C NMR spectroscopies, UV-visible spectroscopy, high-resolution mass spectrometry (HR-MS) and cyclic voltammetry (CV) in by those who supplied the materials. Amorphous polystyrene (PS, $M_n = 350$ kDa), semicrystalline isotactic polystyrene (iPS, $M_n = 400$ kDa) and poly(methyl methacrylate) isotactic (iPMMA), all obtained from Sigma-Aldrich UK except poly (trialryl amine) (PTAA) which was obtained from Merck; all these were used as received (figure 2.2).

Table 2.1: Chemical structure and physical properties of the solvents used in this study.

Solvents	Chemical structure	Molecular Formula	BP (°C)
Decane		$C_{10}H_{22}$	174
Dodecane		$C_{12}H_{26}$	215
Toluene		$C_6H_5CH_3$	110.63
DCM		CH_2Cl_2	40
Chloroform		$CHCl_3$	61.17
Anisole		$C_6H_5CH_3O$	154
THF		C_4H_8O	66
DMF		C_3H_7NO	152
1-Octanol		$C_7H_{15}CH_2OH$	195
3-pentanol		$CH_3CH_2CHOHCH_2CH_3$	115.3
IPA		$CH_3CH(CH_3)OH$	82
Ethanol		C_2H_5OH	78

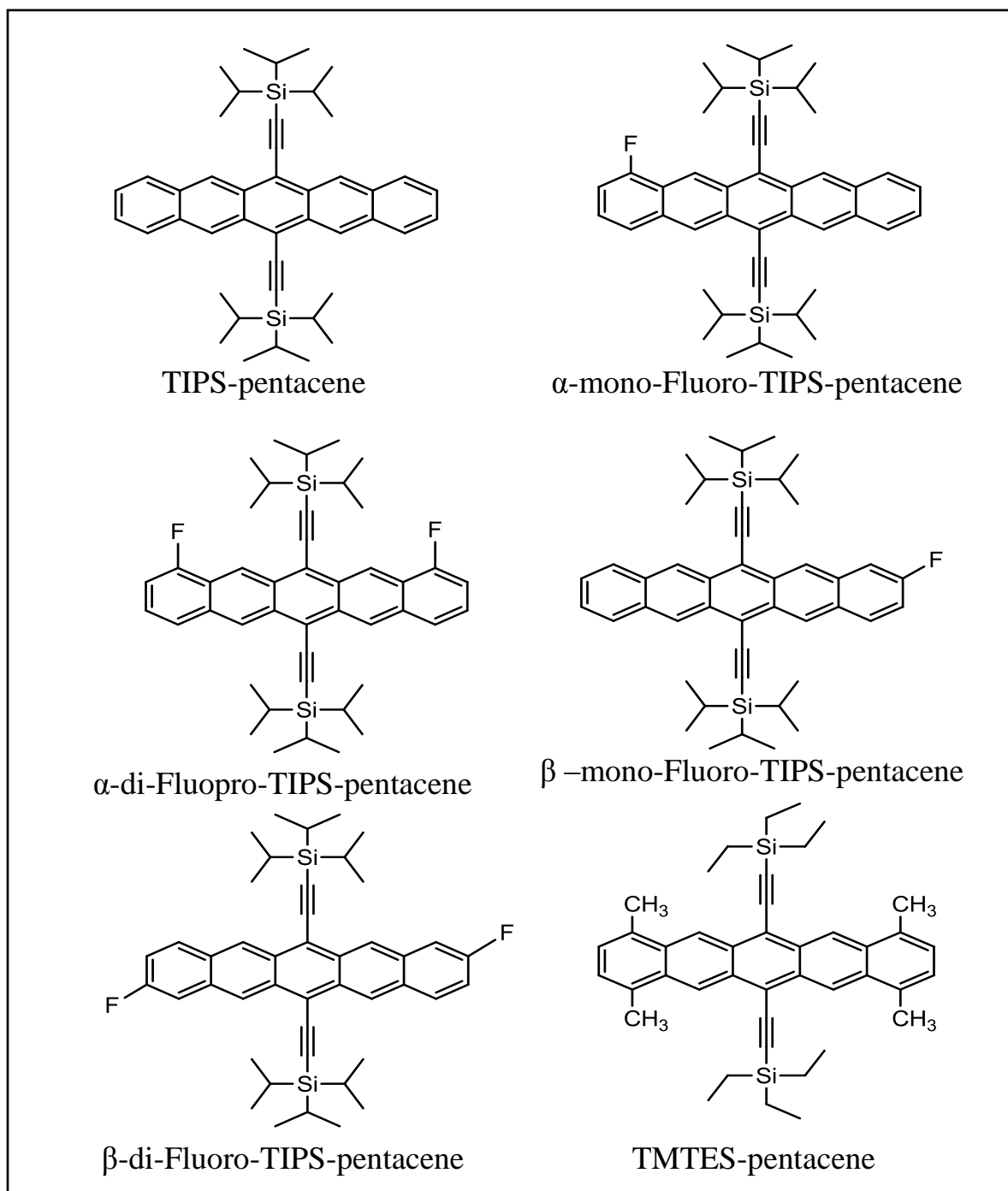


Figure 2.1: Molecular structures of substituted 6, 13- pentacenes derivatives.

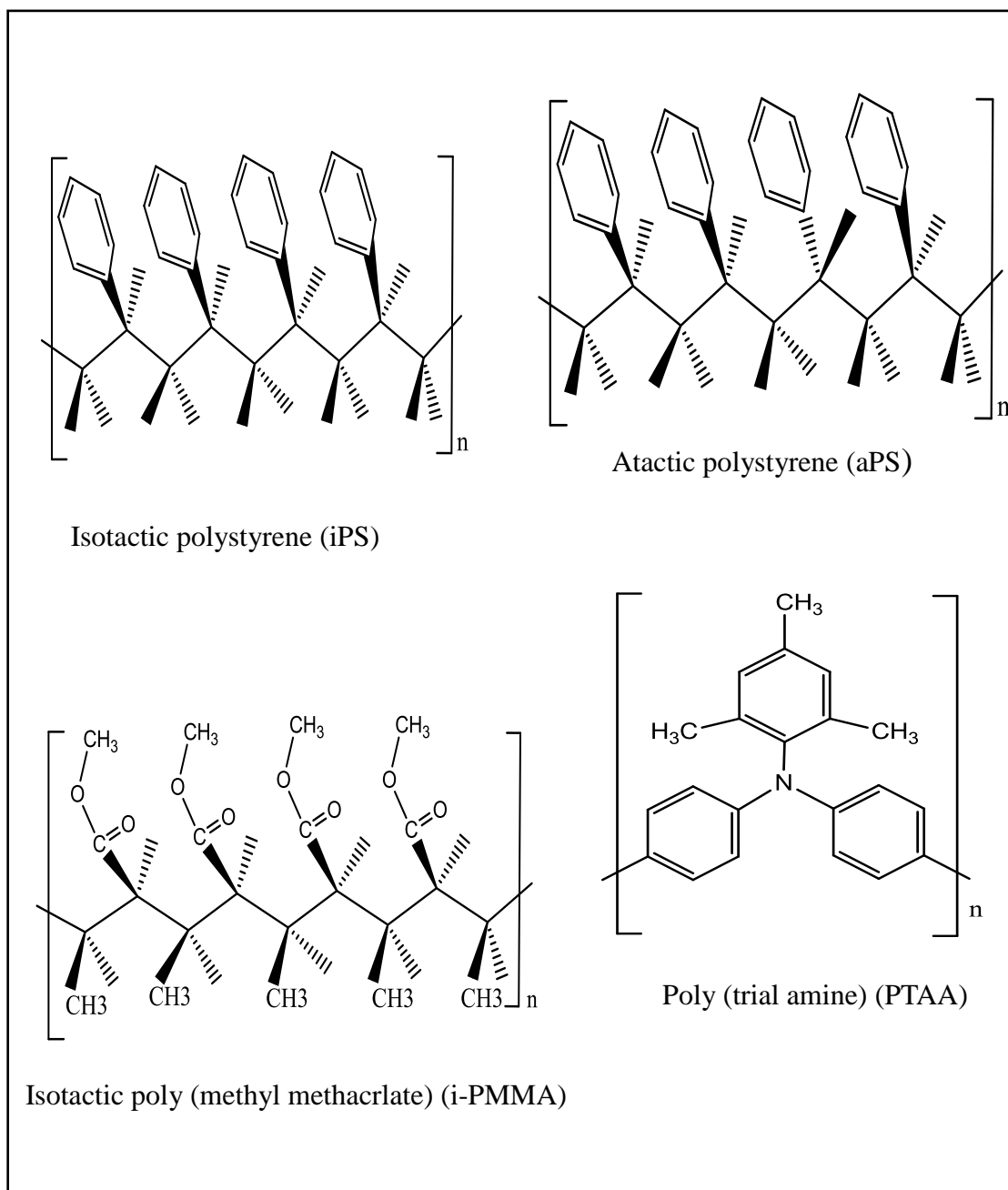


Figure 2.2: Molecular structures of polymers used in this study.

2.2 Ultraviolet and visible (UV-vis) spectroscopy

2.2.1 Absorption process

Ultraviolet (UV) and visible (vis) spectroscopy is a common method of molecular spectroscopy. The technique is based on the interaction of molecules with UV and visible light. The basic setup for measuring the absorption or transmission of light through a sample is shown in Figure 2.3. The molar absorption coefficient (ϵ) of a substance is a measure of how strongly it absorbs light of a given wavelength and is usually measured in $M^{-1} \text{ cm}^{-1}$. The absorbance (A) of an UV band is calculated according to the Beer-Bouguer-Lambert Law:

$$T = I/I_0 \quad 2.1$$

$$I = I_0 10^{-\epsilon c l} \quad 2.2$$

$$A = \text{Log } I_0/I = \epsilon \cdot c \cdot l \quad 2.3$$

where T is the transmittance, I_0 is the intensity of incident light at a given wavelength, I is the intensity of transmitted light; l is the path length through the sample in cm, c is the concentration of the absorbing species in mol^{-1} .

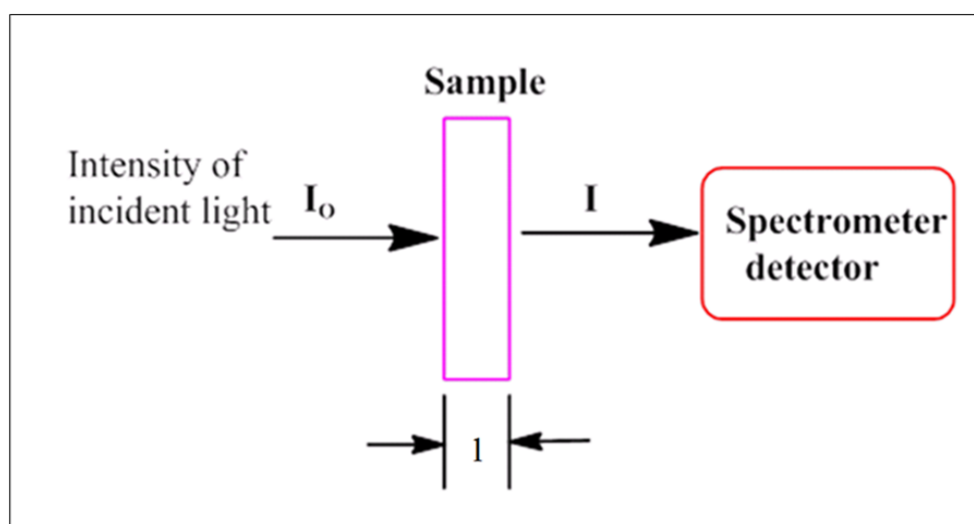


Figure 2.3: Light of intensity I_0 incident upon a sample of thickness t undergoes a loss in intensity upon passing through the sample. The intensity measured after passing through the sample is (I) [92].

Absorption of photons results in an electronic transition of a molecule where electrons are promoted from the ground state to higher electronic states (figure 2.4), usually from the highest occupied molecular orbital (HOMO) to the lowest unoccupied molecular orbital (LUMO). Electronic transitions usually originate from valence electrons in a chromophore, such as the nonbonding (n) or π -electrons in unsaturated functions. The ground state has lower energy (lower band E_i), while the excited state has higher energy (upper band E_f) [92]. The electromagnetic radiation may be described by the wavelength λ (nm), by the frequency ν (s^{-1}), or by the wave number, $\bar{\nu}$ (cm^{-1}), related by energy difference (ΔE), band gap, as following relationships:

$$\lambda\nu = c \quad 2.4$$

$$\bar{\nu} = 1/\lambda \quad 2.5$$

$$\Delta E = h\nu = hc/\lambda \quad 2.6$$

Where h is the universal Planks' constant (6.624×10^{-27} erg sec.), c is velocity of light 2.998×10^{10} cm s^{-1} .

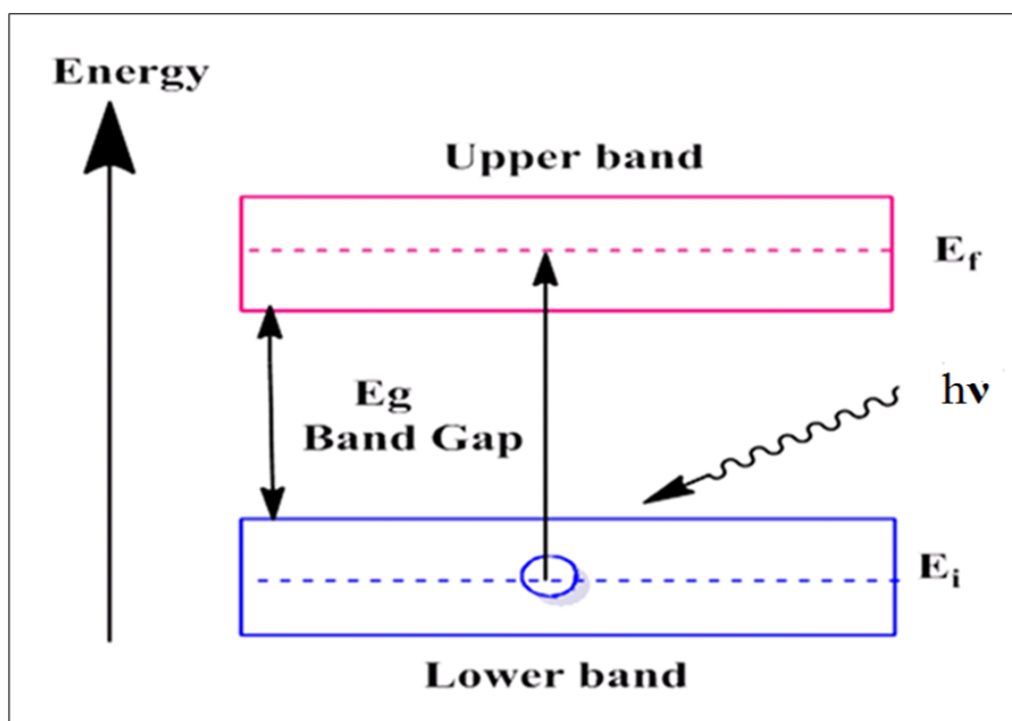


Figure 2.4: Interband optical absorption between an initial state of energy E_i in an occupied lower band and a final state at an energy E_f in an empty upper band. The energy difference between the two bands is the band gap (ΔE)[92].

The electronically excited states may decay unimolecularly back to the ground state by fluorescence (from an excited singlet state) or cross into a different spin system by intersystem crossing (e.g. to a triplet state). Radiative emission from a state of different multiplicity to the ground state is phosphorescence. There are also other non-radiative processes which can occur, particularly vibrational relaxation and quenching. Thus, one can measure the absorption and emission from molecules. The λ_{max} of an absorption band correspond to the excitation energy, ΔE and ϵ_{max} to the intensity of transition, a measure of the probability of promoting an electron, given the excitation energy. For compounds containing double, triple bonds, or aromatic rings; a π electron is excited to an antibonding π^* orbital.

In this project, the UV-visible spectra were obtained on Varian Eclipse 5000 spectrophotometer in the range 200-800 nm using quartz cuvettes with a path-length of 1mm and 10 mm.

2.2.2 Solution preparation

Solvents were equilibrated to air by loosening the cap to allow for free exchange of air, whilst minimizing solvent evaporation for 24 hours before solution preparation. Solutions were then prepared and left over night for complete dissolution in a light shielded vial.

2.2.3 Photostability study in solution

Separate solutions of substituted pentacenes were dissolved in different solvents over a range of concentration and formulations then placed in spectrophotometer cells. The cells were protected from light until each experiment began, at which point an initial spectrum was recorded to define A_0 . Samples in air-saturated solvent were placed on a laboratory bench top and they were then exposed to ambient light irradiation and 60 W, SP35 fluorescent lighting (General Electric, 2850 lm) at room temperature at 30 cm distance for appropriate periods. The UV-visible spectra were recorded without further dilution. For solutions at higher concentration, samples were degraded under the same conditions and further diluted to 1×10^{-5} M immediately prior to the recording of spectra. The decrease in intensity of the long wavelength absorption peak as a function of time was used to monitor the degradation of each compound as a function of time.

In order to compare the data, the half-life of each sample was determined by plots of normalized A_t/A_0 at the long wavelength versus time. From this data, the half-life is obtained for each concentration from the time taken for A_t/A_0 to fall to 0.5. These absorbance-time profiles were found to be reproducible to $\pm 5\%$, with all formulations showing retardation in rate beyond $t_{1/2}$.

2.3 Fluorescence spectroscopy

2.3.1 Emission process

Fluorescence spectroscopy is a very simple but extremely powerful technique to investigate various photochemical processes that occur in the excited state of the molecules. Fluorescence spectroscopy measures the emission of radiation of the molecules from their electronic excited states to the ground state. Any electronically excited molecule comes back to its ground state either by radiative mechanism or non-radiative mechanism. The chromophores following the radiative mechanism emit photons and the process is called fluorescence. The fluorescence photons have information about energy (wavelength), polarization and intensity (number of photons) at a given wavelength. The mechanisms by which electronic excitation of a molecule or a system of molecules and the transitions involved between them are described using a Jablonski diagram as shown in figure 2.5. In this diagram, there are two types of electronic transitions involved, (radiative and non-radiative). The radiative transitions consist of absorption, fluorescence, and phosphorescence and are indicated by straight arrows. The non-radiative transitions are internal conversion (IC), intersystem crossing (ISC), and vibrational relaxation and are indicated by wavy arrows in the diagram. The absorption of a photo takes the molecule from ground state (S_0) to either first excited state (S_1) or second excited state (S_2) (excited from a lower to higher electronic state) and is spin allowed and mostly appears in the absorption spectra. The transitions from S_0 to T_1 or from S_0 to T_n are spin forbidden, but can be observed spectrometrically by using long light paths or intense light sources. The opposite of absorption is luminescence (emission), and can be defined as the radiative de-excitation transition in which the molecule is de-excited from the higher electronic state to lower electronic state by the emission of photon.

Luminescent processes are of two types: the transition from singlet state S_1 to ground state S_0 is fluorescence and it occurs with the same multiplicity. The transition from triplet T_1 to ground singlet state is phosphorescence and it is different multiplicity. Phosphorescence is a spin-forbidden process, and generally is shifted to longer wavelengths relative to the fluorescence. Non-radiative transitions come through several different mechanisms. The vibration relaxation is the relaxation of the excited state to its lowest vibrational level. A second type is internal conversion (IC), which occurs when a vibrational state of an electronically excited state can couple to a vibrational state of a lower electronic state. A third type is the intersystem crossing (ISC), which is a transition to a state with a different spin multiplicity such as from S_1 to T_1 and is responsible for efficient phosphorescence.

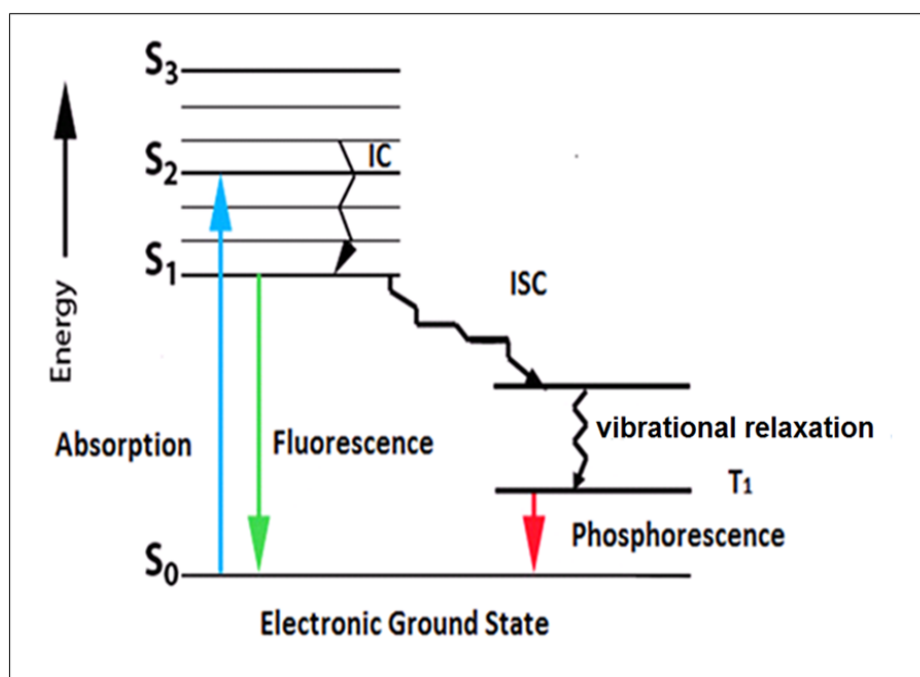


Figure 2.5: Jablonski diagram.

In the present study steady-state fluorescence measurements (fluorescence intensity, excitation spectra or emission spectra) were recorded on a Varian Eclipse fluorescence spectrometer. The sample is excited in a quartz cuvette (either 1mm or 10 mm): the emission wavelength range used here was 600 to 800 nm. A stock solution 1×10^{-3} M TIPS-pentacene in different solvent was prepared and 9 samples of the following concentrations: 5×10^{-4} M, 3×10^{-4} M, 2×10^{-4} M, 1×10^{-4} M, 5×10^{-5} M, 3×10^{-5} M, 2×10^{-5} M, 1×10^{-5} M and 2.5×10^{-6} M were prepared by dilution.

Fluorescence spectroscopy was measured for all of them. The fluorescence parameters are detailed in table 2.2.

Table 2.2: Fluorescence set up parameters.

Excitation	Start	Stop	Excitation slit	Emission slit
550	600	800	2.5	5
643	600	800	2.5	5

2.4 Nuclear magnetic resonance NMR

The ^1H NMR spectra of the organic compounds were recorded using a Varian Inova 300 (300MHz) or (500MHz) spectrometer with 16 transients, and a relaxation time of ten seconds as standard. The solvents used were deuterated chloroform, DCM and toluene.

2.5 Atmospheric pressure chemical ionization (APCI) mass spectrometry

The APCI spectra were recorded on a Fison VG Trio 2000 spectrometer in the Analytical Services unit of the School of Chemistry. Samples are submitted to the service as dilute solutions in sealed ampules. A range of ionisation methods are available and spectra can be requested in positive or negative ion mode (or both).

2.6 Isothermal titration calorimetry (ITC)

ITC is based on the measurement of the heat that is absorbed or generated in an interaction between two molecules. The ITC technique has been used to determine the critical micelle concentration (CMC), stability constants (K_a), interaction enthalpies (ΔH), entropies (ΔS), Gibbs free energies (ΔG) and heat capacity changes (C_p).

A schematic diagram of an ITC instrument is shown in figure 2.6 (A). The difference in temperature between the two cells (sample and reference cell) is maintained by a feedback control system. The ITC systems use a cell feedback network to differentially measure and compensate for heat produced or absorbed between them.

The solution is added to the sample cell in a stepwise fashion with automated stirring to achieve fast mixing. The reference cell acts only as temperature reference. As chemical reaction occurs in the sample cell, heat is generated or absorbed. This temperature difference is kept at a constant value by the addition or removal of heat to the sample cell, as appropriate, using the cell feedback system (CFS), this is called the baseline. Before the titration starts, the feedback system applies a small power to the sample cell which determines the baseline level according to the preset reference power.

For a system where reaction occurs, every single injection triggers further reaction (for example, the binding of a solute to a solvent with the formation of a complex). The process (reaction) either releases heat (exothermic reaction) or absorbs heat (endothermic reaction) that causes a small temperature difference between two cells. Depending on the nature of the process (endo- or exothermic), the feedback system either increases or decreases the thermal power applied to compensate the temperature difference. An example of a binding isotherm (endothermic binding) for a solute to a substrate is shown in figure 2.6 (B). The top panel shows the experimental determination of enthalpy for the binding event with a sequence of peaks and each peak represents each injection of the solution in the syringe. The area under each peak, integrated and normalized per mole of solute injected for each injection point, is plotted against the molar ratio as shown in the bottom panel in figure 2.6 (B). The heat obtained from each injection is proportional to the molar enthalpy according to:

$$\Delta G = -RT \ln K_a = \Delta H - T \Delta S \quad 2.7$$

where ΔG is the free energy of the binding, R is the gas constant and T is the absolute temperature, K_a is the single site binding constant, ΔH is enthalpy of binding and ΔS is the entropy of binding. The inflection point of the curve indicates the stoichiometry (n) of the binding event. And the binding constant (K_a) from the slope in the inflection point and the enthalpy ($-\Delta H$) from the extrapolated step height [93, 94].

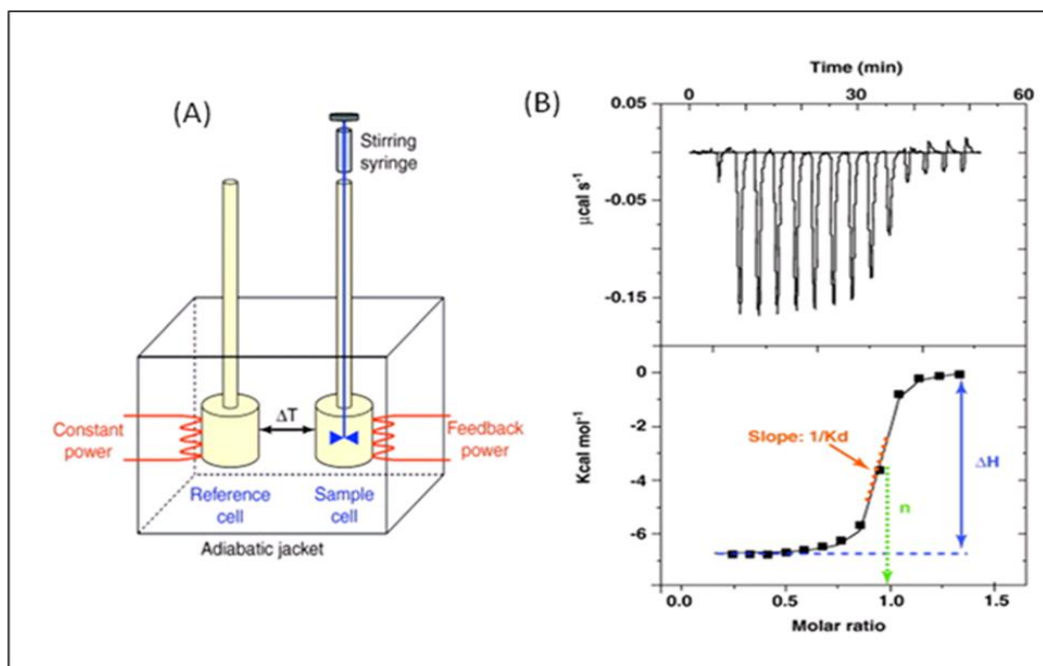


Figure 2.6: Schematic diagram of (A) the Isothermal Titration Calorimetry instrument, and (B) the example of binding profile [94].

ITC experiments of TIPS-pentacene in toluene solutions (0.00001M, 0.0005M and 0.002M) were conducted with a Microcal, ITC200, cell size 200 μl , and maximum volume of syringe 38 μl syringe end modified into a stirrer. Measurements taken at 25 $^{\circ}\text{C}$, stirring at 1000 rpm within the cell, a 120 s delay between injections and an initial injection of 0.5 μl +37 \times 1 μl injections. A small amount of titrate is added multiple times into the sample cell. The end of the pipette is modified so that stirring can take place within the cell (max 1000 rpm). The temperature difference between the cell and the reference cell is kept constant during the experiment using a cell feedback system (CFS). The constant temperature difference between the cell and reference is called the baseline. When binding occurs within the sample cell, a small change in temperature is detected and the appropriate amount of heat is added or removed so that the sample cell returns to the previously established baseline temperature. The integral of the power required to re-establish baseline is proportional to the resulting heat given off due the binding event. The resultant data is plotted using software such as Oracle to give the reaction or binding profile (depending upon the nature of the system under study).

2.7 Small-Angle X-ray scattering (SAXS)

Small-angle X-ray scattering is a very efficient technique to study the formation of particles in solution. Its application is thus particularly useful in studying systems where large conformational change take place, such as in aggregation. Scattering experiments involve emitting well-collimated radiation of wavelength λ through a sample and measuring the variations of the small scattered intensity as a function of the scattering angle θ as shown in figure 2.7. The scattering vector, q , is the parameter that characterizes the scattering geometry and is described by:

$$q = (4\pi/\lambda) \sin \theta/2 \quad 2.8$$

where (λ) is the wavelength in the sample. The magnitude of q (\AA^{-1}) is related to the scattering angle θ , which is the angle between the incident beam and detector.

The SAXS intensity, $I(q)$, at a scattering angle of 2θ as function of the scattering vector (q) is given by

$$I(q) = k N_p P(q) S(q) \quad 2.9$$

where k is a normalization factor that depends on the particle number density, N_p is the scattering number density (number of the molecules per unit volume in the solution), $P(q)$ is the particle form factor, and $S(q)$ is the structure factor, which contains information about the molecules interactions in solution [95-97].

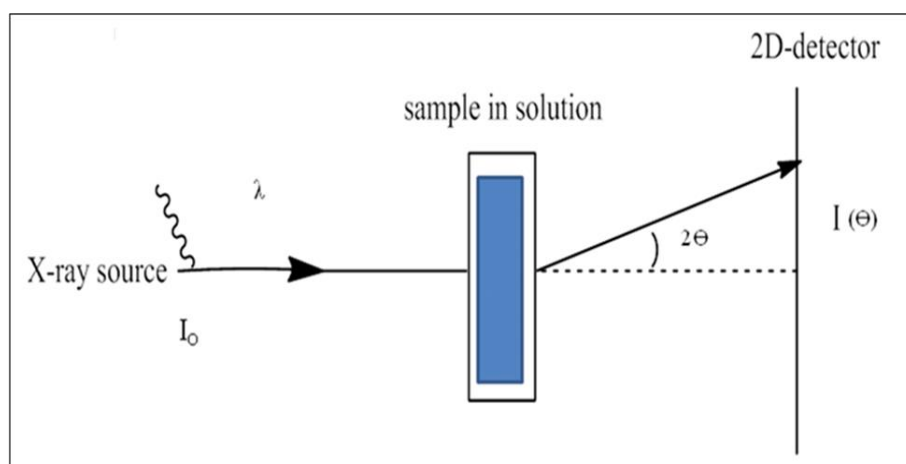


Figure 2.7: Schematic diagram of general scattering experiment measuring the variation in intensity as a function of Θ (scattering angle).

Experiments for TIPS-pentacene solutions were performed using the School of Chemistry's HECUS X-ray systems GMBH GRAZ, S3-Micro and Xenocs Cu K-alpha Microfocus X-Ray Source. The wavelength was 1.5418 Å and the sample-detector distance was 275 mm. The data were collected using a Pilatus 100 K detector. The wave number scale ($q = 4\pi\sin\theta/\lambda$) scattering angle = 2θ , wavelength $\lambda = 1.5418 \text{ \AA}$) was calibrated with silver behenate.

Experiments were performed at 30 °C for 10000 s. Samples solutions were measured in a borosilicate glass capillary 1mm cross section. Temperature control was via controlled sample heater with counter cooling from a water chiller. Scattering curves were monitored over a q -range from 6 to 0.005 Å⁻¹, and the 2D images were converted to 1D using Wavemetrics IGORPro 6.1 and Nika 2D to 1D reductions routines written by the Argonne National Laboratory.

2.8 Thermal stability

2.8.1 Thin film formation

Three different methods were used for TIPS-pentacene and β -DFTIPS-pentacene deposition. In the first method, films were prepared by spin coating at 800 rpm for 30s from 0.3, 0.5 and 1 % w/v toluene solution. In the second method, a small volume of 1 % w/v toluene solution was cast onto glass substrate at room temperature and the solvent slowly evaporated. In the third method 1 % w/v toluene solution of TIPS-pentacene and β -DFTIPS-pentacene were both draw down using number 2 wire bars onto glass substrate at room temperature and the solvent slowly evaporated in the dark. Films were exposed to light and air in the laboratory for two weeks or exposed under UV in ambient air using UV belt for 20 pass as appropriate.

2.8.2 Thermal gravimetric analysis (TGA)

Thermogravimetric analysis (TGA) is a thermal analysis technique (thermal stability of the material) which measures the weight change in a material as a function of temperature and time. TGA analyses were performed on a TGA Q5000 instrument at 10 °C/min under a nitrogen atmosphere.

2.8.3 Differential scanning calorimetry (DSC)

DSC is used to study the thermal transitions of organic semiconductors or polymers such as decomposition, glass transition temperature and their purity. The DSC measures the energy necessary to maintain both pans at an identical temperature. Therefore, the amount of heat absorbed by the sample as it is cooled or heated at a particular rate is measured. Data are recorded as the heat change expressed as heat flow as a function of the temperature. The sample was ground into fine powder and its weight was 6.05 mg, and measurement was performed at a heating and cooling from 50 to 300 °C, at scan rates of 10 °C/min under nitrogen atmosphere.

Chapter 3

3 Solvent-dependent photochemical instability of TIPS-pentacene at low concentration 1×10^{-5} M at 26 °C

3.1 Photooxidative stability of TIPS-pentacene

Although much less reactive than its parent acene, TIPS-pentacene is known to photodegrade in solution via a process involving dissolved oxygen [98]. It is generally accepted that the predominant mechanism for photo-degradation of TIPS-pentacene involves activation of oxygen molecules by the initially-formed excited state; this either generates singlet O_2 species or a superoxide O_2^- species which then adds back across appropriate carbon centres in TIPS-pentacene to produce an endoperoxide (EPO) [98]. This mechanism is supported by the observation of the oxygen adduct as the main product in the mass spectra. Recent studies using chemically generated singlet O_2 [99, 100] have further demonstrated that the superoxide route is the most favoured of the two for TIPS-pentacene, contributing around 90% to the overall rate of EPO formation [98]. Electron transfer rates from excited-state pentacenes are also observed to be fast and solvent-dependent [58]. Deactivations of the initial singlet state by mechanisms which can compete with O_2 activation therefore serve to increase photo-stability. The main non-radiative mechanism for this is singlet fission [101] via interaction with a second TIPS-pentacene molecule to produce a pair of triplets. This has been studied extensively in thin films of pentacene and its derivatives but is less-well characterized in solution [12, 13, 102, 103]. Studies of the photochemistry of pentacene monomers and dimers in host crystals indicate that the singlet lifetime is much shorter in dimers than monomers confirming the importance of pair-wise interactions [104]. Luminescence lifetimes are also strongly environment-dependent, from around 7 ns in dilute solution [105] to sub-ps in thin films. Physical quenching must also be considered as a deactivation route in any condensed medium. Stability in solution is therefore controlled by the rates and quantum yields of these processes, many of which are not known. Recent reports of half-life increase by the attachment of stable radical species to pentacenes is further evidence of the importance of the initial singlet state lifetime [69].

3.2 Effect the solvent on the photooxidative degradation of TIPS-pentacene

Although solvent-processing of organic electronic materials provides an effective route to device fabrication, there are issues of photochemical instability in solution for many species. TIPS-pentacene shows high solubility in common organic solvents. It has been demonstrated that solvents having higher boiling point resulted in a higher degree of orientation with a higher electrical properties stability of TIPS-pentacene devices OTFTs. More importantly TIPS-pentacene film morphology has been found to improve with higher boiling point solvent such as chlorobenzene, anisole and dodecane leading to improvements in the hole mobility and on/off ratio [106-109]. Aromatic solvents such as tetralin and dichlorobenzene are found to solvate the π -electron conjugated segments of conjugated molecules and polymers resulting in better π -stacking and thus better electrical properties [110]. Tetralin has been successfully used for drop casting and furthermore it is an aromatic solvent with the highest reported boiling point [111].

3.3 Literature reports on the photooxidative degradation of TIPS-pentacene in different solvents at low concentration

Table 3.1 gives an overview of the photo-stability in air saturated solution of TIPS-pentacene in different solvents, concentration, and irradiation conditions as reported in the literature [39, 56, 59, 68, 72] . To date there has been no systematic method used for the collection of data across different groups and consequently it is difficult to compare quantitatively the different bodies of work. Furthermore, most individual studies report on the effect of solvent at constant concentration, making comparison therefore difficult (especially when it is considered that there may be concentration-dependent aggregation occurring in some of these solvents). Also, most measurements are reported in air-saturated solvent but it has been shown by Coppo et al that, in the absence of oxygen, the major photoproduct was the Diels- Alder dimer adduct [54].

Table 3.1: Review of literature of photo- oxidation stability of TIPS-pentacene.

Low-energy λ_{\max} (nm)	Solvent	Concentration	Condition	$t_{1/2}$ (min)	Ref.
643	THF	no concentration given	(Rayonet UV light)	500	[39]
643	toluene	no concentration given	Wight light (fluorescent lamp)	2700	[56]
643	DCM	2×10^{-4} M	32 W, SP35 fluorescent lighting 2850 lm	520	[59]
641	THF	1×10^{-4} M	Bright full spectrum light source	296	[72]
642	DCM	5×10^{-5} M	exposed to ambient light and air	300	[68]

Table 3.2: The photochemical conversion of TIPS-pentacene at concentration 1.8×10^{-5} M in different solvents upon irradiation with 15 W lamp at 300nm in the absence of oxygen [54].

Solvents	Low-energy λ_{\max} (nm)	$t_{1/2}$ (min)	Dipole moment
THF	641	7	1.51
DCM	642	3	1.62
Benzene	644	157	2.95×10^{-4}
Toluene	642	18	0.41
Chlorobenzene	646	1	1.68
Hexane	633	28	5.75×10^{-5}
Anisole	646	36	1.47
cyclohexane	636	50	9.96×10^{-3}

3.4 Experimental conditions

TIPS-pentacene samples were dissolved in different solvents (which had been pre-equilibrated with air) at a concentration of 1×10^{-5} M and then placed in 10 mm quartz cells. Samples were placed on a laboratory bench top under conventional 60 W light source irradiation at 30 cm distance for appropriate periods at 26 °C. This temperature was found to be reproducible to +/- 0.5%, with all solvents before and after irradiation. UV-visible spectra measurements were recorded and the decrease in intensity of the long wavelength peak as a function of time was used to monitor the photo-oxidative degradation for each sample. Experimental values for the half-life of each these samples was estimated by plots of normalized A_t/A_0 at λ_{\max} versus time to compare the data in all solvents.

3.5 Photooxidative degradation of TIPS-pentacene at a concentration of 1×10^{-5} M at 26 °C.

Figure 3.1 shows the UV-visible absorption spectra of TIPS-pentacene as measured in toluene solution at a concentration of 1×10^{-5} M. TIPS-pentacene shows three strong peaks at ($\lambda_{\max} = 643, 592$ and 549 nm), corresponding to the excitation to the first singlet excited state ($S_0 \rightarrow S_1$) and mainly implies a one-electron promotion from the HOMO to the LUMO with its associated vibrational structure [112, 113]. These results that matched the absorption spectrum reported for TIPS-pentacene in the tetrahydrofuran (THF) [39], and in chloroform [109,57]. TIPS-pentacene displays a large more than 50 nm red-shifts compared to parent pentacene with ($\lambda_{\max} = 577$ nm) [56]. This red-shift in absorption can be attributed to the stronger extended π -electron delocalization from the pentacene nucleus brought about by triisopropylsilylethynyl (TIPS) at the C-6, C-13 position of pentacene. In increasing order of energy, the two following allowed electronic transitions at ($\lambda_{\max} = 440$ and 416 nm) are in general weaker than the $S_0 \rightarrow S_1$ excitation. These transitions correspond to $S_0 \rightarrow S_3$ and $S_0 \rightarrow S_4$ excitations and are mainly described by the HOMO-2, HOMO-3 to LUMO excitations with a smaller contribution from the HOMO to LUMO+ 2, LUMO + 3 promotions. In addition, the weak UV absorption recorded at 349 nm is assigned to the electronic transition $S_0 \rightarrow S_8$ excitation as shown in figures 3.1 and 3.2 [112]. As can be seen in figure 3.3 the shapes of absorption spectra of TIPS-pentacene are

similar in all solvents and exhibit around 10 nm bathochromic shift (see table 3.3). The possible reason for this behaviour might be too different in dipole moment of these solvents [54, 114-117]. The absence of linear correlation between λ_{\max} of the absorption spectra with dipole moment of the solvent as shown in figure 3.4 is a clear indication that there is a specific interaction of some solvents with TIPS-pentacene in the ground or excited state or both.

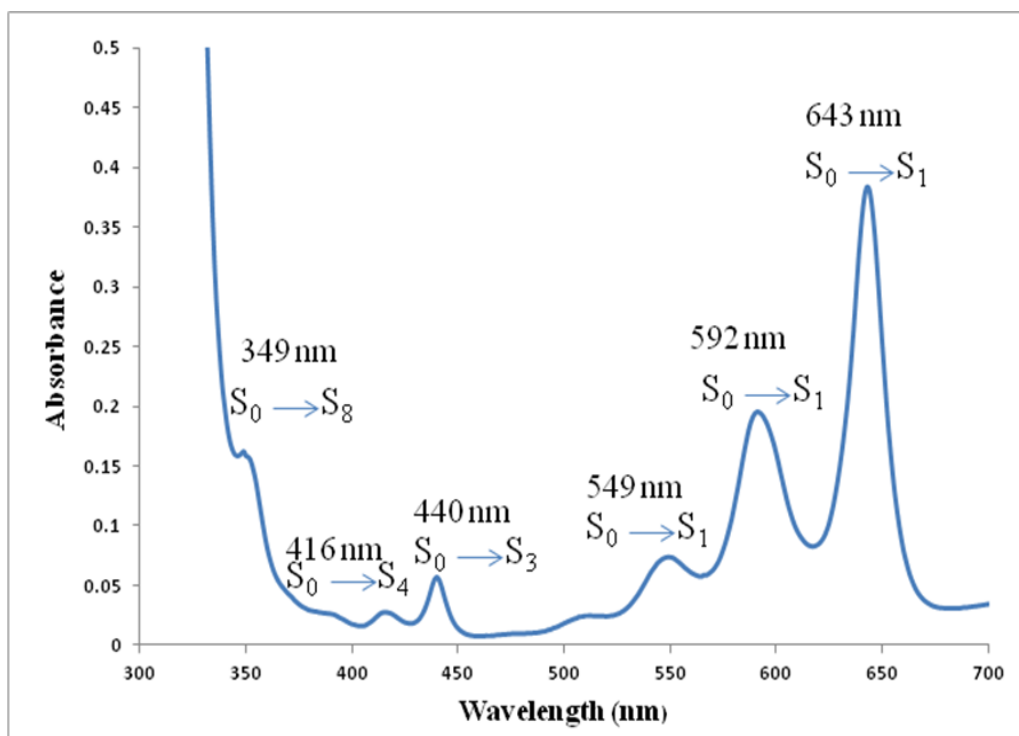


Figure 3.1: UV-visible absorption spectra of TIPS-pentacene in toluene solution at a concentration of 1×10^{-5} M at 26 °C.

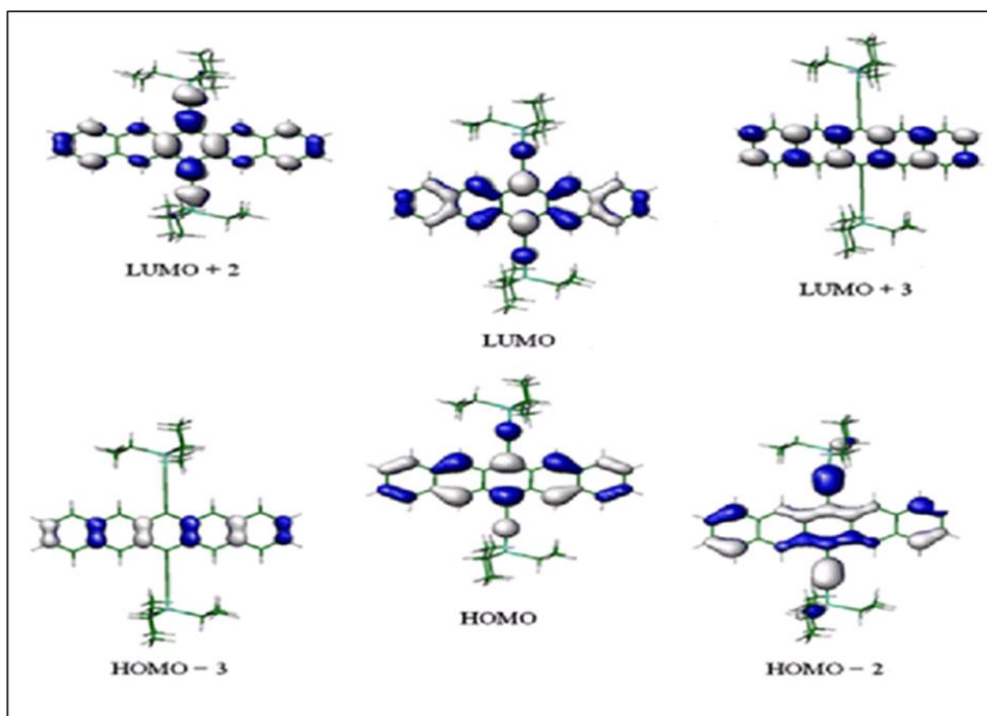


Figure 3.2: HOMO and LUMO of TIPS-pentacene [112].

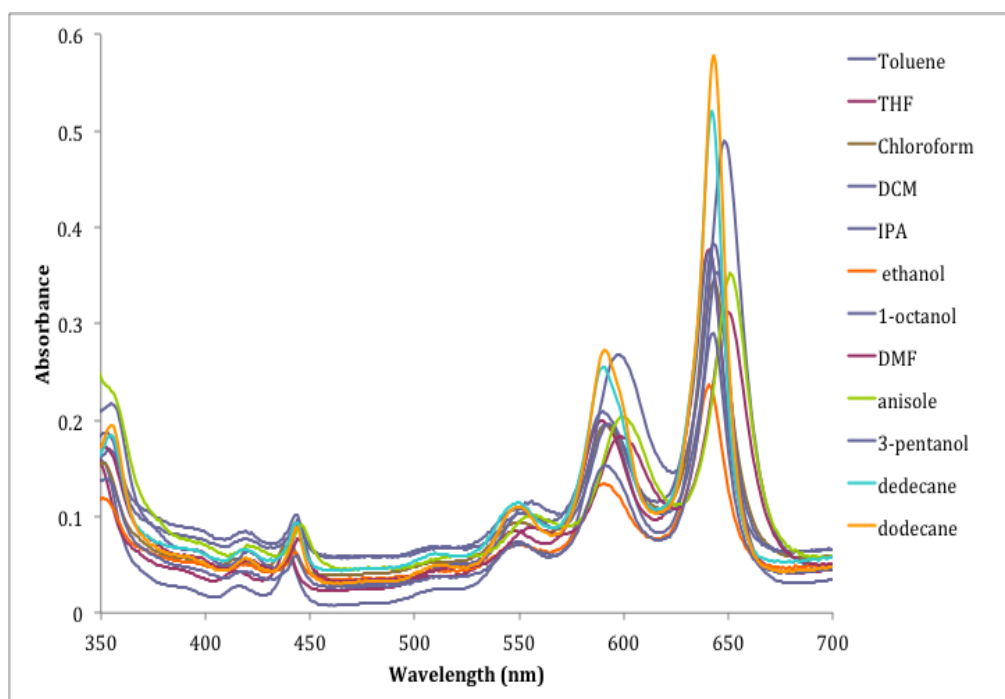


Figure 3.3: UV-visible absorption of TIPS-pentacene in different solvents at a concentration of 1×10^{-5} M at 26 °C.

Table 3.3: The λ_{\max} of TIPS-pentacene at a concentration of 1×10^{-5} M in different solvents at 26°C.

Solvents	λ_{\max}	Solvents	λ_{\max}
Decane	646	THF	641
Dodecane	643	DMF	650
Toluene	643	1-octanol	645
DCM	648	3-pentanol	643
Chloroform	643	IPA	640
Anisole	651	Ethanol	641

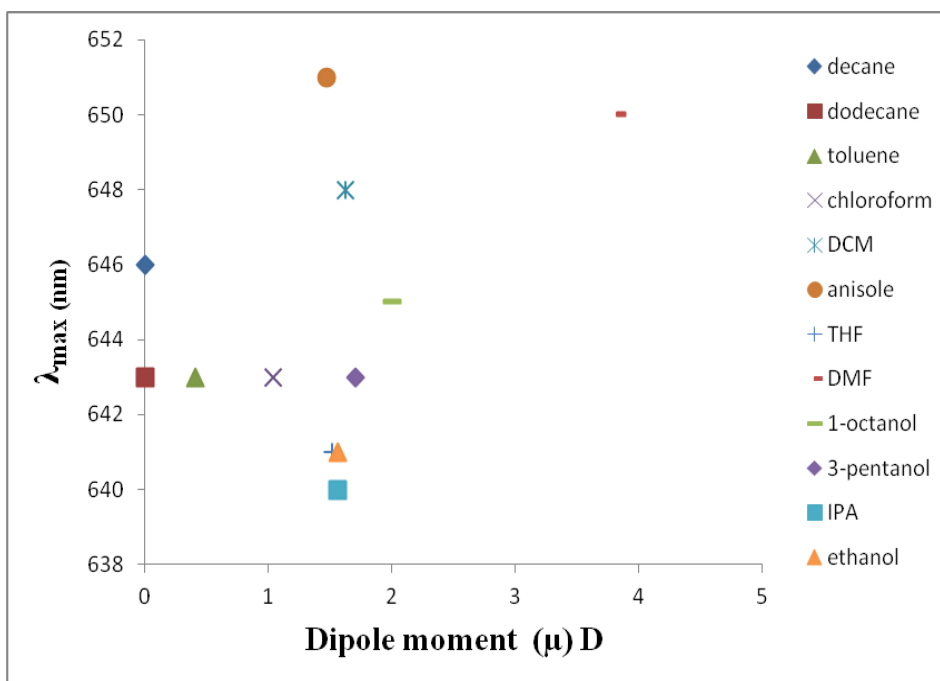


Figure 3.4: Plot of λ_{\max} of the absorption spectra versus the solvent dipole moment for a solution of TIPS-pentacene at a concentration of 1×10^{-5} M at 26°C.

The decrease in intensity of the long wavelength absorption peak ($\lambda_{\text{max}} = 643 \text{ nm}$) as a function of time was used to study the photostability of TIPS-pentacene [39, 56, 59, 68, 72] and data in chloroform is shown in figure 3.5. Comparable decays were also measured for solvents, and it was found that photooxidation stability of TIPS-pentacene is strongly dependant on the solvent used.

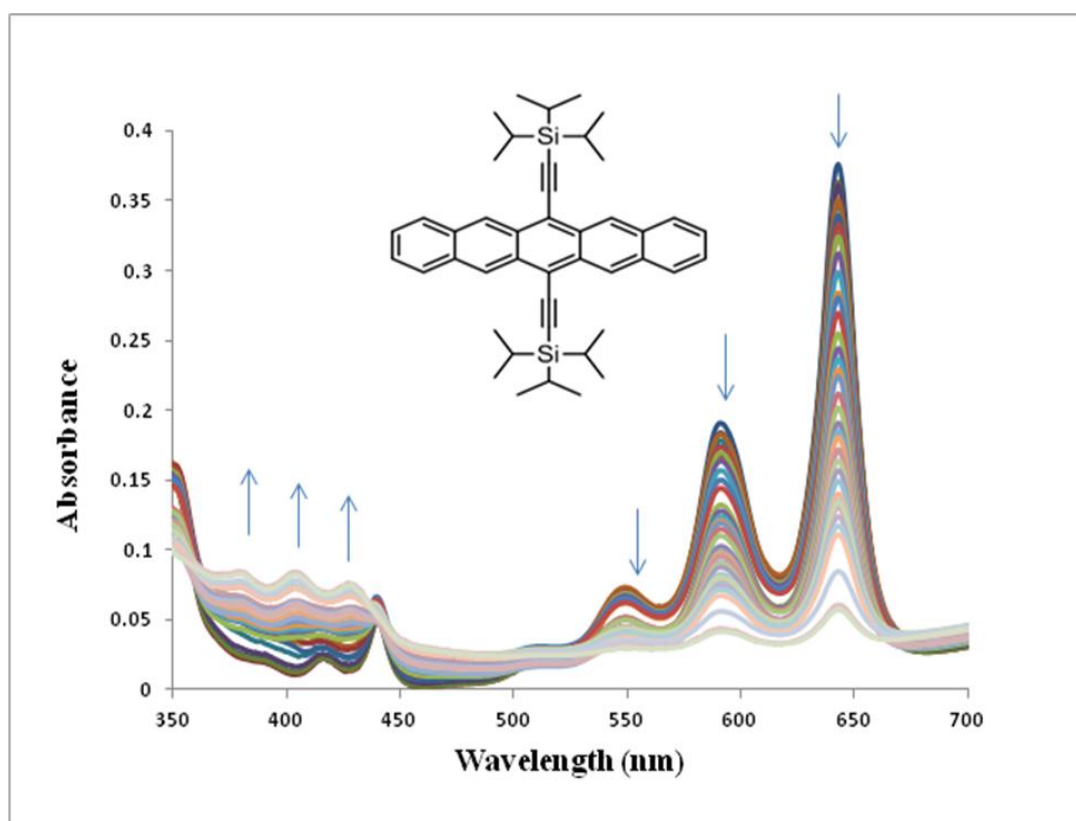


Figure 3.5: UV-visible absorption spectra for the photooxidation of TIPS-pentacene in chloroform at $1 \times 10^{-5} \text{ M}$ in a 10 mm pathlength at 26°C .

The half-life ($t_{1/2}$) for TIPS-pentacene at concentration $1 \times 10^{-5} \text{ M}$ was estimated for each sample in different solvent by plotting of normalized A_t/A_0 at the longest wavelengths absorption with the irradiation time at the same condition from the time taken for A_t/A_0 to fall to 0.5 as shown in figure 3.6. These absorbance-time profiles were found to be reproducible to $\pm 5\%$, with all formulations showing retardation in rate beyond ($t_{1/2}$). As can be seen from table 3.4 TIPS-pentacene showed increasing stability in the order 1-octanol < decane < IPA < dodecane ~ ethanol < anisole < THF < chloroform < DCM < toluene < DMF.

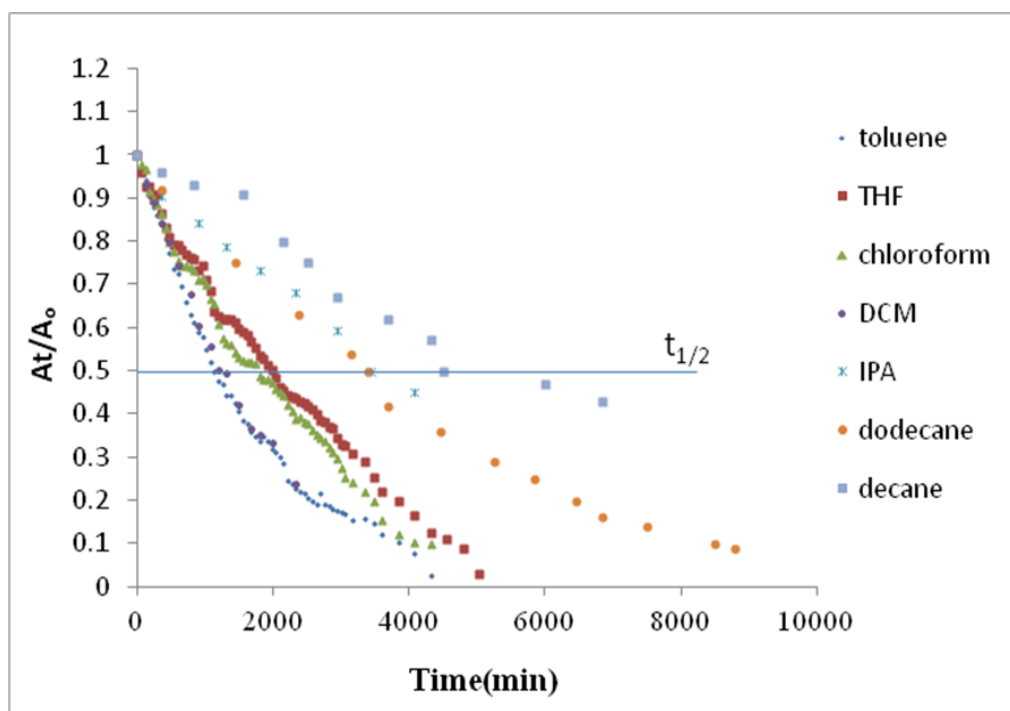


Figure 3.6: Normalised absorbance/ time profiles at λ_{\max} of TIPS-pentacene in different solvents at a concentration $1 \times 10^{-5} \text{ M}$ at 26°C .

Table 3.4: The half-life ($t_{1/2}$) of TIPS-pentacene in different solvents at concentration ($1 \times 10^{-5} \text{ M}$) at 26°C .

Solvents	$t_{1/2}$ (min)	Solvents	$t_{1/2}$ (min)
Decane	4230 +/-540 (3960-4500)	THF	1980
Dodecane	3390	DMF	890 +/- 180 (800-980)
Toluene	1205 +/-190 (1110-1300)	1-octanol	5160
DCM	1200	3-pentanol	2040
Chloroform	1550 +/-360 (1740-1360)	IPA	3450
Anisole	2160	Ethanol	3240

3.6 Photooxidation mechanism of TIPS-pentacene

The electronic excitation of a molecule takes place by absorption of radiation causing an electronic transition from an occupied orbital (e.g. the HOMO) to a higher unoccupied orbital (e.g. the LUMO). The transitions π - π^* within the visible range are necessary for a colour to occur. Pentacene and its derivatives undergo degradation by photooxidation when the excited state(s) react with oxygen to yield products. Pentacene forms products in the form of a transannular endoperoxide and also a dimeric peroxide, and the resulting endoperoxide then converts to pentacenequinone. There have been debates about the mechanisms which actually cause these reactions, because the pertinent to many polycyclic aromatic organic materials. Two main mechanisms have been proposed. In the first, the acene is excited by light and creates singlet oxygen, which subsequently reacts with the acene to form an EPO. This process is denoted a Type-II photooxidation mechanism and is also known as energy transfer (figure 3.7). In the second mechanism, the excited acene serves as an electron donor, transferring an electron to an oxygen molecule causing a radical anion superoxide (O_2^-). The corresponding pentacene radical cation then reacts further with this superoxide radical anion in a Type-I photooxidation process as known electron transfer (figure 3.7) [39, 58, 59, 98]. In solution, singlet oxygen is usually formed by photosensitization (transferring energy of absorbed light): the singlet oxygen sensitization requires a sensitizer with a triplet energy that is larger than the single triplet energy gap in singlet oxygen (greater than 22.5 kcal/mol). Maliakal and co-workers investigated that TIPS-pentacene is approximately 50 times more stable toward degradation in air-saturated in THF solution as compared to pentacene on the basis of measured half-life. They argued that energy transfer can be ignored for TIPS-pentacene, because it has triplet energy of 5.5 kcal/mol which is not large enough to sensitize singlet oxygen even thermodynamically. They proposed that the lower LUMO energy as a result of alkynyl substitution will increase the activation energy and lend enhanced photo-stability of TIPS-pentacene compared to pentacene that it prevents singlet oxygen sensitization [39]. TIPS-pentacenes showed intermolecular (4+4) cycloaddition at 5 and 14 which leads to anthracene and tetracene dimerisation when it exposed to a 15W UV lamp in the absence of oxygen [54]. The photo-degradation of TIPS-pentacene under the influence of light and air in CH_2Cl_2

($2 \times 10^{-4} \text{M}$) has been studied. The UV-visible spectra showed corresponding oxidation products, and the half-life was reported at 520 min [59]. Werner et al. studied the products of TIPS-pentacene obtained from photooxidation in CHCl_3 when it irradiated to sodium lamp (600W) with the direct addition of $^1\text{O}_2$. The photooxygenation of TIPS-pentacene afforded only the product 6, 13-EPO-TIPS-pentacene in 78% yield after isolation by chromatography. However, a trace of a byproduct of 5, 14-EPO-TIPS-pentacene was found in UV-visible spectra. As a result of these studies, it is concluded that TIPS-pentacene can react via either a Type-I (electron transfer) or Type-II (energy transfer) under irradiation but that the Type-I photooxygenation is faster than the Type-II ($^1\text{O}_2$) pathway and is mainly responsible for the photodegradation [98].

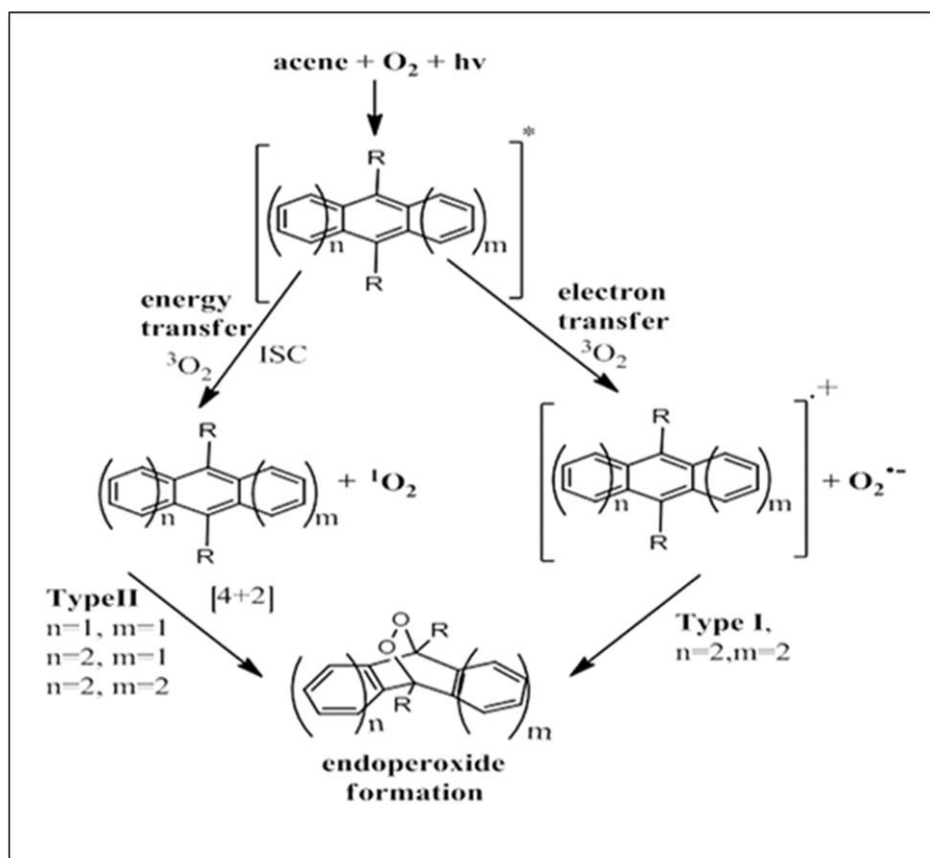


Figure 3.7: Schematic showing two mechanistic pathways to photooxidation of oligoacenes: electron transfer (Type-I) and energy transfer (Type-II) [98].

3.6.1 Analysis of the photooxidation products of TIPS-pentacene

Degradation of TIPS-pentacene in all solvent solutions can be visually observed by a colour change of the solution from blue to yellow during the irradiation to room light, air and white light (60W). The structural elucidation of the various degradation products was based on the UV- visible spectrophotometry, nuclear magnetic resonance (^1H NMR) spectrometry and atmospheric pressure chemical ionization (APCI) mass spectrometry. As can be seen from figures 3.5 and 3.15, the intensity of the peaks at 643, 592 and 549 nm decreases slowly, and new peaks are formed at 377, 405 and 424 nm upon photodegradation in chloroform and toluene solutions. This kind of the UV absorption change around 400 nm may be assigned to an endo-peroxide product indicating a photoaddition reaction of pentacene with oxygen [39]. APCI mass spectrometry of the TIPS-pentacene solution after irradiation was performed as shown in figures 3.8 to 3.11 in toluene and chloroform solutions. The APCI mass spectrometry (AP^+) shows a base peak at 638 corresponding to the molecular ion of TIPS pentacene. This is accompanied by further peaks at $M^{++}16, 32, 48, 64$ etc indicating that additional oxidised species are present. In figures 3.7 and 3.9 the most abundant secondary peak lies at 670 corresponding to a doubly oxidised product. The structure of the oxidation products has been fully elucidated for a double oxidation may support degradation via an endo-peroxide route [98].

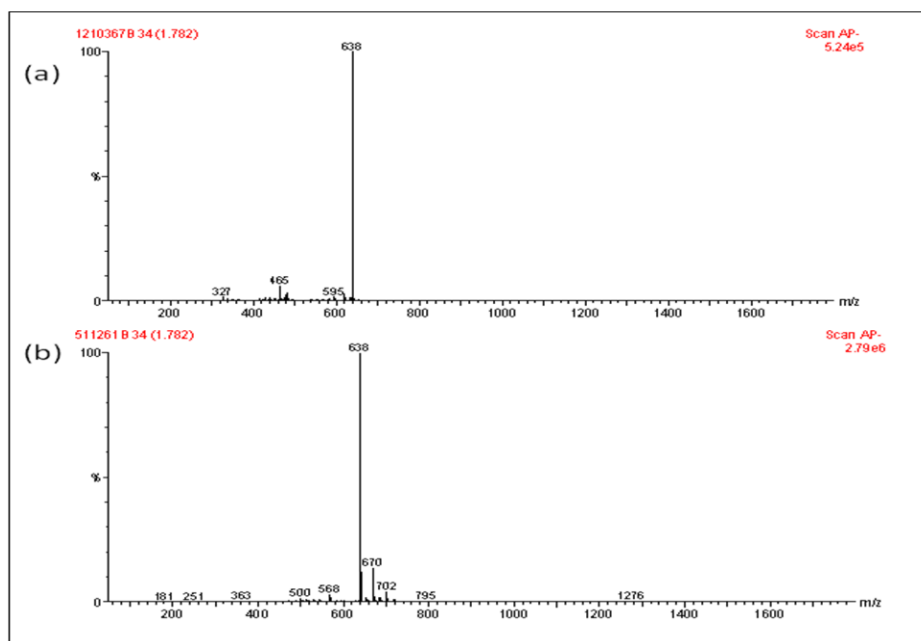


Figure 3.8: Mass spectroscopy (AP⁻) of TIPS-pentacene at 1×10^{-5} M in toluene, (a) before and (b) after photooxidation.

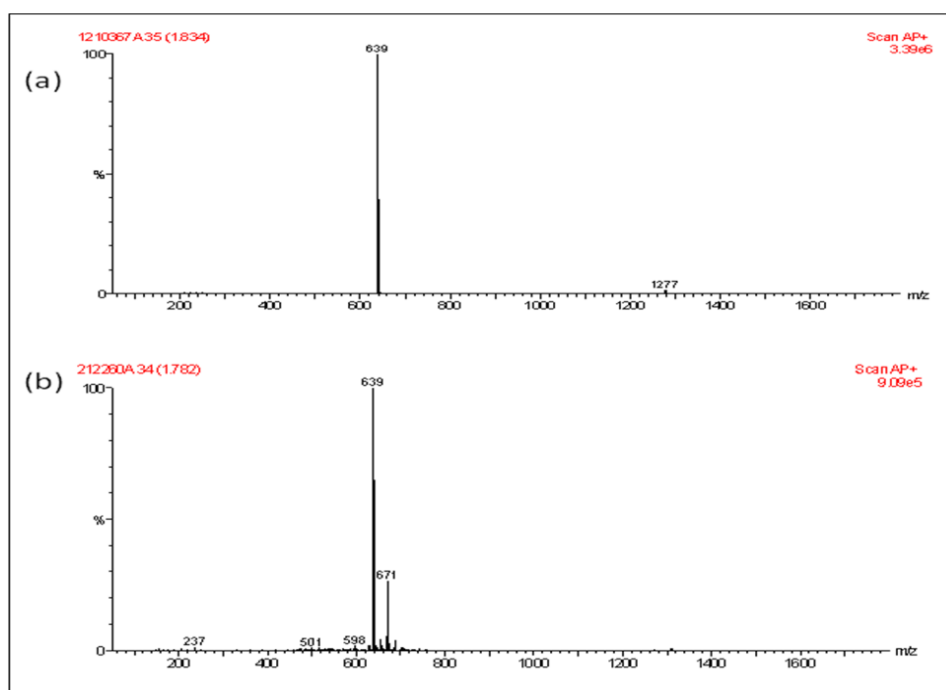


Figure 3.9: Mass spectroscopy (AP⁺) of TIPS-pentacene at 1×10^{-5} M in toluene, (a) before and (b) after photooxidation.

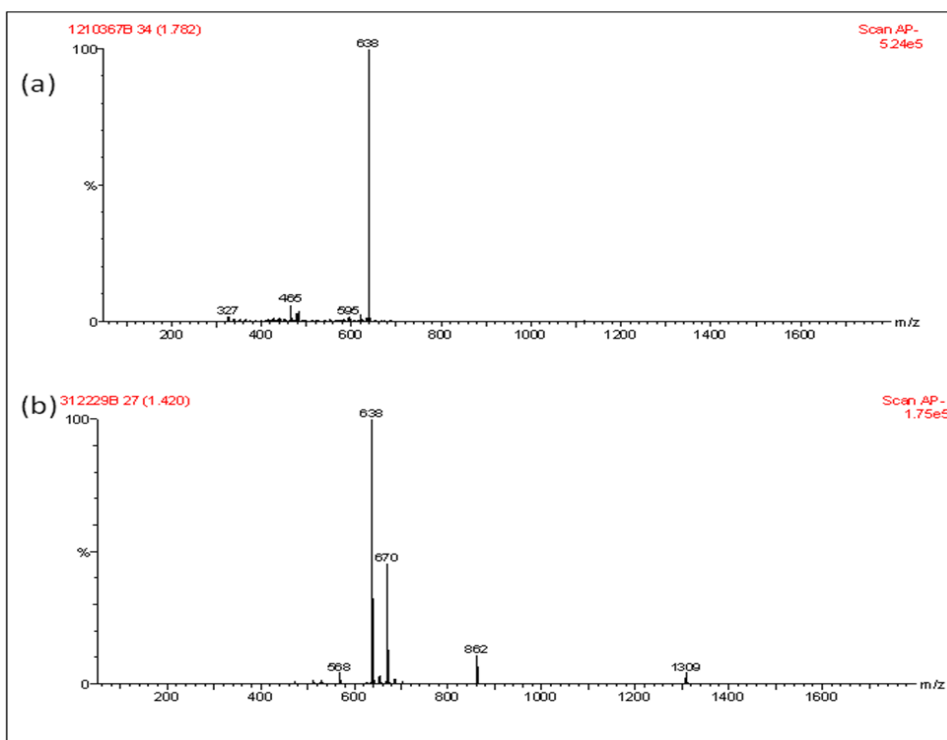


Figure 3.10: Mass spectroscopy (AP⁻) of TIPS-pentacene at 1×10^{-5} M in chloroform, (a) before and (b) after photooxidation.

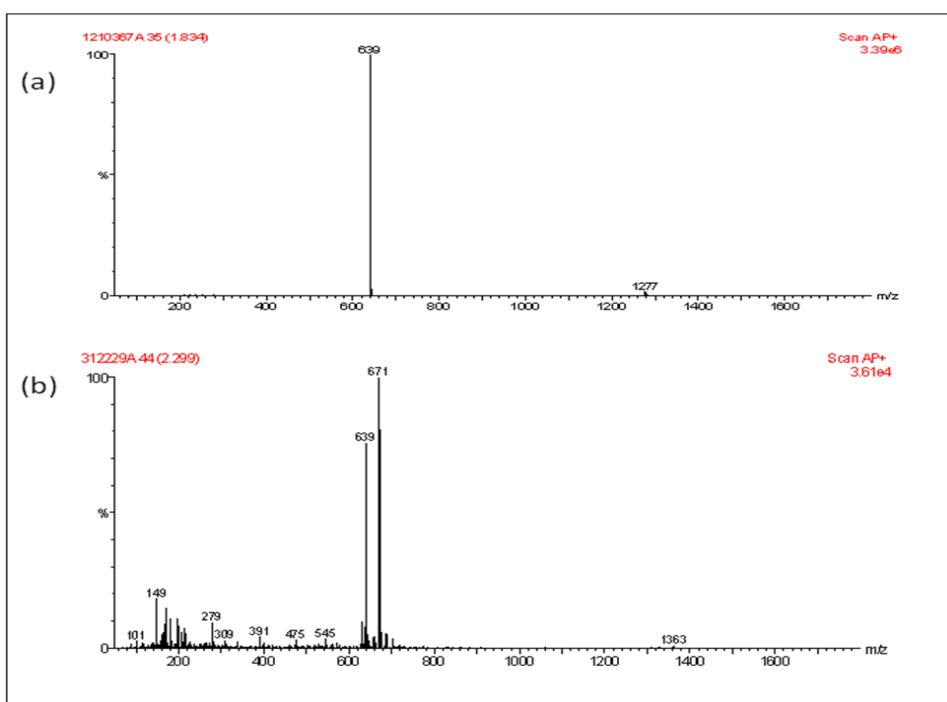


Figure 3.11: Mass spectroscopy (AP⁺) of TIPS-pentacene 1×10^{-5} M in chloroform, (a) before and (b) after photo-oxidation.

The ^1H NMR analysis of TIPS-pentacene in different solvents clarify the structure of 6, 13-endoperoxide directly by the shift from 9.33ppm for (4H,s, H-5, H-7, H-12, H-14) (a) of TIPS-pentacene to 8.23ppm (a) of 6, 13-EPO-TIPS-pentacene as shown in Figures 3.12 and 3.13 before irradiation and after photodegradation in toluene and chloroform. As mentioned above, the formation of the endoperoxide (6,13-EPO-TIPS-pentacene) and (5,14-EPO-TIPS-pentacene) (figure 3.14) has been observed using chemically generated singlet oxygen ($^1\text{O}_2$) [98]. Mass spectra and ^1H NMR spectra confirm that the main product is 6, 13-EPO-TIPS-pentacene of TIPS-pentacene; this shows no features in the visible absorption spectra because the conjugated π -system in the product is too short (comprising two naphthalene rings). The new features observed below 450 nm are due to small quantities of the 5, 14-EPO-TIPS-pentacene (effectively a substituted anthracene) as shown in figure 3.15. In addition, it seems that the main product 6, 13-EPO-TIPS-pentacene can further react to give pentacene-6, 13-dione, shown by the colour change from blue to yellow as shown in figure 3.14. Work by Katsuhiko Ono et al. [48] has shown that a stable and characterisable endoperoxide can be formed with a 6, 13-dithienopentacene. This is presumably assisted by the electron rich thiophene substituents. This oxidation route is suspected to play a part in TIPS pentacene degradation. The degradation to mono and higher oxidation products of sublimed pentacene has been examined by De Angelis et al. The products described are believed to be combinations of quinones and secondary alcohols [41].

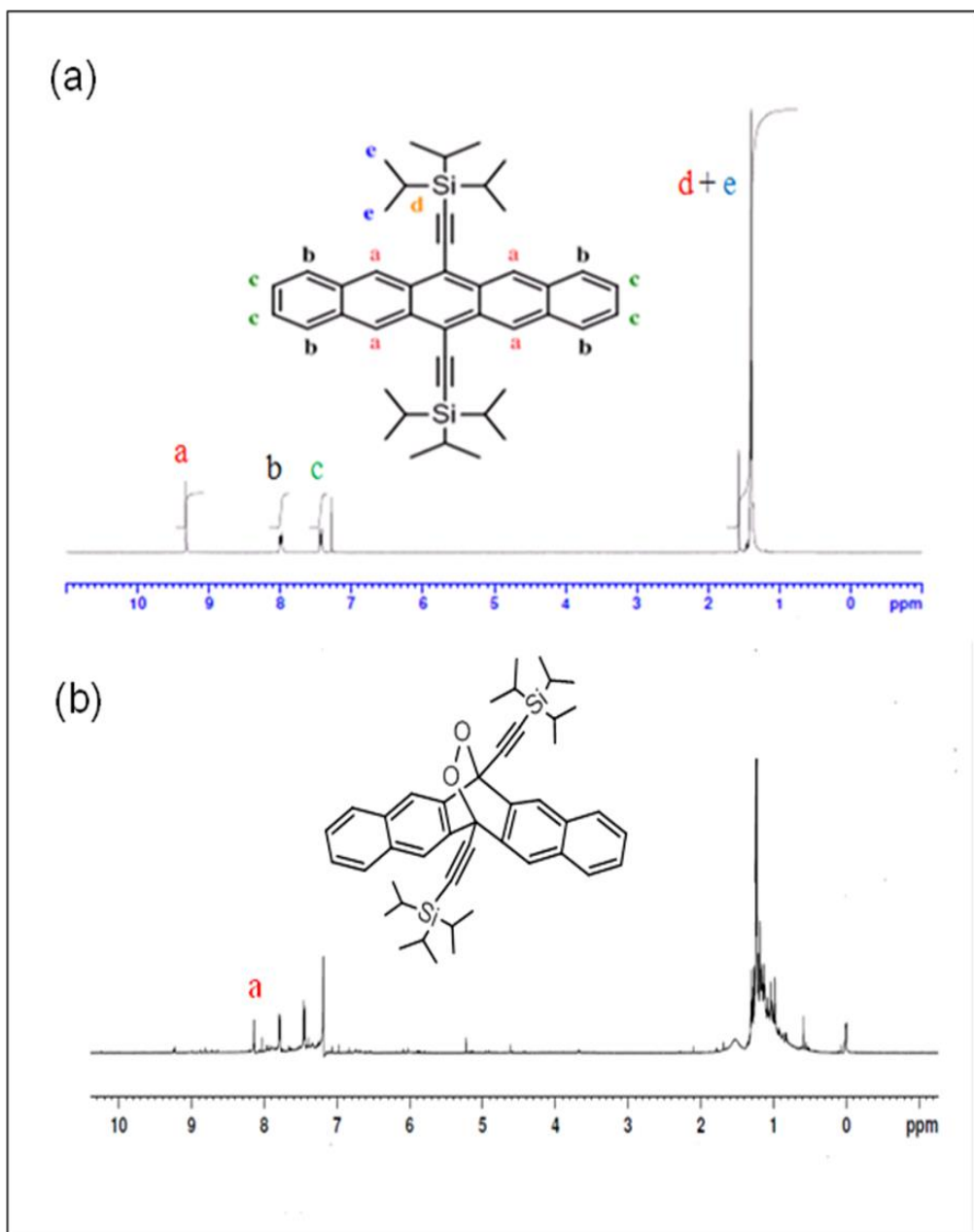


Figure 3.12: ^1H NMR spectra TIPS-pentacene 1×10^{-5} M in toluene, (a) before and (b) after photooxidation.

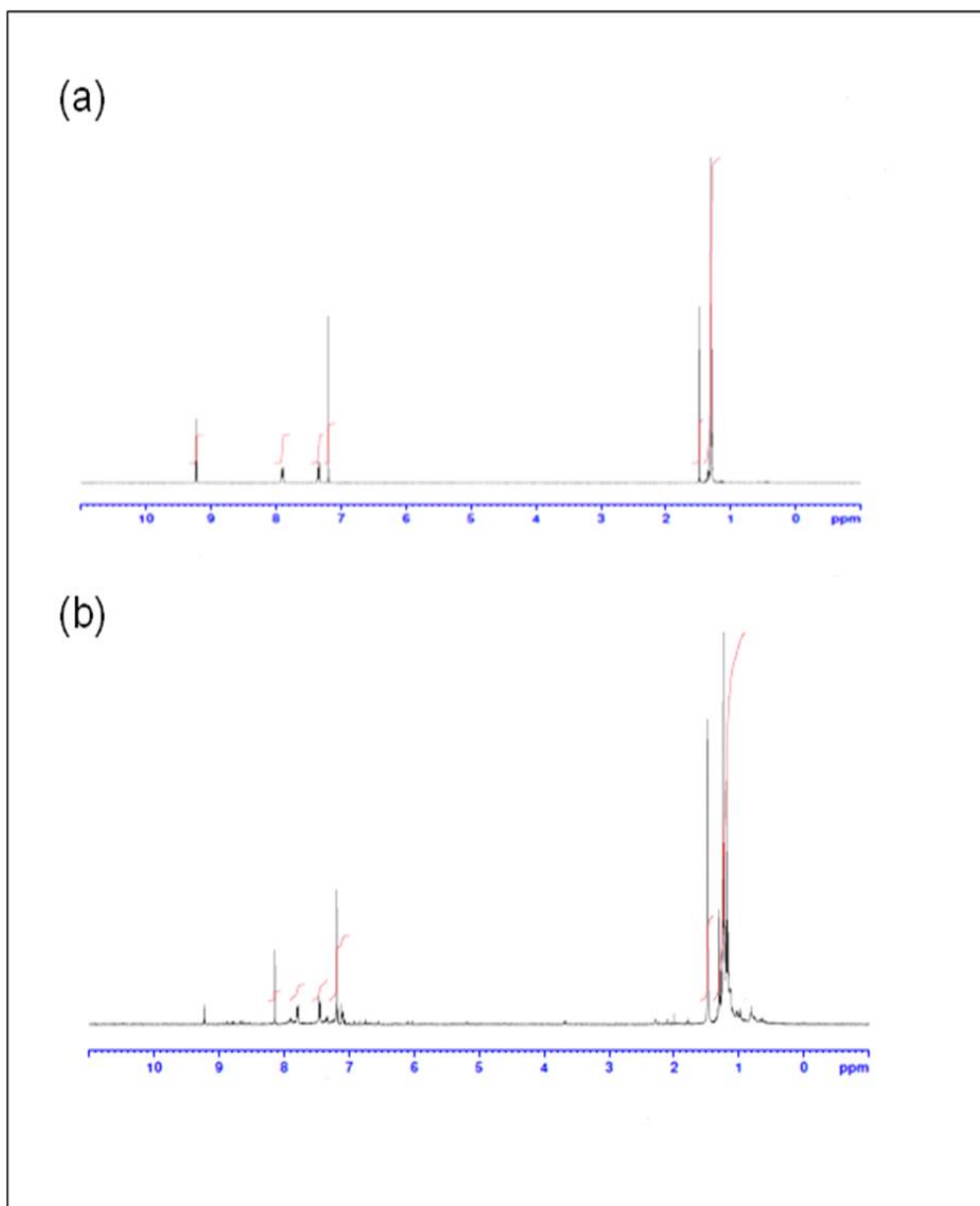


Figure 3.13: ^1H NMR spectra TIPS-pentacene at 1×10^{-5} M in chloroform, (a) before and (b) after photooxidation.

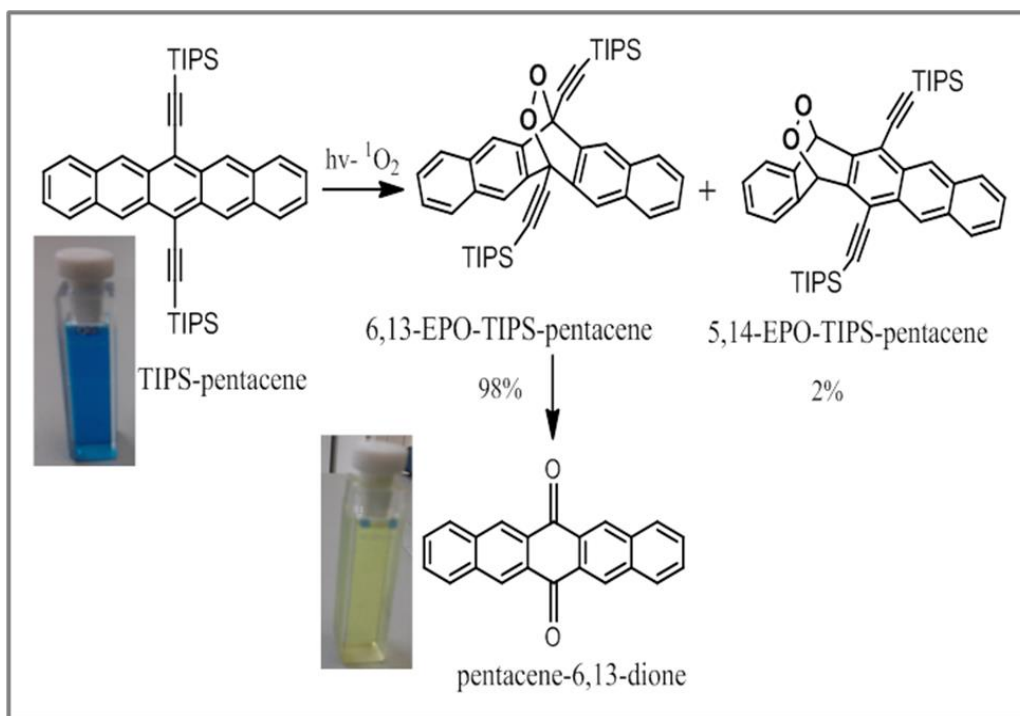


Figure 3.14: Schematic showing photooxidation of TIPS-pentacene.

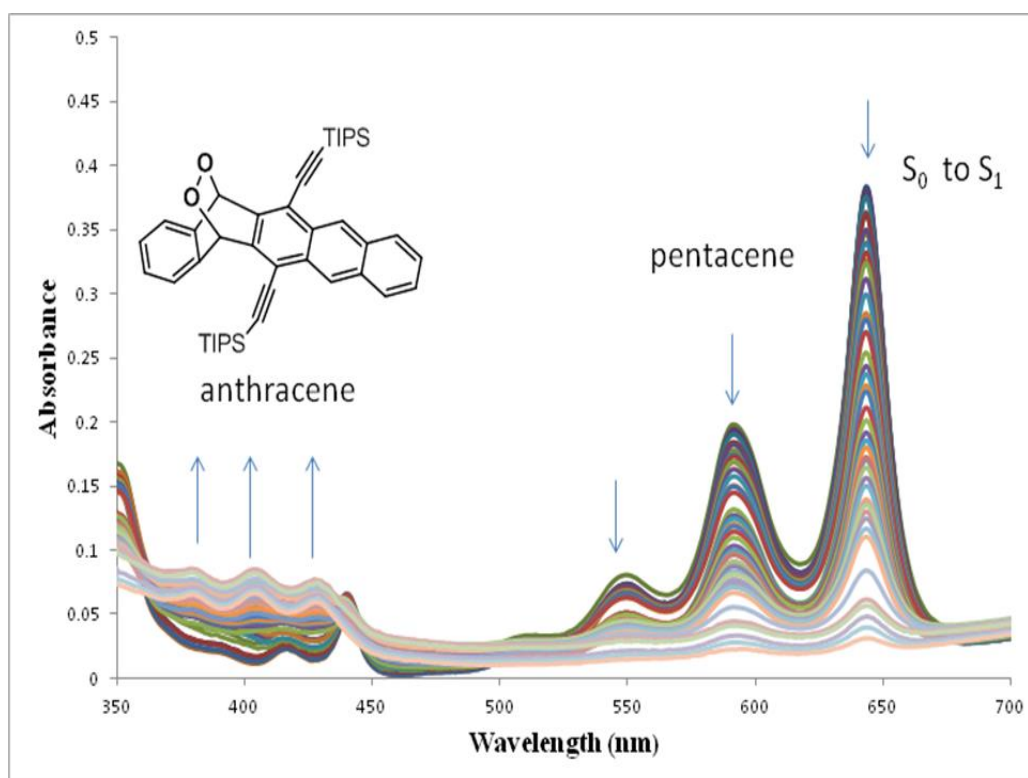
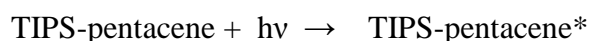


Figure 3.15: UV-visible absorption spectra for the photooxidation of TIPS-pentacene in toluene at 1×10^{-5} M in a 10 mm pathlength at 26°C.

3.7 Kinetics of the photodegradation of TIPS-pentacene in solution

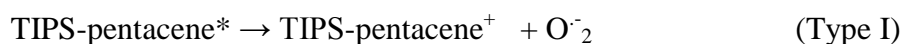
The photodegradation of TIPS-pentacene solutions is controlled by the rates and quantum yields of several processes, as summarised below:

A) The initial step is TIPS-pentacene excitation from the ground electronic state to an excited singlet state ($S_0 - S_1$):



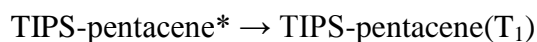
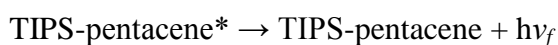
B) Primary photoprocesses then occur, of which there are several possibilities:

1. If dissolved oxygen is present, the excited TIPS-pentacene can activate O_2 molecules by either of the two processes described above:

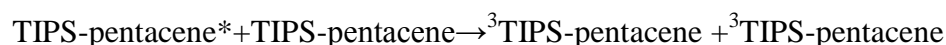


Both singlet oxygen and superoxide produce an endoperoxide (EPO), so these are lumped together in the kinetic scheme (although this treatment assumes that the donor TIPS-pentacene molecule (in either process) is the recipient of the excited O_2 from which the EPO is formed).

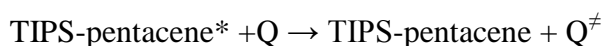
2. Excited state TIPS-pentacene can relax back to its ground state by fluorescence emission, or can undergo intersystem crossing to its lowest triplet excited state (T_1).



3. Singlet fission via interaction with a second TIPS-pentacene molecule can occur to produce a pair of triplets:



4. Deactivation can be accomplished by physical quenching via interaction with some other dissolved component:



[NB. This simple treatment assumes that the formation of the EPO is a secondary process following from step B (1) which goes with 100% efficiency. The validity of this needs to be tested.]

Abbreviating the rate constants as follows: j – photochemical rate constant for initial excitation; k_f – fluorescence rate constant; k_{ex} – rate constant for O₂ excitation; k_q – rate constant for quenching; k_{SF} – rate constant for singlet fission; k_{ISC} – rate constant for intersystem crossing, the rate of loss of TIPS-pentacene (denoted $[M]$) is given by:

$$-\frac{d[M]}{dt} = j[M] - k_f[M^*] - k_q[Q][M^*] - k_{SF}[M][M^*]$$

and the rate of formation of excited state TIPS-pentacene (denoted $[M^*]$) is given by:

$$\frac{d[M^*]}{dt} = j[M] - k_f[M^*] - k_q[Q][M^*] - k_{SF}[M][M^*] - k_{ex}[M^*][O_2] - k_{ISC}[M^*]$$

and since M^* can be treated as steady state (i.e. $\frac{d[M^*]}{dt} = 0$),

$$[M^*] = \frac{j[M]}{k_f + k_q[Q] + k_{SF}[M] + k_{ex}[O_2] + k_{ISC}} = \frac{j[M]}{\sum proc}$$

This results in the following rate equation:

$$-\frac{d[M]}{dt} = j[M] \left(1 - \frac{k_f}{\sum proc} - \frac{k_q[Q]}{\sum proc} - \frac{k_{SF}[M]}{\sum proc} \right)$$

Recognising that

$$\frac{k_f}{\sum proc} = \Phi_f$$

[i.e. the quantum yield for each process, the amount of M lost as EPO is what is left after the three de-excitation processes have occurred].

and, recognising that the terms in the brackets represent the quantum yields of each of the primary processes (except intersystem crossing), this shows that the rate of loss of TIPS-pentacene upon photodegradation in oxygen-containing solvents is determined by the relative efficiencies of fluorescence, quenching and singlet fission (with the latter depending upon the concentration of the co-reactant, i.e. $[Q]$ or $[M]$). Intersystem crossing as a direct process has been neglected in this treatment since it is likely to make only a very small, concentration-independent contribution to the total process (and is included in the M^* processes). This treatment shows that factors which increase the efficiency of quenching (increased $[Q]$) and singlet fission (partly increased $[M]$, but also solvent, see later) will lead to increased stability because they compete to regenerate ground-state TIPS-pentacene from the excited singlet state(s).

Since there are several possible photodegradation products, the kinetics are followed via the loss of TIPS-pentacene by monitoring the absorption at λ_{\max} on as a function of irradiation time. Furthermore, since the rates of these various processes are not known, it is not a simple task to predict the order of the overall degradation reaction so the kinetics need to be deduced empirically. Data were plotted as zero, first and second order as shown below.

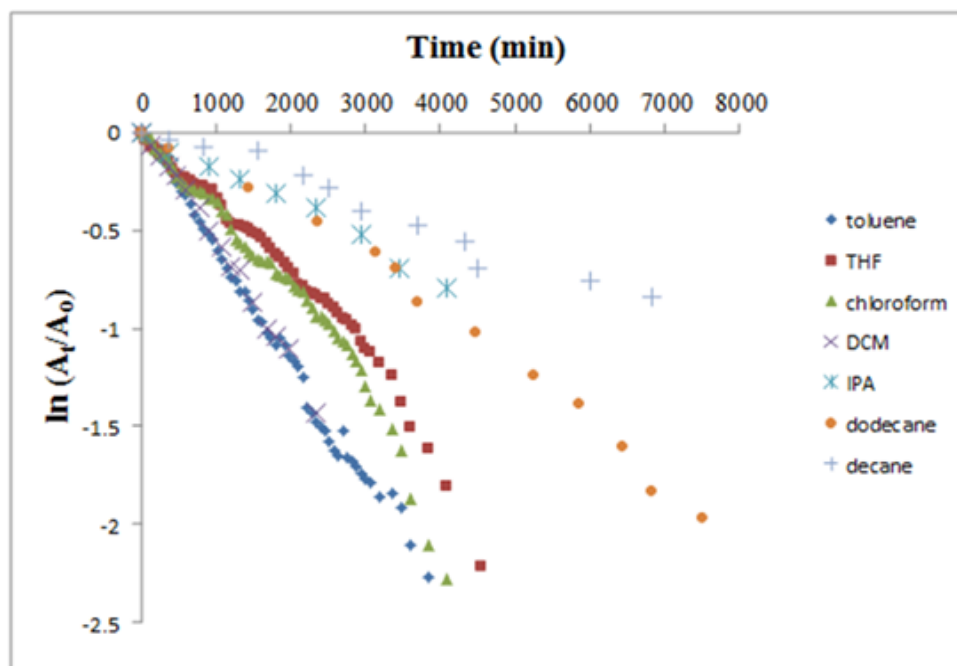


Figure 3.16: Plot of $\ln(A_t/A_0)$ versus time for TIPS-pentacene in a variety of solvents at a concentration of 1×10^{-5} M at 26°C .

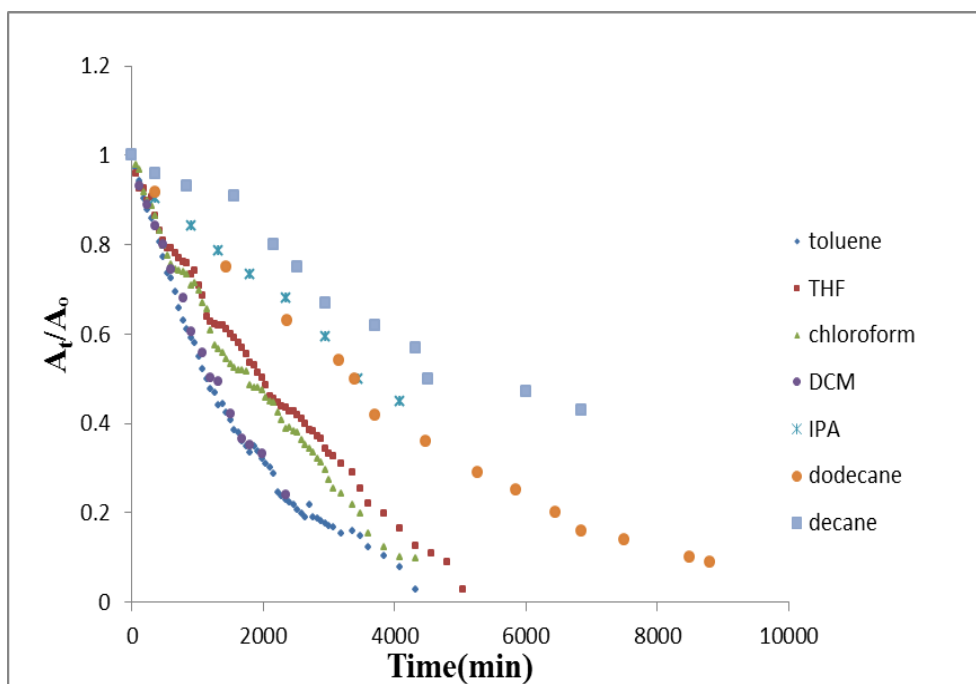


Figure 3.17: Plot of (A_t/A_0) versus time for TIPS-pentacene in a variety of solvents at a concentration of 1×10^{-5} M at 26°C .

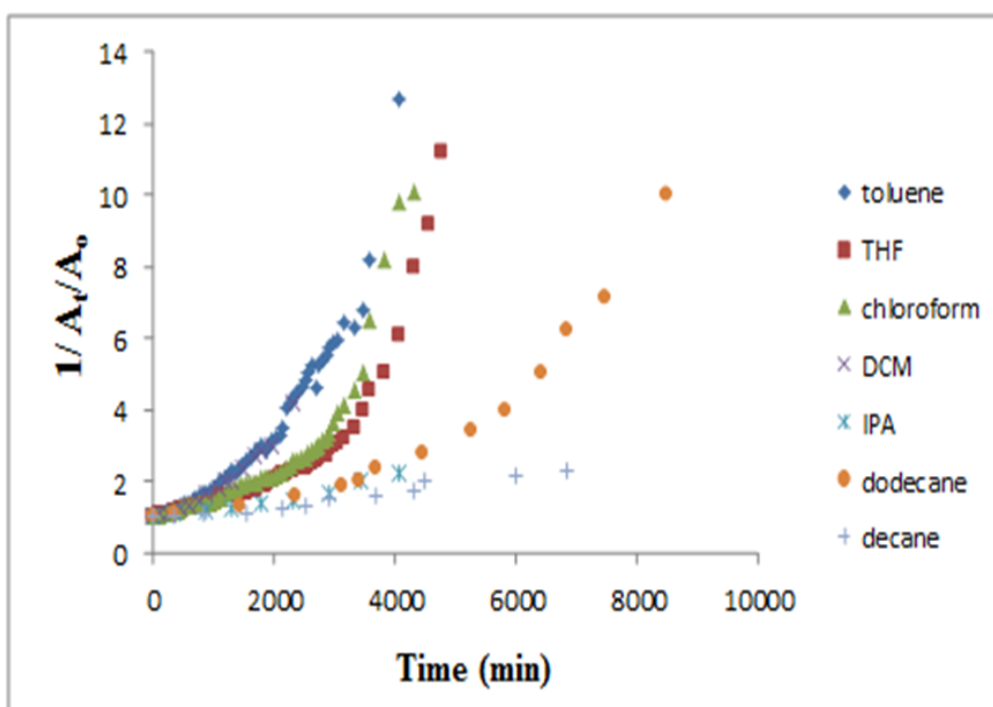


Figure 3.18: Plot of $1/(A_t/A_0)$ versus time for TIPS-pentacene in a variety of solvents at a concentration of 1×10^{-5} M at 26°C .

The kinetics of the photodegradation process are effectively first order, as shown in figure 3.16 which is a plot of $\ln(A_t/A_0)$ versus time. The rate constant k and R^2 values from the linear regression are listed in table 3.5. First order kinetics also found for 6, 13- diphenylpentacene [48, 118].

Table 3.5: Effective reaction rate constants, k' (min^{-1}) determined and R^2 for TIPS-pentacene in different solvents at a concentration of 1×10^{-5} M at 26°C .

solvents	$t_{1/2}$ (min)	R^2 (zero order)	R^2 (first order)	R^2 (second order)	k (min^{-1}) first order constant
Toluene	1205 +/-190 (1110-1300)	0.901	0.995	0.871	0.0006
DCM	1200	0.97	0.991	0.93	0.0006
Chloroform	1550 +/-360 (1740-1360)	0.971	0.952	0.71	0.0005
THF	1980	0.97	0.954	0.70	0.0004
Dodecane	3390	0.95	0.987	0.83	0.0003
IPA	3450	0.99	0.985	0.95	0.0002
Decane	4230 +/-540 (3960-4500)	0.951	0.9703	0.96	0.0001

3.8 TIPS-Pentacene solubility

3.8.1 Solubility parameters: theory

The term solubility parameter (d) was describing by Hildebrandt and Scott and is defined according to equation 3.1 as the square root of the cohesive energy density (CED). The cohesive energy density in equation 3.2 is in turn derived from the heat of vaporization (ΔH), the absolute temperature T and the global ideal gas constant R divided by the molar volume (V_m) ($\text{cm}^3 \text{mol}^{-1}$).

$$d = (\text{CED})^{1/2} \quad 3.1$$

$$\text{CED} = \Delta H - RT / V_m \quad 3.2$$

$$d = \left[\frac{\Delta H - RT}{V_m} \right]^{1/2} \quad 3.3$$

The cohesive energy density is a numerical value that is a direct reflection of the van-der Waals forces holding the molecules together. This correlation between the vaporization and the van der Waals forces translates into a correlation between vaporization and solubility behaviour as the same intermolecular attractive forces have to be overcome to vaporize a liquid as well as dissolve it.

On the other hand, the concept of regular solution is applicable only to non-ionic solutions in which association and dipole interaction do not take place between solvent and solute. However, hydrogen bonding and dipole interactive force should not be ignored in many solvents. It is important to extend the regular solution theory to real solution. Hansen proposed Hildebrand's solubility parameter (HSP) into three terms, the atomic dispersive interaction (van der Waals forces) (d_d) the permanent dipole permanent dipole molecular interaction (polar forces) (d_p), and the molecular hydrogen bonding interaction (d_h) as follows,

$$\text{HSP} = d_t = (d_d^2 + d_p^2 + d_h^2)^{1/2} \quad 3.4$$

The unit of these solubility parameters in the SI unit system is $(\text{MPa})^{1/2}$. The solubility properties can be visualized in a three dimensional coordinates system with the three Hansen parameters as the axis x,y and z (d_d , d_p , d_h) and the radius of sphere, called the interaction radius (R_0) as in figure 3.19.

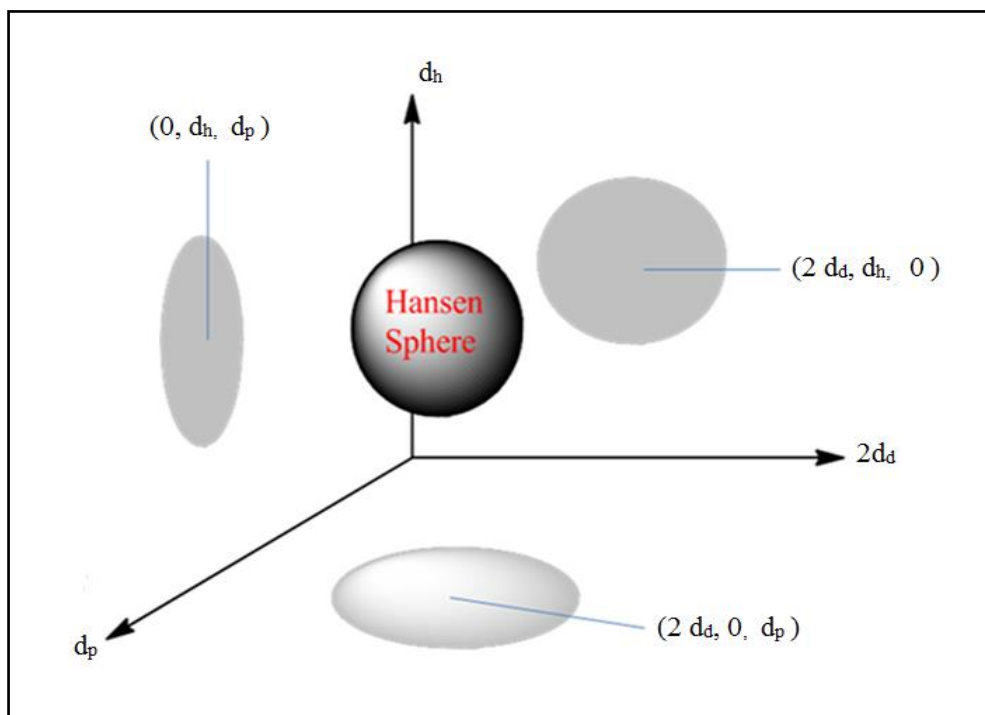


Figure 3.19: schematic of the Hansen solubility sphere.

The HSP coordinates of the solute are determined by analyzing the solubility of this solute in series of solvents with known Hansen parameters. The solubility space is then determined by fitting a spheroid into the solubility space identifies the solubility volume of this solute, with the solvent inside the spheroid and the non-solvents outside (good solvents are within the sphere, bad ones outside).

The solubility parameters of the solute under analysis are the centre coordinates of the sphere and the radius of the sphere R_0 spanning the regime within which the solute is being dissolved. The more a solvent is close to the solute in the Hansen space, the better its affinity for this solute. A solute is soluble in solvent or solvent blend when the Hansen parameters for the solvent lie within the solubility sphere for the solute.

In order to determine this, the distance of the solvent from the centre of the solute solubility sphere is calculated by the following expression,

$$R_a^2 = a (d_{d2} - d_{d1})^2 + b (d_{p2} - d_{p1})^2 + c (d_{h2} - d_{h1})^2 \quad 3.5$$

Where R_a is the distance between solvent and the solute, d_{x2} is Hansen component parameters for solvent, d_{x1} Hansen component parameters for solute and a , b , and c are weighting factors. Hansen has suggested settings of $a=4$ and $b=c=1$ based on empirical testing. If the distance R_a is less than the radius of interaction of the solute, the solvent would be expected to dissolve the solute. This method avoids reliance on graphic plots and can be effectively used in numerical form.

Teas parameters are fractional parameters derived mathematically from the Hansen parameters and indicate the percent contribution that each Hansen parameter contributes to the whole Hildebrand value as shown in equations:

$$f_d = \frac{d_d}{d_h + d_p + d_d} \quad 3.6$$

$$f_p = \frac{d_p}{d_h + d_p + d_d} \quad 3.7$$

$$f_h = \frac{d_h}{d_h + d_p + d_d} \quad 3.8$$

The sum will always be the same if all the fractional parameters are added together.

$$f_d + f_p + f_h = 1 \quad 3.9$$

Teas graph means that the solvents may be positioned relative to each other in three directions. The solvents whose only intermolecular bonding is due to dispersion forces, are located in the far lower right corner of the Teas graph, the corner that corresponds to 100% dispersion force contribution, and 0% contribution from hydrogen bonding or polar forces. Moving upwards from the bottom of the graph area solvents of increasing polarity, due less to hydrogen bonding functional groups then to an increasingly greater dipole moment of the molecule like the ketones and nitro compounds. Moving toward the lower left corner, corresponding to 100% hydrogen bonding contribution are the solvents that exhibit increasing hydrogen bonding.

3.8.2 Solvent effect

According to the relationships described above, the solubility of TIPS-pentacene in different organic solvents was used in this work. Table 3.7 shows the Hansen solubility parameters and solubility values for different solvents as well as the solubility limit for TIPS-pentacene in these solvents. TIPS-pentacene shows high solubility in common organic solvents and it has a large d_d and small d_p and d_h . Toluene, tetrahydrofuran (THF), chloroform, and DCM were found to be the best solvents for this molecule. The solubility parameters and fractional solubility parameters for these solvents are similar to those of TIPS-pentacene [119]. However, decane, dodecane and anisol have similar solubility parameters to the TIPS-pentacene will not dissolve as well as expected.

On the other hand, DMF, ethanol, IPA, 1-octanol and 3-pentanol are bad solvents for TIPS-pentacene and have a large d_p and d_h . The our own solubility tests of TIPS-pentacene in those solvents was established as: toluene ~THF ~DCM~ chloroform (~5%) < anisol, decane, dodecane (0.5- 1.5%) < 3-pentanol, 1-octanol, ethanol, DMF, IPA (0.01-0.07) [120].

Table 3.6: Hansen parameters Fractional solubility parameters, solubility limits and oxygen solubility at different solvents.

Solvents	Parameters parameters (MPa) ^{1/2} [119]				Fractional solubility parameters			Interaction distance	Solubility limit	O ₂ solubility (mole fraction ×10 ⁻⁴) [121-123].
	d _t	d _d	d _p	d _h	f _d	f _p	f _h	R _a	(wt)%	
TIPS- pentacene	19.1	18.8	0.4	3.6	0.82	0.02	0.16			
Decane	15.8	15.8	0.0	0.0	1.00	0.00	0.00	7.0	1	21.8
Dodecane	16.0	16.0	0.0	0.0	1.00	0.00	0.00	6.6	0.5	22.0
Toluene	18.1	18.0	0.7	2.0	0.87	0.03	0.10	2.2	5	9.2
DCM	20.2	18.2	6.1	6.1	0.60	0.20	0.20	6.3	5	5.7
Chloroform	18.9	17.8	3.1	5.7	0.67	0.12	0.21	3.9	5	7.3
Anisole	19.5	17.8	4.1	6.8	0.62	0.14	0.24	5.3	1.5	9.0
THF	19.4	16.8	5.7	8.0	0.55	0.19	0.26	7.9	5	8.0
DMF	24.9	17.4	13.7	11.3	0.41	0.32	0.27	15.6	0.13	
1-octanol	21.0	17.7	3.2	11.0	0.55	0.10	0.34	8.2	0.64	
3-pentanol	21.2	15.9	4.8	13.2	0.47	0.14	0.39	12.0	0.064	7.0
IPA	24.5	15.9	6.8	17.4	0.40	0.17	0.43	16.3	0.01	7.9
Ethanol	26.5	15.8	8.8	19.4	0.36	0.20	0.44	18.9	0.1	5.9

Insight into the role of solvent in determining the half-life is forthcoming from consideration of two factors: the ‘goodness’ of the solvent and the concentration of potential quenching species. The former can be expressed via Hansen solubility parameters as shown in table 3.6 [119]. These parameters are used to define the centre of a solubility sphere for TIPS-pentacene and an interaction radius, R_a , for any solvent. Good solvents will have a small R_a (i.e. the solubility parameters are closely matched; typically the solute will be highly soluble in such solvents). Progressively poorer solvents have higher values (and declining solubility). There is a generally positive, albeit poor, correlation between half-life data for TIPS-pentacene at $1 \times 10^{-5} \text{M}$ with R_a determined across a range of solvents, as shown in figure 3.20, such that to a first order when R_a is small, half-lives are comparably low and when R_a is large half-lives are comparably large. Such a correlation (poor solvent = large half-life) can be interpreted on the basis of simple non-ideal solution thermodynamic arguments, i.e. as evidence that poor solvent drives TIPS-pentacene molecules together with a concomitant increase in the efficiency of singlet fission.

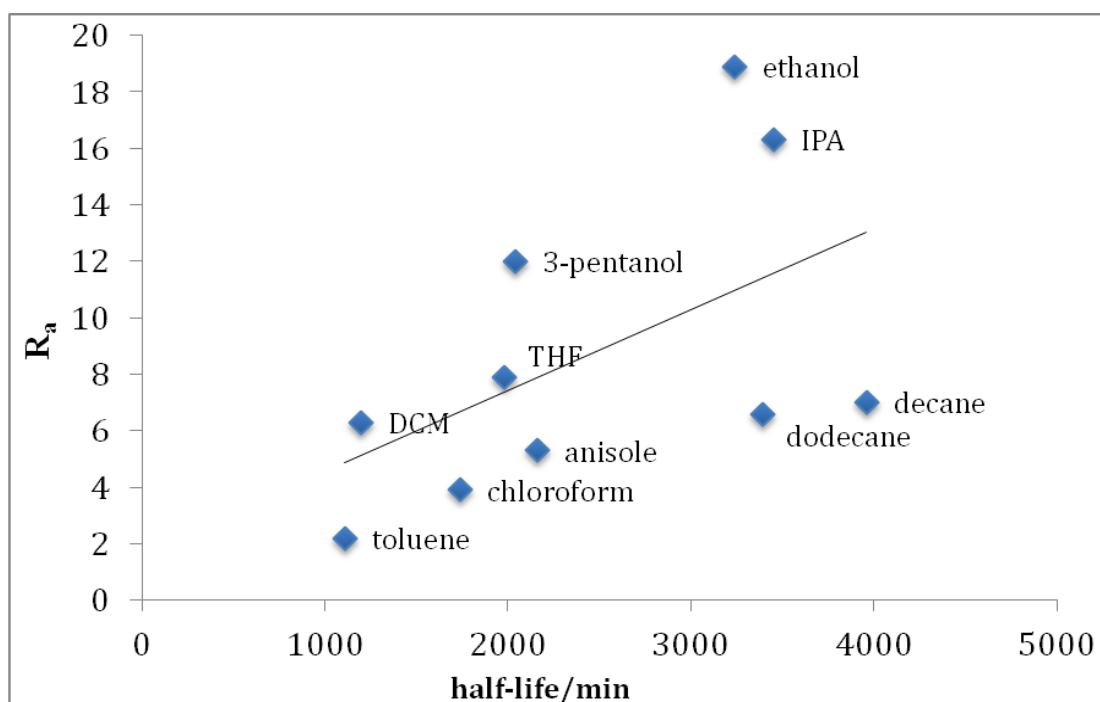


Figure 3.20: Plot of interaction distance (R_a) versus half-life of TIPS-pentacene in different solvents at a concentration of $1 \times 10^{-5} \text{M}$ at 26°C .

A second process which can be invoked to explain the reduction in the lifetime of the singlet state is quenching, for which dissolved oxygen is a prime candidate. Once again, a positive correlation exists between the concentrations of dissolved oxygen [121-123] (expressed as mole-fraction O_2 at saturation) and half-life as shown in figure 3.21 for the concentration 1×10^{-5} M, although again the correlation is not high. A clearer picture of the combination of these two processes can be seen from a plot of the product of the R_a and saturation oxygen solubility versus the half-life, as shown in figure 3.22. Here, the correlation is much improved. It seems clear that, at low concentration, the initial singlet state is deactivated by both intermolecular processes between TIPS-pentacene molecules and by quenching by dissolved oxygen.

The principal factor affecting stability therefore is the lifetime of the initial excited state. The four deactivation processes are luminescence, activation of dissolved O_2 (by whatever route), quenching by solvent and pairwise interaction with a second TIPS-pentacene molecule. Chemical instability towards endoperoxide formation consequently depends upon the relative efficiency of these channels.

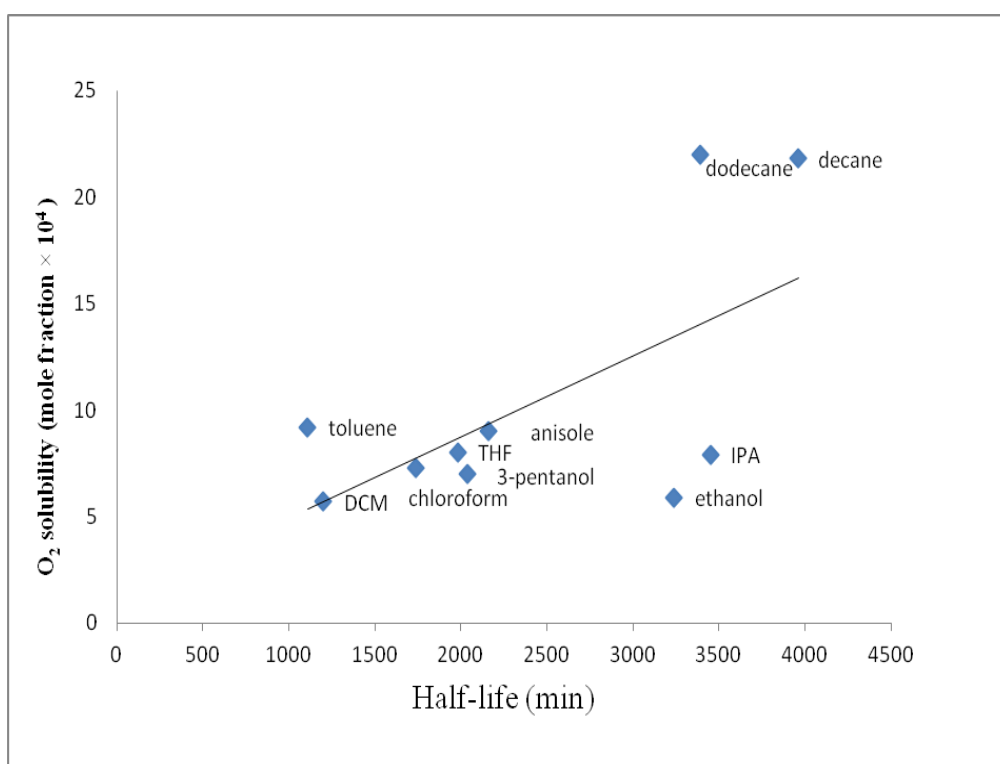


Figure 3.21: Plot of oxygen solubility (mole fraction $\times 10^4$) versus half-life of TIPS-pentacene in different solvents at a concentration of 1×10^{-5} M.

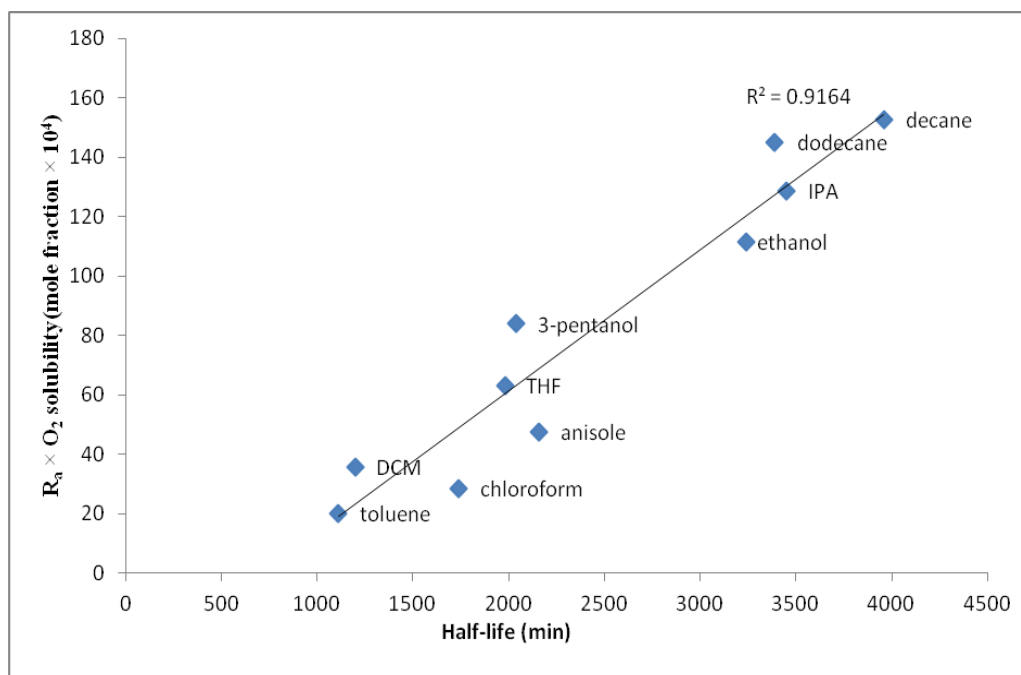


Figure 3.22: Comparison of interaction distance (R_a) \times oxygen solubility (mole fraction $\times 10^4$) versus half-life of TIPS-pentacene in different solvents at a concentration of $1 \times 10^{-5} M$.

3.9 Conclusion

The photooxidative degradation of TIPS-pentacene has been studied in different solvents at low concentration $1 \times 10^{-5} M$. The predominant degradation products of TIPS-pentacene are the same regardless of solvent and concentration, being mainly an endoperoxide resulting from O_2 addition. It is impossible to compare this data of the half-life with published literature values for TIPS-pentacene due to differences in ambient illumination or absence of concentration data. In all solvents the kinetics of the photodegradation process are effectively first order. Photo-stability of TIPS-pentacene in good solvents is observed to vary with solvent, with greater stability in chlorinated solvents and least stability in toluene. Furthermore, good solvents will have a small R_a with progressively poorer solvents having higher values with lifetime increase in alcohols and alkane solvents. This leads to closer proximity between TIPS-pentacene molecules in bad solvents which serve to increase the photostability. Solvents with higher oxygen solubility also show greater stability as a result of more efficient quenching of the initial excited singlet state. A kinetic analysis of these phenomena is consistent with these observations.

Chapter 4

4 Concentration dependent photostability of TIPS-pentacene

In this chapter, TIPS-pentacene samples were dissolved in a variety of solvents over a range of concentrations and degraded under the same conditions of samples at low concentration, confirming that stability is strongly influenced by quenching, pairwise interactions and aggregation behaviour.

4.1 The effect of concentration on the photooxidative degradation kinetics of TIPS-pentacene in toluene solution

As described previously, UV-visible spectra for TIPS-pentacene in toluene solution are characterized by three long-wavelength bands at 643, 592, and 549 nm, with the longest corresponding to the know HOMO-LUMO gap. The λ_{max} values of the longest wavelength absorption do not appear to vary with concentration (figure 4.1). For each sample, plots of normalized A_t/A_0 at 643 versus time were made as shown in figure 4.2 From this data, the half-life is obtained for each concentration from the time taken for A_t/A_0 to fall to 0.5. As shown in figure 4.2, the photostability of TIPS-pentacene increases with increasing concentration.

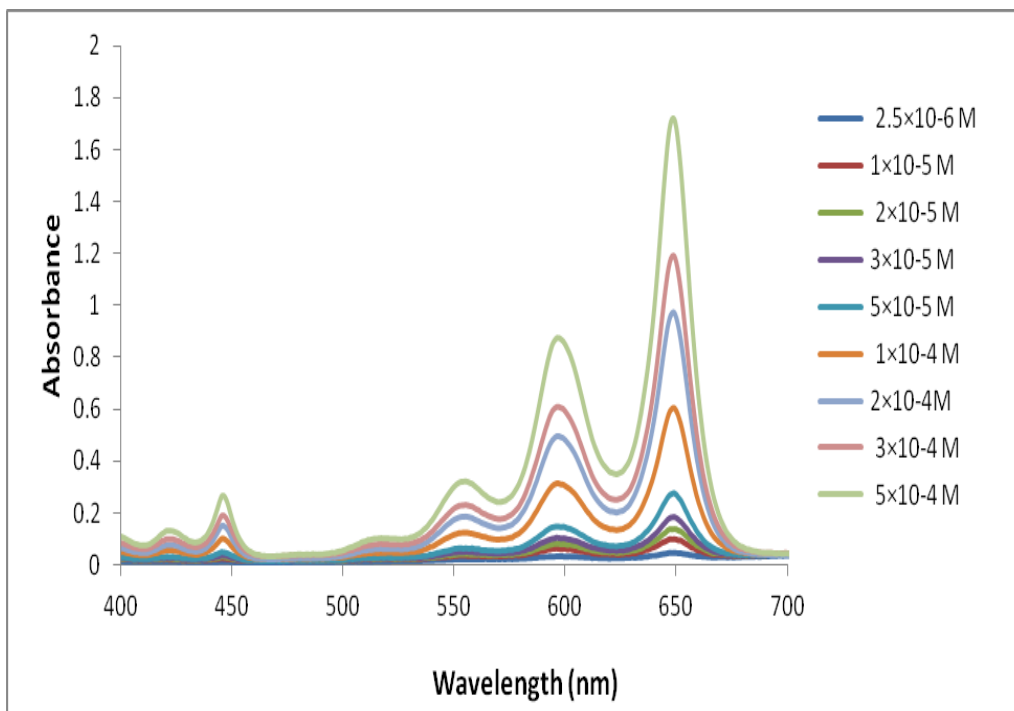


Figure 4.1 :UV-visible absorption spectra of TIPS-pentacene in toluene solution at concentrations ranging from 2.5×10^{-6} M to 5×10^{-4} M in 1mm pathlength at 26°C.

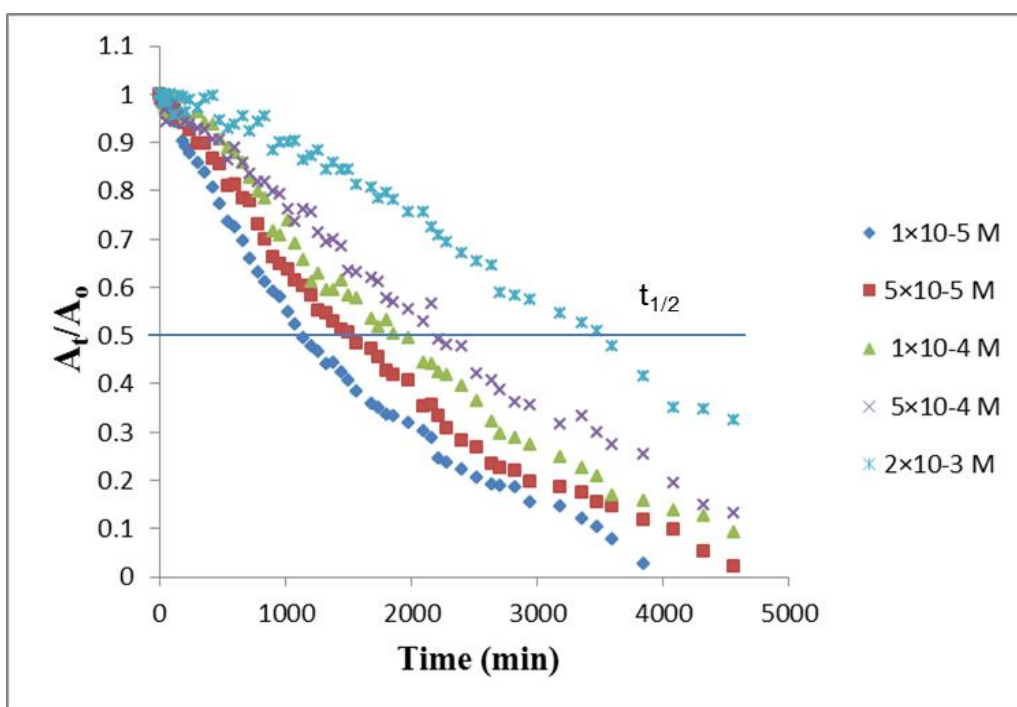


Figure 4.2: Normalised absorbance/time profiles for photooxidation of TIPS-pentacene in toluene solutions for a range of concentration at 26°C.

4.2 The effect of concentration on the photo-oxidative degradation kinetics of TIPS-pentacene at different solvents

Comparable decays were also measured in chloroform, dichloromethane, THF, IPA, dodecane and decane over the same concentration range and the half-life was estimated for each solvent (table 4.1). Note that the data range is limited by solubility in IPA, decane and dodecane. Figure 4.3 shows a summary plot of half-life data for TIPS-pentacene photo-oxidation at concentrations ranging from 2.5×10^{-6} M to 5×10^{-2} M. For all solvents, shortest lifetimes are observed for lowest concentrations, with lifetime increasing as concentration increases. For a number of solvents, the curves show inflection, typically between 5×10^{-5} M and 5×10^{-4} M. This is particularly pronounced in the case of the chlorinated solvents and toluene.

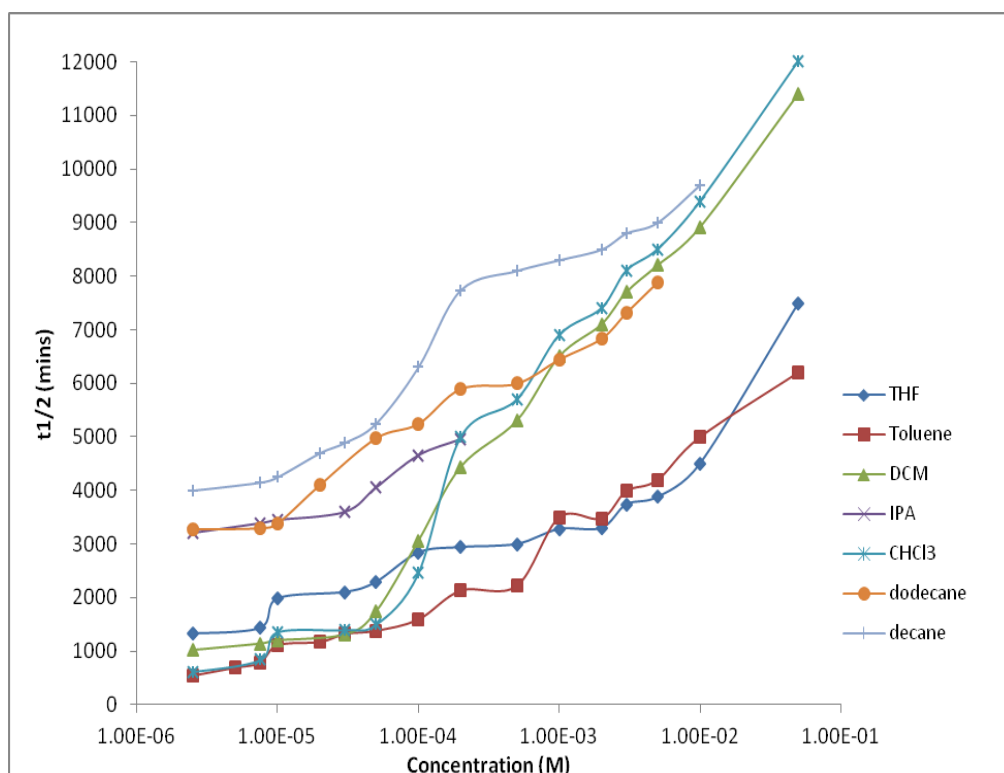


Figure 4.3: Variation of half-life ($t_{1/2}$ min) as function of concentration (M) of TIPS-pentacene in a variety of solvents between 2.5×10^{-6} M to 2×10^{-2} M at 26°C .

Table 4.1: Comparison of experimental $t_{1/2}$ (min) of TIPS-pentacene in toluene, THF, chloroform, DCM, IPA, dodecane and decane at different concentration at 26°C, the (*) solubility limit.

Con. (M)	Toluene	THF	Chloroform	DCM	IPA	Dodecane	Decane
2.5×10^{-6}	827.5 +/-575 (540- 1115)	1320	620	1020	210	3280	4000
5×10^{-6}	690						
7.5×10^{-6}	990 +/-420 (780-1200)	1430	840	1140	3390	3300	4150
1×10^{-5}	1205 +/-190 (1110-1300)	1980	1550 +/-380 (1360- 1740)	1200	3450	3390	4230+/-540 (3960-4500)
2×10^{-5}	1170					4110	4700
3×10^{-5}	1320	2100	1400	1310		4300	4890
5×10^{-5}	1380	2220	1500	1740	4050	4725 +/- 510 (4980- 4470)	5250
1×10^{-4}	1590	2840	2460	3060	4650	5250	6300
1.5×10^{-4}	1680						
2×10^{-4}	2145 +/- 30 (2130-2160)	2940 +/-180 (3120-2760)	5000	4440	4950	5900	7740
5×10^{-4}	2220	3000	5700	5300	*	6000	8100
1×10^{-3}	3500	3280	6900	6500	*	6450	8300
2×10^{-3}	3480	3300	7400	7100	*	6840	8500
3×10^{-3}	3990	3740	8100	7700	*	7320	8800
5×10^{-3}	4200	3880	8500	8200	*	7890	9000
1×10^{-2}	5000	4500	9390	8910	*	9330	9700
5×10^{-2}	6210	7500	12000	11400	*	*	*

Figure 4.4 shows a summary plot of $\ln(A_t/A_0)$ versus time for TIPS-pentacene photo-oxidation at concentration ranging from 1×10^{-5} to 2×10^{-3} M in toluene solution. The variation of $\ln(A_t/A_0)$ with time can be seen to approximately linear up to concentration around 2×10^{-4} M. Within this concentration range, the kinetics of the photodegradation process is effectively first order. Above this concentration, up to the solubility limit (e.g. $\sim 2 \times 10^{-3}$ M), the relationship between $\ln(A_t/A_0)$ and time is nonlinear and the kinetics of oxidation are no longer first order. Given the known tendency of acenes to aggregate in solution [114]. It seems likely that this behaviour reflects the onset of substantial aggregation formation.

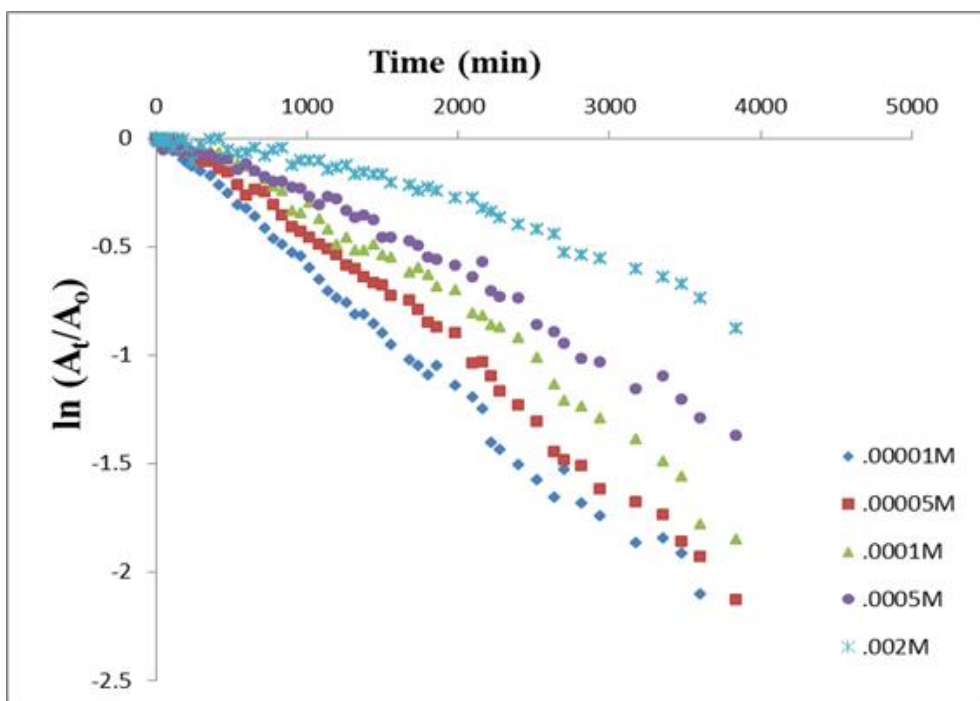


Figure 4.4: Plot of $\ln(A_t/A_0)$ versus time for TIPS-pentacene in toluene solution at different concentrations at 26°C.

4.3 Experimental observations of TIPS-pentacene in solution as a function of concentration

Recent reports have shown evidence of concentration dependent TIPS-pentacene aggregation behaviour in a good solvent solution and it was found that aggregates can be observed in solution well before the solubility limit at very high concentration [114]. Here evidence is given of aggregation behaviour of TIPS-pentacene in good and bad solvents by different techniques, including fluorescence spectra, isothermal titration calorimetry (ITC) and small angle x-ray scattering (SAXS).

4.3.1 Fluorescence spectra of TIPS-pentacene in solution

Fluorescence spectra for TIPS-pentacene in different solvents over a range of concentrations in a 10 mm pathlength cuvette were obtained at excitation wavelengths of 643nm and 550 nm (the two longest wavelength maxima in the absorption spectra from the $S_0 \rightarrow S_1$ transition). These are characterized by fluorescence in the 650-750 nm range as shown in figures 4.5 and 4.6. Two bands are present, one centred on ~ 650 nm and one at 709 nm. The lower wavelength band is observed to shift to longer wavelength as concentration increases, as shown in figure 4.7, whilst the 709 nm band does not shift at all. Given the wavelength, the ~ 650 nm band is undoubtedly the $S_1 \rightarrow S_0$ ($v''=0 \rightarrow v'=0$) transition, with the wavelength shift being due to pairwise interactions in the solution with increasing concentration. The origin of the 709 nm band and the reason why it does not shift with concentration is unclear and will require further experiments (currently underway).

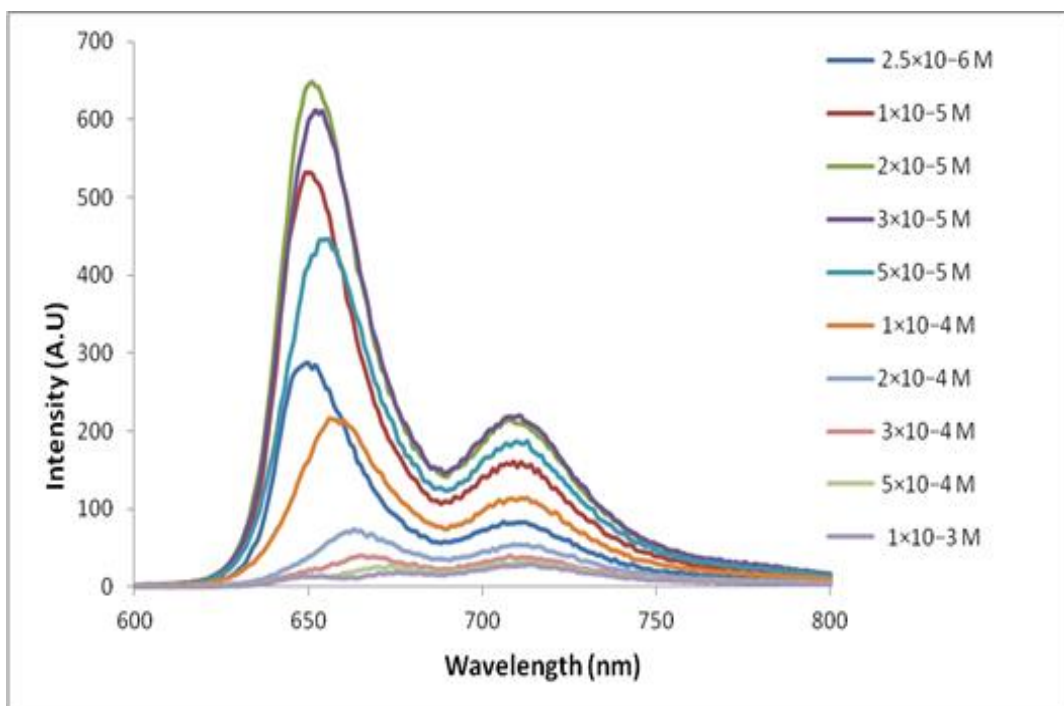


Figure 4.5: Fluorescence emission intensity of TIPS-pentacene in toluene at concentrations ranging from 2.5×10^{-6} M to 1×10^{-3} M in 10mm pathlength cuvette (excitation at 643nm).

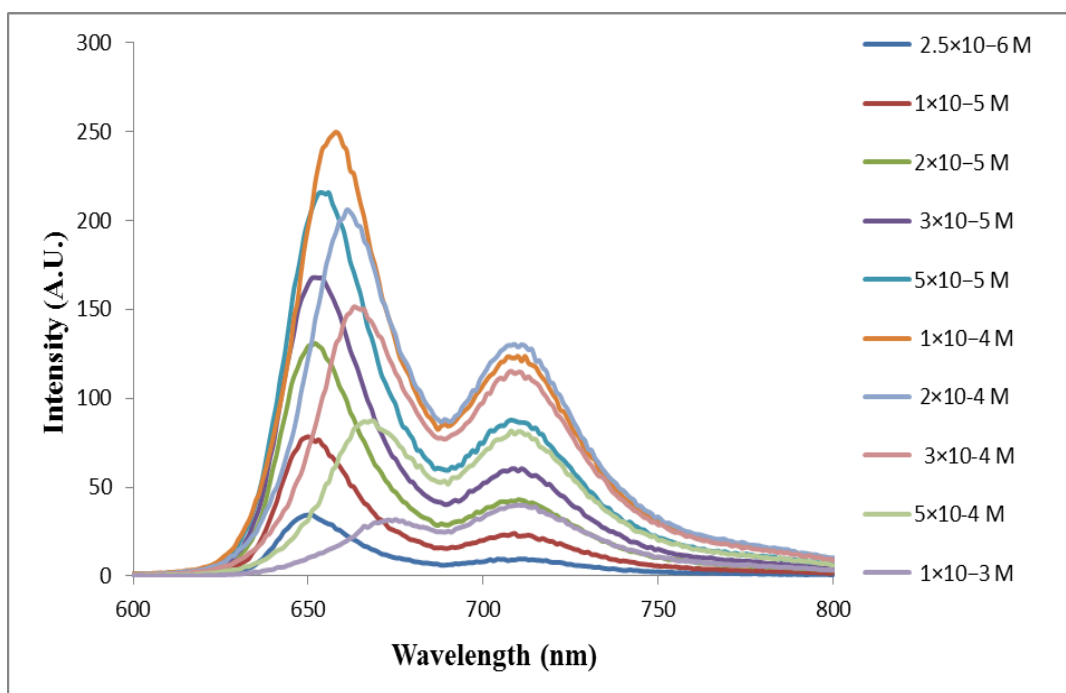


Figure 4.6: Fluorescence emission intensity of TIPS-pentacene in toluene at concentrations ranging from 2.5×10^{-6} M to 1×10^{-3} M in 10mm pathlength cuvette (excitation at 550nm).

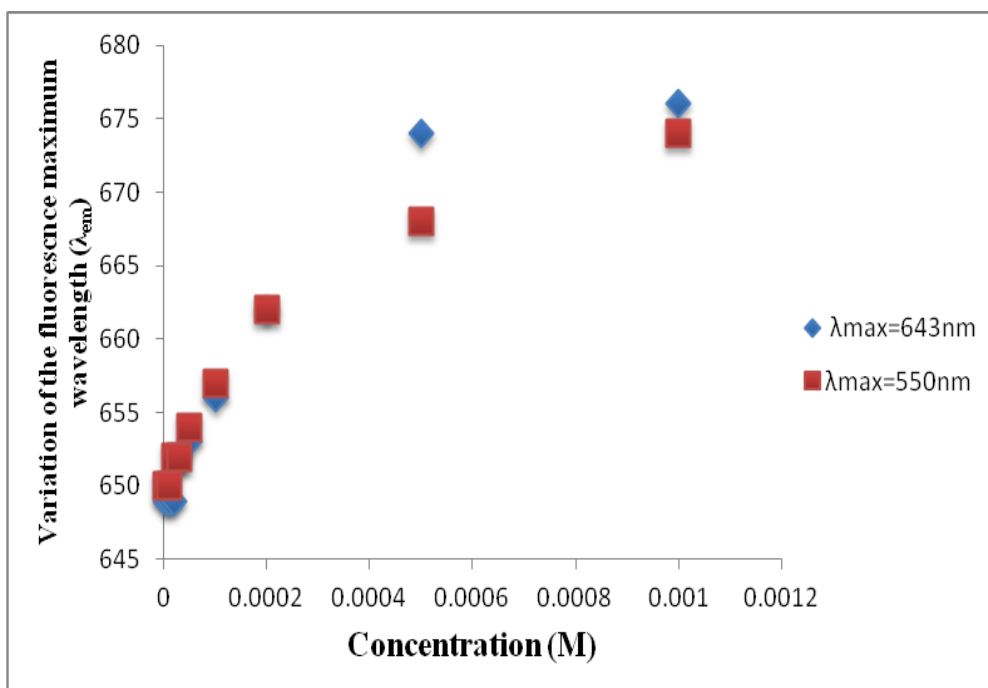


Figure 4.7 : Variation of the wavelength of the maximum fluorescence intensity of TIPS-pentacene in toluene at concentrations ranging from 2.5×10^{-6} M to 1×10^{-3} M for the ~ 650 nm emission band for excitation at 643 and 550 nm.

Figures 4.8 and 4.9 have shown the variation of fluorescence intensity of both bands as a function of TIPS-pentacene concentration. Figure 4.8 shows the results for the 650 nm band, where excitation at 643 nm results in an initial sharp increase as concentration increases, followed by a rapid decay as the concentration exceeds 3×10^{-5} M. In comparison, the emission intensity for excitation at 550 nm shows a more gradual increase with maximum intensity at around 1×10^{-4} M. A slower decay with increasing concentration follows, with emission intensity being approximately equal for both excitation wavelengths at the highest concentration (1×10^{-3} M). The intensity of the 709 nm band shows exactly the same trend (figure 4.9).

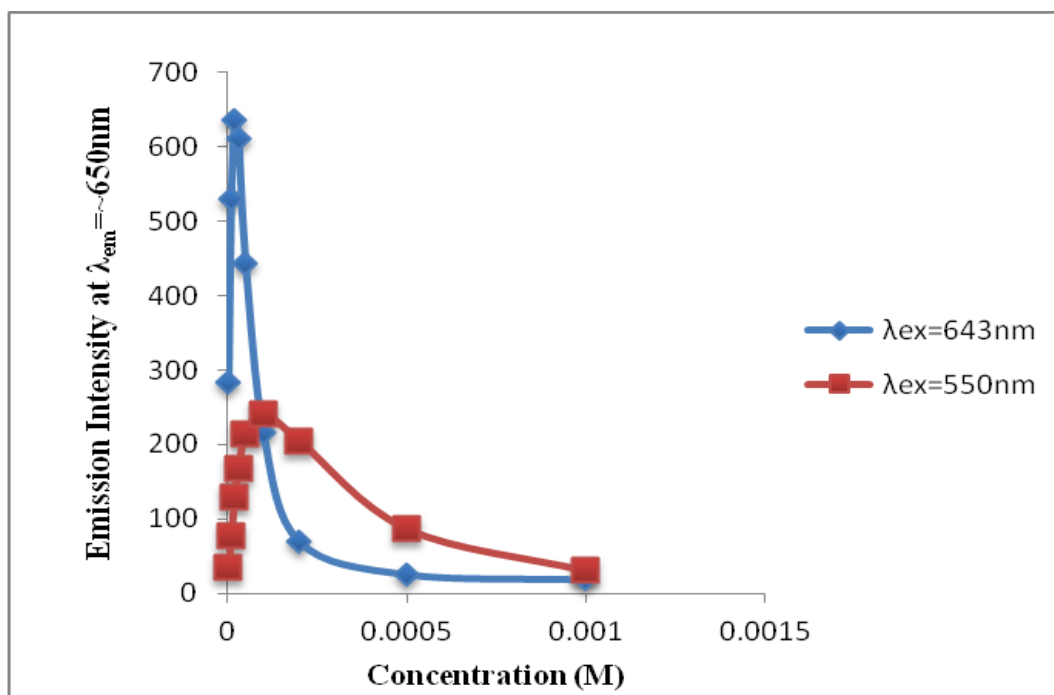


Figure 4.8: Variation of the fluorescence intensity of TIPS-pentacene in toluene between 2.5×10^{-6} M to 1×10^{-3} M for the ~ 650 nm emission band for excitation at 643 and 550 nm.

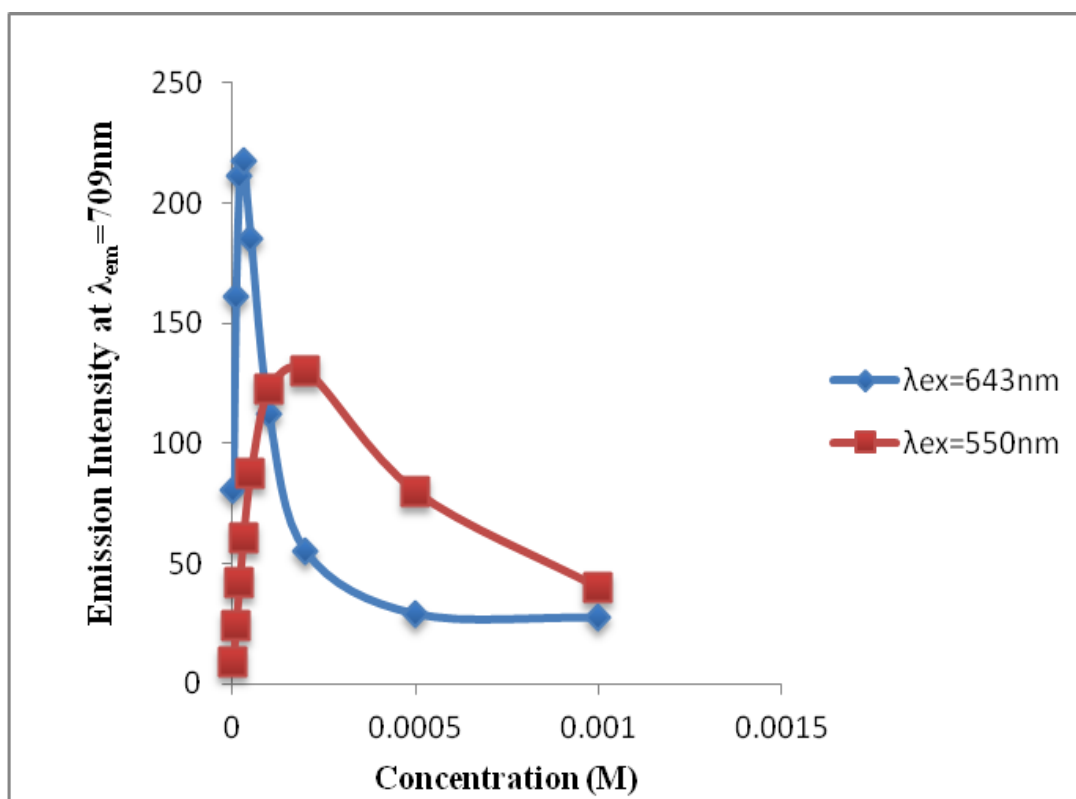


Figure 4.9 : Variation of the fluorescence intensity of TIPS-pentacene in toluene between 2.5×10^{-6} M to 1×10^{-3} M for the 709 nm emission band for excitation at 643 and 550 nm.

The fact that both bands display exactly the same intensity versus concentration behaviour (regardless of excitation wavelength) suggests that they arise from the same species, i.e. they are not due to, say, monomer and dimer. It is likely that they both arise from the monomer, initially increasing in intensity with increasing concentration as the number of monomers increases. As nearest neighbour interactions start to occur, fluorescence becomes less favourable as energy transfer to neighbouring molecules starts to occur and hence the fluorescence intensity decreases with further increase in concentration (cf. the kinetic scheme in chapter 3). A possible explanation for the behaviour of the fluorescence emission with excitation at 550 nm is that the initial excitation at this wavelength produces an electronically and vibrationally excited molecule, which needs to relax before fluorescence emission. In this case, the excited molecule may be less susceptible to pairwise de-excitation and so fluorescence emission is seen to higher concentration. Further evidence to support this suggestion is that fluorescence from both excitation wavelengths collapses to the same value at higher concentrations when pairwise interactions and aggregation become much more significant.

4.3.2 ITC of TIPS-pentacene

A good way of examining the thermodynamics of particles in solution (micelles or aggregates) is isothermal titration calorimetry (ITC). For example, it is a well-known phenomenon that surfactants form micellar aggregates in liquid solution. The micelles' aggregation number (number of compounds per micelle) is high in water but low in nonaqueous solution, and decreases with temperature and increases with concentration [124]. Basically, the surfactant structure consists of a lipophilic group (polar head) and a hydrophilic part (the non-polar hydrocarbon chain). In the dilute water solutions, the strong hydrophobic nature makes the molecules stick to the interface with air, keeping the polar head in solution while the hydrophobic chain is airborne. When the concentration of surfactant is high, the molecules in the bulk liquid gather and micelles with the polar heads on the outer surface of the aggregate to protect the non-polar alkyl chains. The concentration at which these micelles are formed is called Critical Micellar Concentration (CMC) [125].

In ITC experiments, CMCs are calculated by a change in a given measured macroscopic property as a function of concentration. Positive peaks represent endothermic processes, as the heat signal recorded is the heat supplied by the control system of the calorimeter. If the injection developed exothermic heat, the control system would have to remove heat from the cell and the heat signal recorded would be negative. The enthalpogram can be divided into three regions: first, a plateau of high developed, in which the micelles break because the concentration in the cell is below CMC. Second, a transition region appears, which corresponds to the CMC. Third, at cell concentration higher than CMC, a plateau of low heat developed is observed, which is related only to the dilution of micelles. The inflexion point in the curve is assigned to the CMC and it can be calculated by the plot of heat of mixing versus concentration [125, 126]. The advantage of ITC is allowed the determination of both the Critical Micellar Concentration (CMC) and enthalpy of surfactant micellation in one single experiment. The determination of CMC at several temperatures allows the calculation of the free energy and also the entropy, giving a complete thermodynamic characterization of surfactant micellation. For example of titration of surfactants is sodium dodecyl sulphate (SDS) in water as shown in figure 4.10. The value of CMC of (SDS) using ITC is 2.4 g/L, and the enthalpy of micellization (ΔH_{mic}) is usually calculated as the difference between the two plateaus of the first third region and it reported -2.7 kJ/mol [125].

This work reports our experiences with ITC in the investigation of association and interaction of TIPS-pentacene in toluene solution. Isothermal titration calorimetry (ITC) has previously supported the observation of aggregation in TIPS-pentacene in toluene solution at concentrations above 1×10^{-5} M [114].

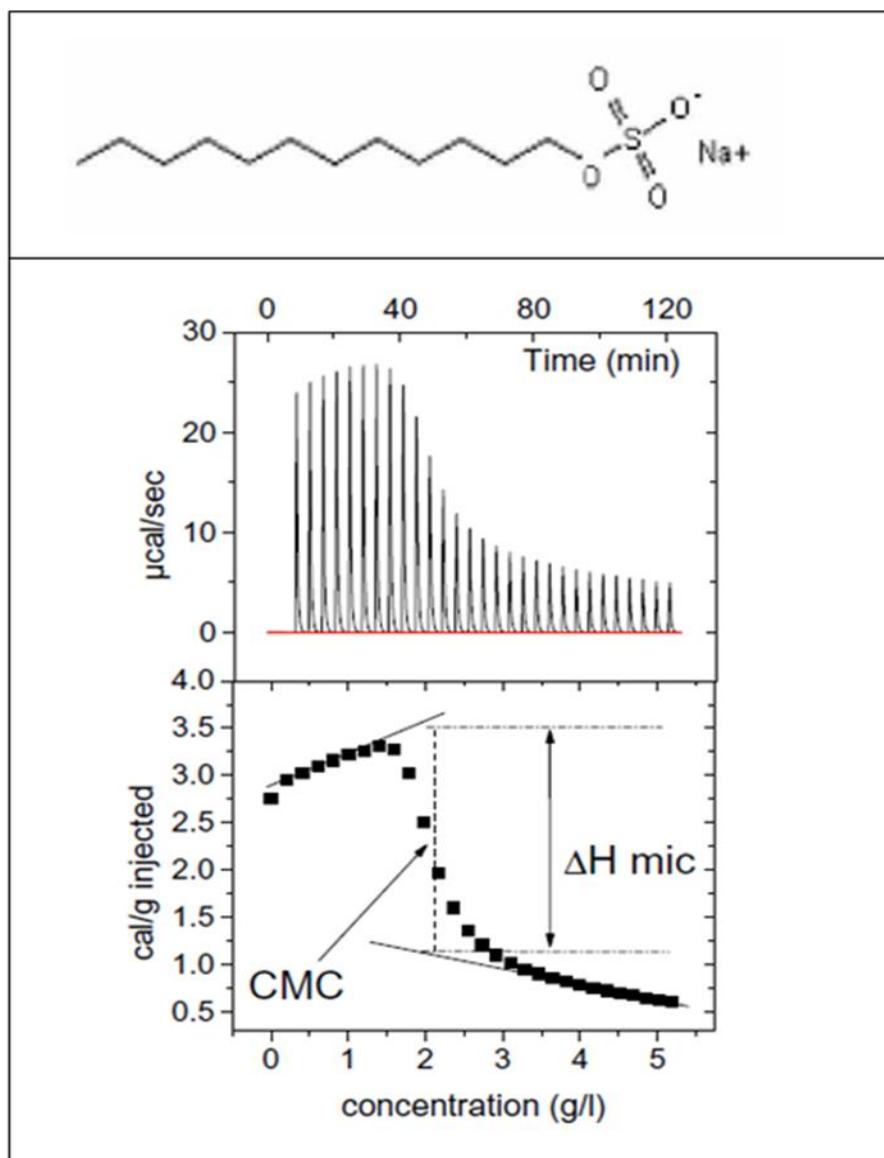


Figure 4.10: The chemical structure of sodium dodecyl sulphate (SDS), and Titration of 30g/l of sodium dodecyl sulphate (SDS) in water at 30°C [125].

Figures 4.11, 4.12 and 4.13 show the data obtained in the titration of TIPS-pentacene in toluene. The first chart (a) displays the raw data heat detected by ITC. The positive peaks indicate that the dilution is endothermic at 25°C. The integration of the area below each peak gives the heat developed per injection (the enthalpy profile obtained from the integration of each individual peak), as shown in the second chart (b) in figures 4.11, 4.12 and 4.13. Figure 4.11 shows the titration of TIPS-pentacene at low concentration (1×10^{-5} M) in toluene solution, the heat developed decreases with increasing concentration in the cell. There is not a first region in which the heat developed is constant.

The absence of this plateau suggests that TIPS-pentacene do not have an aggregation point (equivalent to a CMC) in this concentration region. Figure 4.12 shows the enthalpograms of TIPS-pentacene at concentration 2×10^{-4} M, the behaviour observed is the same with no plateau at low concentration and the heat developed linear. The heat developed depends on the syringe concentration, which is due to the gradual change in the aggregation number of TIPS-pentacene with increasing concentration. The enthalpogram shows that, as the concentration in the cell increases, the heat developed has an exponential decay, due to the fact that the solution in the cell becomes more similar to the one in the syringe and less aggregates dissociate. However, titrations with different syringe concentration of TIPS-pentacene at 2×10^{-3} M show that the heat developed injected increases with concentration, which implies aggregates of TIPS-pentacene are present at this concentration as shown in figure 4.13. As a result ITC experiments, it is observed that there is not an initial region of constant heat developed when the solution of TIPS-pentacene is injected into the cell and the concept of CMC is not applicable to TIPS-pentacene in solution. However, it presents a similar behaviour to asphaltenes in toluene solution, that is to say, they seem to associate step-wise and the aggregation number is too small to consider TIPS-pentacene aggregates as typical micelles[125].

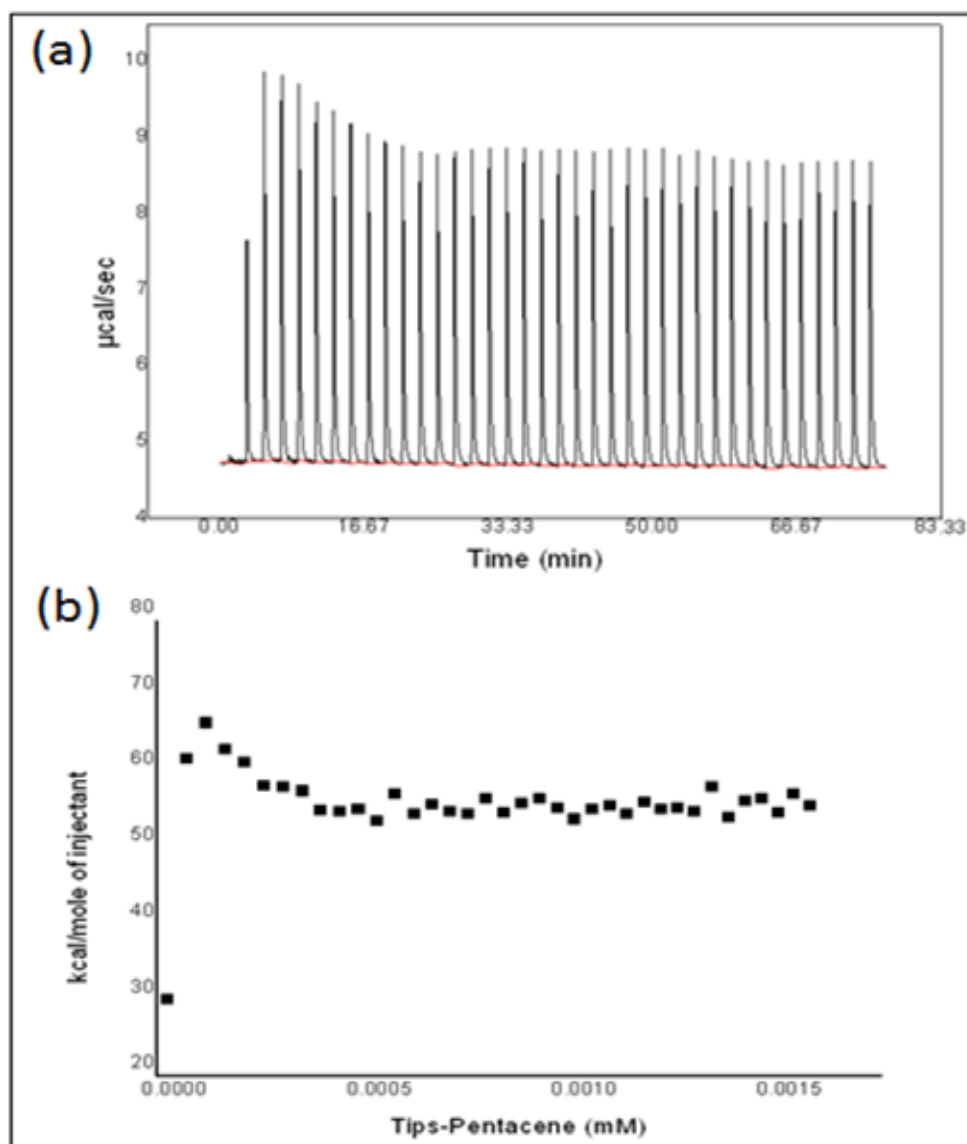


Figure 4.11 : ITC raw heats (a) and the ITC thermogram (b) of TIPS-pentacene in toluene solution at concentration 1×10^{-5} M in 25°C .

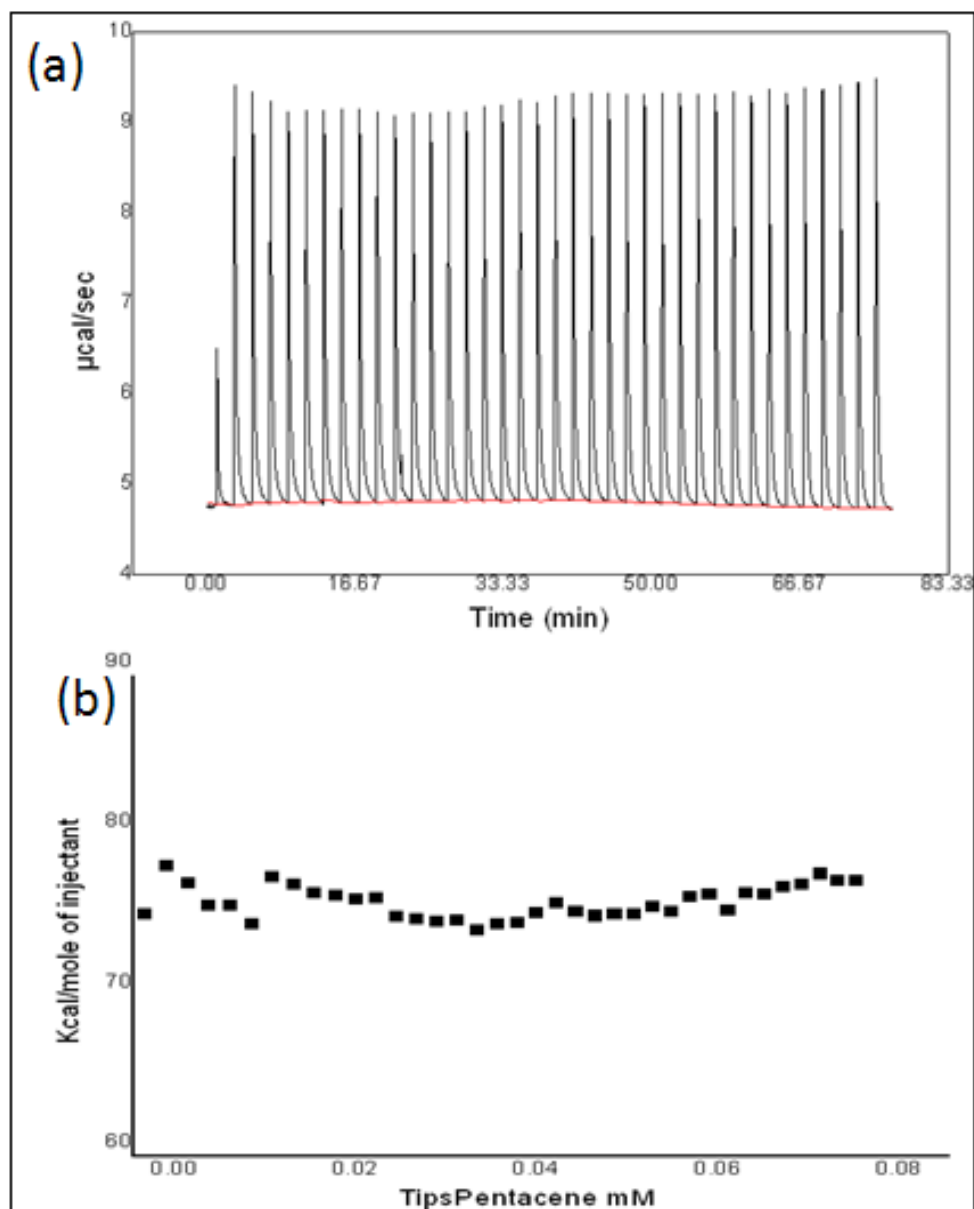


Figure 4.12: ITC raw heats (a) and the ITC thermogram (b) of 5×10^{-4} M TIPS-pentacene in toluene at 25°C .

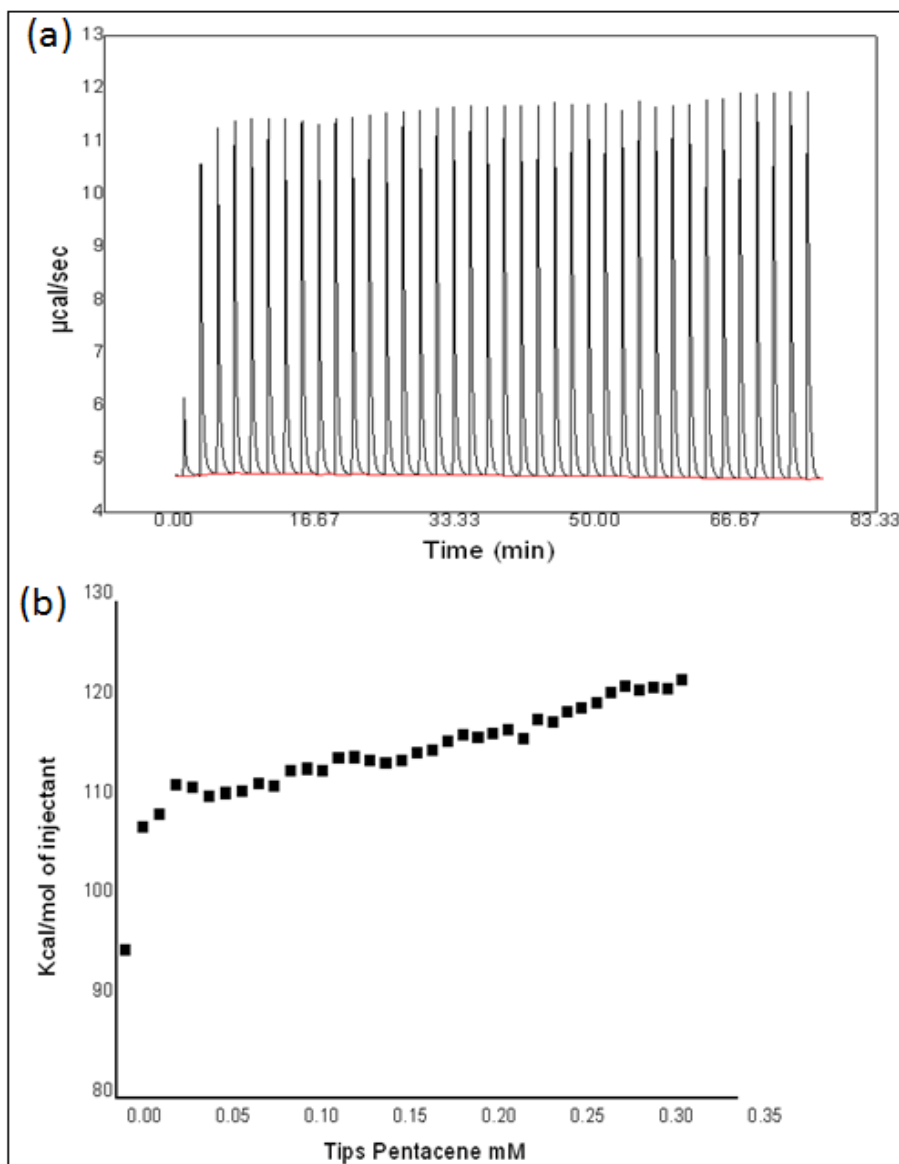


Figure 4.13: ITC raw heats (a) and the ITC thermogram (b) of 2×10^{-3} M TIPS-pentacene in toluene at 25°C .

4.3.3 Small-Angle X-ray scattering (SAXS)

In this work, small angle x-ray scattering was used to study aggregation of TIPS-pentacene in different concentrations and in different solvents. However, the SAXS results for TIPS-pentacene are not very revealing, as hard evidence for aggregation is not present in most samples. However, the SAXS curve of TIPS-pentacene in DCM at a concentration of 1×10^{-3} M appears to be composed of small aggregates. The intensity curves $\log I(q)$ vs q^2 (shown in figure 4.14) show a peak corresponding to ($q^2 = 3.6 \text{ \AA}^{-2}$), from which $\theta = 6.6^\circ$ according to equation (2.8). From reference [127] such a peak at 6.6° corresponds to the 001 peak from crystalline TIPS-pentacene .

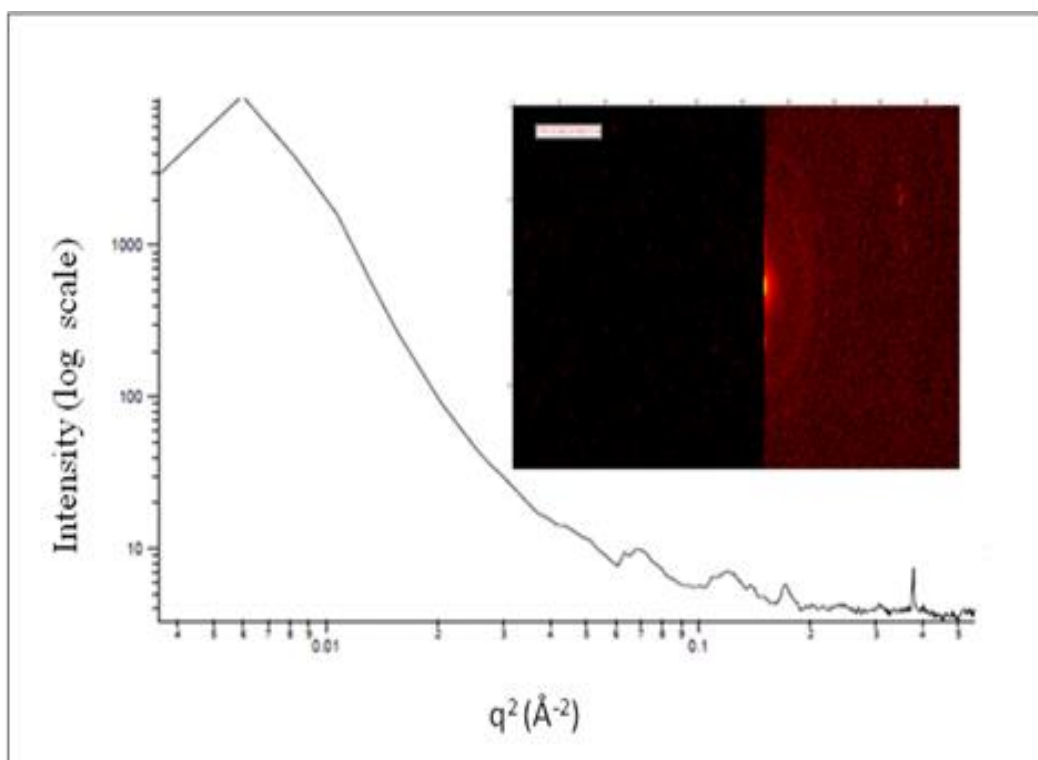


Figure 4.14: A 2-Dimensional scattering detector image, and experimental SAXS data from TIPS-pentacene in DCM solution at concentration 1×10^{-3} M at 25 °C.

4.4 Models and mechanisms for TIPS-pentacene photodegradation

In this section, a variety of factors which are likely to play a role in the determination of TIPS-pentacene lifetime in solution are considered.

4.4.1 Interaction distance and oxygen solubility

As discussed in chapter 3, there is a positive correlation between half-life for TIPS-pentacene at low concentration with R_a determined across a range of solvents, such that to a first order when R_a is small, half-lives are comparably low and when R_a is large. Half-lives are comparably long as shown in figure 4.15. A second process was invoked to explain the reduction in the lifetime of the singlet state by quenching, for which dissolved oxygen is a prime candidate. Once again, a positive correlation exists between the concentrations of dissolved oxygen and half-life as shown in figure 4.16 for a concentration of 1×10^{-4} M, although again the correlation is not high. A clearer picture of the combination of these two processes can be seen from a plot of the product of the R_a and saturation oxygen solubility versus the half-life, as shown in figure 4.17 (which corresponds to that for 1×10^{-5} M given in chapter 3). However, at a concentration of 1×10^{-3} M as shown in figure 4.18 the correlation is poor. A possible reason for this cut-off point is aggregation, which appears to start as concentration exceeds $\sim 2 \times 10^{-4}$ M. It seems clear however that, at low concentration, the initial singlet state is deactivated by both intermolecular processes between TIPS-pentacene molecules and by quenching by dissolved oxygen.

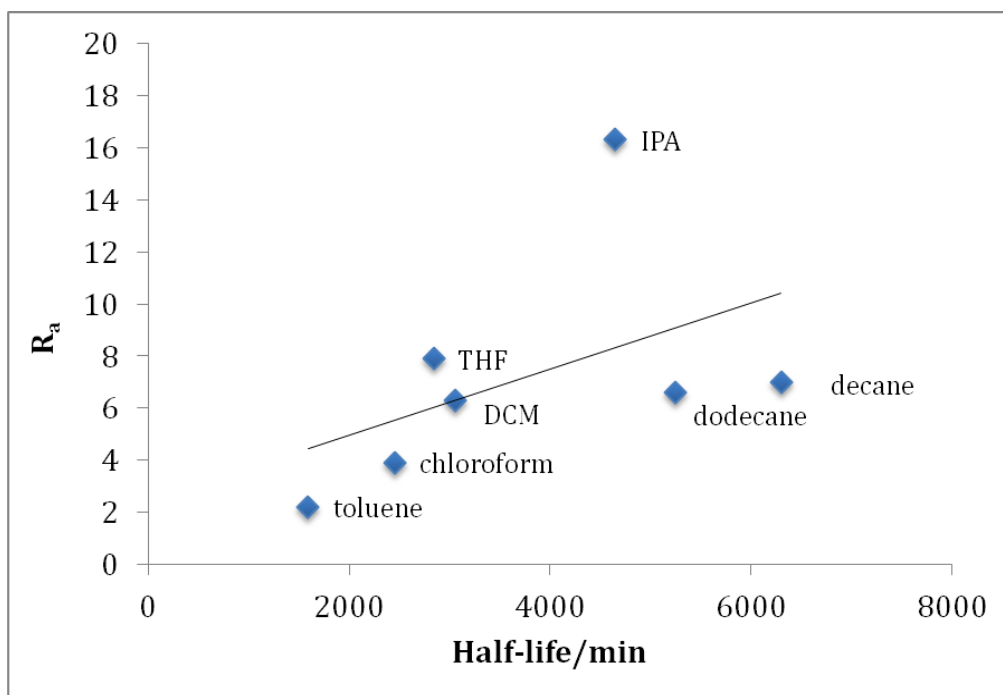


Figure 4.15: Plot of interaction distance (R_a) versus half-life of TIPS-pentacene in different solvents at a concentration of 1×10^{-4} M at 26°C .

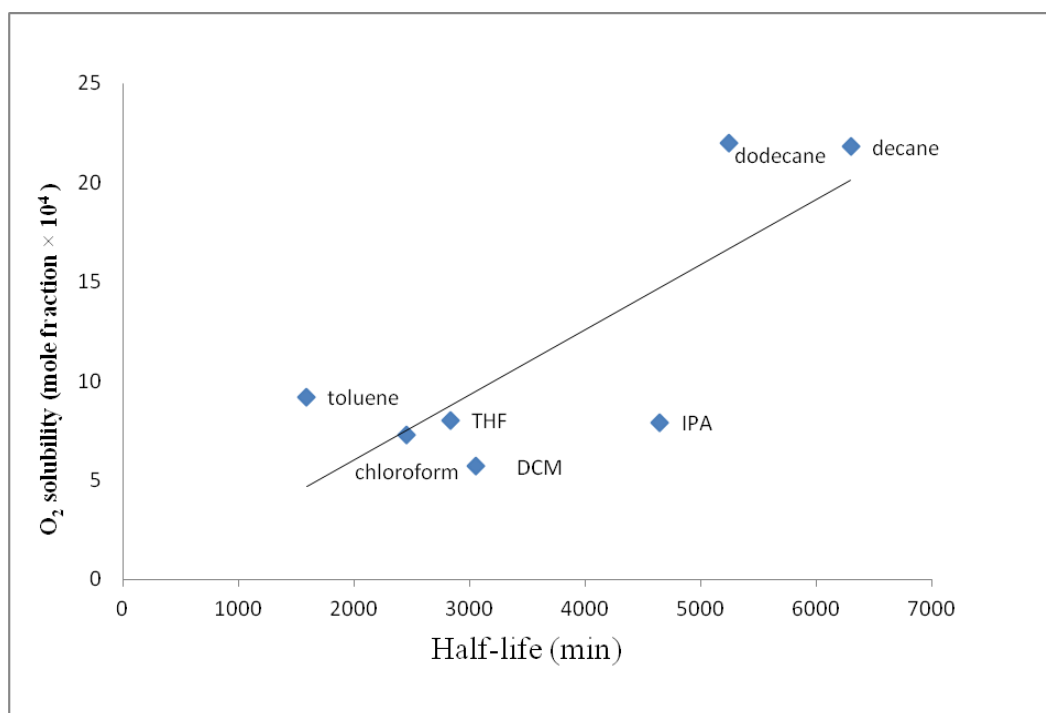


Figure 4.16: Plot of oxygen solubility (mole fraction $\times 10^4$) versus half-life of TIPS-pentacene in different solvents at a concentration of 1×10^{-4} M.

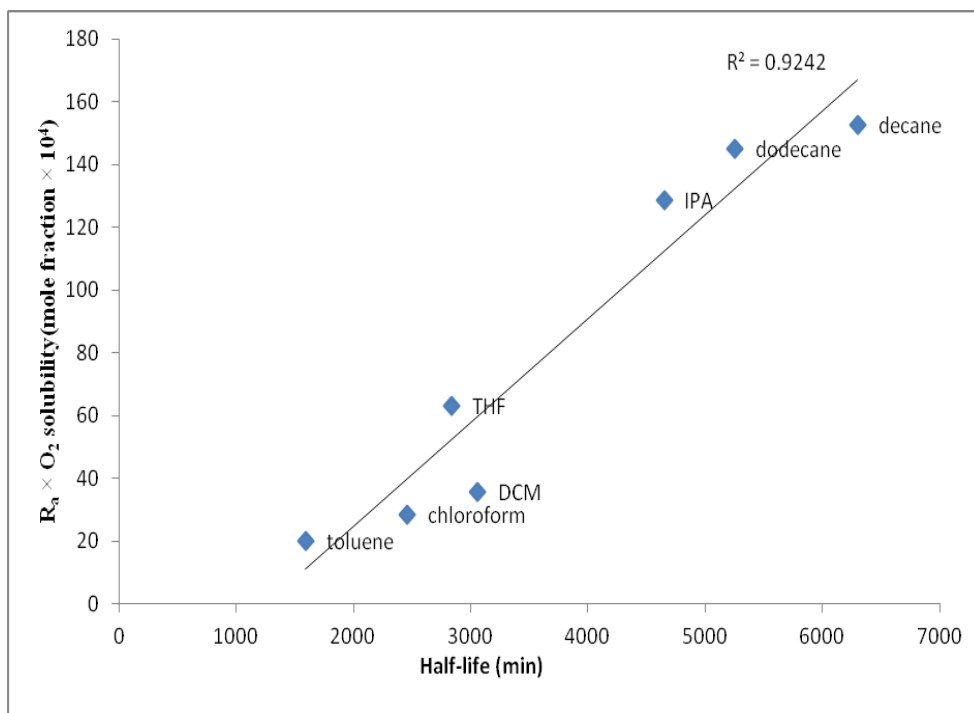


Figure 4.17: Comparison of interaction distance(R_a) \times oxygen solubility (mole fraction $\times 10^4$) versus half-life of TIPS-pentacene in different solvents at a concentration of 1×10^{-4} M.

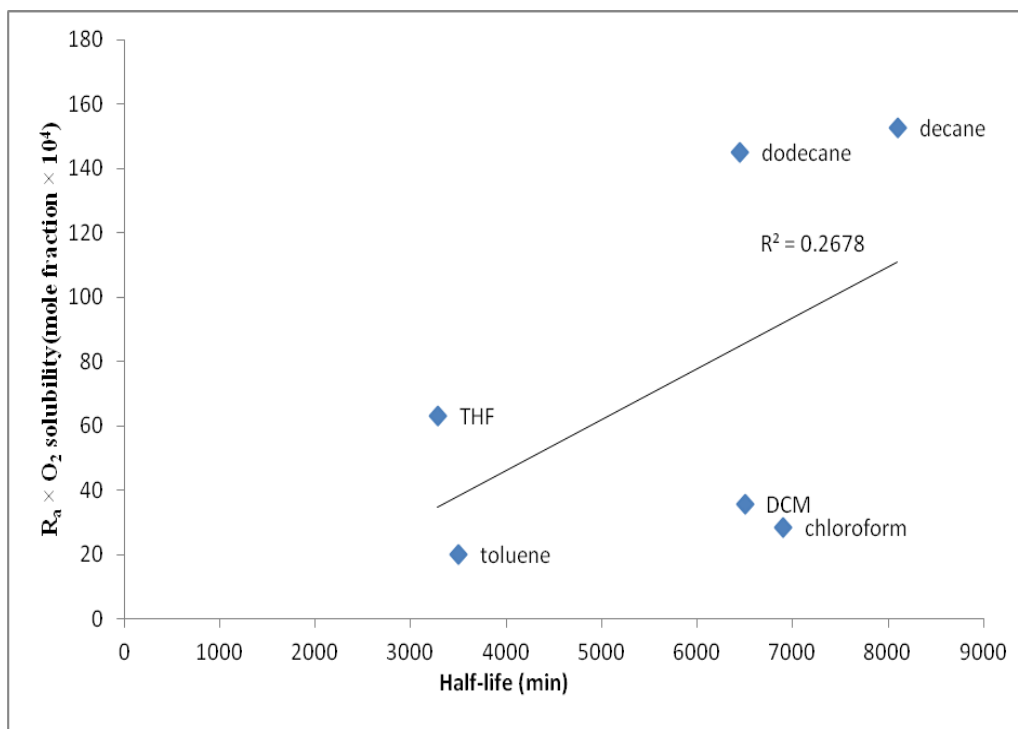


Figure 4.18: Comparison of interaction distance (R_a) \times oxygen solubility (mole fraction $\times 10^4$) versus half-life of TIPS-pentacene in different solvents at a concentration of 1×10^{-3} M.

4.4.2 Aggregation of TIPS-pentacene in solution

Aggregation is likely to have two principal effects upon photo-degradation: first, since proximity to another TIPS-pentacene molecule serves to deactivate the initial excited singlet, molecules associated with aggregates (either on the surface or within the bulk) are therefore not susceptible to oxidation; second, any molecule within an aggregate is physically separated from O₂ in solution and therefore incapable of O₂-activation.

The mode of aggregation is also likely to play a role in determining the concentration-dependence of stability. There are two simple treatments of aggregation that can be considered here: isodesmic and cooperative [128-130]. Figure 4.19(a), displays the degree of aggregation (α) as a function of the concentration. Increasing the cooperativity has a clear influence on the growth profile of the aggregate species whereas for the isodesmic growth a gradual increase in aggregate species is observed with increasing concentration. Another remarkable feature of cooperative aggregation is its bimodal mass distribution which is the result of the presence of (non-activated) monomers and activated molecules that have rapidly elongated after activation as shown in figure 4.19(b). For both mechanisms the size distribution in the high molecular weight limit corresponds to a broad exponential distribution [128].

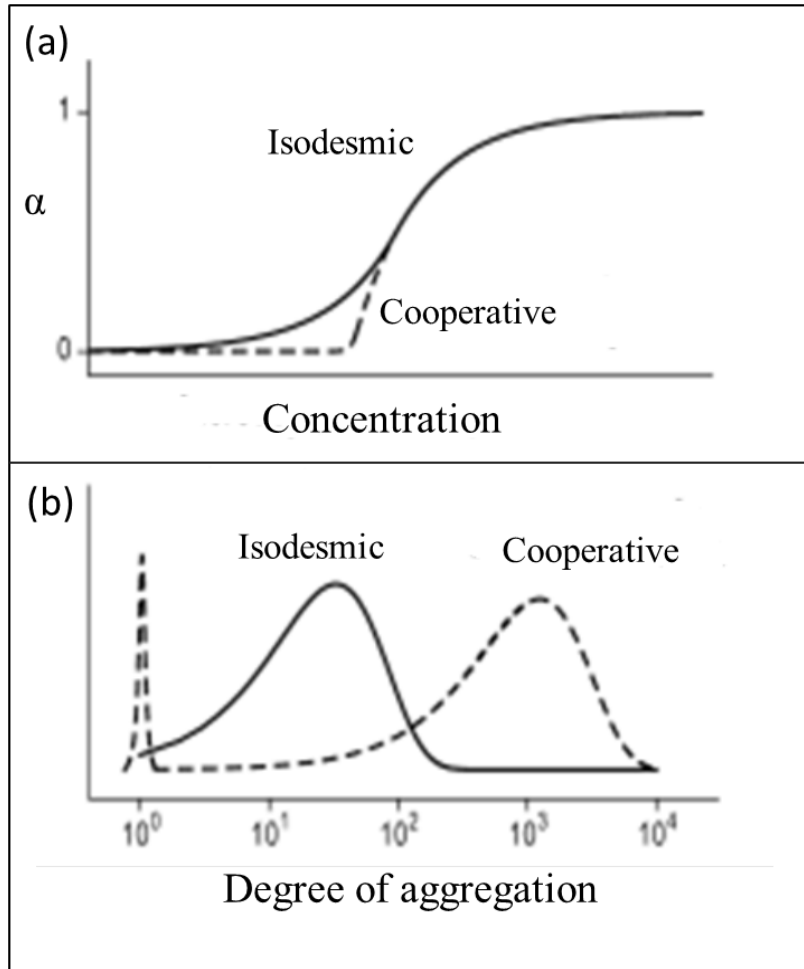


Figure 4.19: Schematic representation of the degree of aggregation versus concentration, (b) schematic molecular weight distribution for an isodesmic and cooperative aggregation mechanism [128].

4.4.3 Isodesmic aggregation model

The isodesmic (equal K) model, assumes that a range of aggregate sizes are formed from successive linear aggregate pairs M_{n-1} and M_n in equilibrium as follows:



Where, M represents a monomer. If the equilibrium constants K (M^{-1}) for each successive addition step are equal, the residual monomer concentration C_1 as a function of total concentration C_T is given by:

$$C_1 = \frac{2KC_T + 1 - \sqrt{4KC_T + 1}}{2K^2C_T} \quad 4.2$$

From this, the normalised residual monomer concentration for each value of the total concentration can be obtained from the ratio C_I/C_T , or the corresponding value, the degree of aggregation can be extracted. This procedure requires a value of K to be chosen. According to the literature, this can vary over a wide range and is of course also dependent upon solvent and temperature. The value of K can be extracted from data fitting with variation of either temperature or concentration if the aggregation is purely isodesmic. A linear fit of half-life to residual monomer concentration for relevant solution concentrations should therefore give K . In this case, it was not found possible to fit the entire data range for a single value of K , with curvature at either end of the data for any chosen value of K .

If the aggregation is isodesmic therefore, the aggregation occurs by equilibrium between free monomer and a series of successively higher numbers (dimer, trimer, tetramer etc.) with a single equilibrium constant for the addition of a further monomer to each number. In this case, the number of molecules which are aggregated (i.e. from dimers upwards) increases with concentration according to a predictable model (with a dependence upon the choice of K , which is not known a priori but requires the data to be fitted). If deactivation is linked to isodesmic aggregation, the half-life should therefore scale linearly with the proportion of non-aggregated molecules (if an appropriate value of K is used). However, there is no value of K that allows the data to be fitted across the entire concentration range for any solvent as shown in figure 4.20.

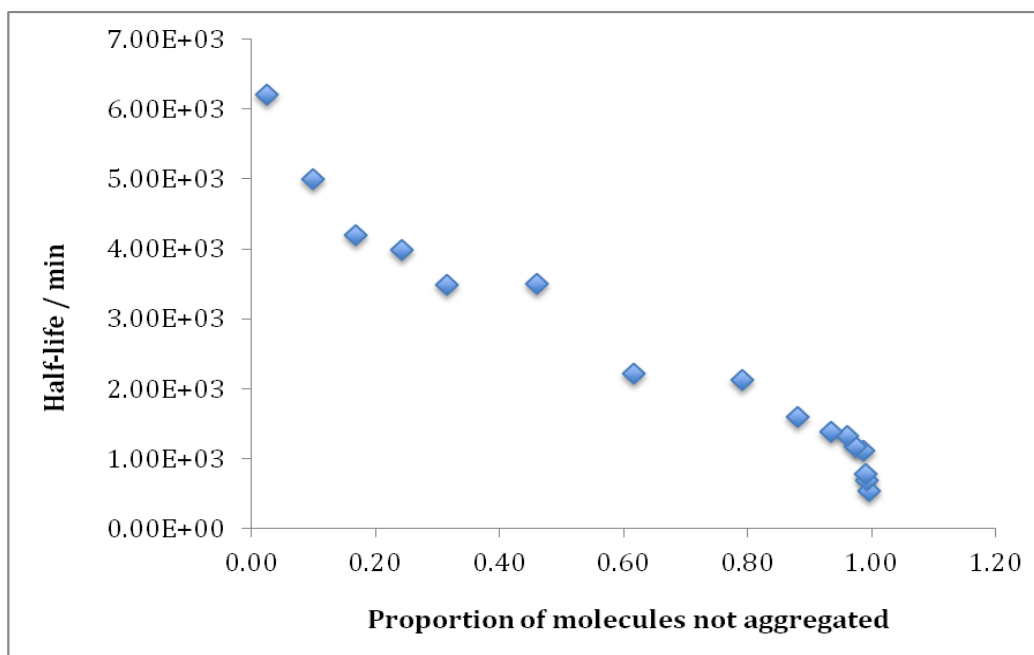


Figure 4.20: Plot of half-life versus time for TIPS-Pentacene in toluene at concentrations ranging from 2.5×10^{-6} M to 5×10^{-2} M using $K = 1000 \text{ M}^{-1}$.

4.4.4 Cooperative aggregation model

An alternative model for aggregate formation, termed cooperative aggregation, involves two separate steps: initial monomer-dimer equilibrium with K' and subsequent chain extension steps as for the isodesmic model with equilibrium constant K . The behaviour of the resulting model depends strongly upon the relative values of the two equilibrium constants. If K' is larger than K , dimer dominates over much of the concentration range whereas if K' is smaller, monomer dominates up to a critical concentration. Direct data fitting (concentration or temperature-dependent) is not possible for this model since it cannot be inverted to calculate the residual monomer concentration without knowledge of both K' and K . It is at low concentrations that these models differ; above the critical concentration, the degree of aggregation shows similar trend. Particularly in the case where K' is less than K , the solution at low concentration is dominated by monomer below the critical concentration. In this case, the proportion of aggregated molecules shows an onset threshold concentration above which aggregation occurs [128]. Given a definite onset of lifetime increase in the data for most of the solvents, this seems to suggest that cooperative aggregation exists in TIPS-pentacene solutions for most solvents.

4.4.5 Nearest Neighbour Interactions.

Studies of the photochemistry of TIPS-pentacene at a concentration around 1×10^{-4} M indicate that in the absence of O_2 the initial singlet excited state persists for no more than a few hundred femtoseconds, with the main route for de-excitation being singlet fission into two triplets (on adjacent TIPS-pentacene molecules). This occurs faster than fluorescence. The singlet fission process requires the proximity of a second TIPS-pentacene molecule, which implies that the efficiency of singlet fission should scale with nearest-neighbour distance in pure solvent, which in turn is a function of solution concentration.

An estimate of the nearest neighbour distance $D(x)$ as a function of solution concentration x (mol dm^{-3}) can be obtained from cube root of the concentration, i.e.

$$D = \sqrt[3]{\frac{1}{1000xN_A}} \quad 4.3$$

If this average nearest neighbour distance is viewed as relating to the probability that an acceptor molecule is in sufficiently close to participate in energy transfer, plotting the half-life against $D(x)$ should yield a straight line.

Figure 4.21 shows a plot of the half-lives versus mean intermolecular distance for the data presented in figure 4.3. The variation of lifetime with $D(x)$ can be seen to approximately linear up to concentrations around 5×10^{-4} M (corresponding to a nearest neighbour distance of $(1.5 \times 10^{-8}$ m). Within this concentration range, the kinetics of the photo-degradation process are effectively first order, as shown in figure 4.4 which is a plot of $\ln(A_t/A_0)$ versus time. From these observations, it is clear that the increase in half-life is (in part) due to an increase in the likelihood of a second TIPS-pentacene molecule being in sufficiently close proximity to participate in triplet formation (and thereby deactivate the singlet state in preference to energy/ electron transfer to O_2). Above this concentration, the half-life increases non-linearly up to the solubility limit and the kinetics of oxidation are no longer first order (e.g. the 0.002 M trace in figure 4.2).

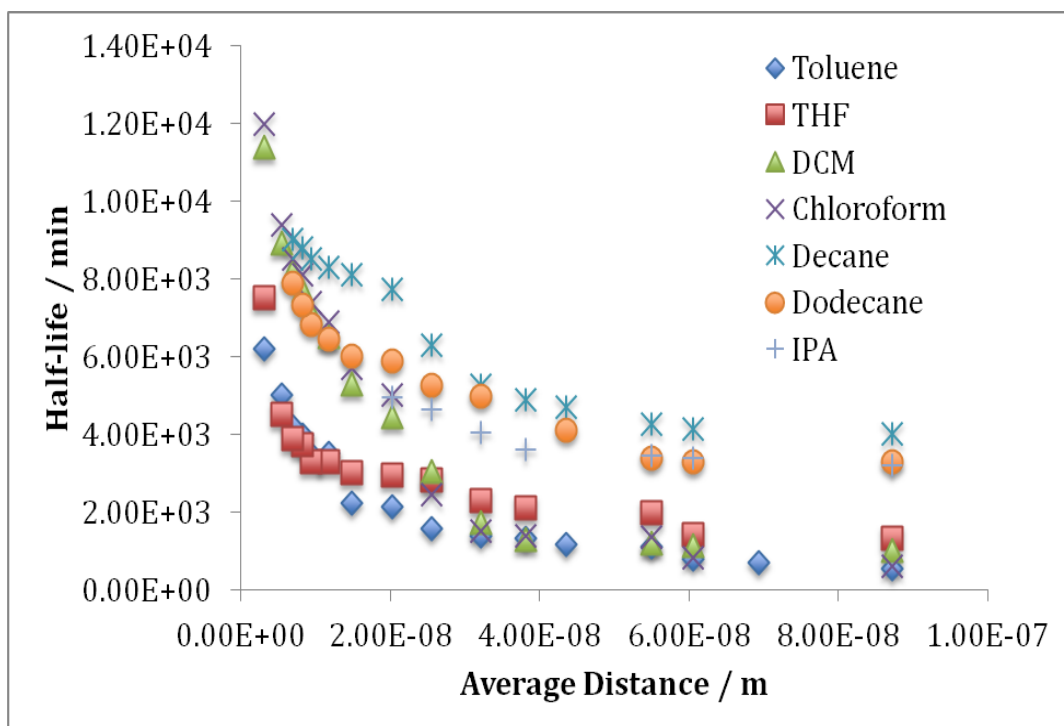


Figure 4.21: Variation of half-life versus average intermolecular distance between 2.5×10^{-6} M to 2.0×10^{-2} M at 25 °C.

4.4.6 Concluding remarks on concentration effects

In fact, it seems likely that this deviation from first-order behaviour at higher concentrations is due to several processes. Given the known tendency of acenes to aggregate in solution [114], this behaviour is in part related to the onset of aggregate formation. A sudden increase in aggregation should therefore be expected to be accompanied by an increase in half-life. Since this is what is observed here (particularly in the case of the chlorinated solvents, which show a substantial increase in half-life at 1×10^{-4} M), it is concluded that the perturbation which increases the half-life beyond that controlled by HSPs and quenching (both by nearest-neighbour interaction and O_2) is therefore cooperative aggregation with an onset around $2-5 \times 10^{-4}$ M, with some slight variation between solvents, compounded by the increasingly significant quadratic term for SF in the kinetic scheme. Indeed, the kinetics of aggregation should depend upon the solvent, with good solvent restricting aggregation (and may indeed have an influence on the mode of aggregation) and keeping TIPS-pentacene molecules uniformly distributed. It is not however possible to separate out such an effect from the data presented here and hence further studies are required.

In addition, the efficiency of singlet de-excitation by singlet fission is also dependent upon the concentration of a second TIPS-pentacene molecule, hence this process, effectively quadratic in [TIPS-pentacene] (see the kinetic scheme in chapter 3), should increase in importance with increasing concentration and move the kinetic behaviour towards second-order.

The linearity of the fit to nearest neighbour distance (which would be perturbed by concentration-dependent aggregation) and first-order kinetics suggests that the degree of aggregation is minimal at low concentrations. This generalization is further modified by variation of solubility, with the longer lifetimes in ‘poor’ solvent (i.e. larger difference in solubility parameters) being attributable to a greater number of TIPS-pentacene molecules in closer proximity to each other in an attempt to ‘avoid’ solvent. In ‘good’ solvent, the dispersion of TIPS-pentacene molecules is more regular throughout the solution and lifetimes are concomitantly shorter.

4.5 Conclusion

The concentration-dependent photooxidation stability in solution for TIPS-pentacene has been studied for a range of different solvents. For all solvents, shortest lifetimes are observed for lowest concentration, with lifetime increasing as concentration increases. Photo-excited (singlet) TIPS-pentacene has a lower probability of deactivation at low concentration and tends to preferentially undergo electron transfer to O₂ leading to EPO formation. Over the lowest concentration range, half-lives scale linearly with decreasing nearest neighbour distance. This effect is mitigated by poor solvent and by high oxygen solubility, which serve to deactivate the initial excited state by forcing solute molecules together (thereby increasing the efficiency of singlet fission) and quenching respectively. At higher concentrations, photostability is further increased by SF-based de-excitation as above and also by the formation of aggregates (which are both incapable of reacting with oxygen and also effectively quench the initial singlet state of TIPS-pentacene, as observed in condensed thin films [12]). In this case, this behaviour shows a specific onset point, suggesting a cooperative rather thanisodesmic aggregation mechanism in most solvents.

Chapter 5

5 Photochemical instability of other substituted pentacene derivatives

In this work, the effects of the chemical structure on the photo-oxidative degradation of TMTES-pentacene and fluorine substituted TIPS-pentacenes and referenced them against unsubstituted one structure of all shown in figure 2.1. Higher photochemical stability of fluoro compounds may be attributed to the electron-withdrawing fluorine on the aromatic, creating more stable molecules. This follows reports that substitution of pentacene with electron- withdrawing chlorine leads to substantially longer-lived species that are also more resistant to photo-oxidation than TIPS-pentacene [59].

5.1 Effect the solvent on rate of photo-oxidative degradation of pentacene derivatives at low concentration

5.1.1 Effect the solvent on rate of photochemical instability of α - mono-Fluoro-TIPS-pentacene

The photo-stability of α -mono-Fluoro-TIPS-pentacene was studied in different solvents. The UV-vis absorption spectra of α -mono-Fluoro-TIPS-pentacene at 1×10^{-5} M in these solvents is shown in figure 5.1. It shows that the λ_{max} values of the longest wavelength absorption are observed to vary slightly with solvent. Here, the long-wavelength bands of α -mono-Fluoro-TIPS-pentacene at 1×10^{-5} M in toluene solution at 643, 591, and 550 nm are all observed to diminish with reaction progress while a new set of bands grow in below 450 nm as shown in figure 5.2. Half-times ($t_{1/2}$) of around 1800 (toluene), 2820 (chloroform), 2460 (DCM) and 2500 (THF) min were obtained by plotting the A_t/A_0 at the absorption maximum with the irradiation time as shown in figure 5.3.

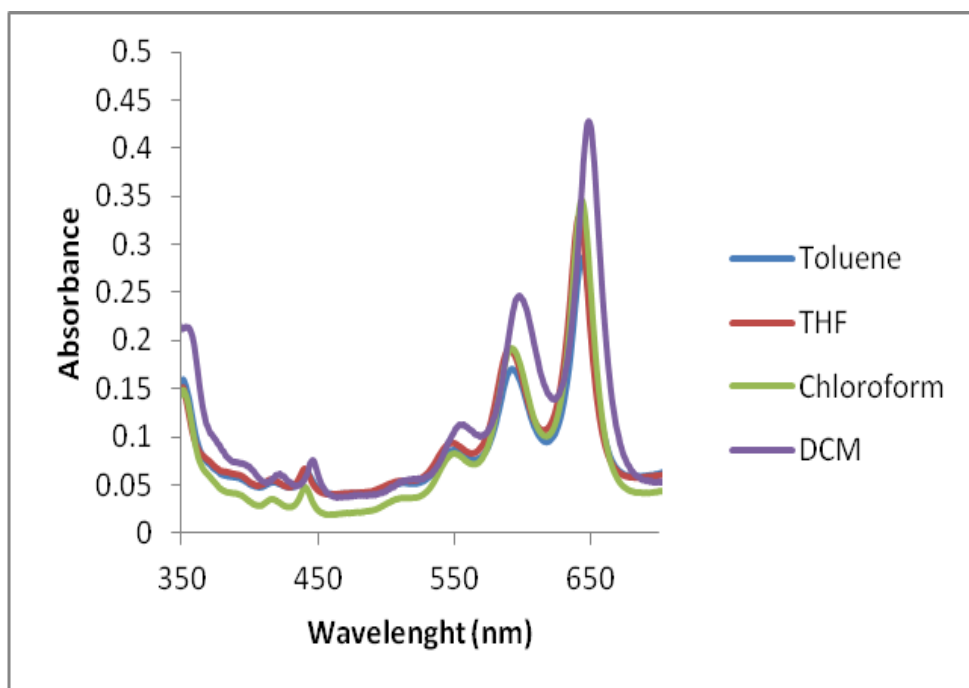


Figure 5.1: V-visible absorption of 1×10^{-5} M solutions of α -mono-Fluoro-TIPS-pentacene in different solvents at 26°C .

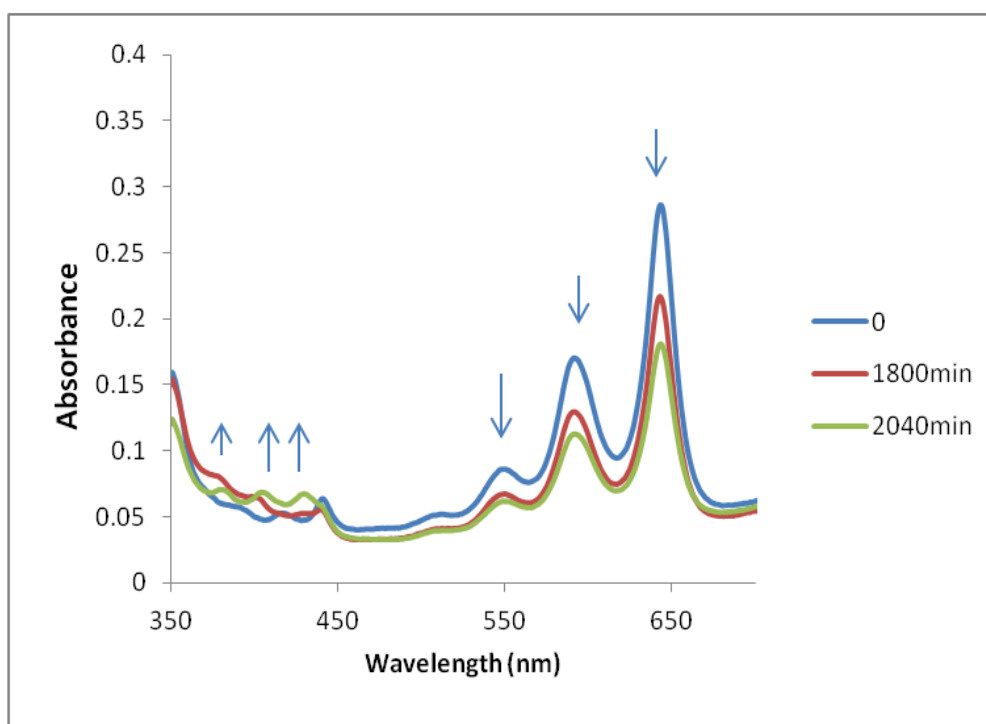


Figure 5.2: UV-visible absorption spectra of for the photodegradation of α -mono-Fluoro-TIPS-pentacene in toluene solution at 1×10^{-5} M in a 10mm pathlength at 26°C .

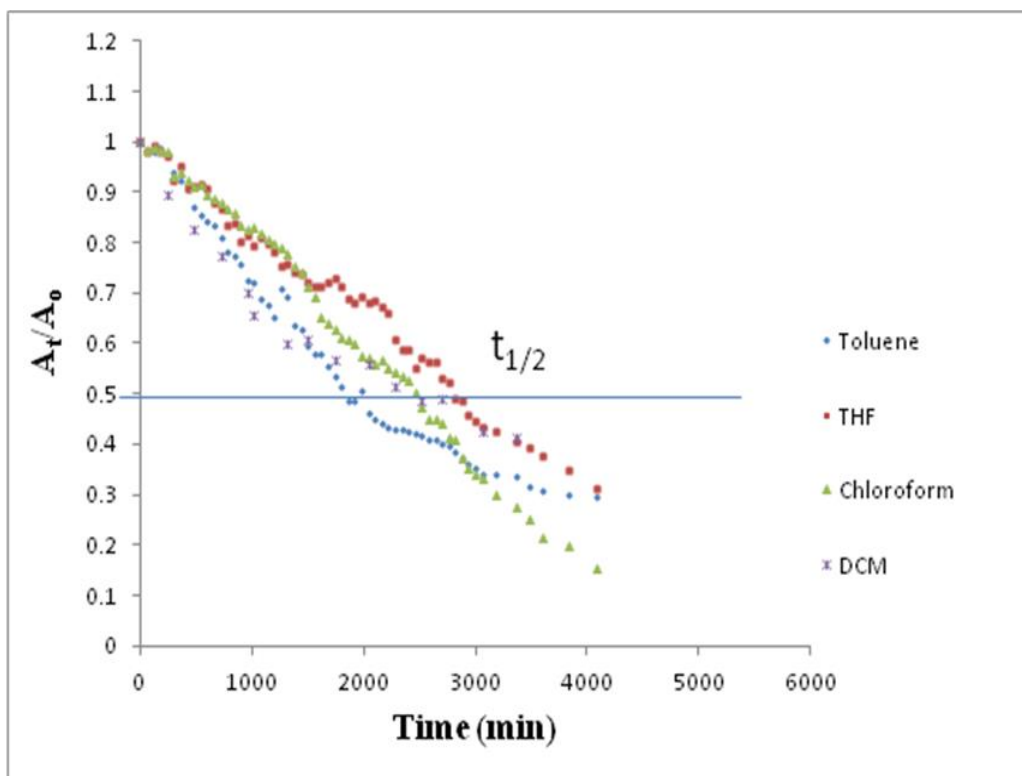


Figure 5.3: Normalised absorbance/ time profiles for α -mono-Fluoro-TIPS-pentacene 1×10^{-5} M at different solvent at 26°C.

5.1.2 Effect the solvent on rate of photochemical instability of β -mono-Fluoro-TIPS-pentacene

UV-visible absorption spectra of β -mono-Fluoro-TIPS-pentacene 1×10^{-5} M at different solvents is shown in figure 5.4. Half-tives ($t_{1/2}$) of around 1560 (toluene), 2880 (DCM), 2580 (chloroform) and 2280 (THF) min were obtained as before from monitoring the decay versus time (figure 5.5) and plotting A_t/A_0 (figure 5.6).

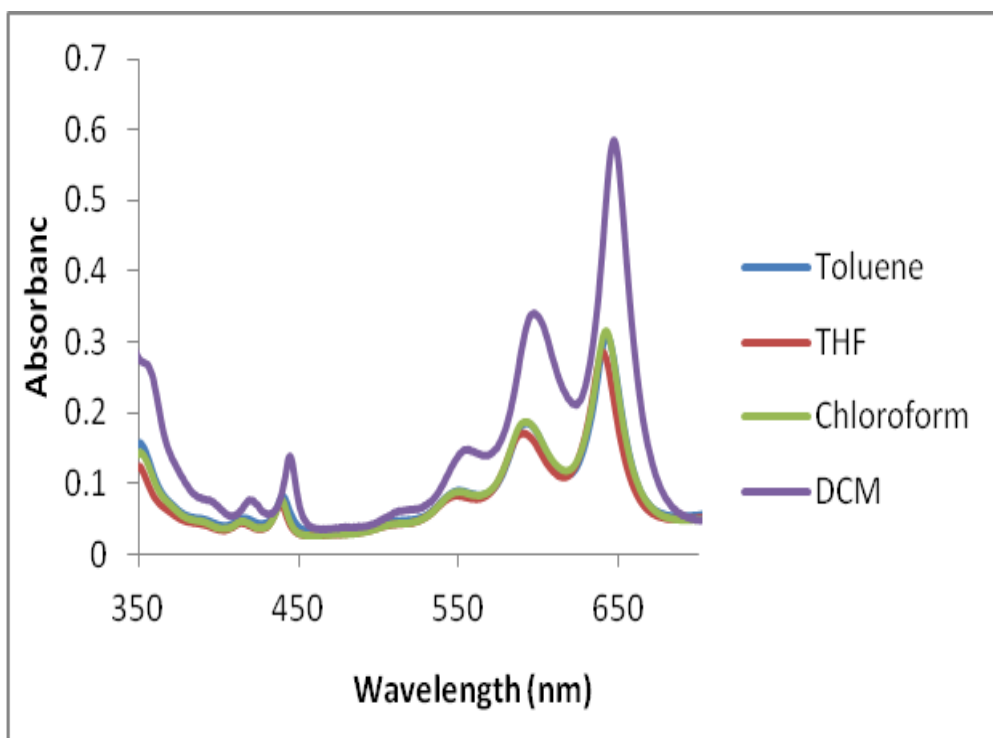


Figure 5.4: UV-visible absorption spectra of 1×10^{-5} M solutions of β -mono-Fluoro-TIPS-pentacene in different solvents at 26°C.

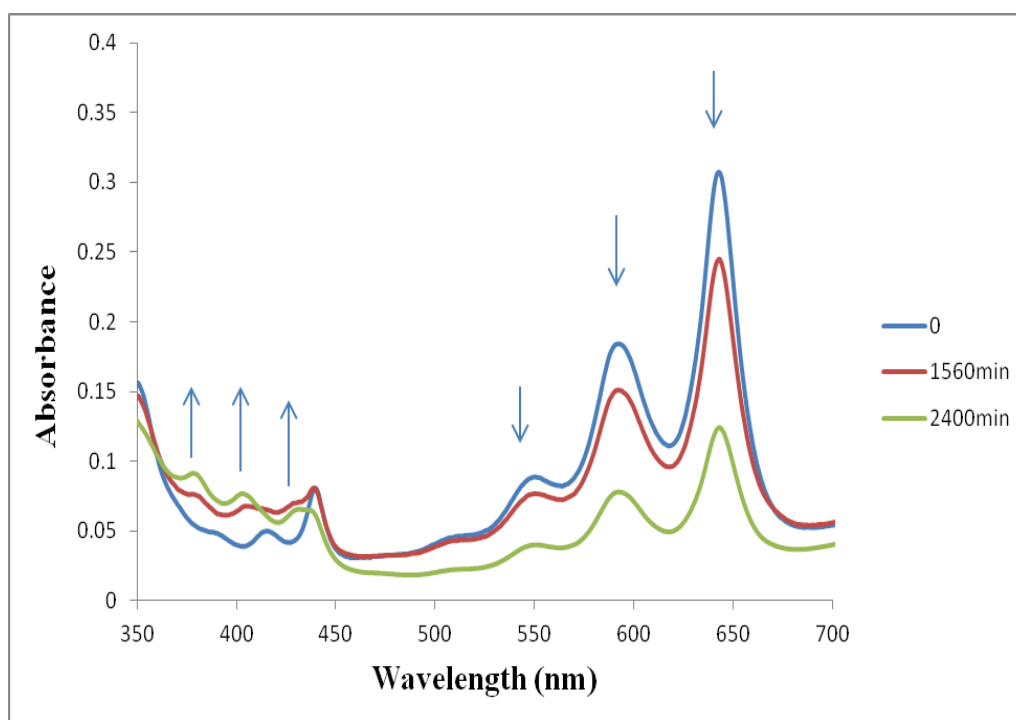


Figure 5.5: UV-visible absorption spectra for the photodegradation of β -mono-Fluoro-TIPS-pentacene in toluene solution at 1×10^{-5} M in a 10mm pathlength at 26°C.

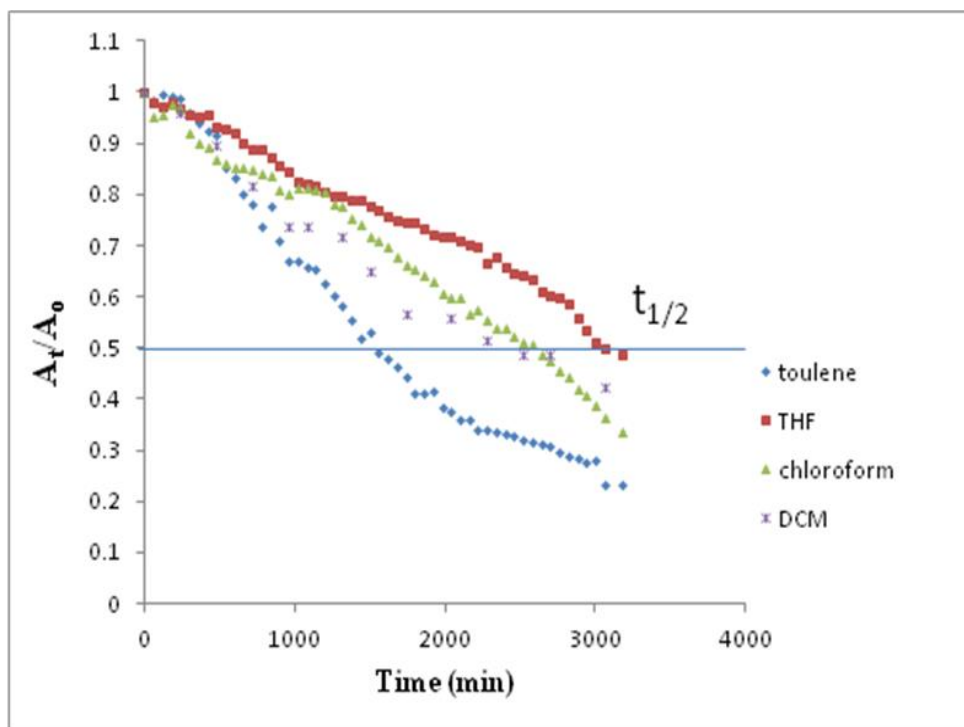


Figure 5.6: Normalised absorbance/ time profiles for β -mono-Fluoro-TIPS-pentacene 1×10^{-5} M at different solvents at 26°C .

5.1.3 Effect the solvent on rate of photochemical instability of α -di-Fluoro-TIPS-pentacene

UV-visible absorption spectra for photodegradation of α -di-fluoro-TIPS-pentacene at 1×10^{-5} M in different solvents is shown in figure 5.7. Half-lives ($t_{1/2}$) of around 2820 (toluene), 3840 (DCM), 3480 (chloroform) and 3060 (THF) min were obtained as before (figure 5.8 and 5.9)s.

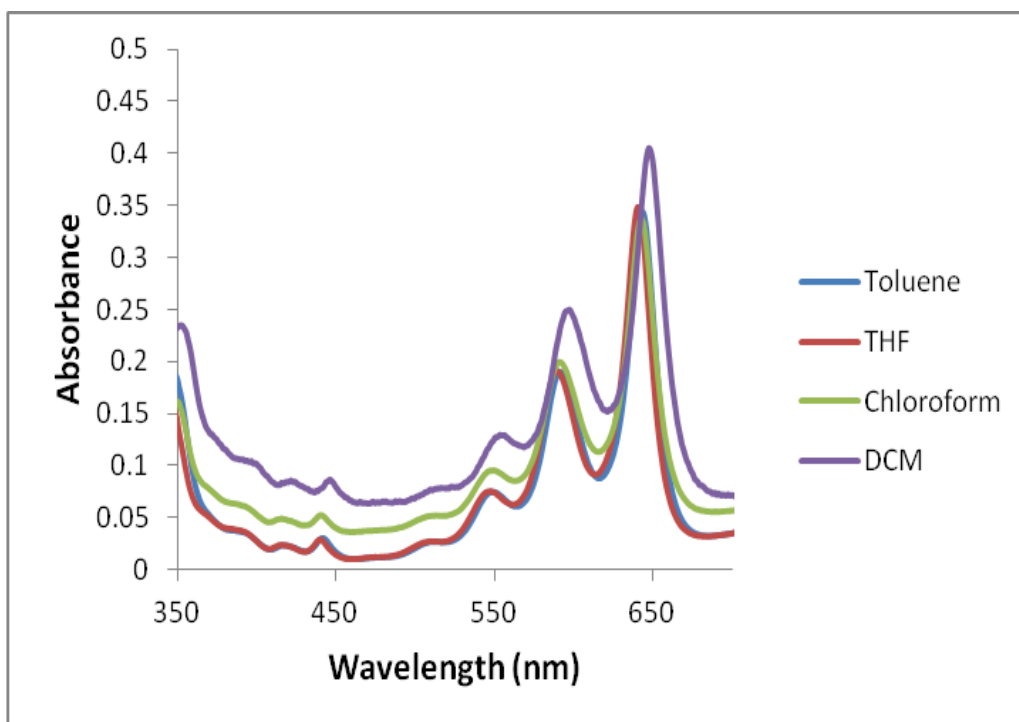


Figure 5.7: UV-visible absorption spectra of 1×10^{-5} M solutions of α -di-Fluoro-TIPS-pentacene in different solvent at 26°C.

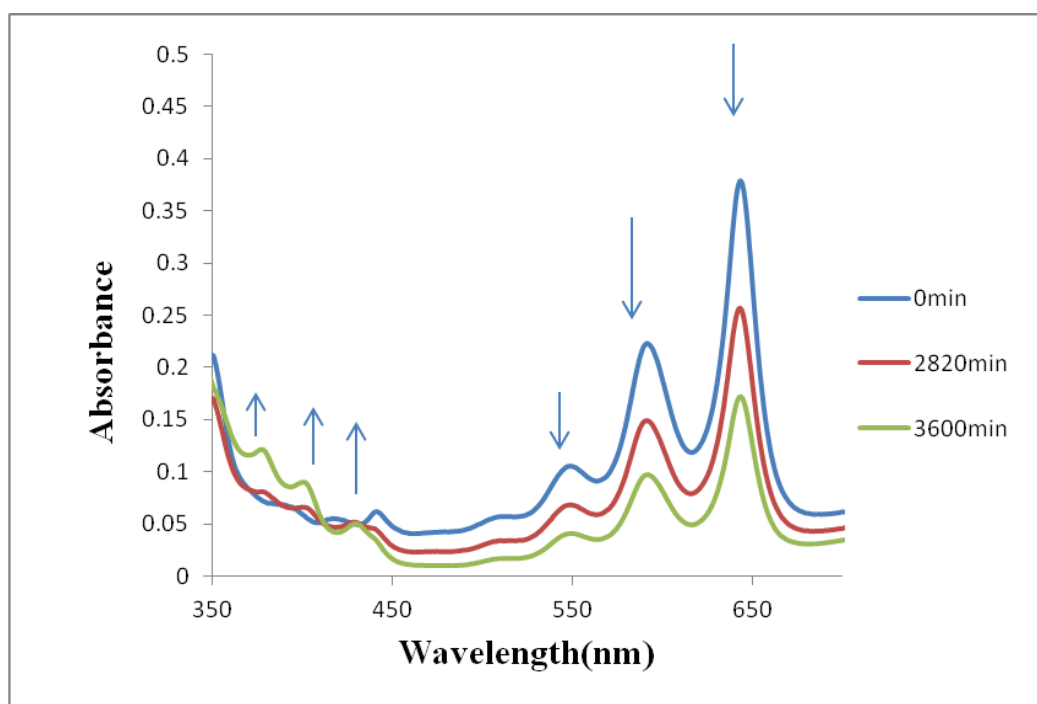


Figure 5.8: UV-visible absorption spectra for the photodegradation of α -di-Fluoro-TIPS-pentacene in toluene solution at 1×10^{-5} M in a 10mm pathlength at 26°C.

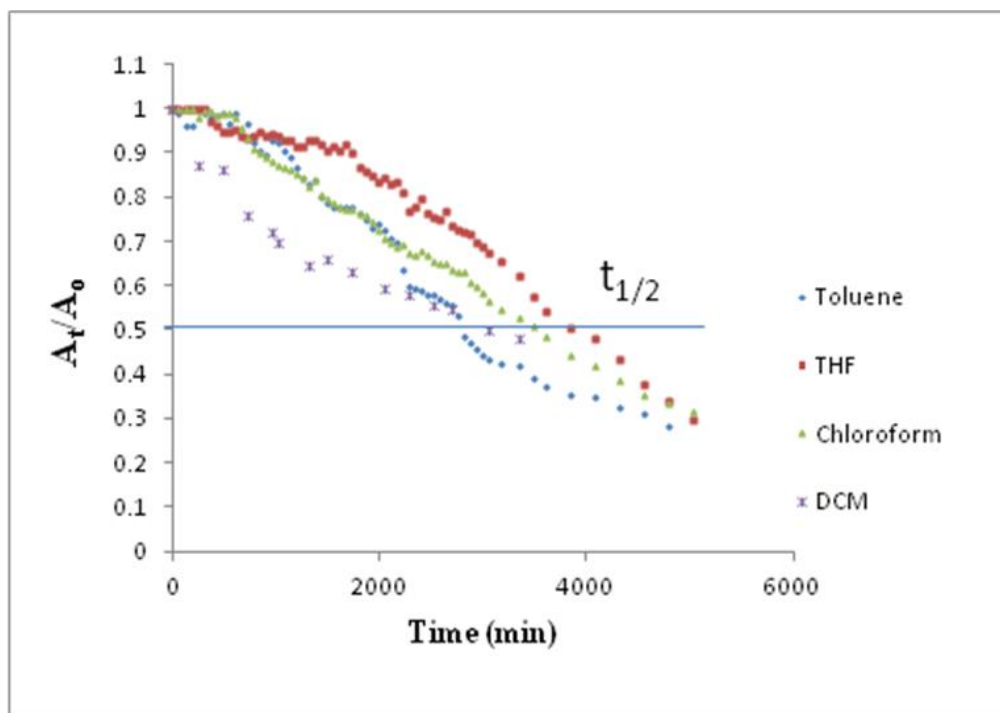


Figure 5.9: Normalised absorbance /time profiles for α -di-Fluoro-TIPS-pentacene 1×10^{-5} M at different solvents at 26°C .

5.1.4 Effect the solvent on rate of photochemical instability of β -di-Fluoro-TIPS-pentacene

UV-visible absorption spectra for the photodegradation of β -di-Fluoro-TIPS-pentacene 1×10^{-5} M in different solvents is shown in figure 5.10. The half-lives ($t_{1/2}$) of around 1560 (toluene), 2460 (THF), 2640 (chloroform) and 2880 (DCM) min were obtained as before (figure 5.11 and 5.12) s.

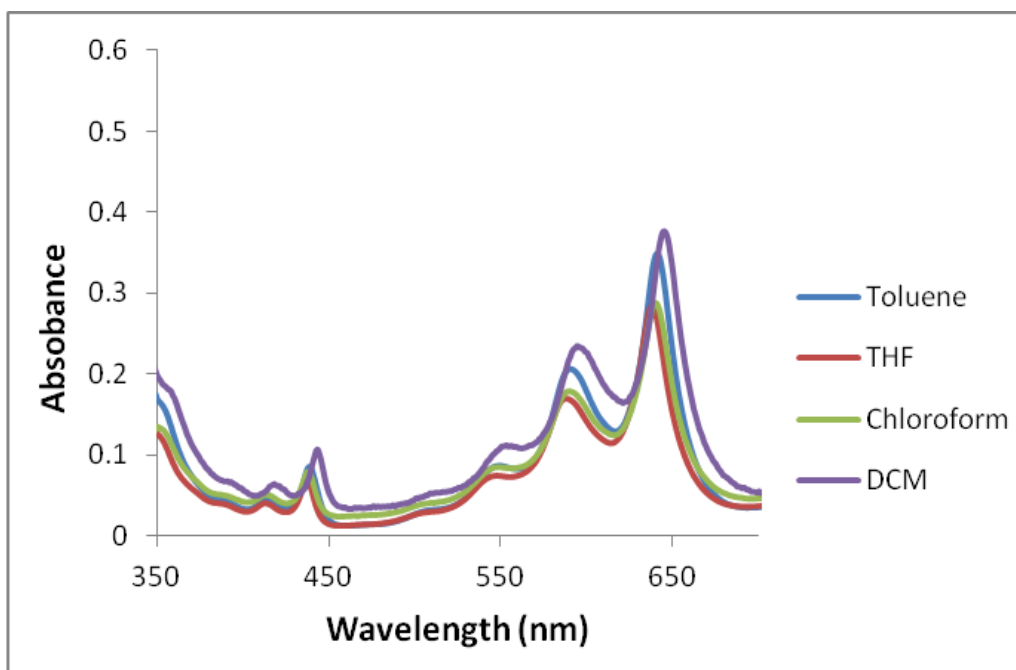


Figure 5.10: UV-visible absorption spectra of 1×10^{-5} M solutions of β -di-Fluoro-TIPS-pentacene in different solvents at 26°C.

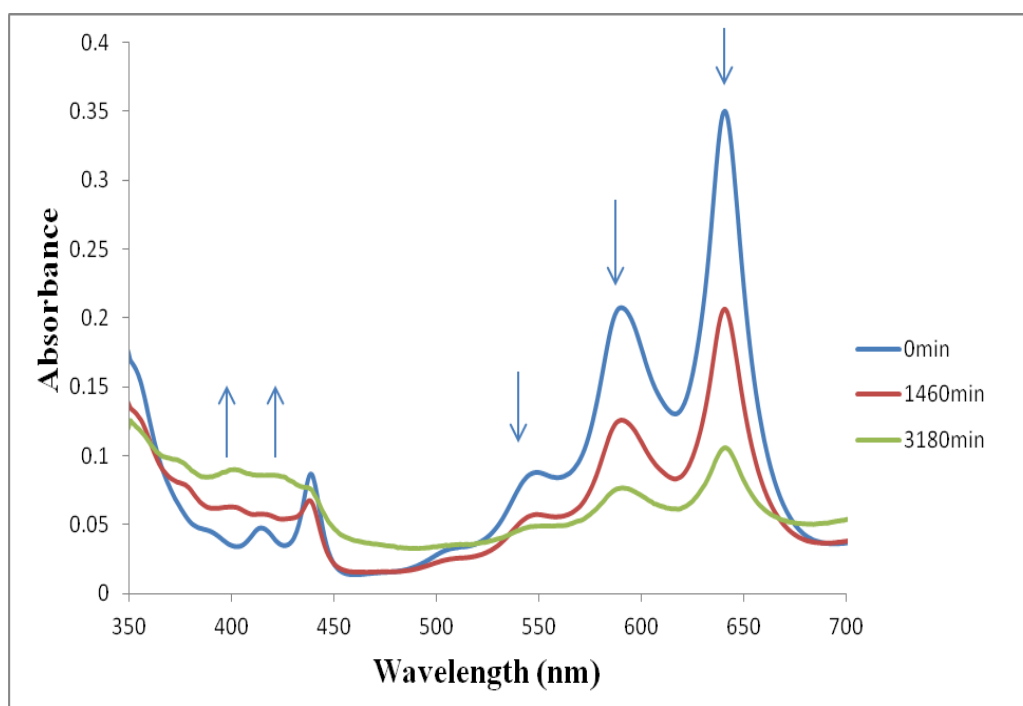


Figure 5.11: UV-visible absorption spectra for the photodegradation of β -di-Fluoro-TIPS-pentacene in toluene at 1×10^{-5} M in a 10mm pathlength at 26°C.

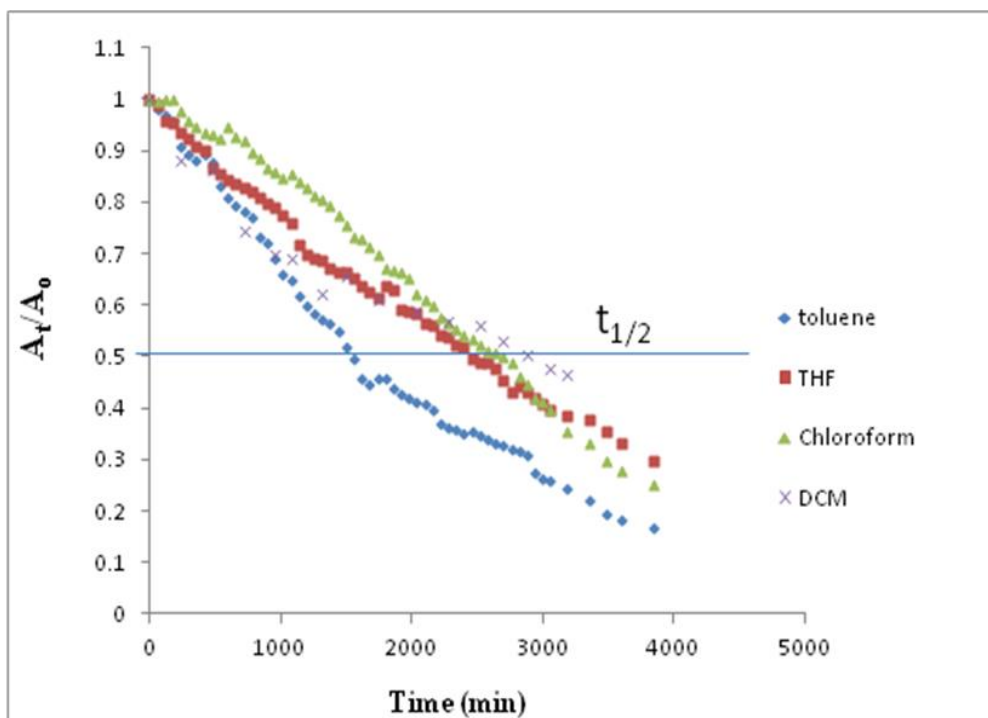


Figure 5.12: Normalised absorbance/ time profiles for β -di-Fluoro-TIPS -pentacene 1×10^{-5} M at different solvents at 26°C .

5.1.5 Effect the solvent on rate of photochemical instability of TMTES-pentacene

UV-visible absorption spectra for photodegradation of TMTES-pentacene at 1×10^{-5} M in different solvents is shown in figure 5.13. The half-lives ($t_{1/2}$) of around 720 (DCM), 1080 (toluene), 1200 (chloroform) and 1260 (THF) min were obtained as before (figure 5.14 and 5.15)s.

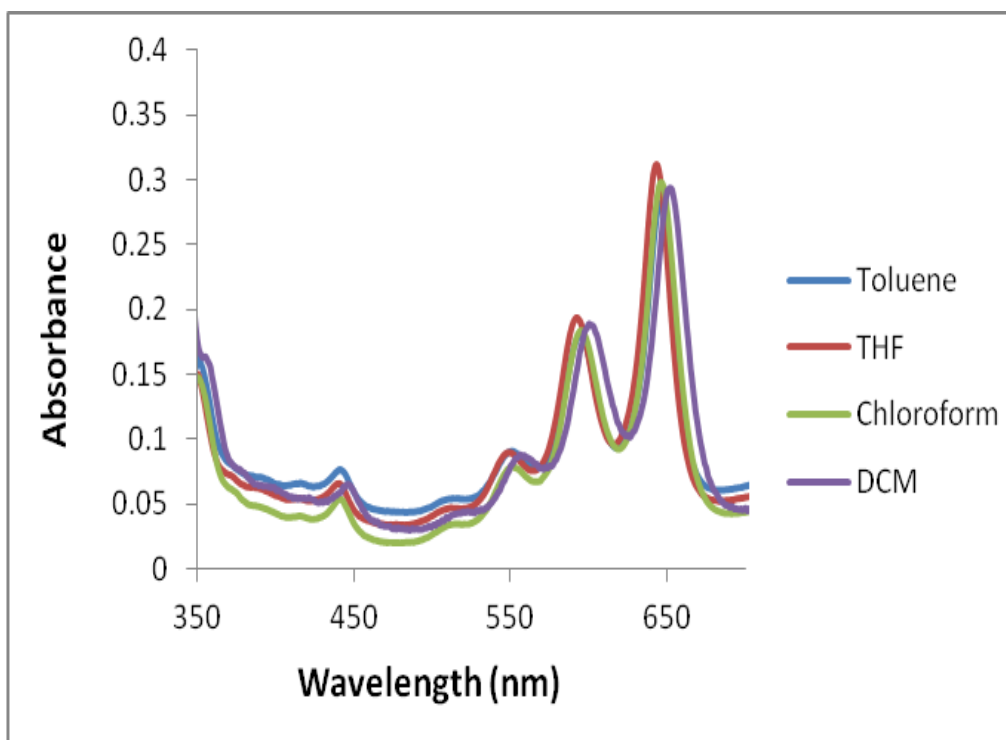


Figure 5.13: UV-visible absorption spectra of 1×10^{-5} M solutions of TMTES-pentacene in different solvent at 26°C.

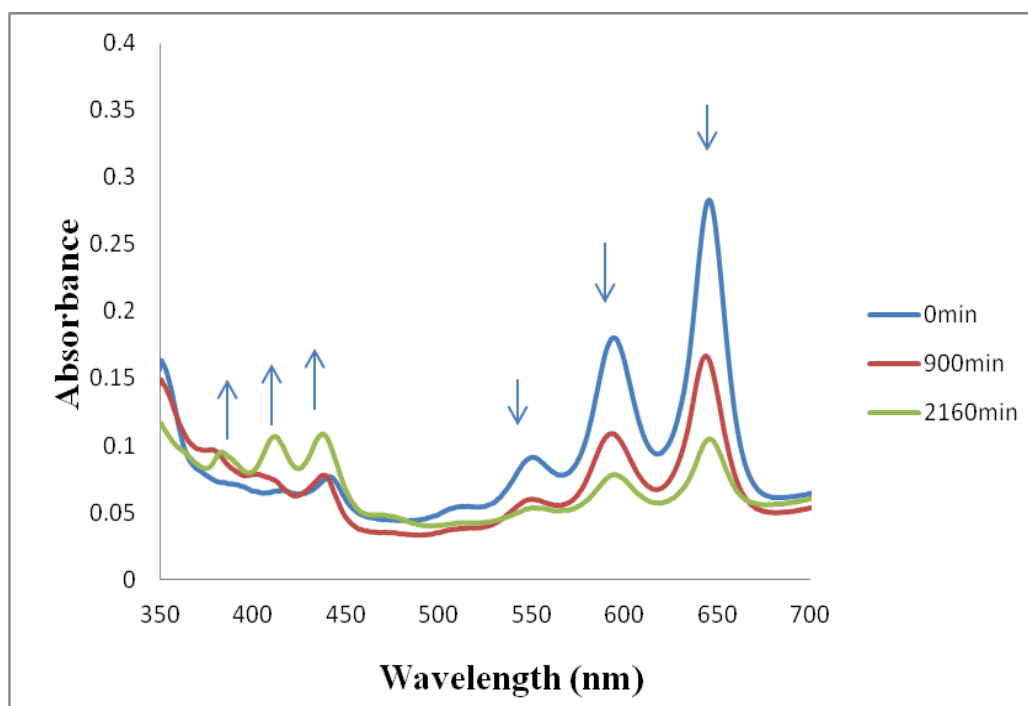


Figure 5.14: UV-visible absorption spectra for the photodegradation of TMTES-pentacene in toluene solution at 1×10^{-5} M in a 10mm pathlength at 26°C.

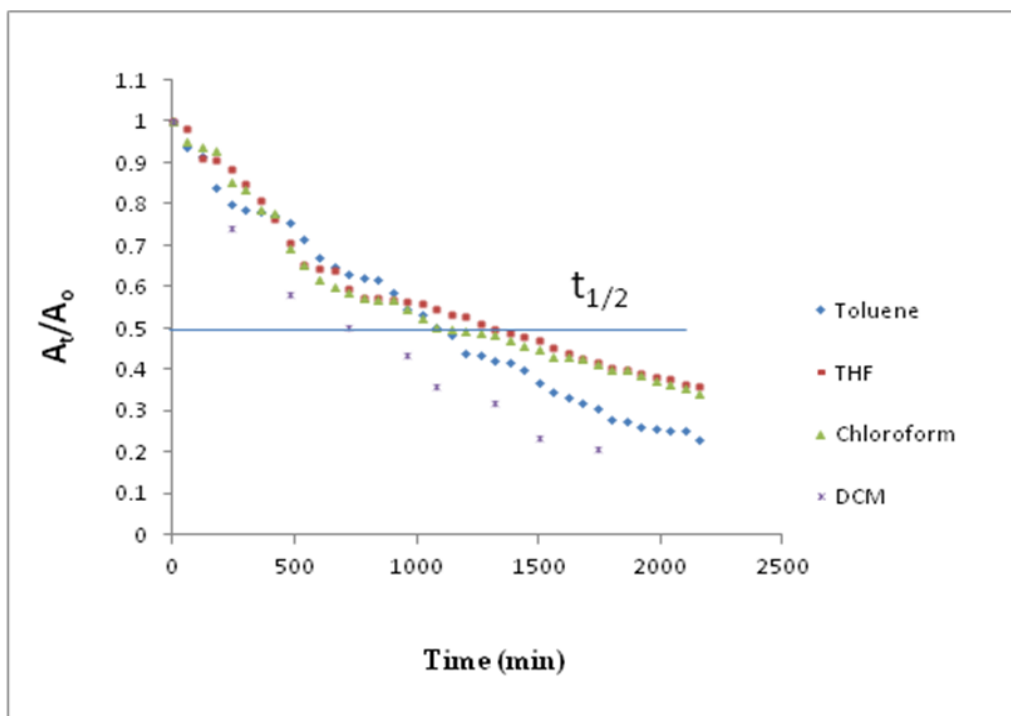


Figure 5.15: Normalised absorbance/ time profiles for TMTES-pentacene 1×10^{-5} M at different solvents at 26°C .

Figures 5.16, 5.17, 5.18 and 5.19 show absorbance-time profile in toluene and chloroform solutions for each pentacene derivative at a concentration 1×10^{-5} M. These reveal a relative ordering of photostability follows: α -di-Fluoro-TIPS-pentacene > β -di-Fluoro-TIPS-pentacene, α -mono-Fluoro-TIPS-pentacene, β -mono-Fluoro-TIPS-pentacene > TIPS-pentacene > TMTES-pentacene. As can be seen from table 5.1 the mono and di-fluorinated-TIPS-pentacene are more stable than TIPS-pentacene because the addition of electron withdrawing fluorine atoms to the pentacene chromophore reduces the electron density at (5,14) and (7,12) carbon atoms thereby reducing the reactivity at these positions. However, TMTES-pentacene possessed the lowest stability because the electron donating groups at the 2, 3,9,10 positions have just the opposite effect.

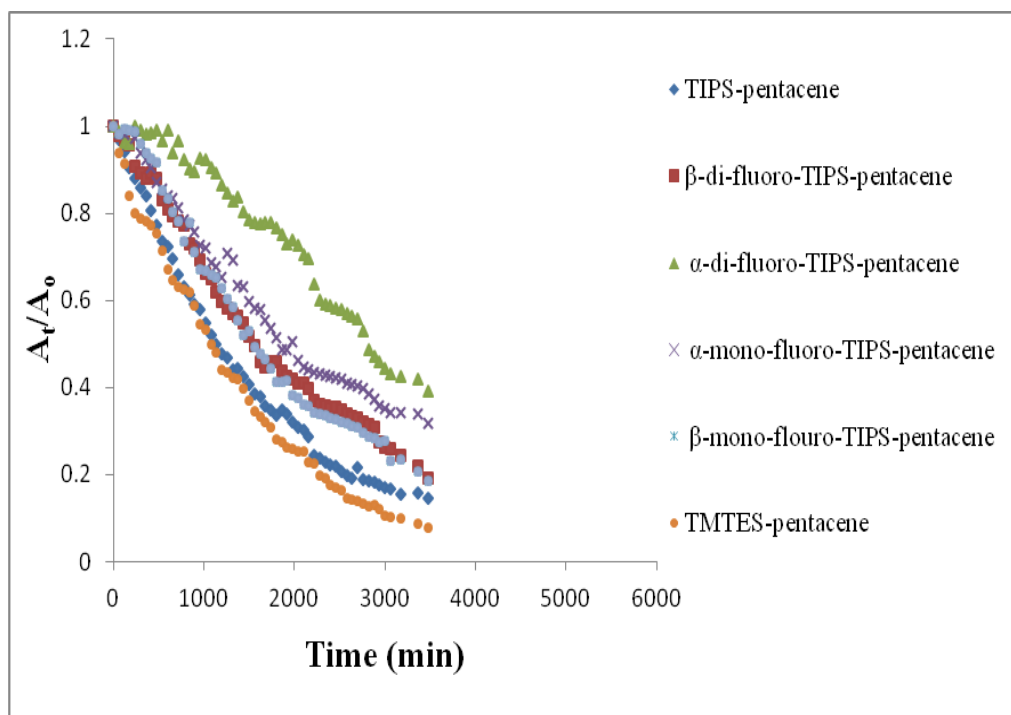


Figure 5.16: Normalised absorbance/time profile of pentacene derivatives (1×10^{-5} M) at λ_{\max} in toluene at 26°C.

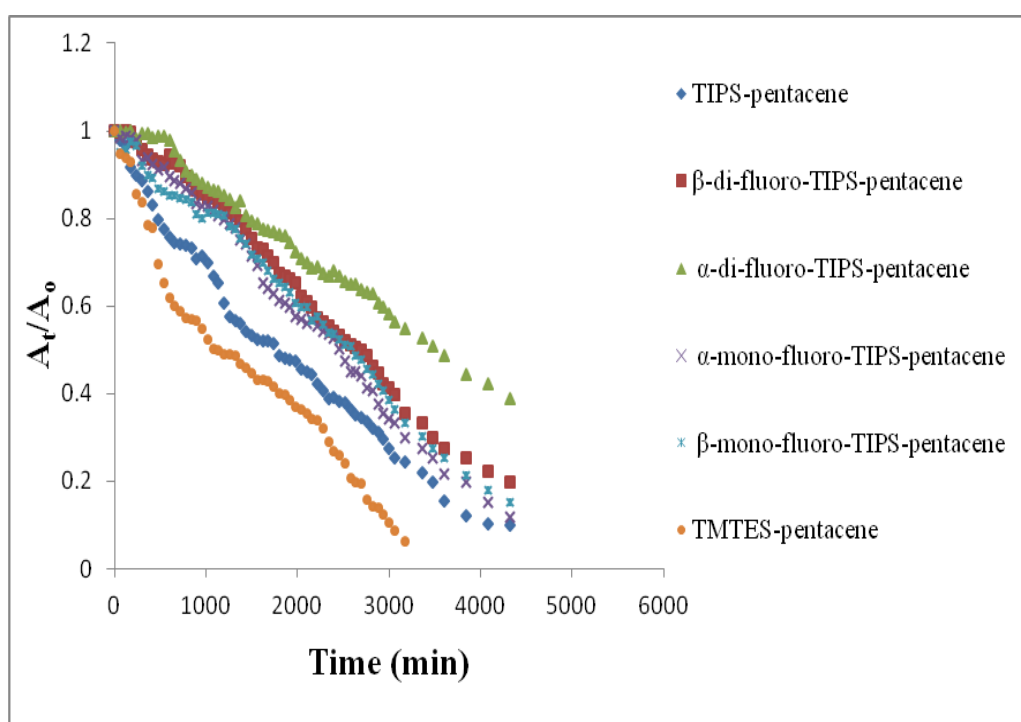


Figure 5.17: Normalised absorbance/time profile of pentacene derivatives (1×10^{-5} M) at λ_{\max} in chloroform at 26°C.

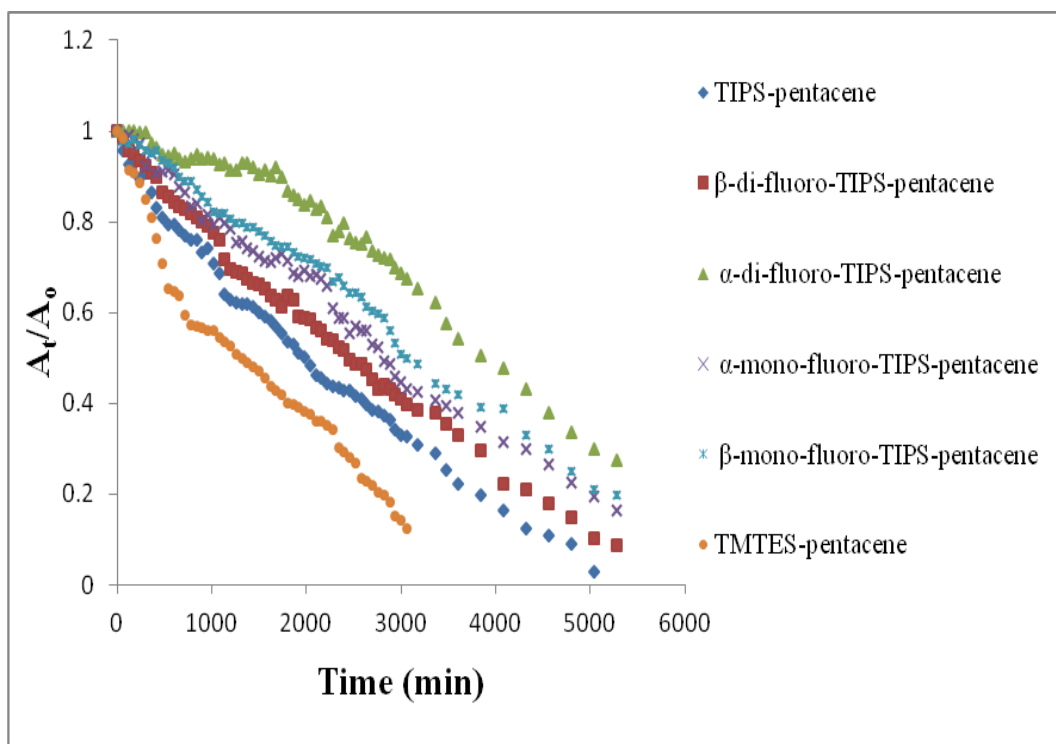


Figure 5.18: Normalised absorbance/time profile of pentacene derivatives (1×10^{-5} M) at λ_{\max} in THF at 26°C .

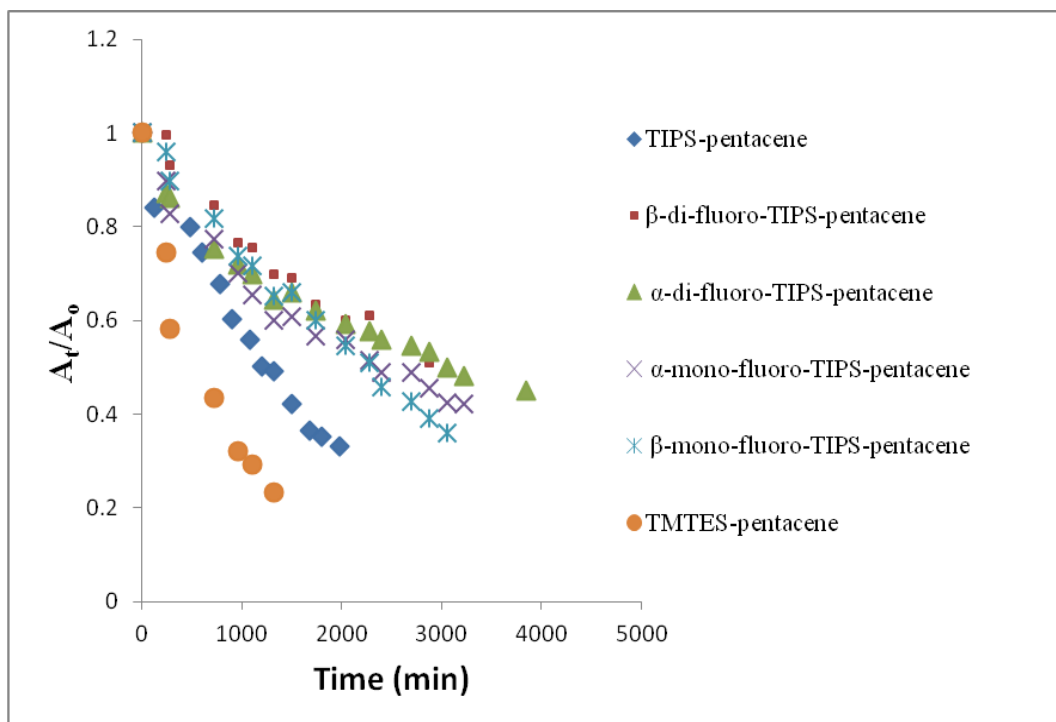


Figure 5.19: Normalised absorbance/time profile of pentacene derivatives (1×10^{-5} M) at λ_{\max} in DCM at 26°C .

Table 5.1: The λ_{\max} and $t_{1/2}$ (min) of pentacene derivatives in toluene, THF, Chloroform and DCM solutions at concentration 1×10^{-5} M at 26°C.

Pentacene derivatives	Toluene		THF		Chloroform		DCM	
	λ_{\max}	$t_{1/2}$ (min)	λ_{\max}	$t_{1/2}$ (min)	λ_{\max}	$t_{1/2}$ (min)	λ_{\max}	$t_{1/2}$ (min)
TIPS-pentacene	643	1205 +/- 190 (1110-1300)	641	1980	643	1550 +/- 360 (1740-1360)	648	1200
α -mono-Fluoro-TIPS-pentacene	643	1800	641	2820	643	2460	648	2500
β -mono-Fluoro-TIPS-pentacene	643	1560	640	2880	642	2580	647	2280
α -di-Fluoro-TIPS-pentacene	643	2885 +/- 130 (2820-2950)	640	3840	643	3480	647	3060
β -di-Fluoro-TIPS-pentacene	641	1567.5 +/- 15 (1560-1575)	638	2460	640	2640	645	2880
TMTES-pentacene	646	1080	643	1260	646	1200	652	720

5.2 Photostability kinetics of pentacene derivatives

The kinetics of the photodegradation of pentacene derivatives are effectively first order at concentration 1×10^{-5} M in all solvents, as shown in figures 5.20, 5.21, 5.22 and 5.23 which is a plot of $\ln(A_t/A_0)$ versus time. These figures are all approximately linear up to time of the half-life. The rate constant k and correlation coefficients R^2 from the liner regression are listed in table 5.2.

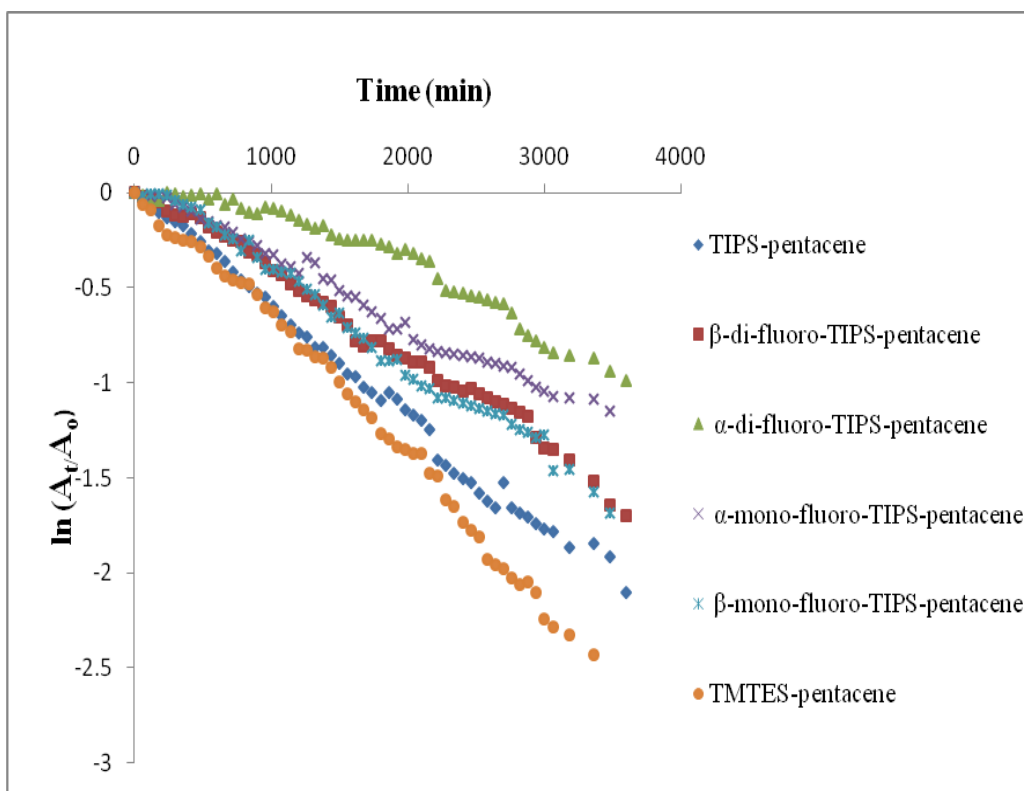


Figure 5.20: Plot of $\ln(A_t/A_0)$ versus time for pentacene derivatives in toluene at a concentration of 1×10^{-5} M at 26°C .

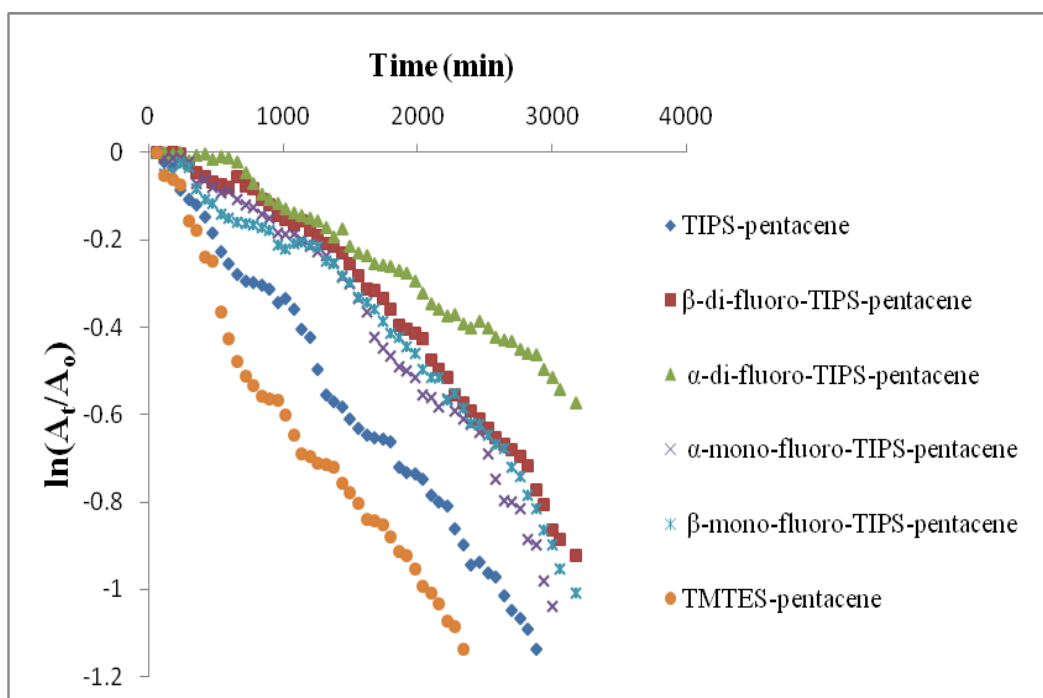


Figure 5.21: Plot of $\ln(A_t/A_0)$ versus time for pentacene derivatives in chloroform at a concentration of 1×10^{-5} M at 26°C .

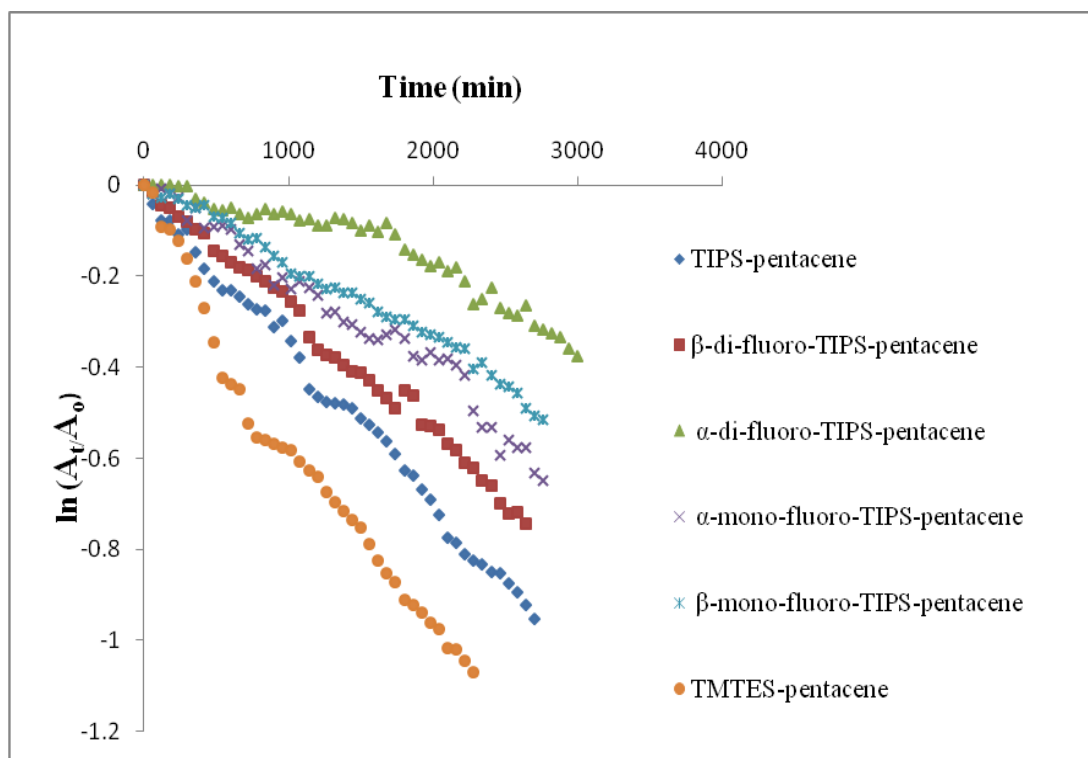


Figure 5.22: Plot of $\ln(A_t/A_0)$ versus time for pentacene derivatives in THF at a concentration of 1×10^{-5} M at 26°C .

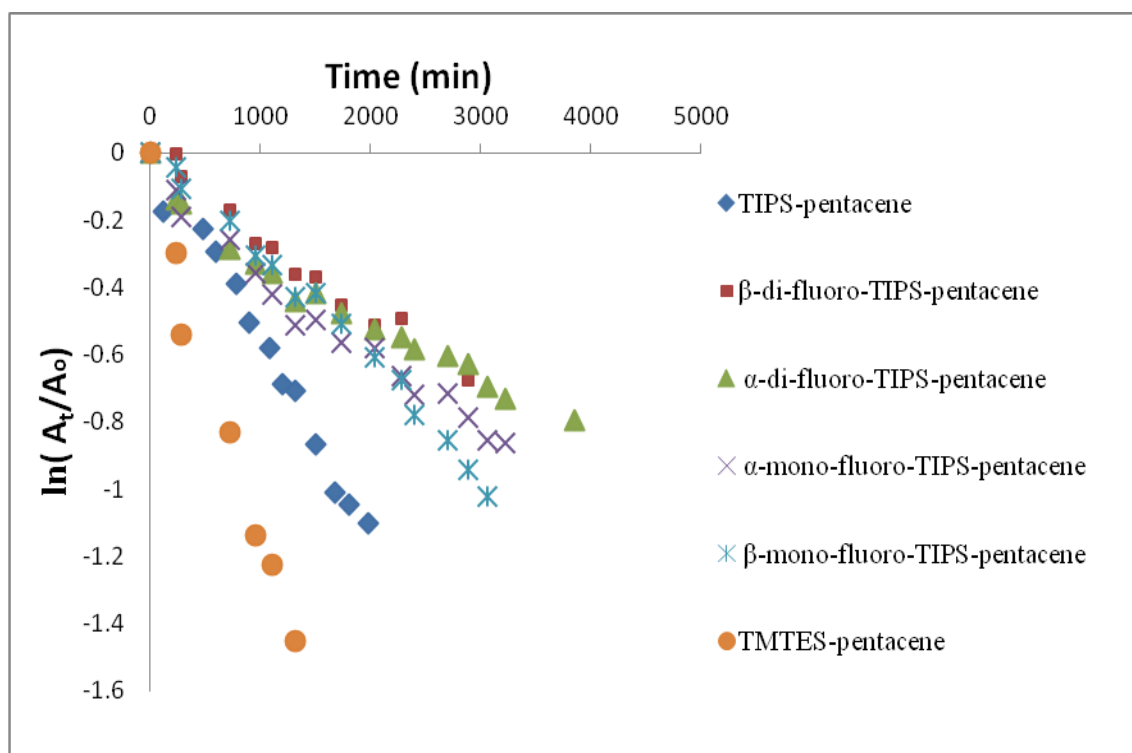


Figure 5.23: Plot of $\ln(A_t/A_0)$ versus time for pentacene derivatives in DCM at a concentration of 1×10^{-5} M at 26°C .

Table 5.2: The kinetic data of pentacene derivatives in toluene, THF, Chloroform and DCM solutions at concentration 1×10^{-5} M at 26°C.

Pentacene derivatives	Toluene		THF		Chloroform		DCM	
	k (min^{-1})	R^2	k (min^{-1})	R^2	k (min^{-1})	R^2	k (min^{-1})	R^2
TIPS-pentacene	0.0006	0.994	0.0003	0.99	0.0004	0.99	0.0006	0.98
α -mono-Fluoro-TIPS-pentacene	0.0004	0.99	0.0002	0.97	0.0003	0.96	0.0002	0.97
β -mono-Fluoro-TIPS-pentacene	0.0005	0.99	0.0002	0.99	0.0003	0.96	0.0003	0.99
α -di-Fluoro-TIPS-pentacene	0.0003	0.93	0.0001	0.91	0.0002	0.99	0.0002	0.96
β -di-Fluoro-TIPS-pentacene	0.0005	0.99	0.0003	0.99	0.0003	0.97	0.0002	0.98
TMTES-pentacene	0.0007	0.99	0.0004	0.97	0.0005	0.96	0.0003	0.98

5.3 Effect the concentration on rate of photo-oxidative degradation of pentacene derivatives in toluene solution

The photochemical stability of pentacene derivatives has been studied in toluene solution at concentrations ranging from 2.5×10^{-6} M to 5×10^{-3} M. For each sample, plots of normalized A_t/A_o at λ_{max} versus time were made to estimate the half-life for each concentration e.g. normalised absorbance/time profiles of β -di-Fluoro-TIPS-pentacene in toluene for a range of concentration as shown in figure 5.24. Experimental values for the half-life of pentacene derivatives in toluene solution at a range of concentrations are shown in figure 5.25 and tabulated in table 5.3. For all derivatives, the data indicate a dramatic increase in photo-stability with increasing the concentration. As can be seen from figure 5.25 the curves show inflection typically between 5×10^{-5} M and 5×10^{-4} M for all pentacene derivatives. As discussed in chapter 4, it is likely that this behaviour reflects the onset of substantial aggregate formation.

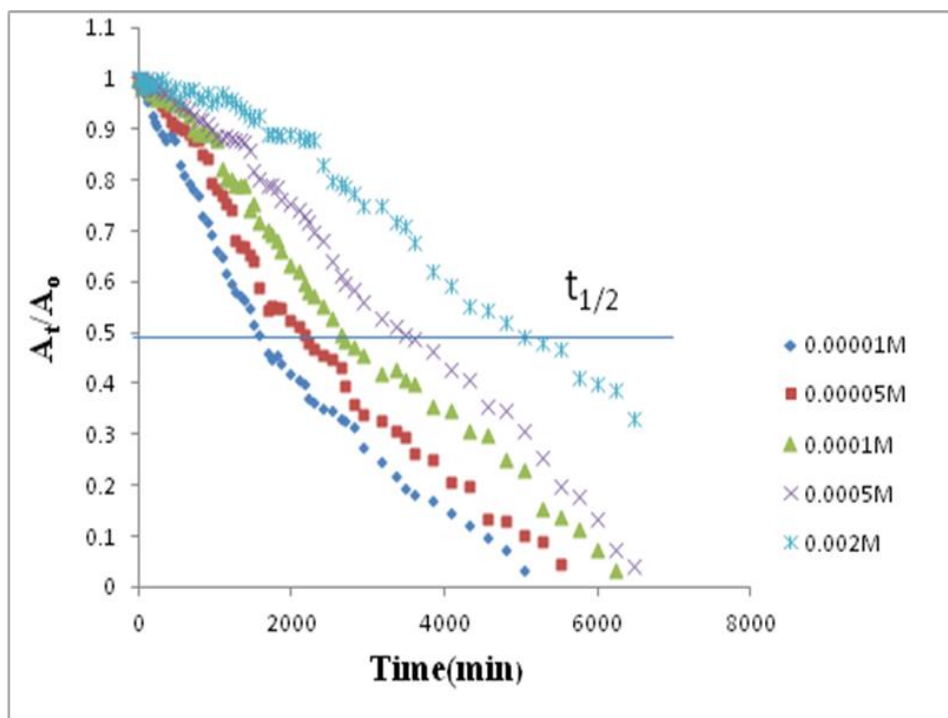


Figure 5.24: Normalised absorbance/time profiles for photooxidation of β -di-Fluoro-TIPS-pentacene in toluene solutions for a range of concentration at 26°C.

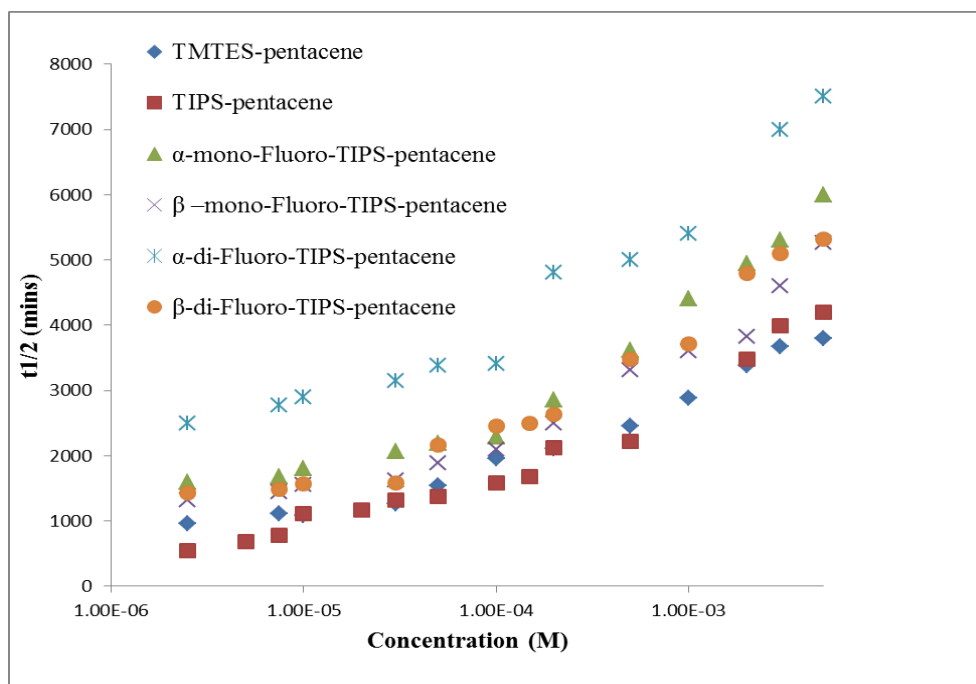


Figure 5.25: plot of half-life ($t_{1/2}$ min) vs concentration (M) of pentacene derivatives in toluene solution between 2.5×10^{-6} M to 5×10^{-3} M at 26°C.

Table 5.3: The $t_{1/2}$ min of pentacene derivatives in toluene solutions at different concentrations at 26°C.

Concentration (M)	TIPS-pentacene	α -mono-Fluoro-TIPS-pentacene	β -mono-Fluoro-TIPS-pentacene	α -di-Fluoro-TIPS-pentacene	β -di-Fluoro-TIPS-pentacene	TMTES-pentacene
2.5×10^{-6}	827.5 +/-575 (540-1115)	1600	1320	2660	1430	960
5×10^{-6}	690					
7.5×10^{-6}	990+/-420 (780-1200)	1680	1440	2780	1490	1120
1×10^{-5}	1205 +/-190 (1110-1300)	1800	1560	2885 +/-130 (2820-2950)	1567.5 +/- 15 (1560- 1575)	1080
2×10^{-5}	1170					
3×10^{-5}	1320	2070	1620	3150	1590	1260
5×10^{-5}	1380 +/-120 (1500,1260)	2190	1890	3380	2160	1540
1×10^{-4}	1590	2290	2100	3410	2640	1960
1.5×10^{-4}	1680				2500	
2×10^{-4}	2145 +/-30 (2130-2160)	2860	2500	4810	2460	2110
5×10^{-4}	2220	3620	3320	5000	3480	2450
1×10^{-3}	3500	4410	3600	5400	3720	2880
2×10^{-3}	3480	4950	3820	6000	4800	3380
3×10^{-3}	3990	5300	4600	6990	5100	3680
5×10^{-3}	4200	6000	5200	7500	5320	3800

For comparison, the photostability of pentacene derivatives in THF at two different concentrations was also obtained at 1×10^{-4} M and 2×10^{-4} M. As can be seen from table 5.4 the half-lives also increase dramatically with increased concentration. Insufficient time was available to collect full dataset of kinetic information for all derivatives in full range of solvents but this data serve to convince that the trends observed for TIPS-pentacene in a range of solvents are also seen in the derivatives.

Table 5.4: the λ_{\max} and $t_{1/2}$ min of pentacene derivatives at concentration (1×10^{-4} M and 2×10^{-4} M) in THF solutions.

Pentacene derivatives	1×10^{-4} M		2×10^{-4} M	
	λ_{\max}	$t_{1/2}$ (min)	λ_{\max}	$t_{1/2}$ (min)
TIPS-pentacene	641	1980	644	3130
α -mono-Fluoro-TIPS-pentacene	641	2820	645	3720
β -mono-Fluoro-TIPS-pentacene	640	2880	644	3660
α -di-Fluopro-TIPS-pentacene	641	2820	644	5400
β -di-Fluoro-TIPS-pentacene	638	2460	641	4140
TMTES-pentacene	638	1260	647	3060

5.4 Comparison with TIPS pentacene

Figure 5.25 shows a summary plot of half-life data versus concentration for pentacene derivatives in toluene solution at concentration ranging from 2.5×10^{-6} M to 3×10^{-3} M. once again, an inflection is observed above 1×10^{-4} M which suggests the onset of aggregation. Figure 5.26 shows a plot of the half-lives versus mean intermolecular distance for pentacene derivatives (cf. figure 4.21 for TIPS-pentacene). The variation of lifetime with $D(x)$ is once again seen to be approximately linear up to concentrations around 5×10^{-4} M and the kinetics of the photodegradation process are effectively first order reaction below this. Above this concentration, the half-life increases non-linearly up to the solubility limit as the photostability is increased by SF de-excitation and also by the formation of aggregates.

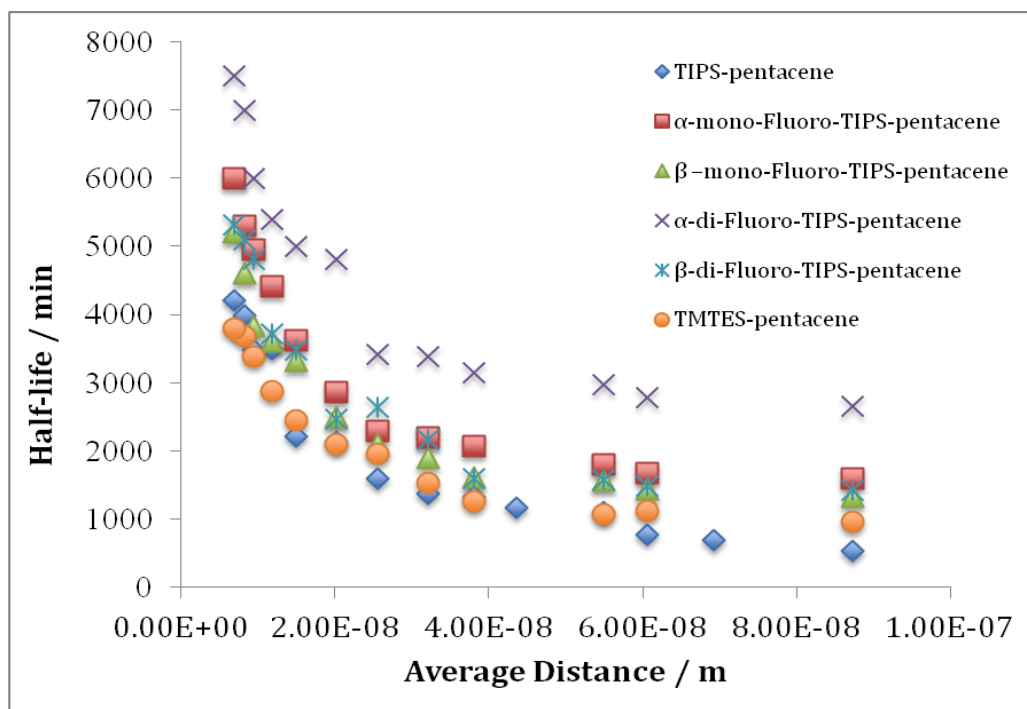


Figure 5.26: Variation of half-life versus average intermolecular distance between 2.5×10^{-6} M to 5.0×10^{-3} M for pentacene derivatives in toluene solution.

5.5 Conclusions

In conclusion, reported for the first time is the photooxidative stability of substituted 6,13 trialkylsilylethynylpentacene derivatives in a variety of common solvents. The absorption spectra of these molecules were found to be systematically red shifted with $\lambda_{\max} = 638\text{-}646$ nm in different solvents. Independent of solvent and at constant concentration the relative ordering of photooxidative resistances were: α -di-Fluoro-TIPS-pentacene > β -di-Fluoro-TIPS-pentacene > α -mono-Fluoro-TIPS-pentacene > β -mono-Fluoro-TIPS-pentacene > TMTES-pentacene. This is correlated with the electron withdrawing/donating effects of the substituent. Whilst the same rank order was maintained upon varying concentration, on going from the most dilute concentration, 2.5×10^{-6} M to the most concentrated 5×10^{-3} M, stability to photooxidation increased with increasing concentration. Photooxidative stability was found also to be a function of solvent, although it was not possible to correlate this with R_a and $[O_2]$ as was done for TIPS-pentacene because of the lack of HSP data. Empirically however it seems reasonable to deduce that the derivatives behave in the same way as TIPS-pentacene with regard to solution properties.

Chapter 6

6 Effect of solvent mixtures and additive aromatic solvent and polymer on rate of photooxidative degradation of TIPS-pentacene

Organic field effect transistors (OFETs) based upon solution processed blends films of small molecular semiconductors and an insulating polymer as the active layer show promise for high performance organic electronics applications, such as high field effect mobility, good solution processability, threshold voltage, on-off ratio and good film uniformity. In particular acenes such as TIPS-pentacene blended with an insulating or semiconducting polymer has been shown to improve the electronic properties and stability of organic thin film transistor devices and has been studied by several groups to better understand the materials [131-139].

Many studies have developed techniques for the solution processing of TIPS-pentacene, with the aim of establishing a greater degree of control over the process of film deposition from the TIPS-pentacene solution and improved hole motilities. In order to solve these problems, solvent mixtures has been accepted as a simple and effective way to achieve morphological tuning and optimal phase separation. Another noteworthy approach is TIPS-pentacene blended with polymers with excellent film forming properties in order to reduce localized crystal anisotropy and to improve film uniformity. The influence of the solvent mixture such as (isopropanol/toluene, acetonitrile/toluene, chloroform/toluene, mesitylene/anisole, P-xylene/toluene, tetralin/toluene, and acetophenon/anisole) [136, 140-143], and TIPS-pentacene:polymer blends such as amorphous polystyrene (aPS), isotactic polystyrene (iPS), poly(α -methyl styrene) (P α MS), poly(triethylamine) (PTAA), poly(4-vinylbiphenyl) (PVBP), isotactic poly(methyl methacrylate) (i-PMMA), have exhibited high mobilities and improved uniformity and thermal stability of TIPS-pentacene in OTFTs devices [132, 133, 135, 136, 144-146]. The aim of this chapter is to explore aspects of the effect of these additives on the solution behaviour of TIPS-pentacene as necessary requirements to the development of a predictive capability for structural control over solution-processed thin films.

6.1 Effect of solvent mixtures on rate of photooxidative degradation of TIPS-pentacene

The effect of solvent and additives on the performance of TIPS-pentacene field effect transistors has been reported using stable binary solvent mixtures containing two solvents with opposing polarities (IPA/toluene) with different ratios [141]. The morphologies of polycrystalline thin films of TIPS-pentacene from azeotropic binary solvent mixtures are large single crystals with predominately parallelepiped shape, indicating facile self assembled in well controlled manner suitable for use in OFET device fabrication. TIPS-pentacene packs in supramolecular aggregates with the transition dipole moments of neighbouring molecules parallel (H-aggregation) in IPA/toluene mixtures. Electronic interaction between the two transition dipole moments in H-aggregates exhibits a blue-shifted absorption band with respect to the absorption of isolated TIPS-pentacene molecules at transition point 563 and 615 nm with increased IPA/toluene ratios [141].

In this work, the photochemical stability of TIPS-pentacene has been studied in mixtures of solvents (toluene, isopropanol (IPA), DCM, dodecane, anisole and THF) with different ratios (v/v) at a TIPS-pentacene concentration 5×10^{-5} M. The half-life is obtained for each sample under the same conditions in chapter 3 and the data is tabled in table 6.1. Figure 6.1 shows a summary plot of half-life data for TIPS-pentacene photooxidation at concentration 5×10^{-5} M in solvent mixtures. For all solvents, shortest half-lives are observed for lowest ratio of additives solvent in toluene mixed solvent, with life time increasing as ratio increases. For mixtures of toluene/dodecane the curve shows inflection when the ratio of dodecane was above 60 vol%. The mixtures of toluene with IPA and THF both rise rapidly even at (90/10) ratio. However, the variation of lifetime with volume ratios (v/v) of toluene in solvent mixtures, (DCM and anisole) can be seen to approximately linear scale from 100% toluene to 100% other solvents, it seems that means no effect of additives of these solvents on the photostability of TIPS-pentacene in toluene mixed solvent.

Table 6.1: The half-lives for TIPS-pentacene in mixed solvent at concentration 5×10^{-5} M.

V/V ratio	Toluene/ Dodecane	Toluene/ Anisole	Toluene/ THF	Toluene/ DCM	Toluene/ IPA
0/100	4980	2250	2940	1740	4050
10/90	3810	2100	3090	1590	3280
20/80	2370	2040	3030	1470	3160
40/60	1500	1740	2970	1420	3040
50/50	1440	1560	2940	1360	2980
60/40	1560	1320	2820	1260	2490
80/20	1500	1220	2680	1230	2370
90/10	1020	1160	2320	1160	2130
100/0	1160	1160	1160	1160	1160

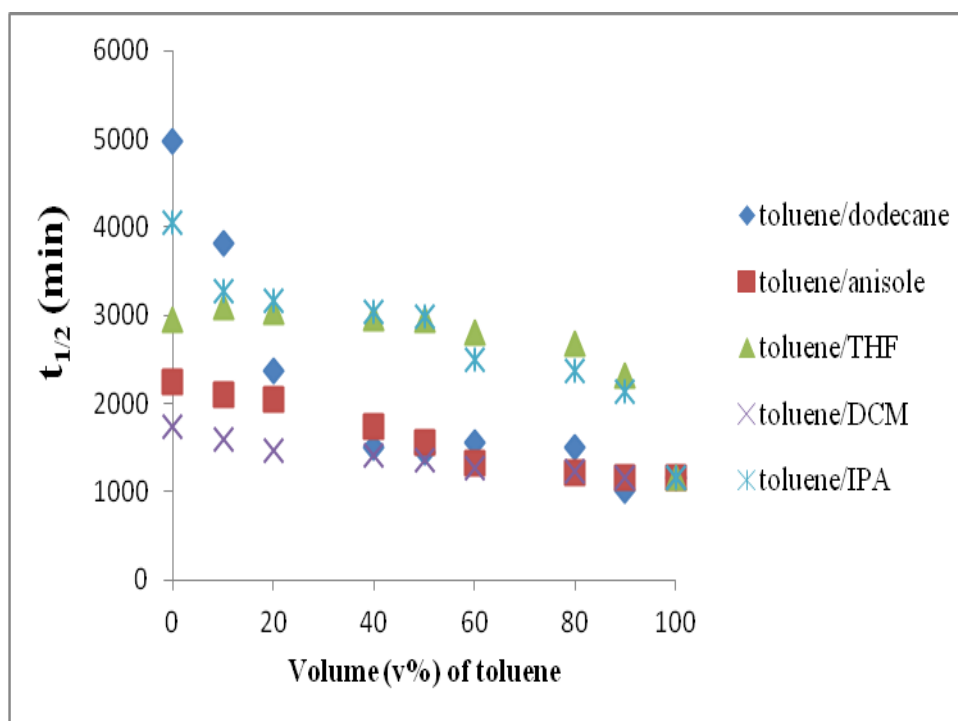


Figure 6.1: Variation of half-lives as a function of volume (v%) of toluene in solvent mixtures for TIPS-pentacene at concentration 5×10^{-5} M at 26°C .

The half-lives were obtained in different mixed solvent (THF/anisole) at the same concentration 5×10^{-5} M in order to observe how the photostability of TIPS-pentacene is affected by change of mixed solvent system. When small amounts of additives are used about 20 vol% from anisole to THF mixed solvent, TIPS-pentacene exhibit larger half-life and increases photostability. As the ratio of anisole is increased to 90 vol %, the half-life decreases linearly up to the ratio 0 vol % as shown in table 6.2 and figure 6.2.

Table 6.2: The half-lives for TIPS-pentacene at concentration 5×10^{-5} M in mixed solvent THF/anisole.

V/V ratio THF/anisole	0/100	10/90	20/80	40/60	50/50	60/40	80/20	90/10	100/0
$t_{1/2}$ (min)	2250	2160	2580	2940	3000	3240	3540	3360	2940

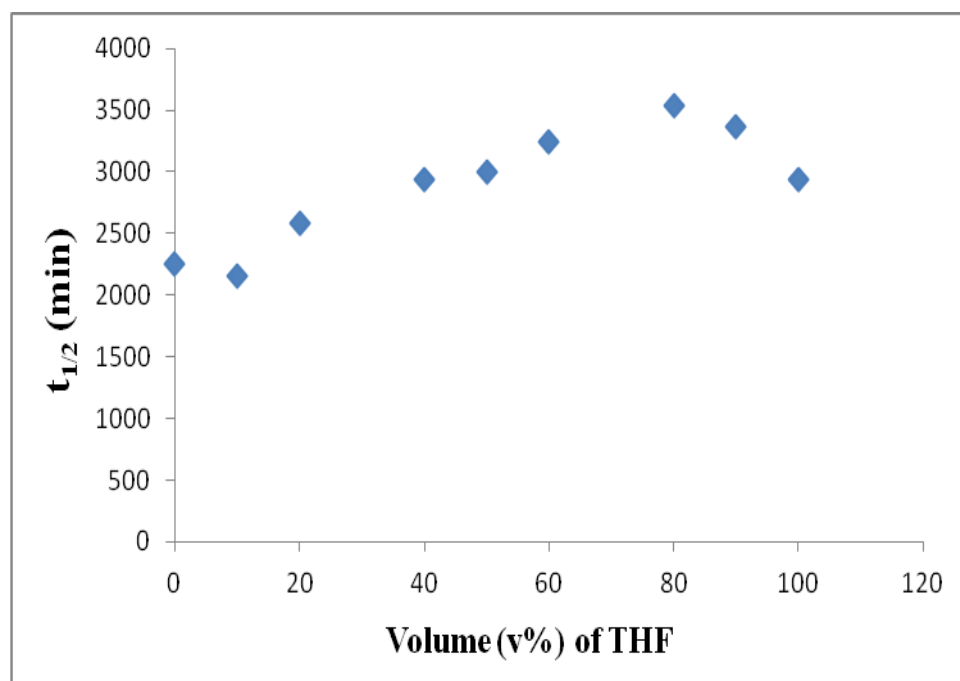


Figure 6.2: Variation of half-lives as a function of volume (v %) of THF in solvent mixtures (THF/anisole) for TIPS-pentacene at concentration 5×10^{-5} M at 26°C.

In order to understand how solvent additives are able to influence the photostability in solution, modification of the photodegradation of TIPS-pentacene by increases in the level at concentration 2×10^{-4} M was studied. As in the samples, the TIPS-pentacene solutions were prepared from anisole with various ratio of decane at concentration 2×10^{-4} M. The half-life data for TIPS-pentacene in mixed solvent anisole/decane increases with the ratio of decane increasing, as shown in table 6.3. Interestingly, increases in half-life were observed when the ratio of decane was above 60 vol %, as displayed in figure 6.3 which is similar behavior in mixed solvent toluene/dodecane at concentration 5×10^{-4} M. In general, it is accepted that half-life is highly sensitive to the kind of two solvents and depends on the volume ratio of TIPS-pentacene photostability in solution.

Table 6.3: The half-lives for TIPS-pentacene 2×10^{-4} M in mixed solvent anisole/ decane

V/V ratio anisole/decane	0/100	10/90	20/80	40/60	50/50	60/40	80/20	90/10	100/0
$t_{1/2}$ (min)	7740	7660	7080	6120	5960	5880	5820	5700	5670

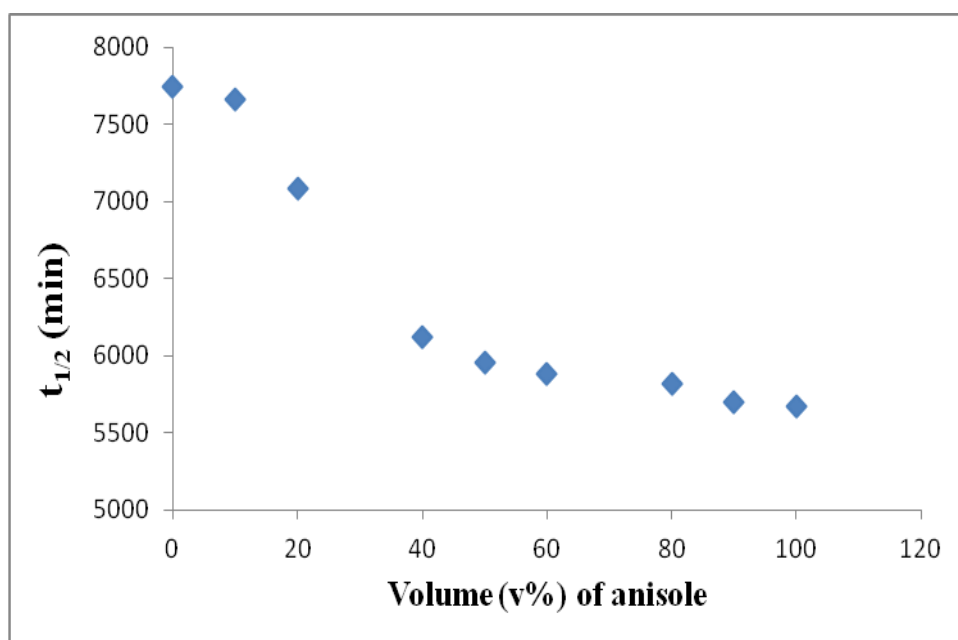


Figure 6.3: Variation of half-lives as a function of volume (v %) of anisole in solvent mixtures (anisole/decane) for TIPS-pentacene at concentration 2×10^{-4} M at 26°C.

6.2 Effect additive aromatic solvent on rate of photo-oxidative degradation of TIPS-pentacene in THF (2×10^{-4} M) at different light conditions

Returning to the subject of interactions within the solution which affect the interaction between TIPS-pentacene molecules, further insight can hopefully be gained by the selective addition of components of different polarity compared to the main solvent. The photostability of a TIPS-pentacene solution at concentration 2×10^{-4} M in THF was studied with the addition of toluene in various ratio under light and dark conditions, as shown in figure 6.4. Dark conditions effectively mean leaving the sample for the same length of time as for the irradiation samples but without illumination. The half-life for TIPS-pentacene in THF in the dark at this concentration is 4500min, whereas in the light it is 2940min. The addition even a small proportion of toluene causes an immediate reduction in the half-life in both cases. The half-life of these samples is tabulated in table 6.4.

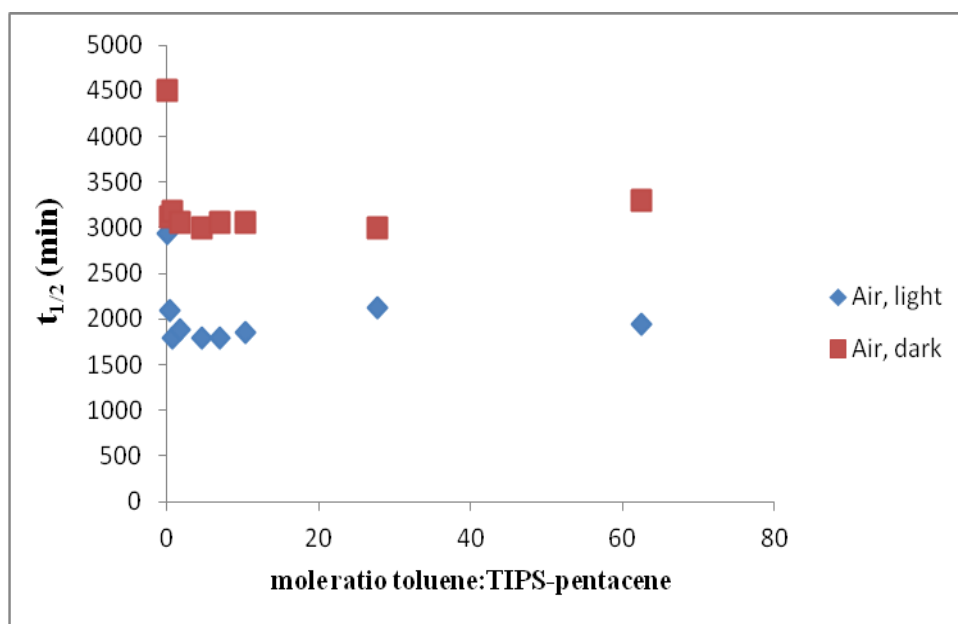


Figure 6.4: The $t_{1/2}$ vs mole ratio of toluene/TIPS-pentacene in THF (2×10^{-4} M) under different conditions at 26°C.

Table 6.4: The half-lives for TIPS-pentacene / toluene at concentration (2×10^{-4} M) in THF solutions at different ratio (w/w) under different irradiation conditions at 26°C.

w/w ratio TIPS-pentacene/ toluene	Mole ratio of Toluene/TIPS -pentacene	t _{1/2} (min) in O ₂ / white light (60W) and ambient light	t _{1/2} (min) in O ₂ / in dark
100/0	0	2940 +/- 180 (3120,2760)	4500
95/5	0.35	2100	3120
90/00	0.76	1800	3180
80/20	1.73	1890+/-90 (1980,1800)	3060
60/40	4.58	1790 +/- 10 (1800,1780)	3000
50/50	6.94	1860	3060
40/60	10.4	2120	3060
20/80	27.8	1950 +/- 90 (2040,1860)	3000
10/90	62.4	1920	3300

6.3 Effect of added polymer on rate of photo-oxidative degradation of TIPS-pentacene in THF (2×10^{-4} M)

Next, the effect of added polymer to TIPS-pentacene photostability in good solvent was studied by varying the ratio (w/w) % of TIPS-pentacene polymer blends under different conditions. Four types of solutions blended containing of TIPS-pentacene with aPS, iPS, i-PMMA, and PTAA were by mixing the two solids at various ratio (w/w) % in THF (2×10^{-4} M) and stirring the solutions for several hours at 26°C.

6.3.1 Effect of added amorphous polystyrene on rate of photo-oxidative degradation of TIPS-pentacene in THF (2×10^{-4} M)

The influence of atactic polystyrene on the photostability with TIPS-pentacene in toluene is shown in figure 6.5 and tabulated in table 6.5. The addition of aPS has a dramatic effect on the photostability, decreasing the half-life in all ratio of the blends in light conditions. There is however no effect on the dark lifetime, suggesting that the effect is in some way photoactivated.

Table 6.5: The half-lives for TIPS-pentacene/amorphous polystyrene (aPS) at concentration (2×10^{-4} M) in THF solution at different ratio (w/w) under different irradiation conditions at 26°C.

w/w ratio TIPS-pentacene/aPS	Mol ratio of aPS/ TIPS-pentacene	$t_{1/2}$ (min) in O ₂ / white light (60W) and ambient light	$t_{1/2}$ (min) in O ₂ / in dark
100/0	0	2940	4500
95/5	0.309735	2160	4320
90/10	0.672566	1980	4380
80/20	1.530973	2250	4260
60/40	4.053097	1910	4300
50/50	6.141593	1740	4440
40/60	9.20354	1790	4350
20/80	24.60177	1680	4260
10/90	55.22124	1740	4680

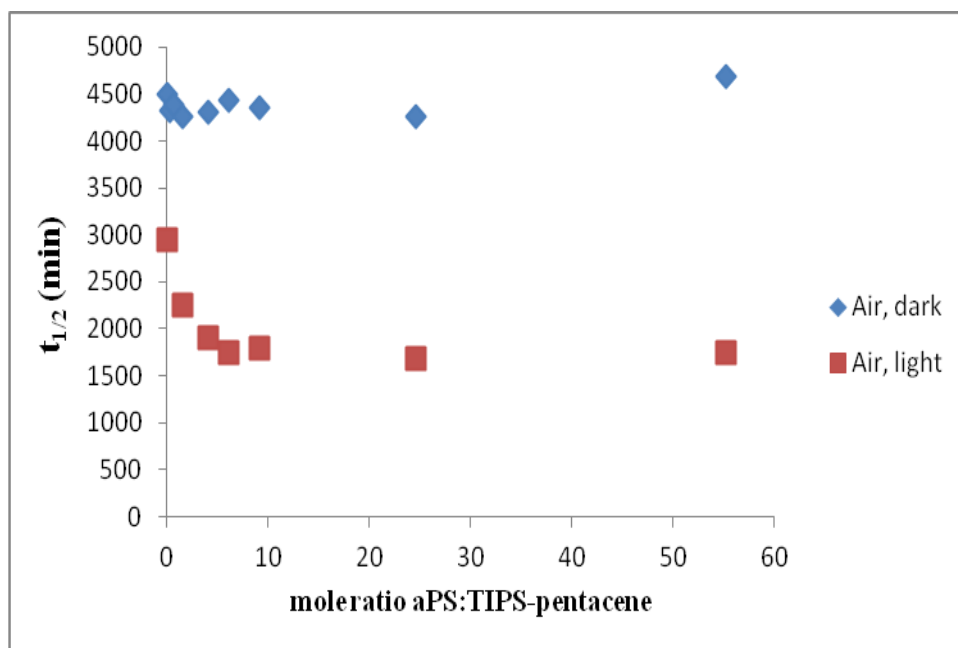


Figure 6.5: The $t_{1/2}$ vs mole ratio amorphous polystyrene (aPS) polystyrene/ TIPS-pentacene in THF (2×10^{-4} M) under different conditions at 26°C.

6.3.2 Effect of added isotactic polystyrene on rate of photo-oxidative degradation of TIPS-pentacene at concentration (2×10^{-4} M) in THF

A similar decrease in half-life was observed when iPS was used, as displayed in figure 6.6 under different irradiation conditions. To compare the data reported in figure 6.6, the half-life of each of these samples is tabulated in table 6.6. Added atactic polystyrene and isotactic polystyrene were found to reduce photooxidative degradation, which means that adding anything which can act as an acceptor to the solution will slow down the degradation and anything which impairs pair-wise energy transfer speeds up the degradation.

Table 6.6 : The half-lives for TIPS-pentacene / isotactic polystyrene at concentration (2×10^{-4} M) in THF solution at different ratio (w/w) under different irradiation conditions at 26°C.

w/w ratio TIPS-pentacene/ iPS	Mole ratio of iPS/ TIPS-pentacene	$t_{1/2}$ (min) in O ₂ / white light (60W) and ambient light	$t_{1/2}$ (min) in O ₂ / in dark
100/0	0	2940	4500
95/5	0.309	2820	3960
90/10	0.672	2280	4080
80/20	1.530	2340	4020
60/40	4.053	1660	3840
50/50	6.141	1800	4020
40/60	9.203	1860	4140
20/80	24.60	2160	4020
10/90	55.22	2280	4012

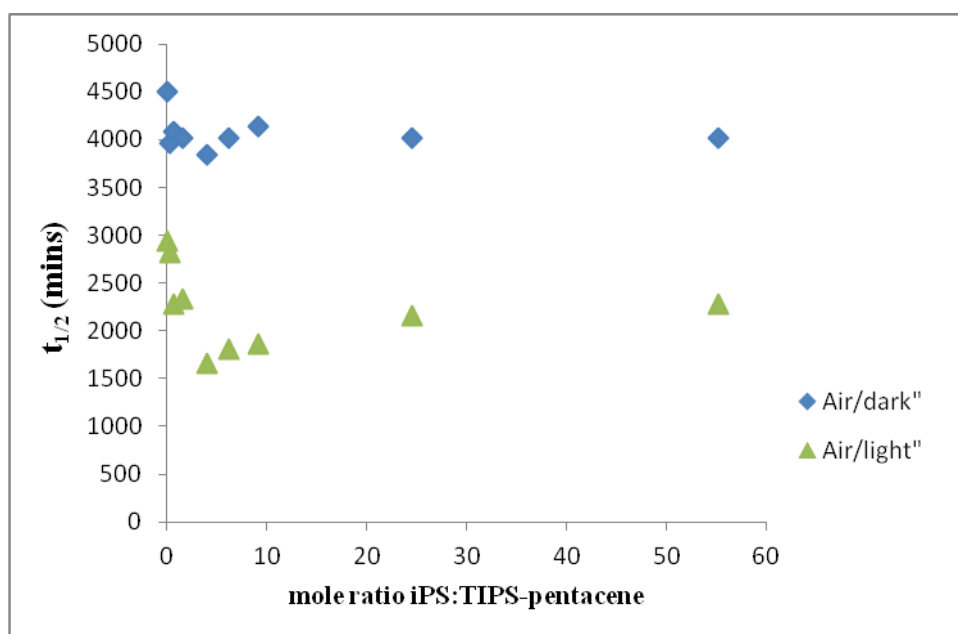


Figure 6.6: The $t_{1/2}$ vs mole ratio isoatactic polystyrene/ TIPS-pentacene in THF (2×10^{-4} M) under different conditions at 26°C.

6.3.3 Effect of added isotactic poly (methacrylate) i-PMMA and poly(triethylamine) (PTAA) on rate of photo-oxidative degradation of TIPS-pentacene at concentration (2×10^{-4} M) in THF

The half-life results from TIPS-pentacene blends with i-PMMA and PTAA with different ratios are shown in table 6.7 and figure 6.7. The data indicate similar photostability in both blends at all ratios. This means addition of PTAA or i-PMMA has no effect and it is therefore concluded that it does not interact with the solute.

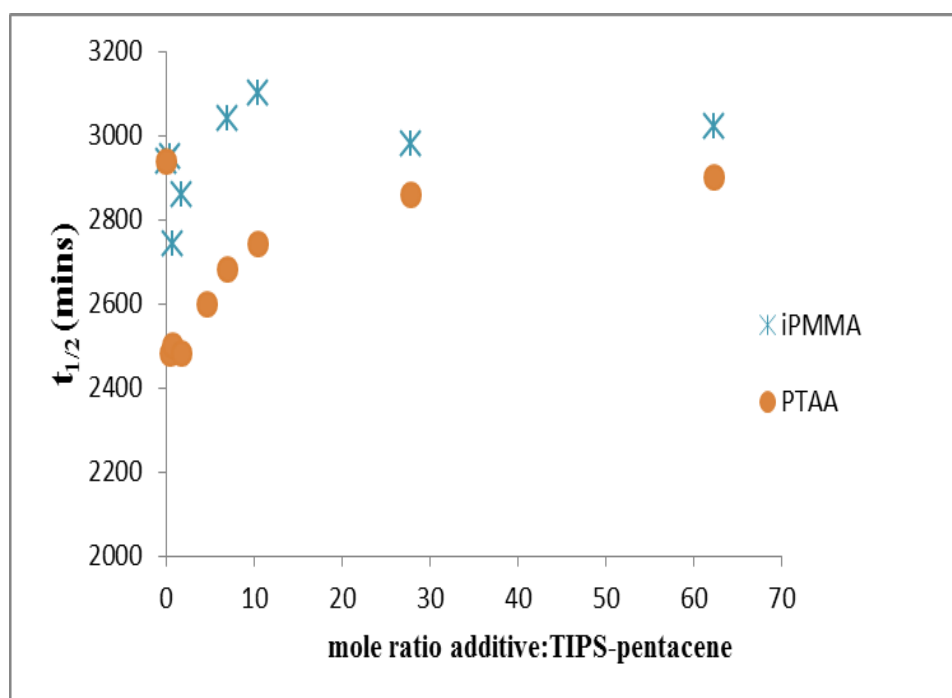


Figure 6.7: The $t_{1/2}$ vs mole ratio TIPS-pentacene/ i-PMMA and TIPS-pentacene/ PTAA in THF (2×10^{-4} M) under light conditions at 26°C.

Table 6.7: The half-lives for TIPS-pentacene/ i-PMMA and TIPS-pentacene/ PTAA at concentration (2×10^{-4} M) in THF solution at different ratio (w/w) under light conditions at 26°C.

w/w ratio TIPS-pentacene/ i-PMMA or PTAA	Mol ratio of i-PMMA, or PTAA / TIPS- pentacene	$t_{1/2}$ (min) in O₂/ white light (60W) and ambient light of TIPS-pentacene/ iPMMA	$t_{1/2}$ (min) in O₂/ white light (60W) and ambient light of TIPS-pentacene/ PTAA
100/0	0	2940	2940
95/5	0.309	2950	2480
90/00	0.672	2740	2500
80/20	1.530	2860	2480
60/40	4.053	2500	2600
50/50	6.141	3040	2680
40/60	9.203	3100	2740
20/80	24.60	2980	2860
10/90	55.22	3020	2900

Figure 6.8 shows the effect of the addition of up to 10 mole-equivalents of aromatic solvent (toluene) and poly(styrene) on the half-life of TIPS-pentacene in THF. The addition of PTAA and i-PMMA has no effect and it is therefore concluded that it does not interact with the solute. Toluene however has a dramatic effect, decreasing the half-life by ~40% with the addition of 1 mole-equivalent. Similar but less dramatic decreases are seen with the addition of poly (styrene) – the effect can be seen to occur over a wider mole-equivalent range. That this effect occurs at TIPS-pentacene concentrations sufficiently low such that aggregation is insignificant suggests that the addition of material which is either ‘good’ solvent (toluene) or for which a strong π - π interaction is possible serves to reduce TIPS-pentacene pairwise interactions and therefore reduce cooperative singlet exciton deactivation.

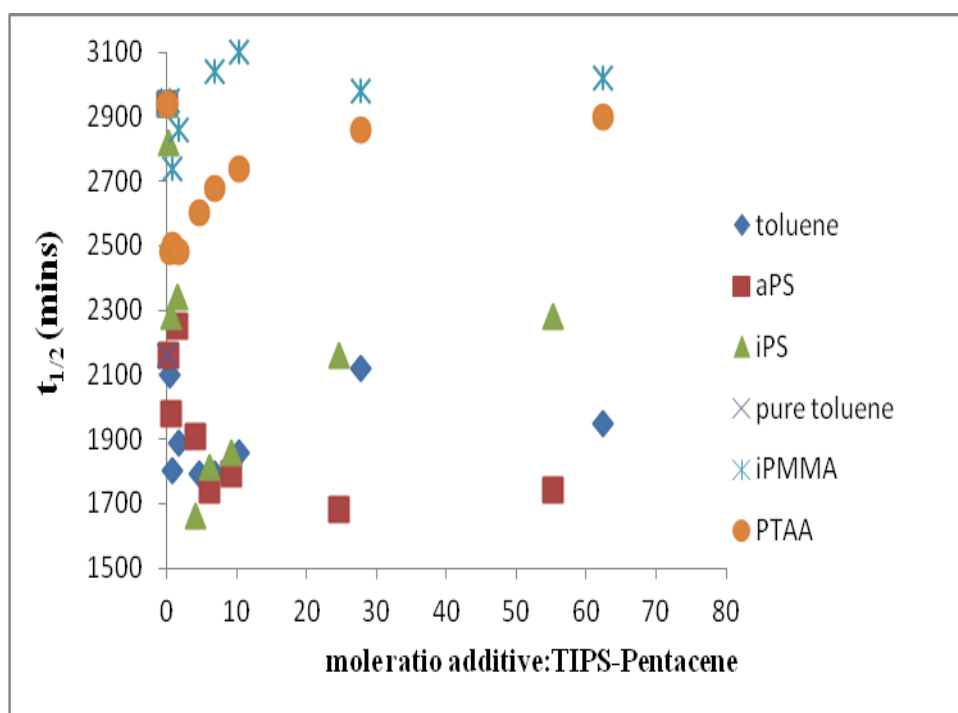


Figure 6.8: Effect of added toluene and polymer to half-life of photo-oxidation of TIPS-pentacene in THF (2×10^{-4} M) under light conditions at 26°C.

6.4 Conclusion

Toluene was found to accelerate photooxidative degradation compared with THF or CH₂Cl₂. Added atactic polystyrene and isotactic polystyrene were found to accelerate photooxidative degradation whilst isotactic poly(methylmethacrylate) and PTAA had no effect. It appears that adding anything which impairs pair-wise energy transfer speeds up the degradation. This is further evidence of the addition polystyrene influencing the solution aggregation interaction behaviour of 6,13 substituted pentacene's through competitive π - π interaction. In the case the stereo-regular nature of the side chain aromatic groups of isotactic polystyrene allow for a more enhanced π - π interaction leading to the formation of a supramolecular complex in solution. It is likely this is a co-operative mechanism in the positive effect of binder on enhanced thin film semi-conductor performance. Further work is needed to explore this phenomenon.

Chapter 7

7 Conclusion and Further work

7.1 Conclusion

In summary, these measurements clearly demonstrate the effects of concentration, solvent, solution polarity, oxygen solubility and aggregation on photo-stability of acenes in solution. At low concentration, photo-excited TIPS-pentacene molecules have a lower probability of deactivation and tend to preferentially undergo electron-transfer to O₂, leading to short life-times with respect to endoperoxide formation. This effect is mitigated by poor solvent and by high oxygen solubility, which serve to deactivate the initial excited state by singlet fission and quenching respectively. At higher concentrations, photostability is increased by two parallel mechanisms – de-excitation by a near-neighbour molecule (of which there are more) and by the formation of aggregates (which are both incapable of reacting with oxygen and also effectively quench the initial singlet state of TIPS-pentacene, as observed in condensed thin films [12]). The addition of small quantities of additives with a strong affinity for TIPS-pentacene also serves to reduce the half-life. These observations have ramifications for device fabrication. If the concentration is too low, the rate of photo-degradation is significant and is likely that decomposition products with unfavourable optical or electronic properties will be incorporated into devices. At higher concentration, the aggregates are present in significant numbers which increases photostability. The incorporation of preformed aggregation into films may have implications for the structure (and therefore electronic and/or optical properties) of the resulting devices. However, these effects might be mitigated or controlled by careful manipulation of the solute/solvent/additive blend: such as intermolecular interactions in ternary blends.

7.2 Further work

Further work along the following lines is necessary to resolve some of the uncertainties in these data and conclusions:

- 1- To continue to focus upon those parameters which influence environmental stability of organic semiconductors.
 - Solution state.
 - Presence of polymers such as polystyrene and functionalised polystyrene.
 - Solvent blends (identifying tailored solvent mixtures based upon HSPs)
 - Dissolved quenching species such as O₂
- 2- To probe the aggregation behaviour of organic semiconductors in solution using fluorescence spectroscopy, light scattering, X-ray diffraction and ITC.
- 3- To relate solution aggregation to thin film morphology using TOF-SIMS, G₁XRD, thermal analysis and other spectroscopic techniques.

Further projects will also need to consider the following areas:

- To develop a more sophisticated description of the photochemistry and photophysics of substituted pentacenes in solution in different solvents at different concentrations.
- To extend the range of measurements to other oligoacenes in a variety of polymer and solvent mixtures.
- To study similar effects in polythiophene and C₇₀-PCBM materials which are used in solar cell application.

8 References

1. Brutting, W., *Introduction to physics of organic semiconductors*. 2005: Wiley-VCH.
2. Filo, J. and M. Putala, *Semiconducting Organic Molecular Materials*. Journal of Electrical Engineering-Elektrotechnicky Casopis, 2010. **61**(5): p. 314-320.
3. Facchetti, A., et al., *Building blocks for n-type organic electronics: Regiochemically modulated inversion of majority carrier sign in perfluoroarene-modified polythiophene semiconductors*. Angewandte Chemie-International Edition, 2003. **42**(33): p. 3900-3903.
4. Newman, C.R., et al., *Introduction to organic thin film transistors and design of n-channel organic semiconductors*. Chemistry of Materials, 2004. **16**(23): p. 4436-4451.
5. Jiang, L., H. Dong, and W. Hu, *Organic single crystal field-effect transistors: advances and perspectives*. Journal of Materials Chemistry, 2010. **20**(24): p. 4994-5007.
6. Mas-Torrent, M. and C. Rovira, *Novel small molecules for organic field-effect transistors: towards processability and high performance*. Chemical Society Reviews, 2008. **37**(4): p. 827-838.
7. Reese, C., et al., *Organic thin film transistors*. Mater. Today (Oxford, U. K.), 2004. **7**(9): p. 20-27.
8. Bredas, J.L., et al., *Organic semiconductors: a theoretical characterization of the basic parameters governing charge transport*. Proc. Natl. Acad. Sci. U. S. A., 2002. **99**(9): p. 5804-5809.
9. *What are organic semiconductors*. The bonding of sp²-hybridised carbon, Small-molecule organic semiconductors, Polymer organic semiconductors 2011.
10. Köhler, A. and H. Bässler, *Triplet states in organic semiconductors*. Materials Science and Engineering: R: Reports, 2009. **66**(4-6): p. 71-109.
11. Köhler, A. and H. Bässler, *What controls triplet exciton transfer in organic semiconductors?* Journal of Materials Chemistry, 2011. **21**(12): p. 4003-4011.
12. Wilson, M.W.B., et al., *Ultrafast Dynamics of Exciton Fission in Polycrystalline Pentacene*. Journal of the American Chemical Society, 2011. **133**(31): p. 11830-11833.
13. Zimmerman, P.M., et al., *Mechanism for Singlet Fission in Pentacene and Tetracene: From Single Exciton to Two Triplets*. Journal of the American Chemical Society, 2011. **133**(49): p. 19944-19952.
14. Sirringhaus, H., *Materials and Applications for Solution-Processed Organic Field-Effect Transistors*. Proceedings of the IEEE, 2009. **97**(9): p. 1570-1579.
15. Anthony, J.E., *Functionalized acenes and heteroacenes for organic electronics*. Chemical Reviews, 2006. **106**(12): p. 5028-5048.
16. Mei, J., et al., *Integrated Materials Design of Organic Semiconductors for Field-Effect Transistors*. Journal of the American Chemical Society, 2013. **135**(18): p. 6724-6746.
17. Kline, R.J., et al., *Dependence of regioregular poly(3-hexylthiophene) film morphology and field-effect mobility on molecular weight*. Macromolecules, 2005. **38**(8): p. 3312-3319.
18. Street, R.A. and A. Salleo, *Contact effects in polymer transistors*. Applied Physics Letters, 2002. **81**(15): p. 2887-2889.
19. Sun, Y., Y. Liu, and D. Zhu, *Advances in organic field-effect transistors*. J. Mater. Chem., 2005. **15**(1): p. 53-65.
20. Mas-Torrent, M. and C. Rovira, *Role of Molecular Order and Solid-State Structure in Organic Field-Effect Transistors*. Chemical Reviews, 2011. **111**(8): p. 4833-4856.
21. Antonio, F., *Semiconductors for organic transistors*. Materials Today, 2007. **10**(3): p. 28-37.

22. Stallinga, P. and H.L. Gomes, *Modeling electrical characteristics of thin-film field-effect transistors: I. Trap-free materials*. Synthetic Metals, 2006. **156**(21–24): p. 1305-1315.
23. Miozzo, L., A. Yassar, and G. Horowitz, *Surface engineering for high performance organic electronic devices: the chemical approach*. Journal of Materials Chemistry, 2010. **20**(13).
24. Gupta, D., N. Jeon, and S. Yoo, *Modeling the electrical characteristics of TIPS-pentacene thin-film transistors: Effect of contact barrier, field-dependent mobility, and traps*. Organic Electronics, 2008. **9**(6): p. 1026-1031.
25. Dimitrakopoulos, C.D. and P.R.L. Malenfant, *Organic Thin Film Transistors for Large Area Electronics*. Advanced Materials, 2002. **14**(2): p. 99-117.
26. Ling, M.M. and Z.N. Bao, *Thin film deposition, patterning, and printing in organic thin film transistors*. Chemistry of Materials, 2004. **16**(23): p. 4824-4840.
27. Diao, Y., et al., *Solution coating of large-area organic semiconductor thin films with aligned single-crystalline domains*. Nat Mater, 2013. **12**(7): p. 665-671.
28. Pasquarelli, R.M., D.S. Ginley, and R. O'Hayre, *Solution processing of transparent conductors: from flask to film*. Chemical Society Reviews, 2011. **40**(11): p. 5406-5441.
29. Wang, Y.W., et al., *Influence of measuring environment on the electrical characteristics of pentacene-based thin film transistors*. Thin Solid Films, 2004. **467**(1-2): p. 215-219.
30. Jang, J., et al., *Effect of active layer thickness on environmental stability of printed thin-film transistor*. Organic Electronics, 2009. **10**(3): p. 421-425.
31. Lee, H.N., et al., *Organic passivation layers for pentacene organic thin-film transistors*. Current Applied Physics, 2008. **8**(5): p. 626-630.
32. Han, S.H., et al., *Lifetime of organic thin-film transistors with organic passivation layers*. Applied Physics Letters, 2006. **88**(7).
33. Simeone, D., et al., *Influence of structural properties on environmental stability of pentacene thin film transistors*. Organic Electronics, 2011. **12**(3): p. 447-452.
34. Anthony, J.E., D.L. Eaton, and S.R. Parkin, *A road map to stable, soluble, easily crystallized pentacene derivatives*. Organic Letters, 2002. **4**(1): p. 15-18.
35. Roberson, L.B., et al., *Pentacene disproportionation during sublimation for field-effect transistors*. Journal of the American Chemical Society, 2005. **127**(9): p. 3069-3075.
36. Zong, X., et al., *Control of structure, morphology and property in electrospun poly(glycolide-co-lactide) non-woven membranes via post-draw treatments*. Polymer, 2003. **44**(17): p. 4959-4967.
37. Ruiz, R., et al., *Pentacene thin film growth*. Chemistry of Materials, 2004. **16**(23): p. 4497-4508.
38. Berg, O., et al., *s-dipentacene: Structure, spectroscopy, and temperature- and pressure-dependent photochemistry*. Journal of Physical Chemistry A, 1999. **103**(14): p. 2451-2459.
39. Maliakal, A., et al., *Photochemical stability of pentacene and a substituted pentacene in solution and in thin films*. Chemistry of Materials, 2004. **16**(24): p. 4980-4986.
40. Reddy, A.R. and M. Bendikov, *Diels-Alder reaction of acenes with singlet and triplet oxygen - theoretical study of two-state reactivity*. Chemical Communications, 2006(11).
41. De Angelis, F., et al., *Direct mass spectrometry investigation on Pentacene thin film oxidation upon exposure to air*. Chemical Physics Letters, 2009. **468**(4–6): p. 193-196.

42. Afzali, A., C.D. Dimitrakopoulos, and T.L. Breen, *High-Performance, Solution-Processed Organic Thin Film Transistors from a Novel Pentacene Precursor*. Journal of the American Chemical Society, 2002. **124**(30): p. 8812-8813.
43. Wolak, M.A., et al., *Functionalized pentacene derivatives for use as red emitters in organic light-emitting diodes*. Journal of Physical Chemistry B, 2004. **108**(18): p. 5492-5499.
44. Afzali, A., C.R. Kagan, and G.P. Traub, *N-sulfinylcarbamate-pentacene adduct: A novel pentacene precursor soluble in alcohols*. Synthetic Metals, 2005. **155**(3): p. 490-494.
45. Chow, T.J., et al., *A new type of soluble pentacene precursor for organic thin-film transistors*. Chemical Communications, 2007(10): p. 1065-1067.
46. Vets, N., M. Smet, and W. Dehaen, *Reduction versus rearrangement of 6,13-dihydro-6,13-diarylpentacene-6,13-diols affording 6,13- and 13,13'-substituted pentacene derivatives*. Synlett, 2005(2): p. 217-222.
47. Miao, Q., et al., *Organization of acenes with a cruciform assembly motif*. Journal of the American Chemical Society, 2006. **128**(4): p. 1340-1345.
48. Ono, K., et al., *Photooxidation and reproduction of pentacene derivatives substituted by aromatic groups*. Tetrahedron, 2007. **63**(39): p. 9699-9704.
49. Wang, J., et al., *New Oligothiophene-Pentacene Hybrids as Highly Stable and Soluble Organic Semiconductors*. Organic Letters, 2009. **11**(12): p. 2563-2566.
50. Sheraw, C.D., et al., *Functionalized pentacene active layer organic thin-film transistors*. Advanced Materials, 2003. **15**(23): p. 2009-2011.
51. Kwon, J.-H., et al., *A flexible organic thin-film transistor with 6,13-bis(triisopropylsilylethynyl)pentacene and a methyl-siloxane-based dielectric*. Solid-State Electronics, 2009. **53**(3): p. 266-270.
52. Payne, M.M., et al., *Organic Field-Effect Transistors from Solution-Deposited Functionalized Acenes with Mobilities as High as 1 cm²/V·s*. Journal of the American Chemical Society, 2005. **127**(14): p. 4986-4987.
53. Griffith, O.L., et al., *Electronic Properties of Pentacene versus Triisopropylsilylethynyl-Substituted Pentacene: Environment-Dependent Effects of the Silyl Substituent*. Journal of the American Chemical Society, 2009. **132**(2): p. 580-586.
54. Coppo, P. and S.G. Yeates, *Shining light on a pentacene derivative: The role of photoinduced cycloadditions*. Advanced Materials, 2005. **17**(24): p. 3001-+.
55. Anthony, J.E., et al., *Functionalized pentacene: Improved electronic properties from control of solid-state order*. Journal of the American Chemical Society, 2001. **123**(38): p. 9482-9483.
56. Li, Y., et al., *Stable Solution-Processed High-Mobility Substituted Pentacene Semiconductors*. Chem. Mater., 2007. **19**(3): p. 418-423.
57. Palayangoda, S.S., et al., *Synthesis of Highly Soluble and Oxidatively Stable Tetraceno[2,3-b]thiophenes and Pentacenes*. The Journal of Organic Chemistry, 2007. **72**(17): p. 6584-6587.
58. Maliakal, A., B.H. Northrop, and K.N. Houk, *Photostability of pentacene and 6,13-disubstituted pentacene derivatives: a theoretical and experimental mechanistic study*. Photochemical & Photobiological Sciences, 2008. **7**(12): p. 1463-1468.
59. Miller, G.P., et al., *Substituent Effects in Pentacenes: Gaining Control over HOMO-LUMO Gaps and Photooxidative Resistances*. Journal of the American Chemical Society, 2008. **130**(48): p. 16274-16286.
60. Meng, H., et al., *Tetramethylpentacene: Remarkable absence of steric effect on field effect mobility*. Advanced Materials, 2003. **15**(13): p. 1090-+.
61. Swartz, C.R., et al., *Synthesis and characterization of electron-deficient pentacenes*. Organic Letters, 2005. **7**(15): p. 3163-3166.

62. Jiang, J., B.R. Kaafarani, and D.C. Neckers, *Design, Synthesis, and Properties of New Derivatives of Pentacene*. J. Org. Chem., 2006. **71**(5): p. 2155-2158.
63. Wang, Y.-M., et al., *Synthesis, characterization, and reactions of 6,13-disubstituted 2,3,9,10-tetrakis(trimethylsilyl)pentacene derivatives*. Tetrahedron, 2007. **63**(35): p. 8586-8597.
64. Jurchescu, O.D., et al., *Organic Single-Crystal Field-Effect Transistors of a Soluble Anthradithiophene*. Chemistry of Materials, 2008. **20**(21): p. 6733-6737.
65. Kim, C., et al., *Novel soluble pentacene and anthradithiophene derivatives for organic thin-film transistors*. Organic Electronics, 2010. **11**(8): p. 1363-1375.
66. Sakamoto, Y., et al., *Perfluoropentacene: High-performance p-n junctions and complementary circuits with pentacene*. Journal of the American Chemical Society, 2004. **126**(26): p. 8138-8140.
67. Appleton, A.L., et al., *Effects of electronegative substitution on the optical and electronic properties of acenes and diazaacenes*. Nat Commun, 2010. **1**: p. 91.
68. Liang, Z., et al., *Soluble and Stable N-Heteropentacenes with High Field-Effect Mobility*. Advanced Materials, 2011. **23**(13): p. 1535-1539.
69. Kawanaka, Y., et al., *Using Stable Radicals To Protect Pentacene Derivatives from Photodegradation*. Angewandte Chemie International Edition, 2013. **52**(26): p. 6643-6647.
70. Mondal, R., et al., *Synthesis, Stability, and Photochemistry of Pentacene, Hexacene, and Heptacene: A Matrix Isolation Study*. Journal of the American Chemical Society, 2009. **131**(40): p. 14281-14289.
71. Bendikov, M., et al., *Oligoacenes: Theoretical prediction of open-shell singlet diradical ground states*. Journal of the American Chemical Society, 2004. **126**(24): p. 7416-7417.
72. Anthony, J.E., B. Purushothaman, and S.R. Parkin, *Synthesis and Stability of Soluble Hexacenes*. Organic Letters, 2010. **12**(9): p. 2060-2063.
73. Chun, D., Y. Cheng, and F. Wudl, *The most stable and fully characterized functionalized heptacene*. Angew Chem Int Ed Engl, 2008. **47**(44): p. 8380-8385.
74. Qu, H. and C. Chi, *A Stable Heptacene Derivative Substituted With Electron-Deficient Trifluoromethylphenyl and Triisopropylsilylethynyl Groups*. Org. Lett., 2010. **12**(15): p. 3360-3363.
75. Mondal, R., *Synthesis and Study of Higher Poly(acenes)s: Hexacene, Heptacene, and Derivatives* December (2007), Bowling Green State University. p. 155.
76. Takimiya, K., et al., *Design strategy for air-stable organic semiconductors applicable to high-performance field-effect transistors*. Science and Technology of Advanced Materials, 2007. **8**(4): p. 273-276.
77. Chi, X., et al., *5,6,11,12-Tetrachlorotetracene, a tetracene derivative with π -stacking structure: The synthesis, crystal structure and transistor properties*. Organic Electronics, 2008. **9**(2): p. 234-240.
78. Moon, H., et al., *Synthesis, crystal structure, and transistor performance of tetracene derivatives*. Journal of the American Chemical Society, 2004. **126**(47): p. 15322-15323.
79. Zhang, J., et al., *Acene-linked conjugated polymers with ratiometric fluorescent response to 1O₂*. Chemical Communications, 2011. **47**(12): p. 3445-3447.
80. Liang, Z., et al., *Unexpected Photooxidation of H-Bonded Tetracene*. Organic Letters, 2008. **10**(10): p. 2007-2010.
81. Zhang, J., et al., *Structure, photophysics, and photooxidation of crowded diethynyltetracenes*. Journal of Materials Chemistry, 2012. **22**(13): p. 6182-6189.

82. Payne, M.M., S.R. Parkin, and J.E. Anthony, *Functionalized Higher Acenes: Hexacene and Heptacene*. Journal of the American Chemical Society, 2005. **127**(22): p. 8028-8029.
83. Anthony, J.E., *The Larger Acenes: Versatile Organic Semiconductors*. Angewandte Chemie International Edition, 2008. **47**(3): p. 452-483.
84. Lobanova Griffith, O., et al., *Electron Transfer Parameters of Triisopropylsilylethynyl-Substituted Oligoacenes*. The Journal of Physical Chemistry C, 2008. **112**(51): p. 20518-20524.
85. Griffith, O.L., et al., *Intermolecular Effects on the Hole States of Triisopropylsilylethynyl-Substituted Oligoacenes*. The Journal of Physical Chemistry C, 2010. **114**(32): p. 13838-13845.
86. Griffith, O.L., et al., *Substituent Effects on the Electronic Characteristics of Pentacene Derivatives for Organic Electronic Devices: Dioxolane-Substituted Pentacene Derivatives with Triisopropylsilylethynyl Functional Groups*. Journal of the American Chemical Society, 2012. **134**(34): p. 14185-14194.
87. Kim, S.-o., et al., *H-Aggregation Strategy in the Design of Molecular Semiconductors for Highly Reliable Organic Thin Film Transistors*. Advanced Functional Materials, 2011. **21**(9): p. 1616-1623.
88. An, T.K., et al., *Molecular aggregation–performance relationship in the design of novel cyclohexylethynyl end-capped quaterthiophenes for solution-processed organic transistors*. Dyes and Pigments, 2013. **96**(3): p. 756-762.
89. Spano, F.C., *The Spectral Signatures of Frenkel Polarons in H- and J-Aggregates*. Accounts of Chemical Research, 2009. **43**(3): p. 429-439.
90. Xu, Z., et al., *Low-Threshold Nanolasers Based on Slab-Nanocrystals of H-Aggregated Organic Semiconductors*. Advanced Materials, 2012. **24**(35): p. OP216-OP220.
91. Llorente, G.R., et al., *High performance, acene-based organic thin film transistors*. Chemical Communications, 2009(21).
92. Arif, M.A., *Raman Scattering Studies and Charge Transport in Polyfluorenes*, August 2007, Missouri-Columbia. p. 209.
93. Velázquez-Campoy, A., et al., *Isothermal Titration Calorimetry*, in *Current Protocols in Cell Biology*. 2001, John Wiley & Sons, Inc.
94. Núñez, S., J. Venhorst, and C.G. Kruse, *Target–drug interactions: first principles and their application to drug discovery*. Drug Discovery Today, 2012. **17**(1–2): p. 10-22.
95. Blanchet, C.E. and D.I. Svergun, *Small-Angle X-Ray Scattering on Biological Macromolecules and Nanocomposites in Solution*. Annual Review of Physical Chemistry, 2013. **64**(1): p. 37-54.
96. Gonnelli, A., et al., *Small-Angle X-ray Scattering Study of Self-Assembling Lipophilic Guanines in Organic Solvents: G-Quadruplex Formation and Cation Effects in Cyclohexane*. The Journal of Physical Chemistry B, 2013. **117**(4): p. 1095-1103.
97. Rivnay, J., et al., *Quantitative Determination of Organic Semiconductor Microstructure from the Molecular to Device Scale*. Chemical Reviews, 2012. **112**(10): p. 5488-5519.
98. Fudickar, W. and T. Linker, *Why Triple Bonds Protect Acenes from Oxidation and Decomposition*. Journal of the American Chemical Society, 2012. **134**(36): p. 15071-15082.
99. Zehm, D., W. Fudickar, and T. Linker, *Molecular Switches Flipped by Oxygen*. Angewandte Chemie International Edition, 2007. **46**(40): p. 7689-7692.
100. Zehm, D., et al., *9,10-Diarylanthracenes as Molecular Switches: Syntheses, Properties, Isomerisations and Their Reactions with Singlet Oxygen*. Chemistry – A European Journal, 2008. **14**(36): p. 11429-11441.

101. Nozik, A.J. and J. Miller, *Introduction to Solar Photon Conversion*. Chemical Reviews, 2010. **110**(11): p. 6443-6445.
102. Rao, A., et al., *Photophysics of pentacene thin films: The role of exciton fission and heating effects*. Physical Review B, 2011. **84**(19): p. 195411.
103. Ramanan, C., et al., *Competition between Singlet Fission and Charge Separation in Solution-Processed Blend Films of 6,13-Bis(triisopropylsilylethynyl)pentacene with Sterically-Encumbered Perylene-3,4:9,10-bis(dicarboximide)s*. Journal of the American Chemical Society, 2011. **134**(1): p. 386-397.
104. Patterson, F.G., et al., *Intersystem crossing from singlet states of molecular dimers and monomers in mixed molecular crystals: picosecond stimulated photon echo experiments*. Chemical Physics, 1984. **84**(1): p. 51-60.
105. Nijegorodov, N., V. Ramachandran, and D.P. Winkoun, *The dependence of the absorption and fluorescence parameters, the intersystem crossing and internal conversion rate constants on the number of rings in polyacene molecules*. Spectrochimica Acta Part A: Molecular and Biomolecular Spectroscopy, 1997. **53**(11): p. 1813-1824.
106. Kim, C.S., et al., *Solvent-dependent electrical characteristics and stability of organic thin-film transistors with drop cast bis(triisopropylsilylethynyl) pentacene*. Applied Physics Letters, 2008. **93**(10): p. 103302-103302-3.
107. Kwang Nam, C., et al., *Solvent Effect on the Electrical Properties of Triisopropylsilylethynyl (TIPS) Pentacene Organic Thin-Film Transistors*. Device and Materials Reliability, IEEE Transactions on, 2009. **9**(3): p. 489-493.
108. Park, S.K., et al., *High mobility solution processed 6,13-bis(triisopropyl-silylethynyl) pentacene organic thin film transistors*. Applied Physics Letters, 2007. **91**(6).
109. Kim, Y.-H., et al., *Influence of Solvent on the Film Morphology, Crystallinity and Electrical Characteristics of Triisopropylsilyl Pentacene OTFTs*. Journal of The Electrochemical Society, 2007. **154**(12): p. H995-H998.
110. Lee, S.H., et al., *High-performance thin-film transistor with 6,13-bis(triisopropylsilylethynyl) pentacene by inkjet printing*. Organic Electronics, 2008. **9**(5): p. 721-726.
111. Shin, S.-I., et al., *Solution-processed 6,13-bis(triisopropylsilylethynyl) (TIPS) pentacene thin-film transistors with a polymer dielectric on a flexible substrate*. Semiconductor Science and Technology, 2008. **23**(8): p. 085009.
112. Aragón, J., et al., *Functionalized pentacenes: a combined theoretical, Raman and UV-Vis spectroscopic study*. Theoretical Chemistry Accounts, 2011. **128**(4-6): p. 521-530.
113. Zhu, Z., S. Wu, and Y. Zhang, *The electronic structures and spectra of conducting pentacene derivatives*. Russian Journal of Physical Chemistry A, Focus on Chemistry, 2008. **82**(13): p. 2293-2298.
114. Marie-Beatrice Madec, a.S.B., a Pablo Taboada,b Richard Heenan,c Mark Geoghegan and Stephen G. Yeates*a, *The influence of directed p-p interactions in solution on the thin film organic semiconductor device properties of small molecule polymer blends†*. Soft Matter, 2011.
115. Diaz, M.S., M.L. Freile, and M.I. Gutierrez, *Solvent effect on the UV/Vis absorption and fluorescence spectroscopic properties of berberine*. Photochemical & Photobiological Sciences, 2009. **8**(7): p. 970-974.
116. Suppan, P., *Invited review solvatochromic shifts: The influence of the medium on the energy of electronic states*. Journal of Photochemistry and Photobiology A: Chemistry, 1990. **50**(3): p. 293-330.
117. Bag, B. and P.K. Bharadwaj, *Effect of methylation to an ethylenediamine receptor-based fluorescence signaling system: Solvent dependence, metal ion selectivity and photophysical studies*. Journal of Luminescence, 2007. **126**(1): p. 27-36.

118. Wolak, M.A., et al., *Functionalized Pentacene Derivatives for Use as Red Emitters in Organic Light-Emitting Diodes*. J. Phys. Chem. B, 2004. **108**(18): p. 5492-5499.
119. C.M., *Hansen solubility parameters*, 2007: CRC Press, Boca Raton.
120. Chen, J.H., D.C. Martin, and J.E. Anthony, *Morphology and molecular orientation of thin-film bis(triisopropylsilylethynyl) pentacene*. Journal of Materials Research, 2007. **22**(6): p. 1701-1709.
121. Shirono, K., T. Morimatsu, and F. Takemura, *Gas Solubilities (CO₂, O₂, Ar, N₂, H₂, and He) in Liquid Chlorinated Methanes*. Journal of Chemical & Engineering Data, 2008. **53**(8): p. 1867-1871.
122. Fischer, K. and M. Wilken, *Experimental determination of oxygen and nitrogen solubility in organic solvents up to 10 MPa at temperatures between 298 K and 398 K*. The Journal of Chemical Thermodynamics, 2001. **33**(10): p. 1285-1308.
123. Battino, R., et al., *The Solubility of Oxygen and Ozone in Liquids*. Journal of physical and chemical reference data, 1983. **12**(2): p. 163.
124. Majhi, P.R. and A. Blume, *Thermodynamic Characterization of Temperature-Induced Micellization and Demicellization of Detergents Studied by Differential Scanning Calorimetry*. Langmuir, 2001. **17**(13): p. 3844-3851.
125. Merino-Garcia, D. and S.I. Andersen, *Calorimetric Evidence about the Application of the Concept of CMC to Asphaltene Self-Association*. Journal of Dispersion Science and Technology, 2005. **26**(2): p. 217-225.
126. Garidel, P., et al., *Thermodynamic Characterization of Bile Salt Aggregation as a Function of Temperature and Ionic Strength Using Isothermal Titration Calorimetry*. Langmuir, 2000. **16**(12): p. 5267-5275.
127. Nicolas, Y., et al., *TIPS-triphenodioxazine versus TIPS-pentacene: Enhanced electron mobility for n-type organic field-effect transistors*. Organic Electronics, 2012. **13**(8): p. 1392-1400.
128. Smulders, M.M.J., et al., *How to Distinguish Isodesmic from Cooperative Supramolecular Polymerisation*. Chemistry – A European Journal, 2010. **16**(1): p. 362-367.
129. Chen, Z., et al., *Self-assembled [small pi]-stacks of functional dyes in solution: structural and thermodynamic features*. Chemical Society Reviews, 2009. **38**(2).
130. Zhao, D. and J.S. Moore, *Nucleation-elongation: a mechanism for cooperative supramolecular polymerization*. Organic & Biomolecular Chemistry, 2003. **1**(20): p. 3471-3491.
131. Chung, M.-H., et al., *Polymer binder effects on the electrical characteristics of 6, 13-bis(triisopropylsilylethynyl)-pentacene thin-film transistors in different solvents*. Thin Solid Films, 2010. **518**(22): p. 6289-6294.
132. Madec, M.-B., et al., *Organic field effect transistors from ambient solution processed low molar mass semiconductor-insulator blends*. J. Mater. Chem., 2008. **18**(27): p. 3230-3236.
133. Kang, J., et al., *Structure and Properties of Small Molecule-Polymer Blend Semiconductors for Organic Thin Film Transistors*. Journal of the American Chemical Society, 2008. **130**(37): p. 12273-12275.
134. Chung, Y.S., et al., *Zone-Refinement Effect in Small Molecule-Polymer Blend Semiconductors for Organic Thin-Film Transistors*. Journal of the American Chemical Society, 2010. **133**(3): p. 412-415.
135. Park, B., et al., *High-performance organic thin-film transistors with polymer-blended small-molecular semiconductor films, fabricated using a pre-metered coating process*. J. Mater. Chem., 2012. **22**(12): p. 5641-5646.

136. Lada, M., et al., *Morphology control via dual solvent crystallization for high-mobility functionalized pentacene-blend thin film transistors*. J. Mater. Chem., 2011. **21**(30): p. 11232-11238.
137. Lim, J.A., et al., *Control of the Morphology and Structural Development of Solution-Processed Functionalized Acenes for High-Performance Organic Transistors*. Advanced Functional Materials, 2009. **19**(10): p. 1515-1525.
138. Smith, J., et al., *Solution-processed organic transistors based on semiconducting blends*. Journal of Materials Chemistry, 2010. **20**(13): p. 2562-2574.
139. Li, X., et al., *Charge transport in high-performance ink-jet printed single-droplet organic transistors based on a silylethynyl substituted pentacene/insulating polymer blend*. Organic Electronics, 2011. **12**(8): p. 1319-1327.
140. Kim, D.H., et al., *High-Mobility Organic Transistors Based on Single-Crystalline Microribbons of Triisopropylsilylethynyl Pentacene via Solution-Phase Self-Assembly*. Advanced Materials, 2007. **19**(5): p. 678-682.
141. Li, X., et al., *Azeotropic Binary Solvent Mixtures for Preparation of Organic Single Crystals*. Advanced Functional Materials, 2009. **19**(22): p. 3610-3617.
142. Madec, M.-B., et al., *Enhanced reproducibility of inkjet printed organic thin film transistors based on solution processable polymer-small molecule blends*. Journal of Materials Chemistry, 2010. **20**(41): p. 9155-9160.
143. Chae, G.J., et al., *Improved performance in TIPS-pentacene field effect transistors using solvent additives*. Journal of Materials Chemistry C, 2013.
144. Park, J.H., et al., *Self-assembly of organic channel/polymer dielectric layer in solution process for low-voltage thin-film transistors*. Organic Electronics, 2010. **11**(10): p. 1688-1692.
145. Kwon, J.-H., et al., *Channel width effect for organic thin film transistors using TIPS-pentacene employed as a dopant of poly-triarylamine*. Organic Electronics, 2009. **10**(4): p. 729-734.
146. Hwang, D.K., et al., *Solvent and polymer matrix effects on TIPS-pentacene/polymer blend organic field-effect transistors*. Journal of Materials Chemistry, 2012. **22**(12): p. 5531-5537.
147. Kwon, J.-H., et al., *A 6,13-bis(Triisopropylsilylethynyl) pentacene thin-film transistor using a spun-on inorganic gate-dielectric*. IEEE Trans. Electron Devices, 2008. **55**(2): p. 500-505.

9 Appendix

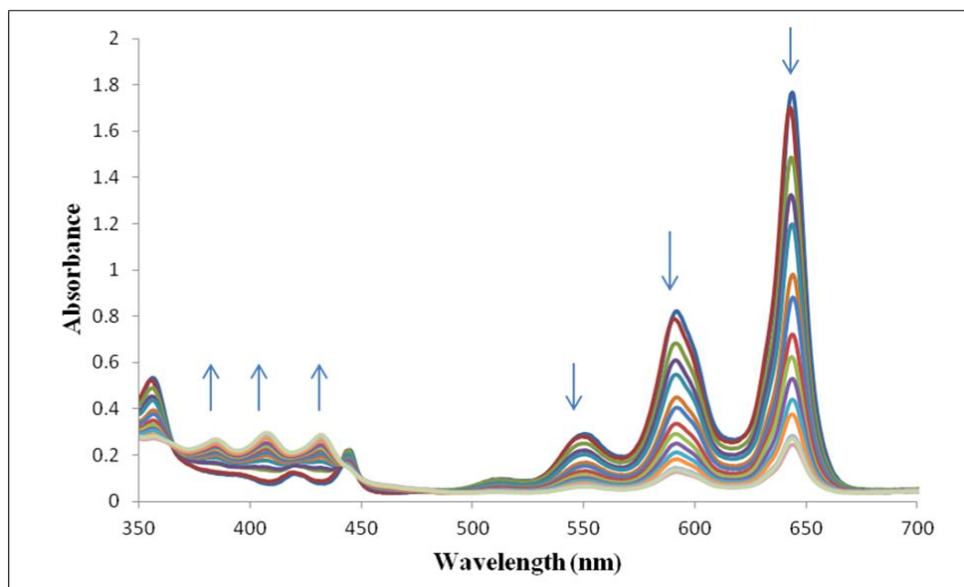


Figure 9.1: UV-visible absorption spectra for the photooxidation of TIPS-pentacene in dodecane at 5×10^{-5} M in a 10 mm pathlength at 26°C.

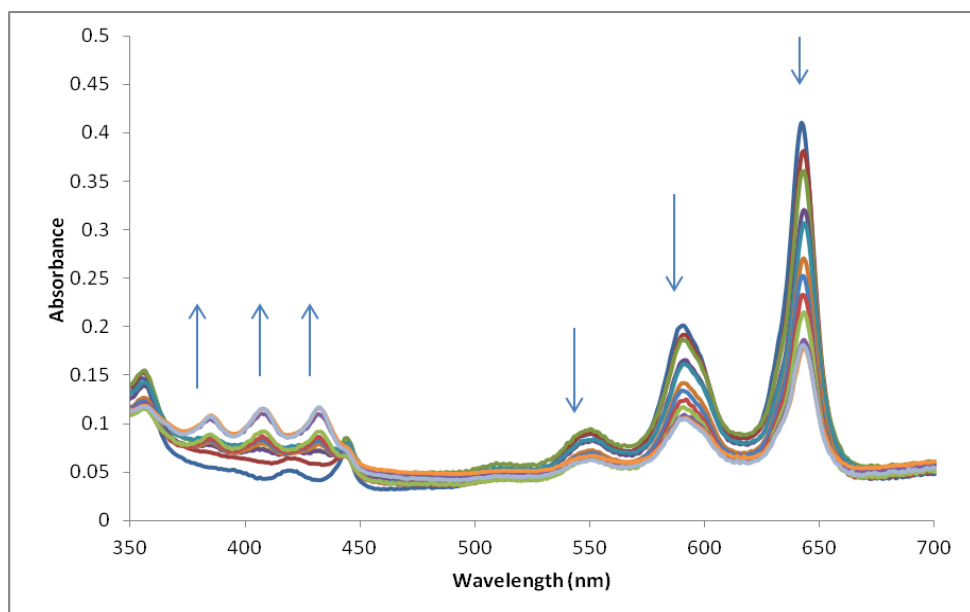


Figure 9.2: UV-visible absorption spectra for the photooxidation of TIPS-pentacene in decane at 5×10^{-5} M in a 10 mm pathlength at 26°C.

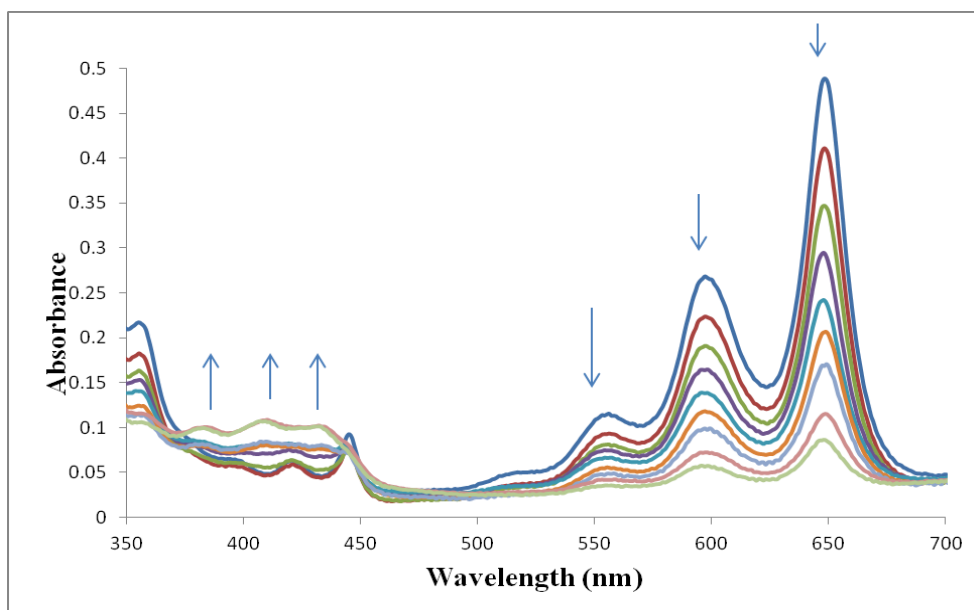


Figure 9.3: UV-visible absorption spectra for the photooxidation of TIPS-pentacene in DCM at 1×10^{-5} M in a 10 mm pathlength at 26°C.

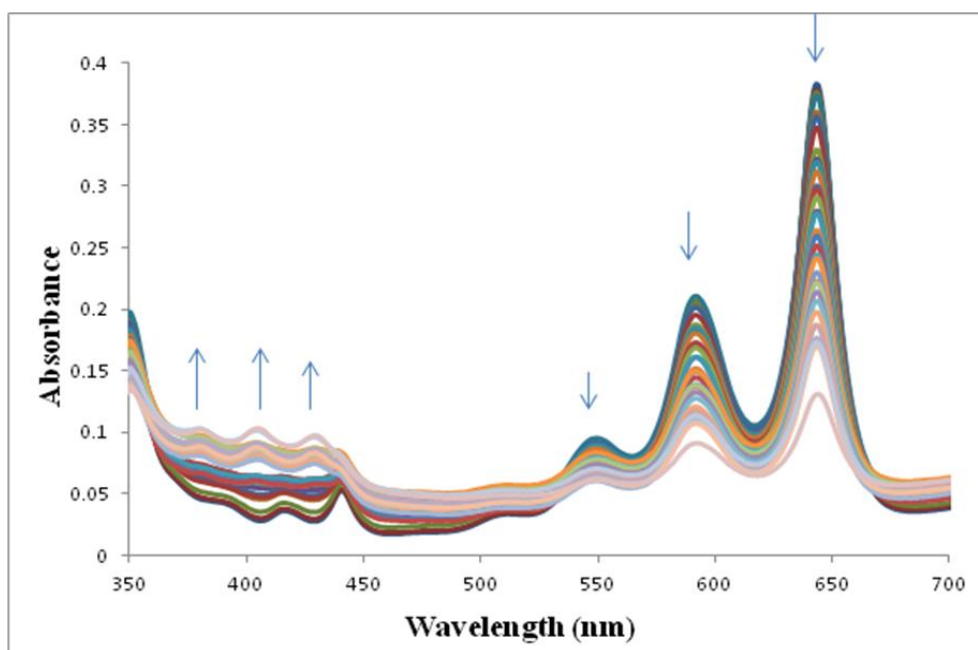


Figure 9.4: UV-visible absorption spectra for the photooxidation of TIPS-pentacene in THF at 1×10^{-5} M in a 10 mm pathlength at 26°C.

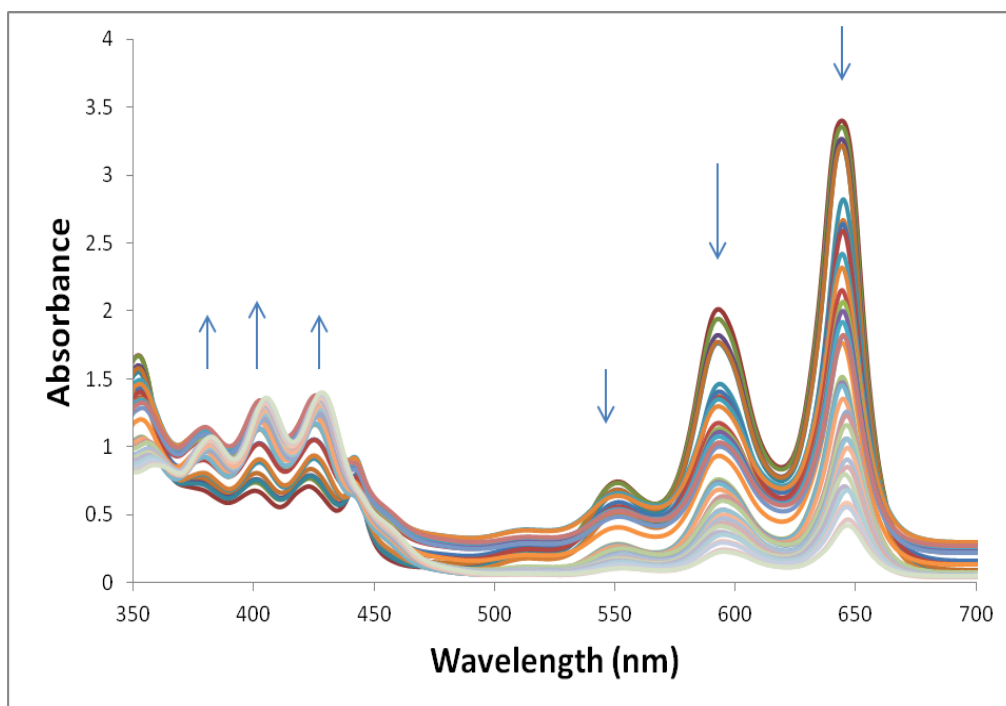


Figure 9.5: UV-visible absorption spectra for the photooxidation of TIPS-pentacene in THF at 1×10^{-4} M in a 10 mm pathlength at 26°C.

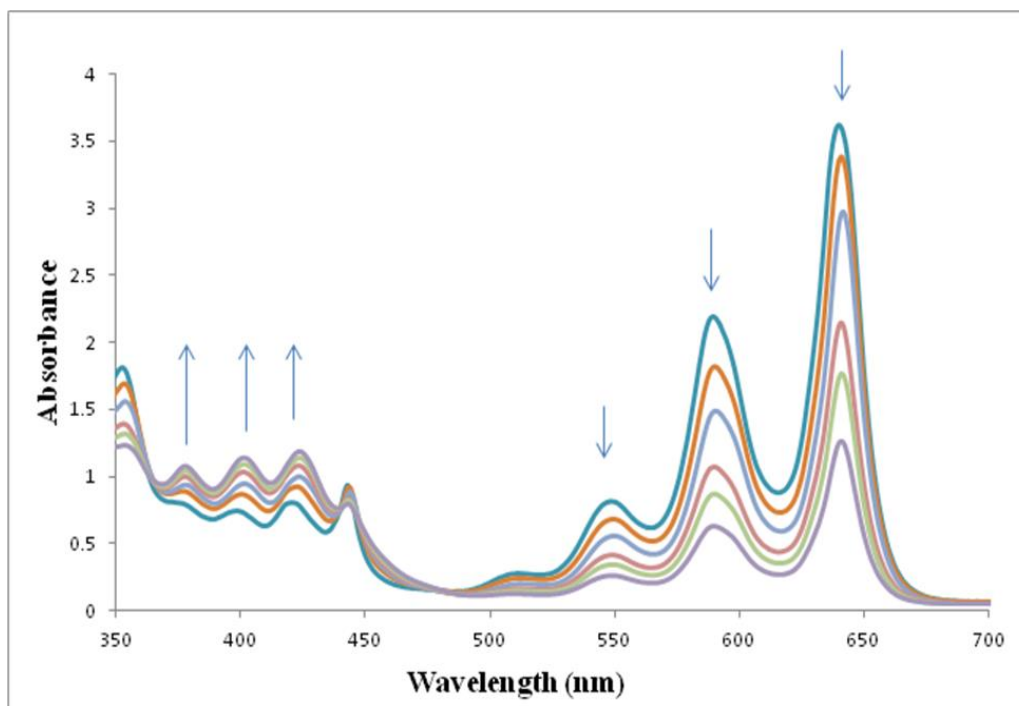


Figure 9.6: UV-visible absorption spectra for the photooxidation of TIPS-pentacene in IPA at 1×10^{-4} M in a 10 mm pathlength at 26°C.

¹H NMR analysis of TIPS-pentacene

¹H NMR (300MHz, CDCl₃): δ=1.40 (42H, m, CH(CH₃)₂), 7.45 (4H, dd, J=3.1 Hz, 6.5 Hz, H-2,H-3, H-9, H-10), 7.99 (4H, dd, J=3.1 Hz, 6.5 Hz, H-1, H-4, H-8, H-11), 9.32 (4H, s, H-5, H-7, H-12, H-14).

¹H NMR analysis of 6, 13-EPO-TIPS-pentacene

¹H NMR (300MHz, CDCl₃): δ=1.33 (42H,s, CH(CH₃)₂), 7.22-7.55 (4H, dd, J=3.2 Hz, 6.1 Hz, H-2,H-3, H-9, H-10), 7.86-7.90 (4H, dd, J=3.2 Hz, 6.1 Hz, H-1, H-4, H-8, H-11), 8.23 (4H,s, , H-5, H-7, H-12, H-14).

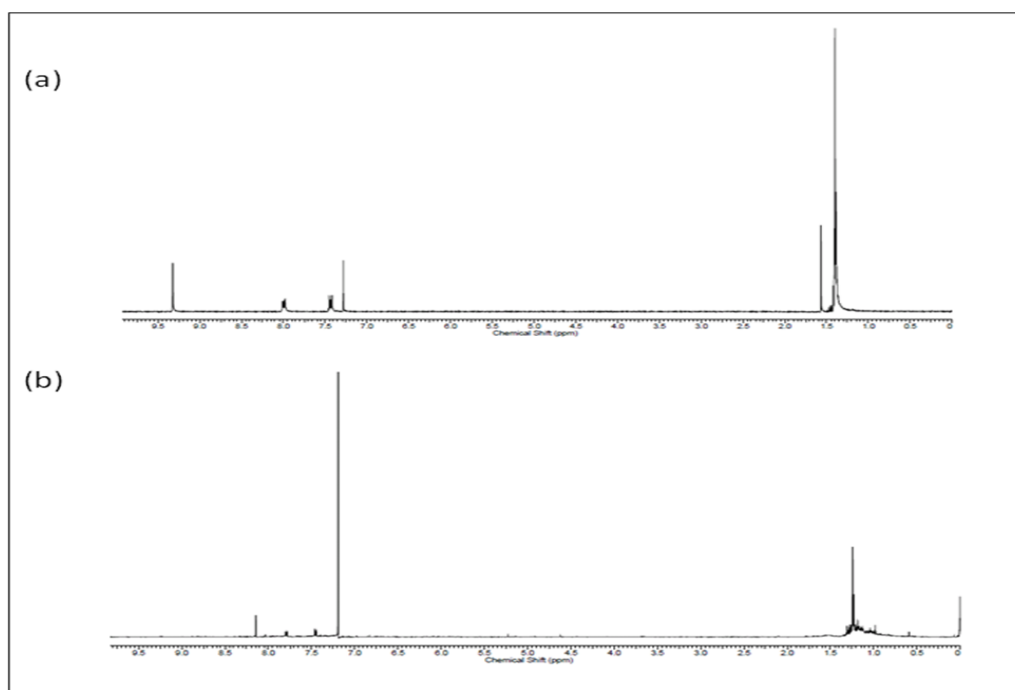
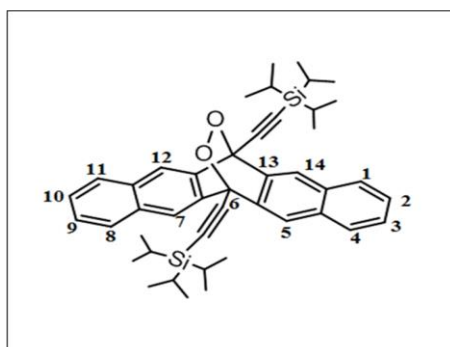


Figure 9.7: ¹H NMR spectra of TIPS-pentacene 1×10^{-5} M in THF, (a) before and (b) after photooxidation.

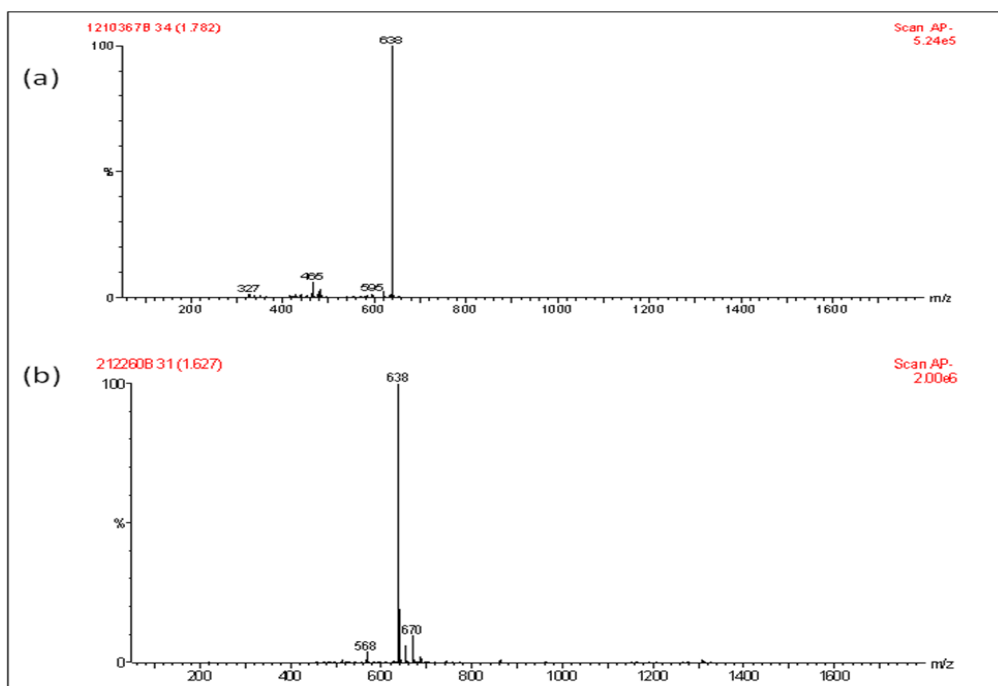


Figure 9.8: Mass spectrometry (APCI) (AP^-) of TIPS-pentacene 1×10^{-5} M in THF, (a) before and (b) after photooxidation.

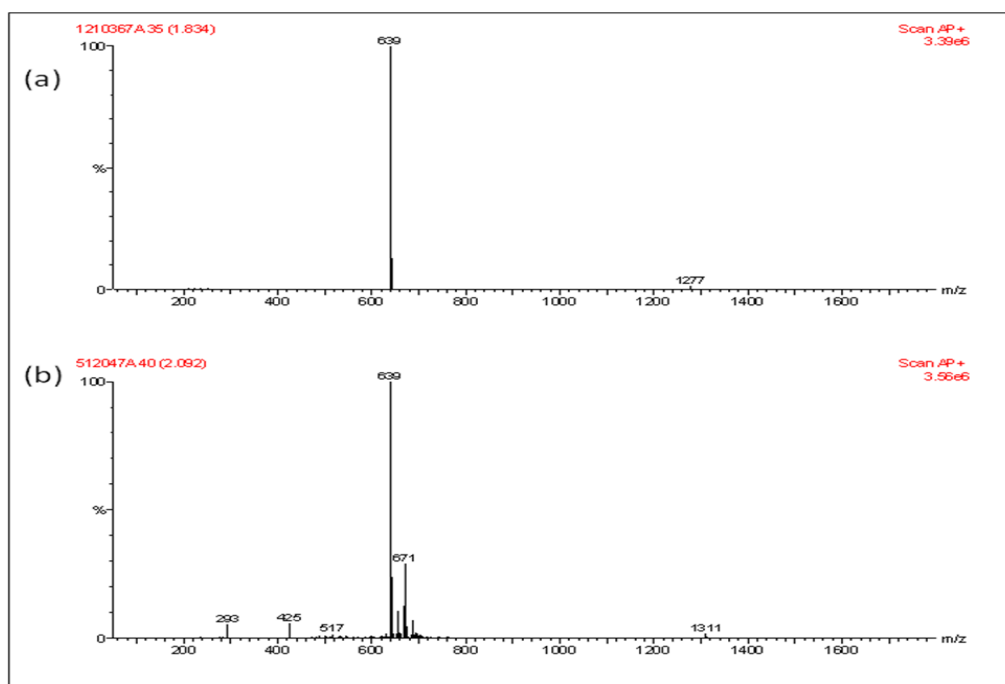


Figure 9.9: Mass spectrometry (APCI) (AP^+) of TIPS-pentacene 1×10^{-5} M in THF, (a) before and (b) after photooxidation.

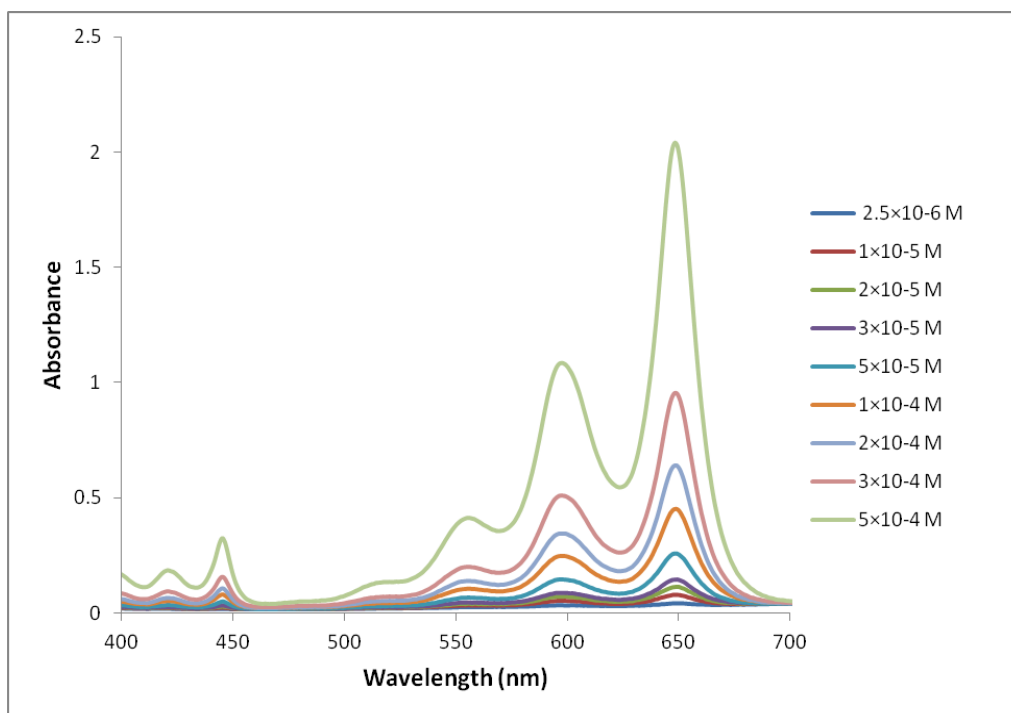


Figure 9.10: UV-vis absorption spectra of TIPS-pentacene in DCM at concentrations ranging from $2.5 \times 10^{-6} \text{ M}$ to $5 \times 10^{-4} \text{ M}$ in 1mm pathlength cuvette.

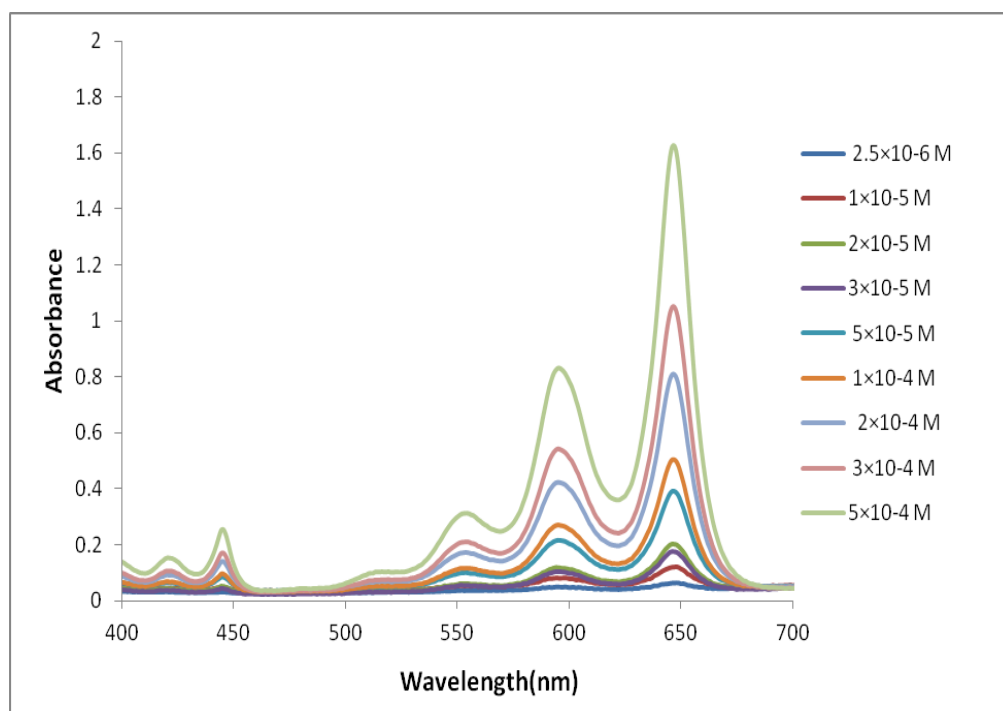


Figure 9.11: UV-vis absorption spectra of TIPS-pentacene in THF at concentrations ranging from $2.5 \times 10^{-6} \text{ M}$ to $5 \times 10^{-4} \text{ M}$ in 1mm pathlength cuvette.

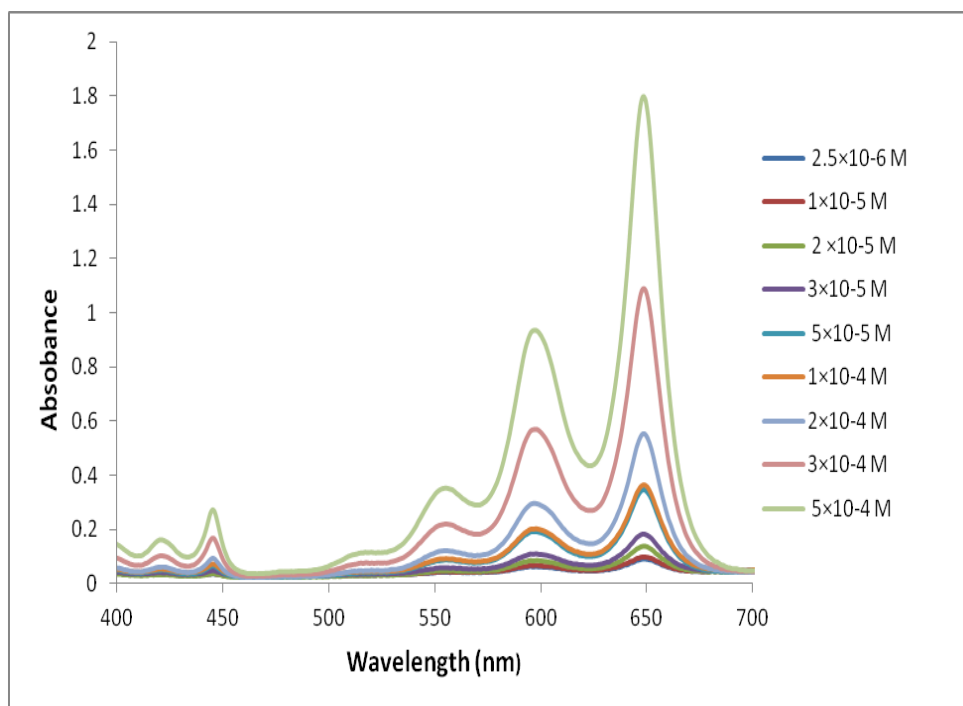


Figure 9.12: UV-vis absorption spectra of TIPS-pentacene in chloroform at concentrations ranging from 2.5×10^{-6} M to 5×10^{-4} M in 1mm pathlength cuvette.

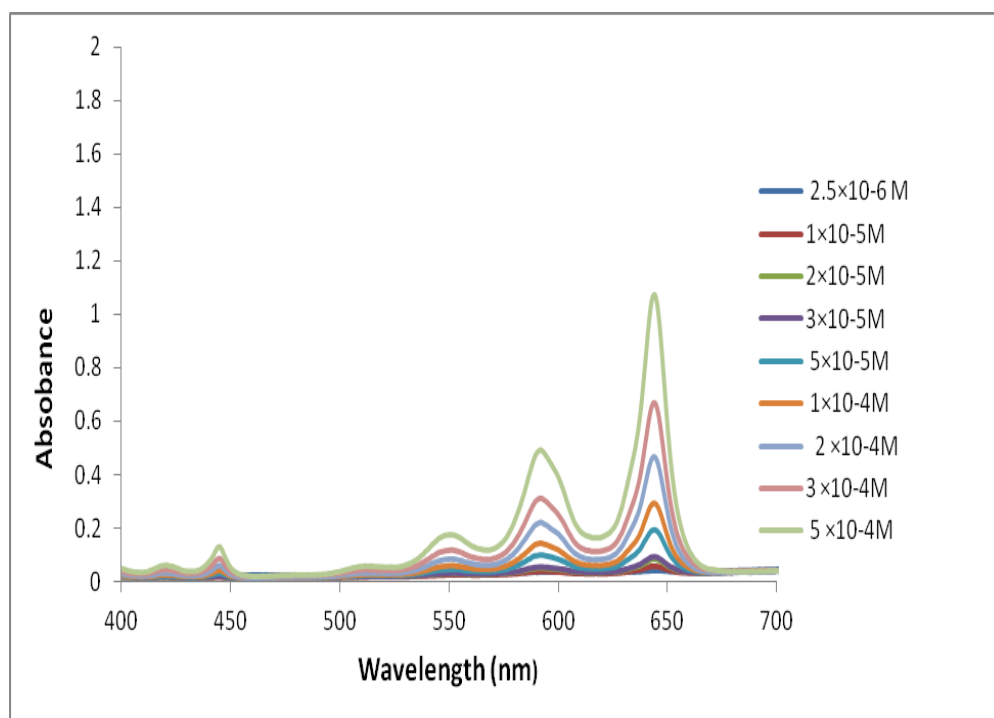


Figure 9.13: UV-vis absorption spectra of TIPS-pentacene in dodecane at concentrations ranging from 2.5×10^{-6} M to 5×10^{-4} M in 1mm pathlength cuvette.

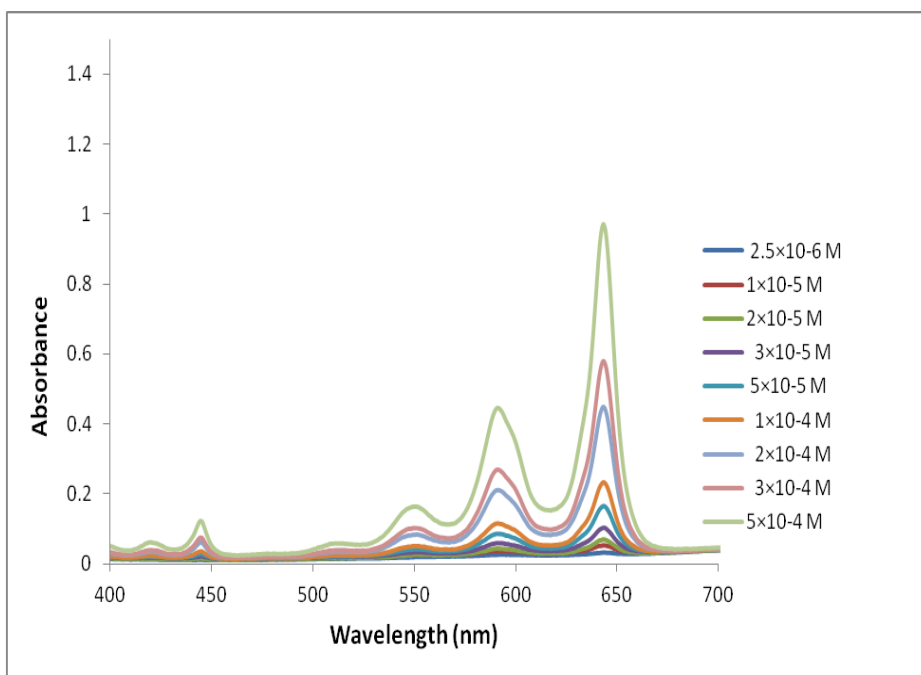


Figure 9.14: UV-vis absorption spectra of TIPS-pentacene in decane at concentrations ranging from 2.5×10^{-6} M to 5×10^{-4} M in 1mm pathlength cuvette.

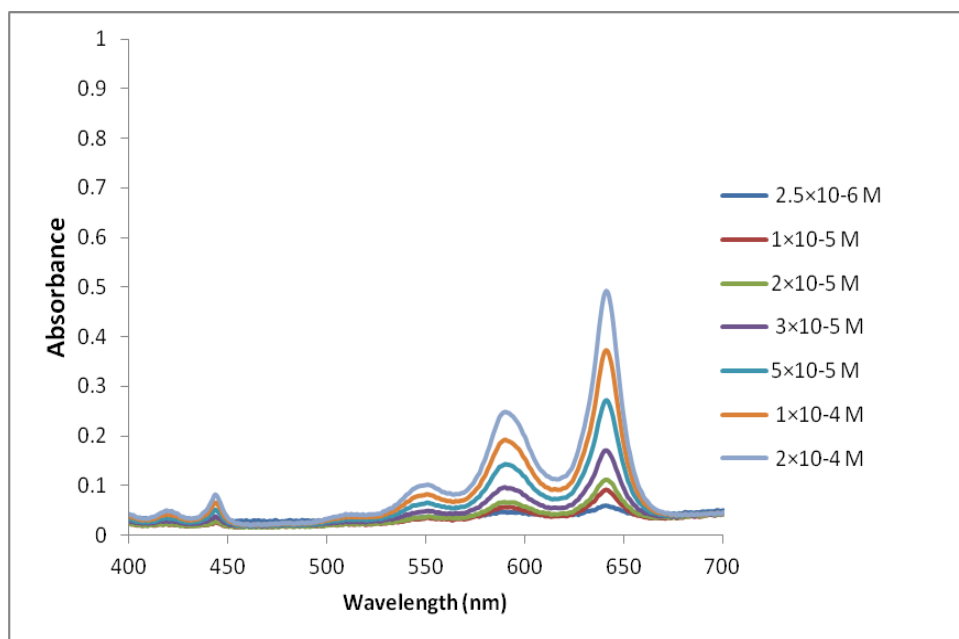


Figure 9.15: UV-vis absorption spectra of TIPS-pentacene in IPA at concentrations ranging from 2.5×10^{-6} M to 5×10^{-4} M in 1mm pathlength cuvette.

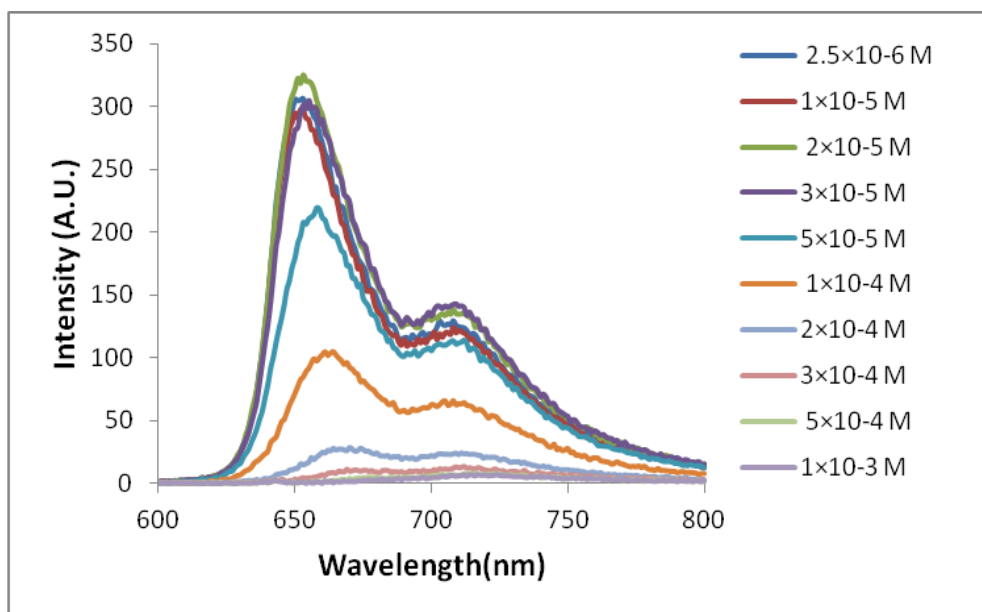


Figure 9.16: Fluorescence emission intensity of TIPS-pentacene in chloroform at concentrations ranging from 2.5×10^{-6} M to 1×10^{-3} M in 10mm pathlength cuvette at an excitation wavelength of 643nm.

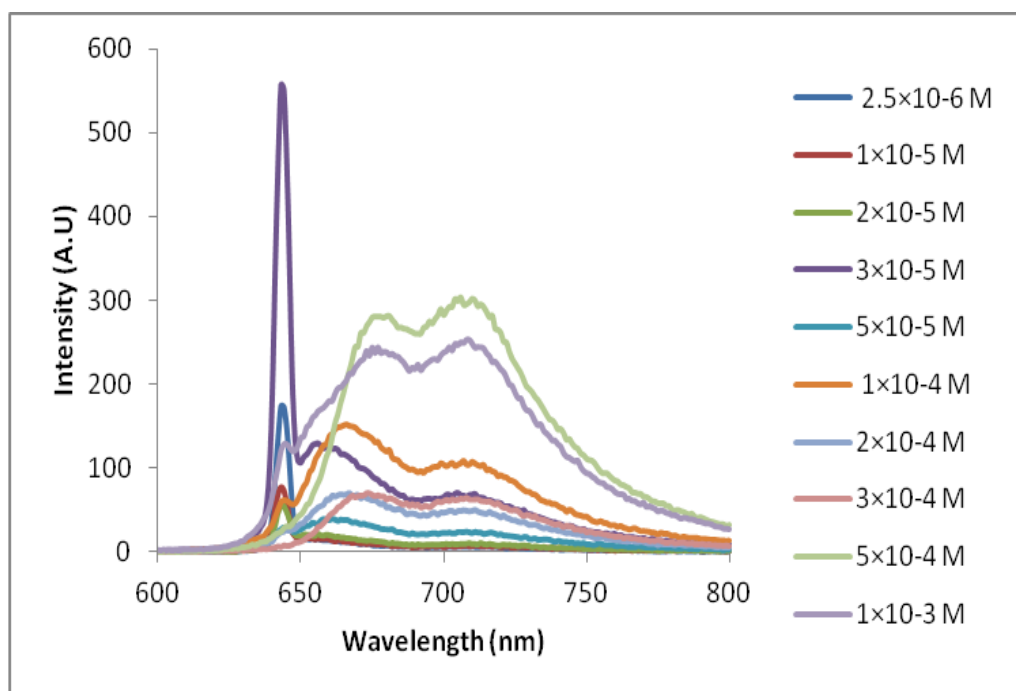


Figure 9.17: Fluorescence emission intensity of TIPS-pentacene in chloroform at concentrations ranging from 2.5×10^{-6} M to 1×10^{-3} M in 1mm pathlength cuvette at an excitation wavelength of 643nm.

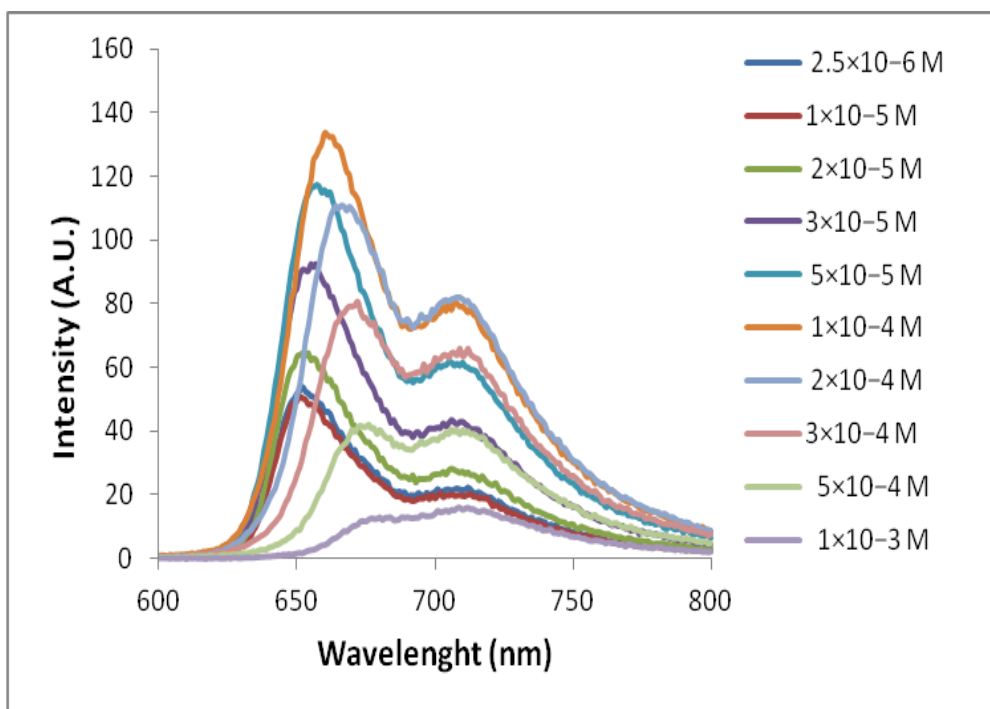


Figure 9.18: Fluorescence emission intensity of TIPS-pentacene in chloroform at concentrations ranging from 2.5×10^{-6} M to 1×10^{-3} M in 10mm pathlength cuvette at an excitation wavelength of 550nm.

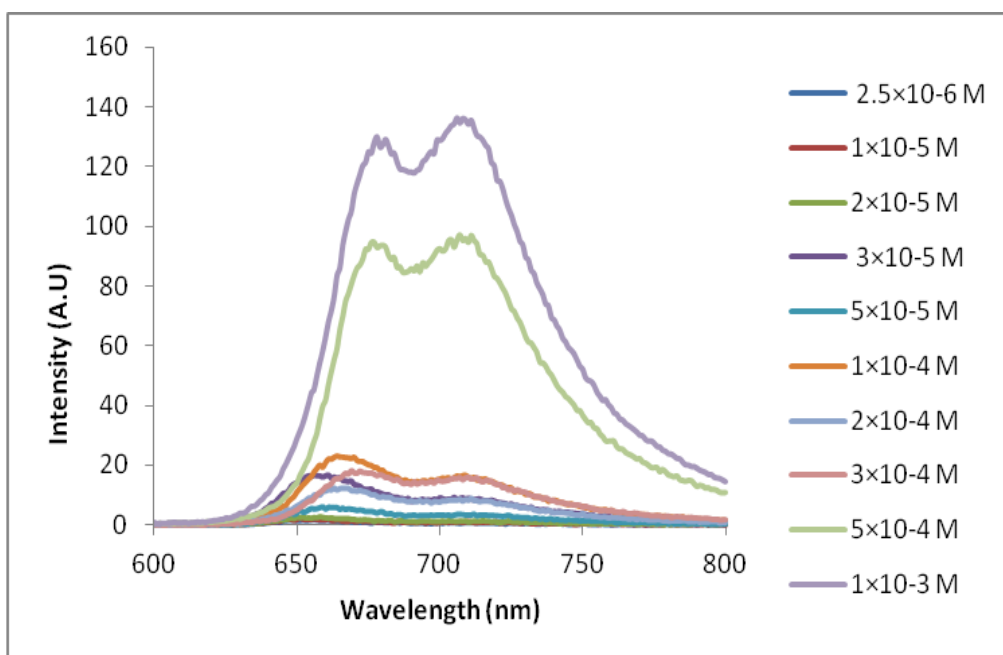


Figure 9.19: Fluorescence emission intensity of TIPS-pentacene in chloroform at concentrations ranging from 2.5×10^{-6} M to 1×10^{-3} M in 1mm pathlength cuvette at an excitation wavelength of 550nm.

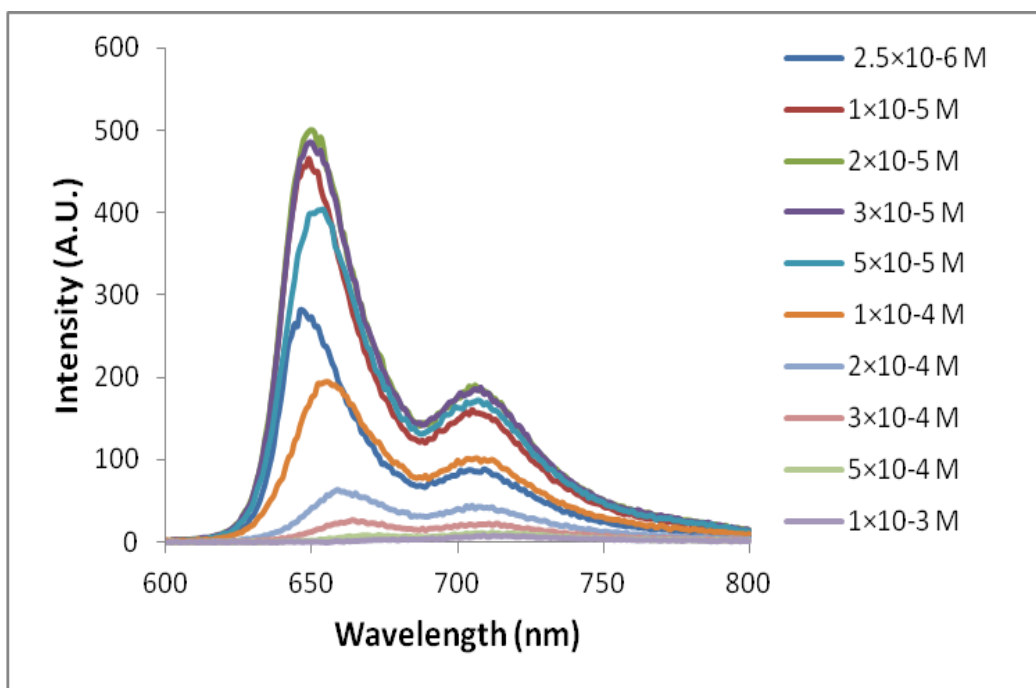


Figure 9.20: Fluorescence emission intensity of TIPS-pentacene in THF at concentrations ranging from 2.5×10^{-6} M to 1×10^{-3} M in 10mm pathlength cuvette at an excitation wavelength of 643nm.

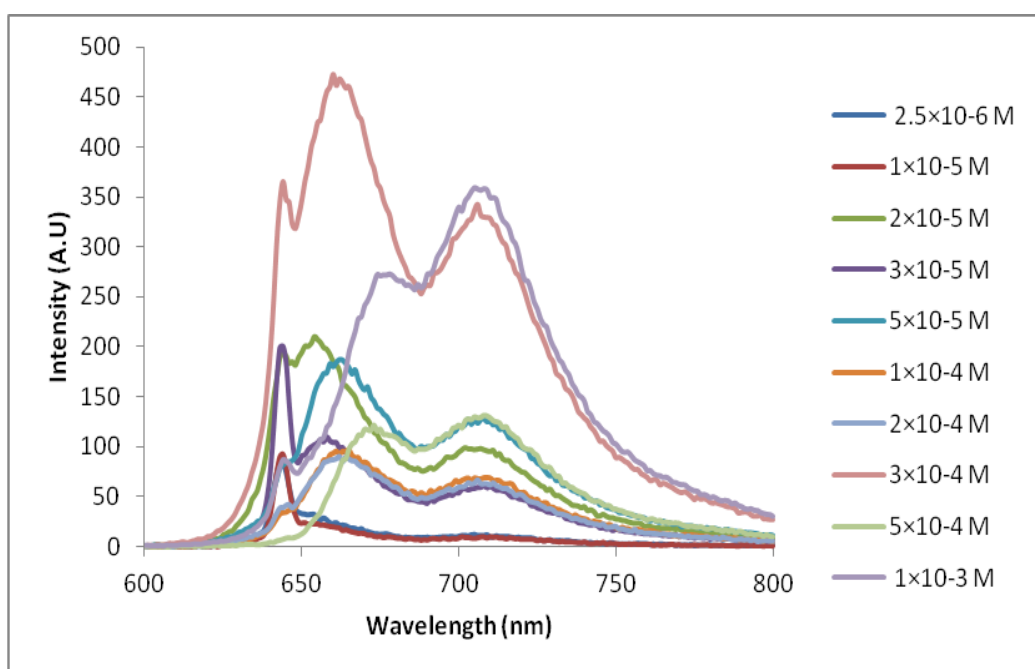


Figure 9.21: Fluorescence emission intensity of TIPS-pentacene in THF at concentrations ranging from 2.5×10^{-6} M to 1×10^{-3} M in 1mm pathlength cuvette at an excitation wavelength of 643nm.

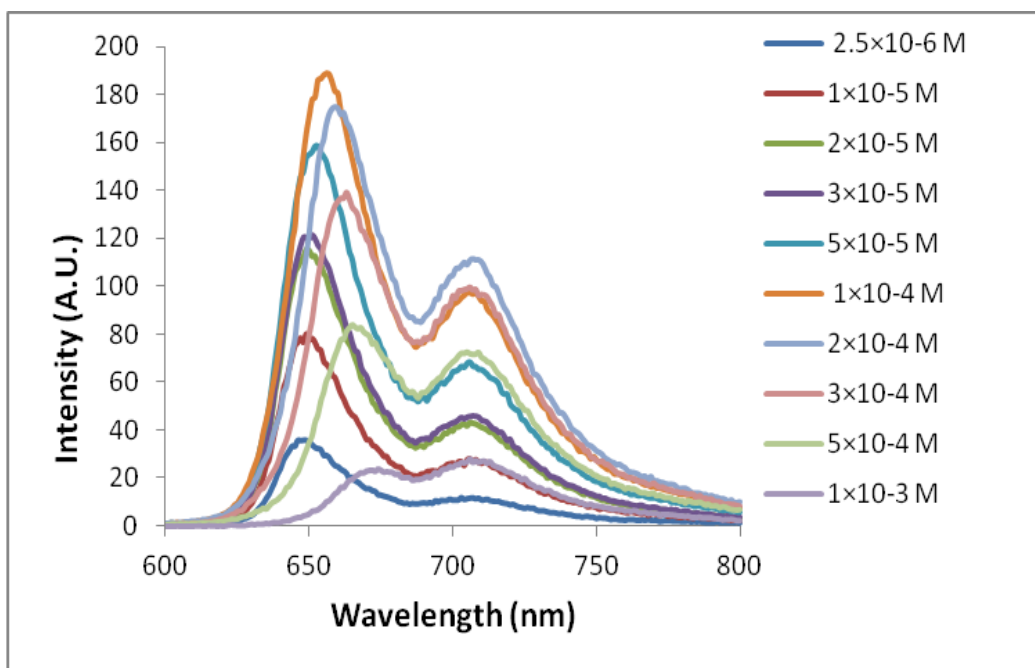


Figure 9.22: Fluorescence emission intensity of TIPS-pentacene in THF at concentrations ranging from 2.5×10^{-6} M to 1×10^{-3} M in 10mm pathlength cuvette at an excitation wavelength of 550nm.

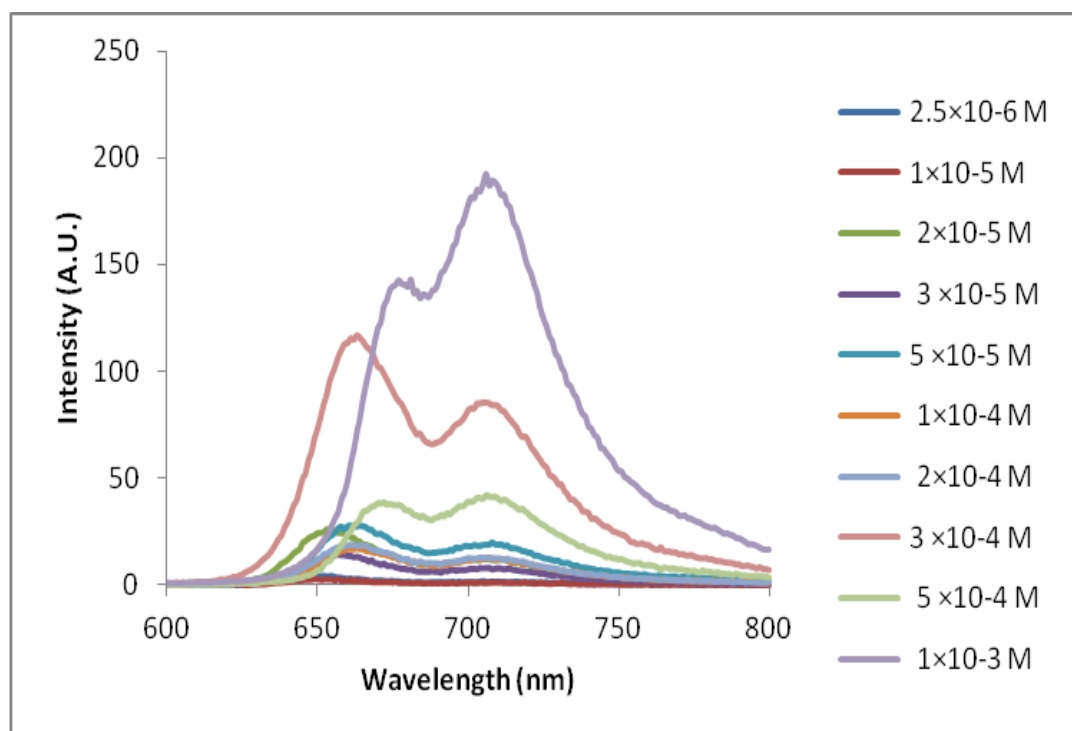


Figure 9.23: Fluorescence emission intensity of TIPS-pentacene in THF at concentrations ranging from 2.5×10^{-6} M to 1×10^{-3} M in 1mm pathlength cuvette at an excitation wavelength of 550nm.

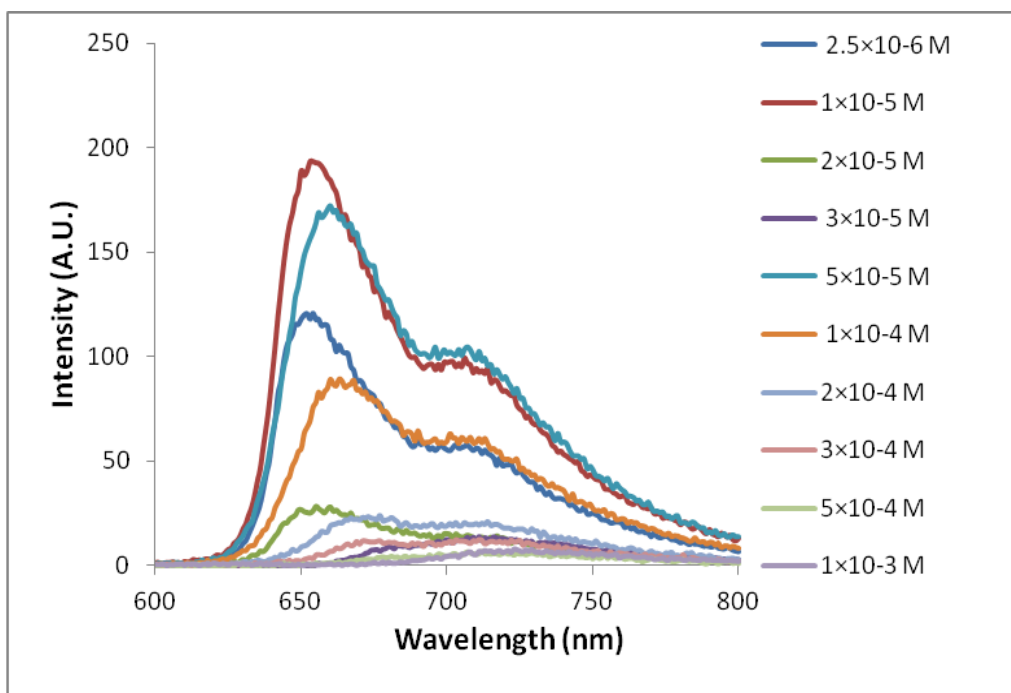


Figure 9.24: Fluorescence emission intensity of TIPS-pentacene in DCM at concentrations ranging from 2.5×10^{-6} M to 1×10^{-3} M in 10mm pathlength cuvette at an excitation wavelength of 643nm.

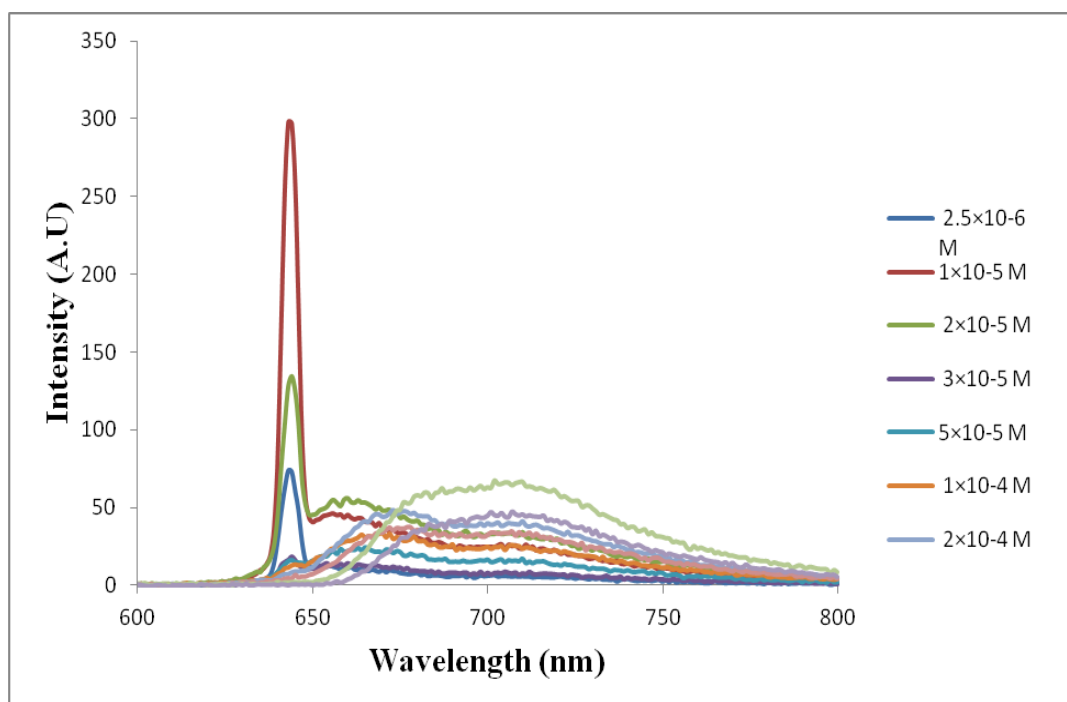


Figure 9.25: Fluorescence emission intensity of TIPS-pentacene in DCM at concentrations ranging from 2.5×10^{-6} M to 1×10^{-3} M in 1mm pathlength cuvette at an excitation wavelength of 643nm.

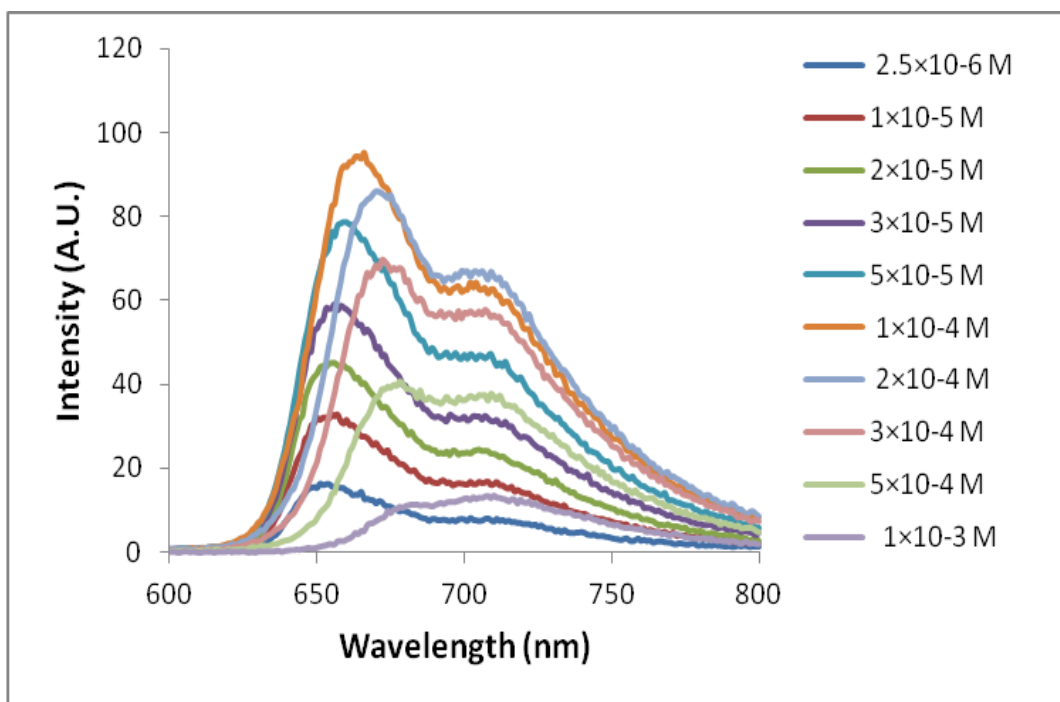


Figure 9.26: Fluorescence emission intensity of TIPS-pentacene in DCM at concentrations ranging from 2.5×10^{-6} M to 1×10^{-3} M in 10mm pathlength cuvette at an excitation wavelength of 550nm.

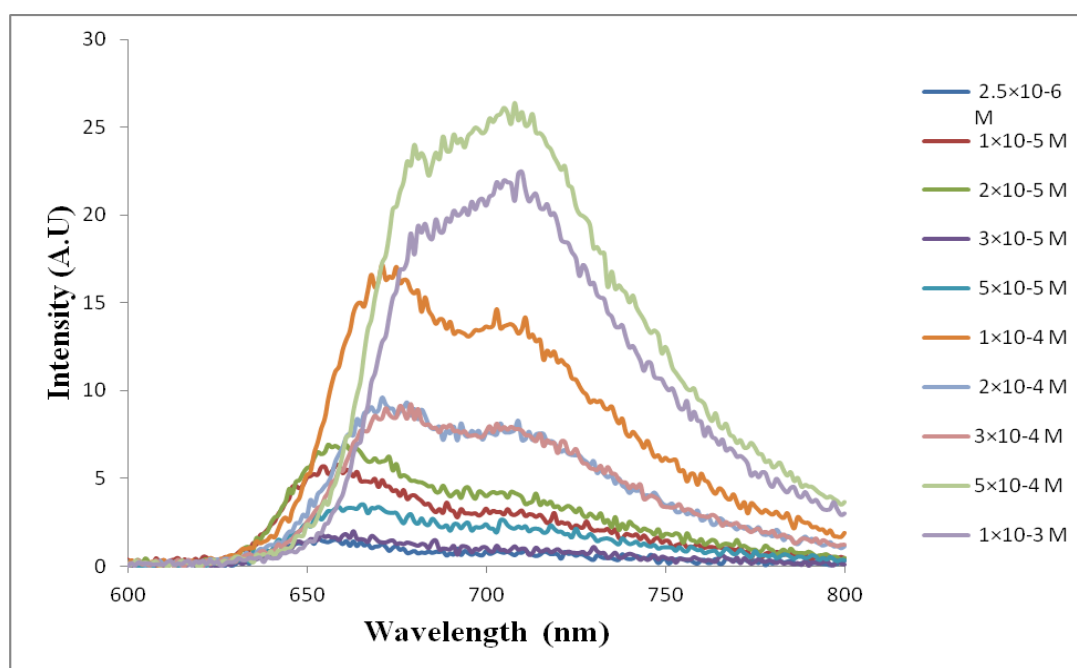


Figure 9.27: Fluorescence emission intensity of TIPS-pentacene in DCM at concentrations ranging from 2.5×10^{-6} M to 1×10^{-3} M in 1mm pathlength cuvette at an excitation wavelength of 550nm.

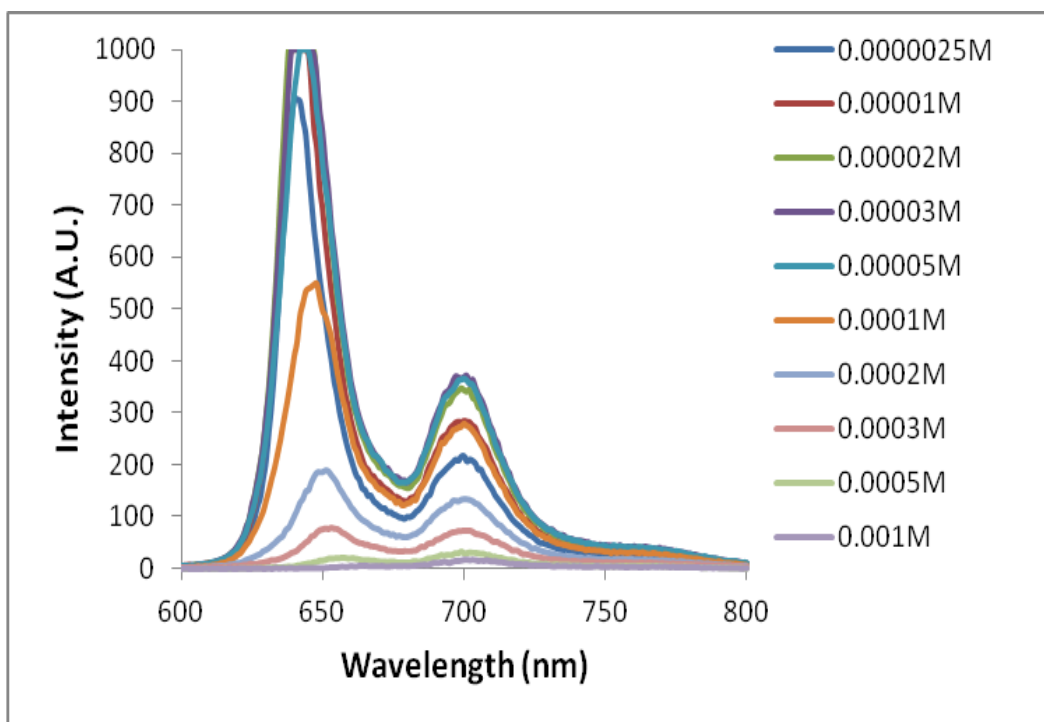


Figure 9.28: Fluorescence emission intensity of TIPS-pentacene in decane at concentrations ranging from 2.5×10^{-6} M to 1×10^{-3} M in 10mm pathlength cuvette at an excitation wavelength of 643nm.

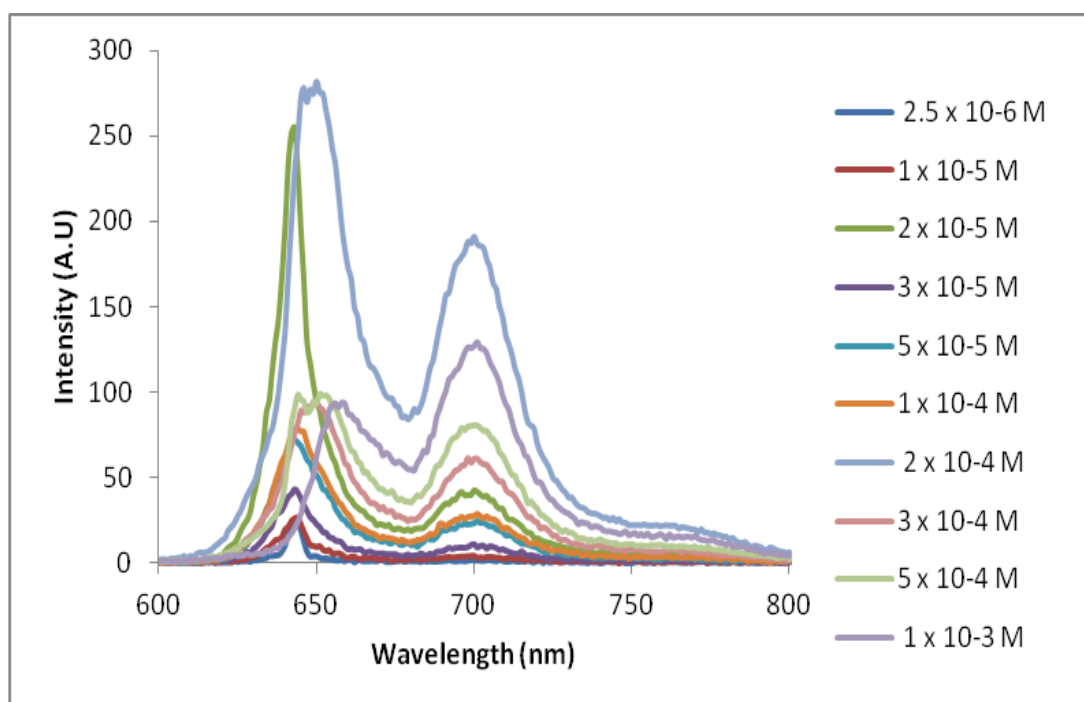


Figure 9.29: Fluorescence emission intensity of TIPS-pentacene in decane at concentrations ranging from 2.5×10^{-6} M to 1×10^{-3} M in 1mm pathlength cuvette at an excitation wavelength of 643nm.

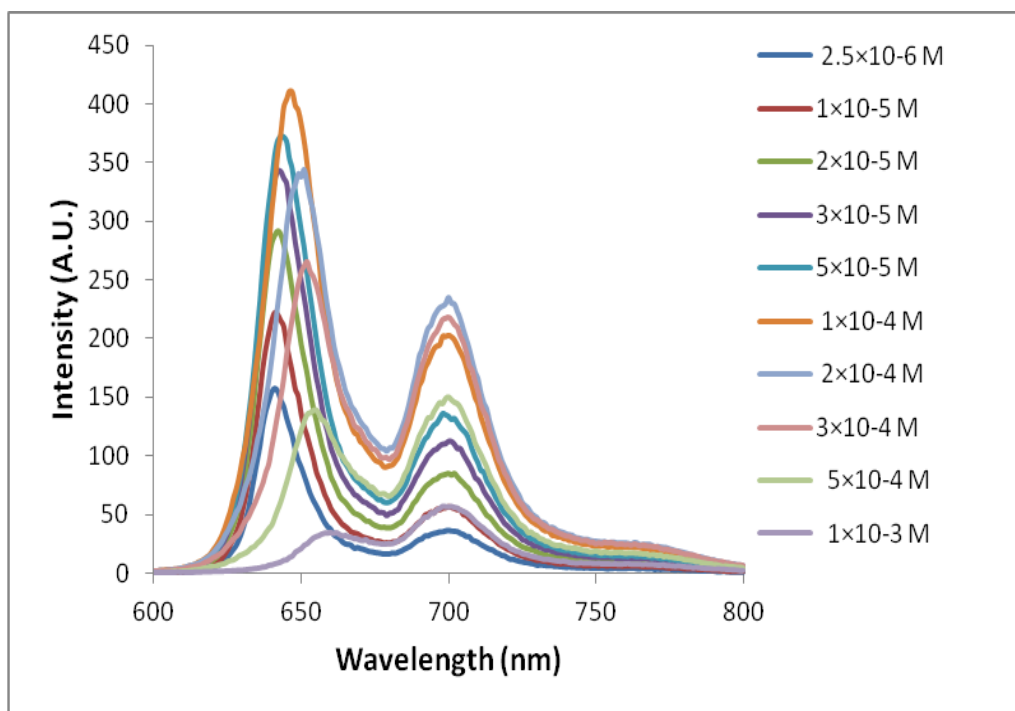


Figure 9.30: Fluorescence emission intensity of TIPS-pentacene in decane at concentrations ranging from 2.5×10^{-6} M to 1×10^{-3} M in 10mm pathlength cuvette at an excitation wavelength of 550nm.

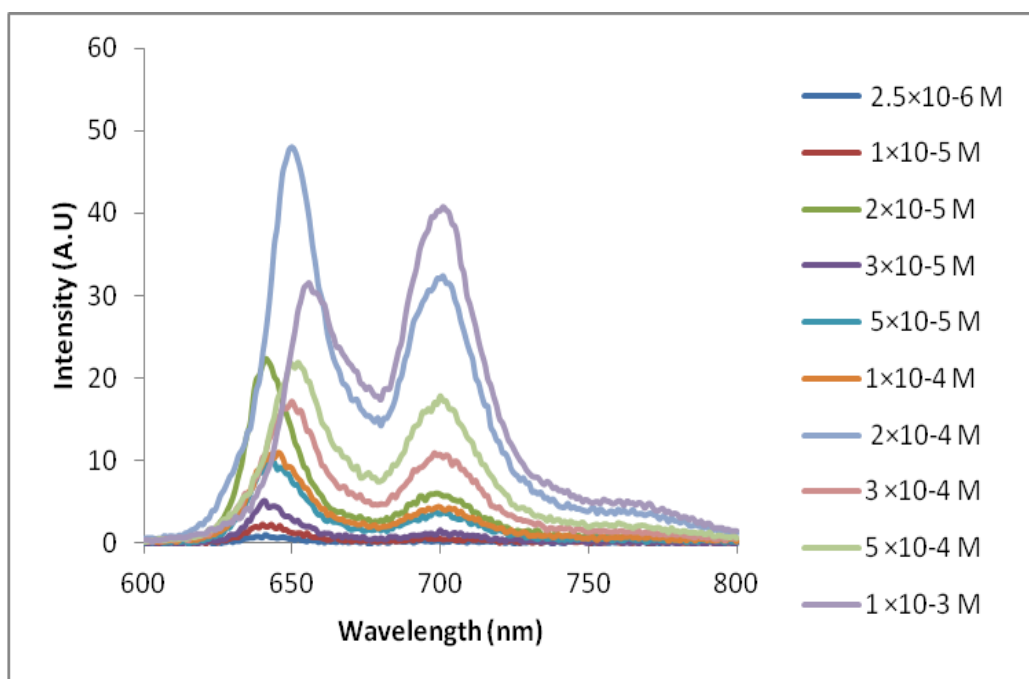


Figure 9.31: Fluorescence emission intensity of TIPS-pentacene in decane at concentrations ranging from 2.5×10^{-6} M to 1×10^{-3} M in 1mm pathlength cuvette at an excitation wavelength of 550nm.

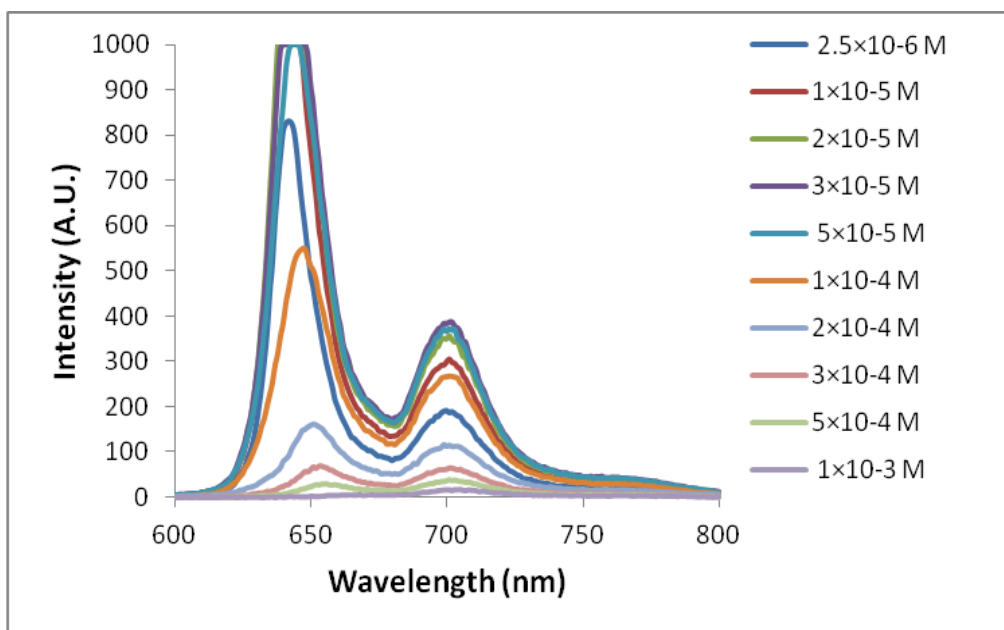


Figure 9.32: Fluorescence emission intensity of TIPS-pentacene in dodecane at concentrations ranging from 2.5×10^{-6} M to 1×10^{-3} M in 10mm pathlength cuvette at an excitation wavelength of 643nm.

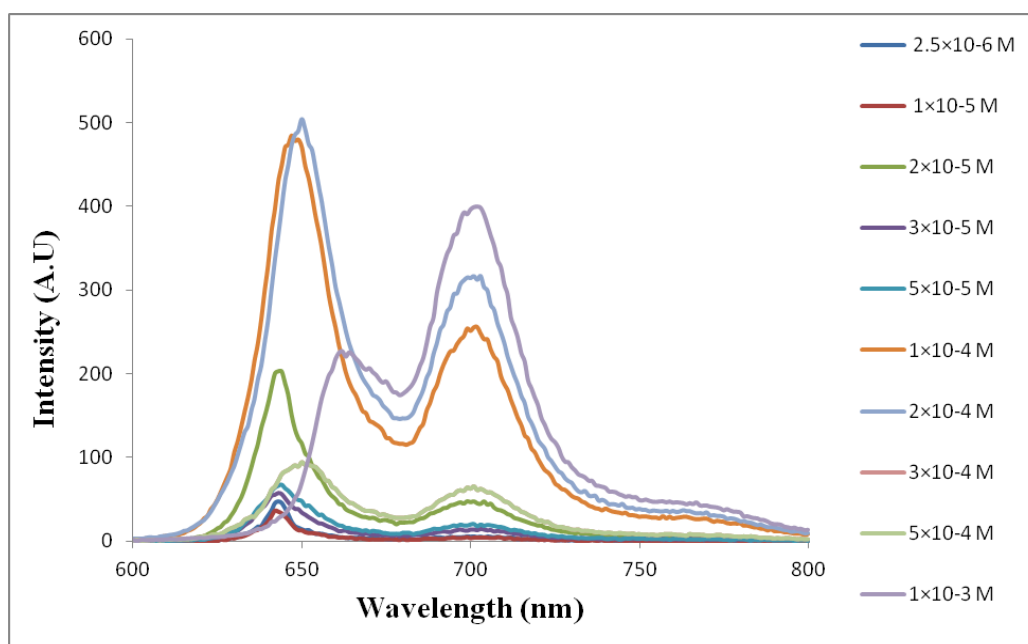


Figure 9.33: Fluorescence emission intensity of TIPS-pentacene in dodecane at concentrations ranging from 2.5×10^{-6} M to 1×10^{-3} M in 1mm pathlength cuvette at an excitation wavelength of 643nm.

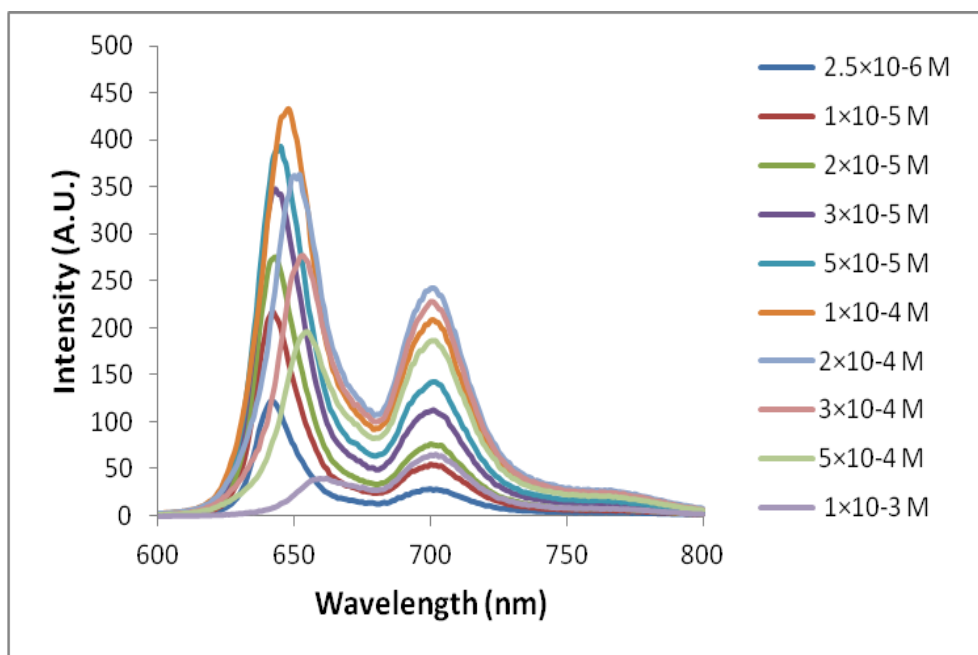


Figure 9.34: Fluorescence emission intensity of TIPS-pentacene in dodecane at concentrations ranging from 2.5×10^{-6} M to 1×10^{-3} M in 10mm pathlength cuvette at an excitation wavelength of 550nm.

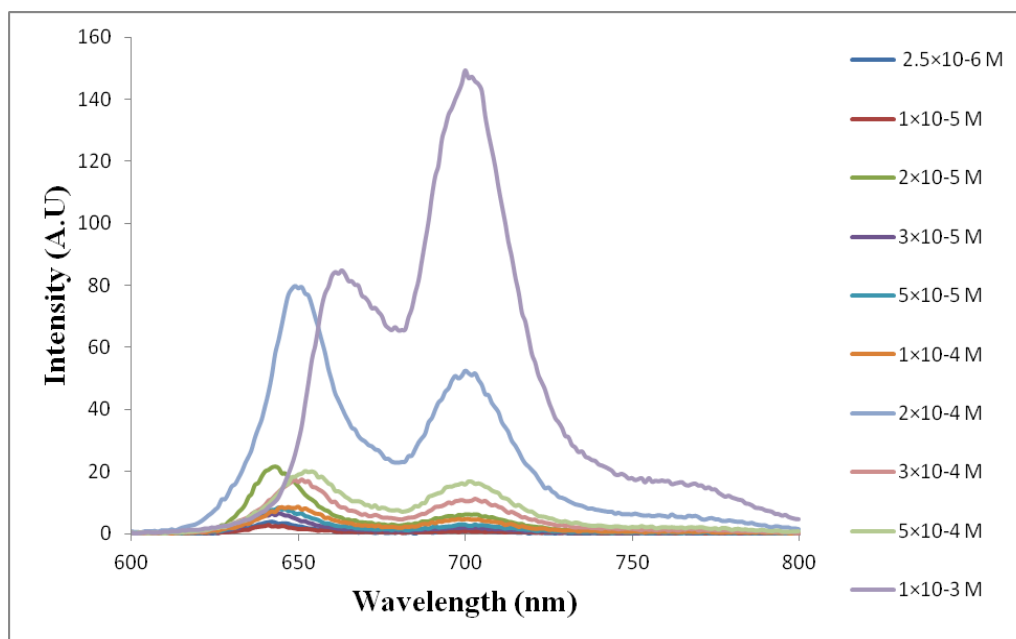


Figure 9.35: Fluorescence emission intensity of TIPS-pentacene in dodecane at concentrations ranging from 2.5×10^{-6} M to 1×10^{-3} M in 10mm pathlength cuvette at an excitation wavelength of 550nm.

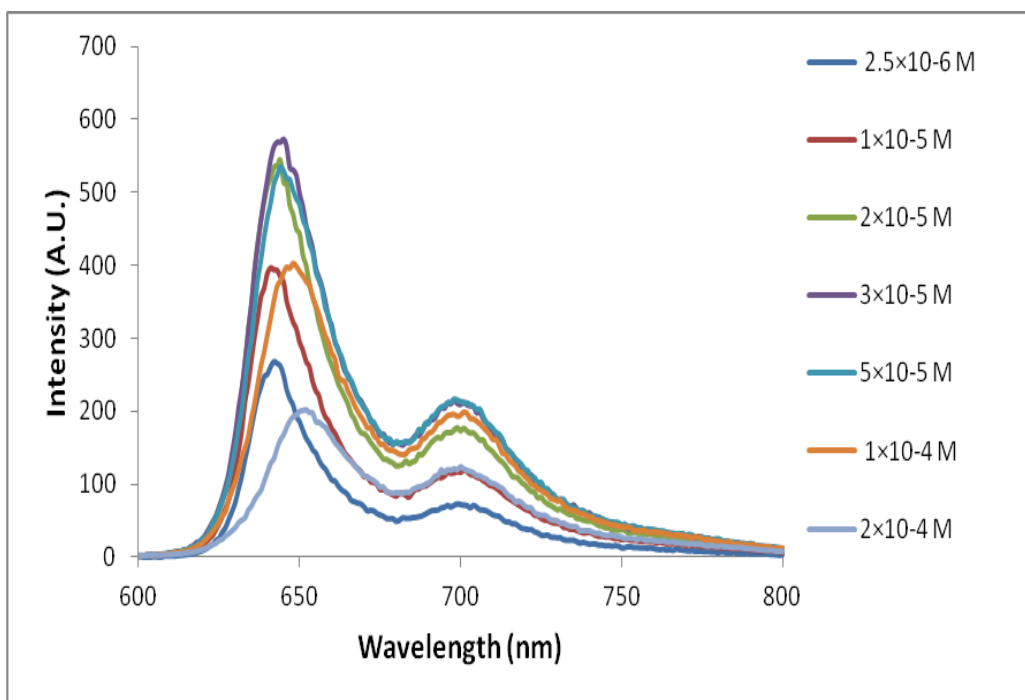


Figure 9.36: Fluorescence emission intensity of TIPS-pentacene in IPA at concentrations ranging from 2.5×10^{-6} M to 2×10^{-4} M in 10mm pathlength cuvette at an excitation wavelength of 643nm.

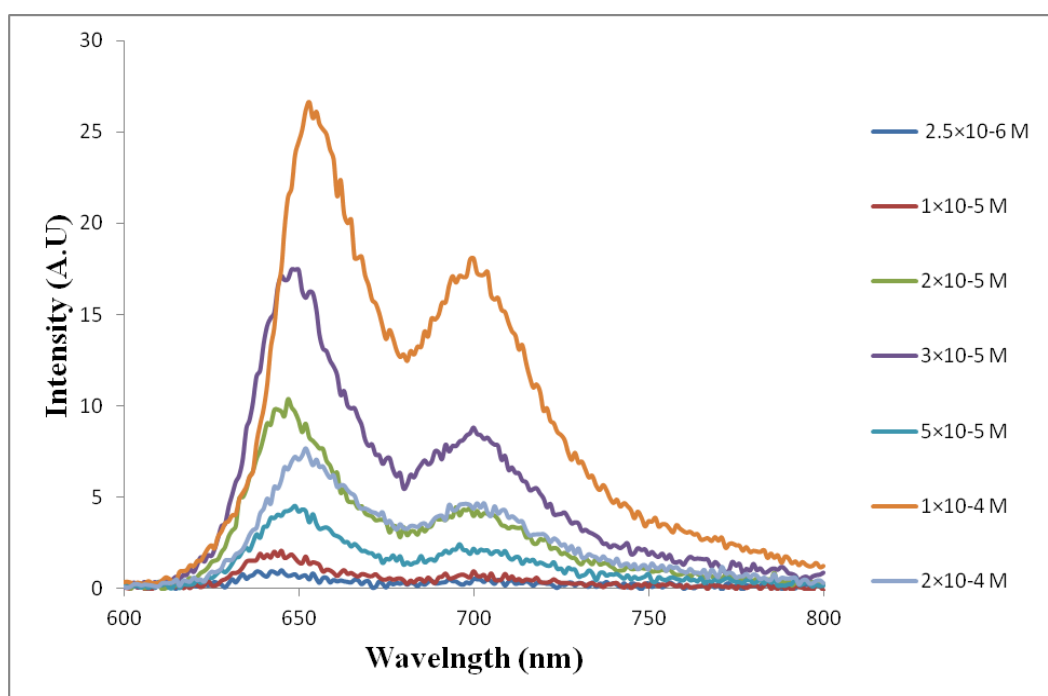


Figure 9.37: Fluorescence emission intensity of TIPS-pentacene in IPA at concentrations ranging from 2.5×10^{-6} M to 2×10^{-4} M in 1mm pathlength cuvette at an excitation wavelength of 643nm.

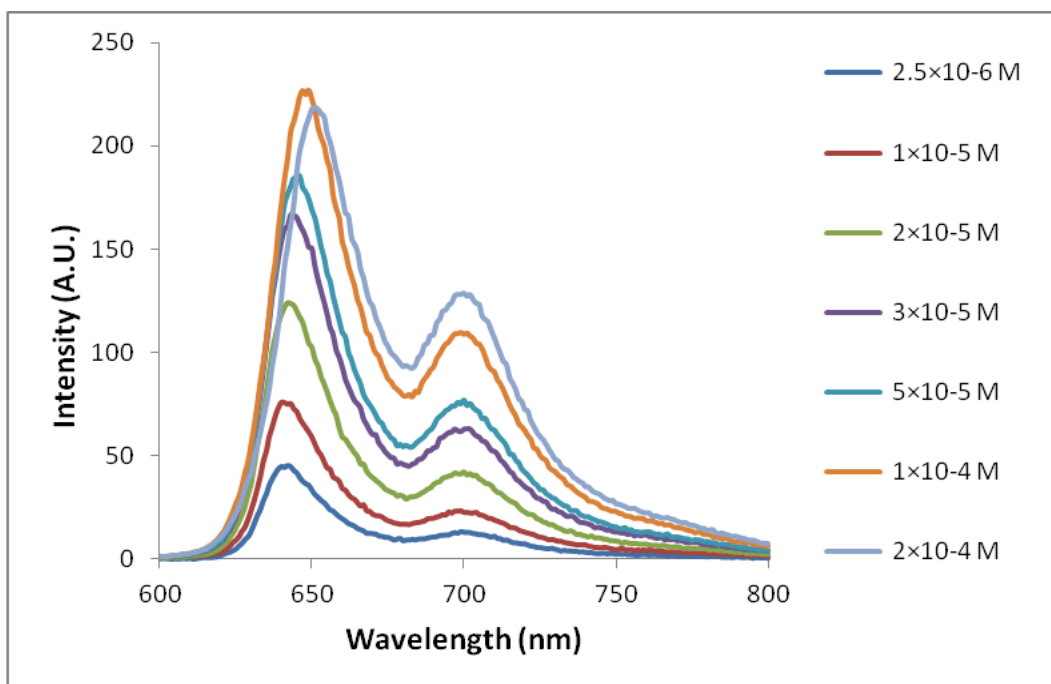


Figure 9.38: Fluorescence emission intensity of TIPS-pentacene in IPA at concentrations ranging from 2.5×10^{-6} M to 2×10^{-4} M in 10mm pathlength cuvette at an excitation wavelength of 550nm.

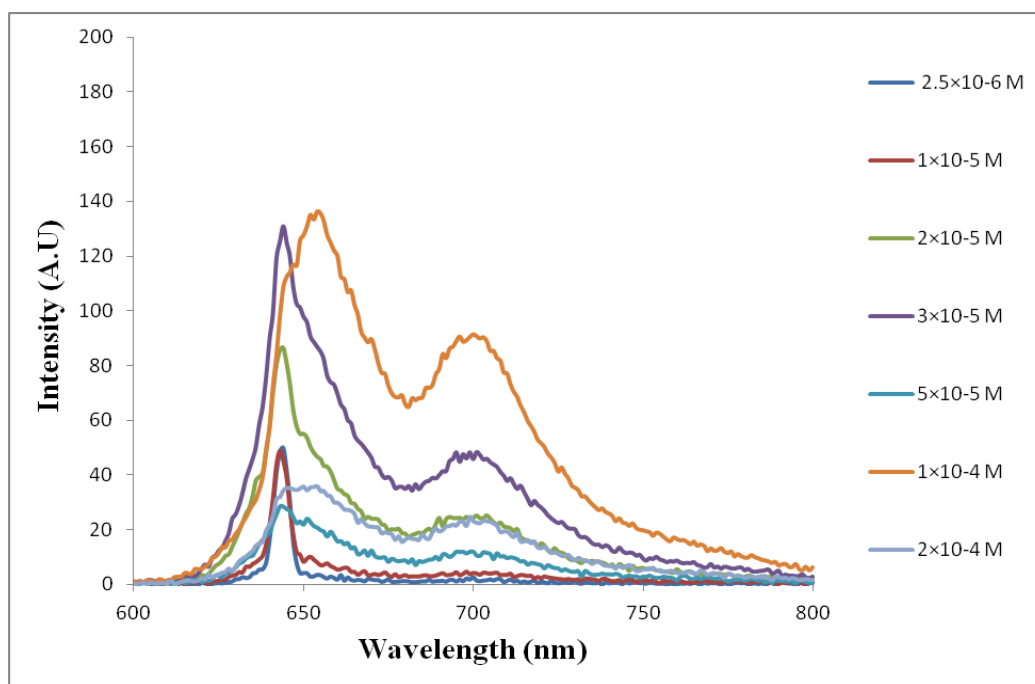


Figure 9.39: Fluorescence emission intensity of TIPS-pentacene in IPA at concentrations ranging from 2.5×10^{-6} M to 2×10^{-4} M in 1mm pathlength cuvette at an excitation wavelength of 550nm.

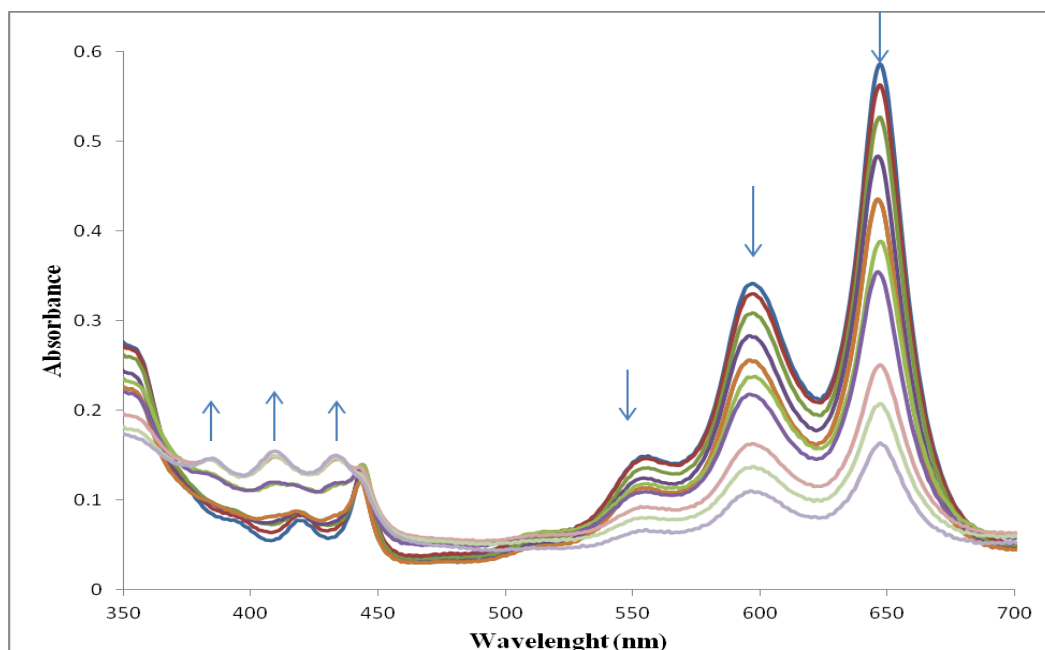


Figure 9.40: UV-visible absorption spectra for the photooxidation of β -mono-FTIPS-pentacene in DCM 1×10^{-5} M in a 10 mm pathlength at 26°C.

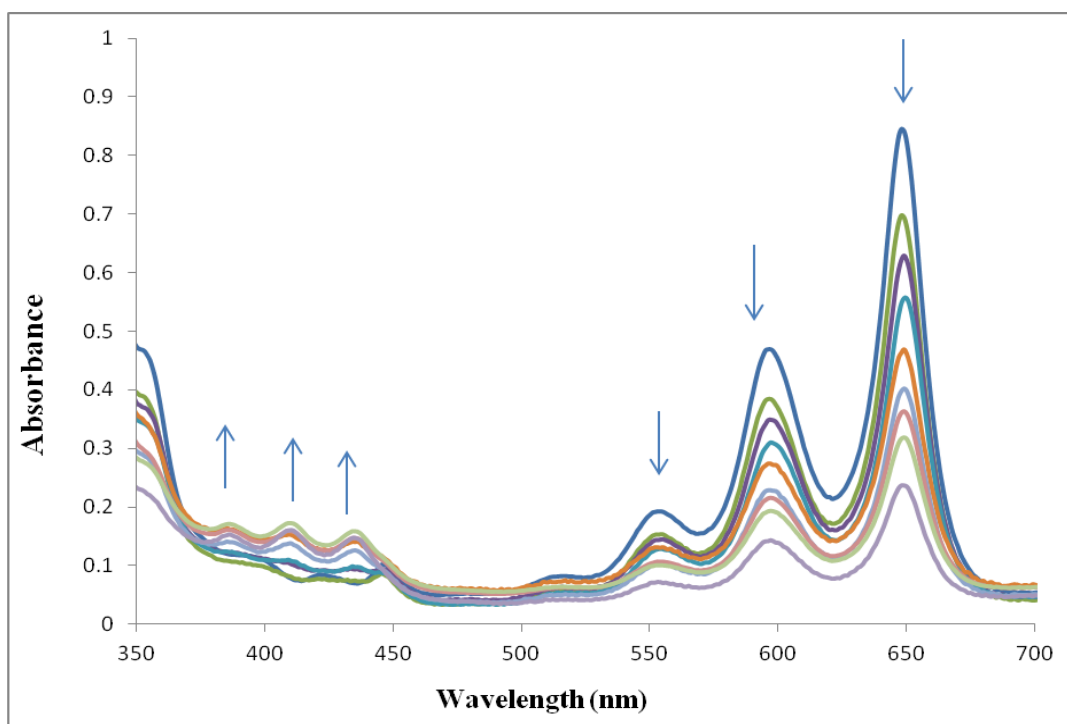


Figure 9.41: UV-visible absorption spectra for the photooxidation of α -di-FTIPS-pentacene 3×10^{-5} M in toluene solution in a 10 mm pathlength at 26°C.

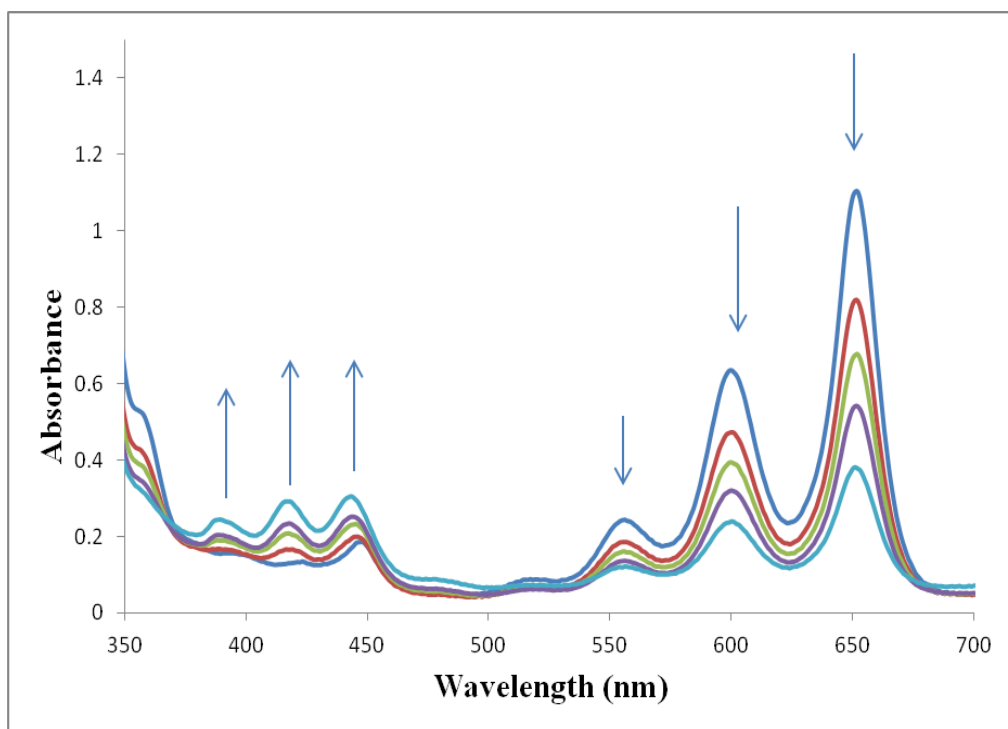


Figure 9.42: UV-visible absorption spectra for the photooxidation of TMTE-pentacene 5×10^{-5} M in toluene solution in a 10 mm pathlength at 26°C.

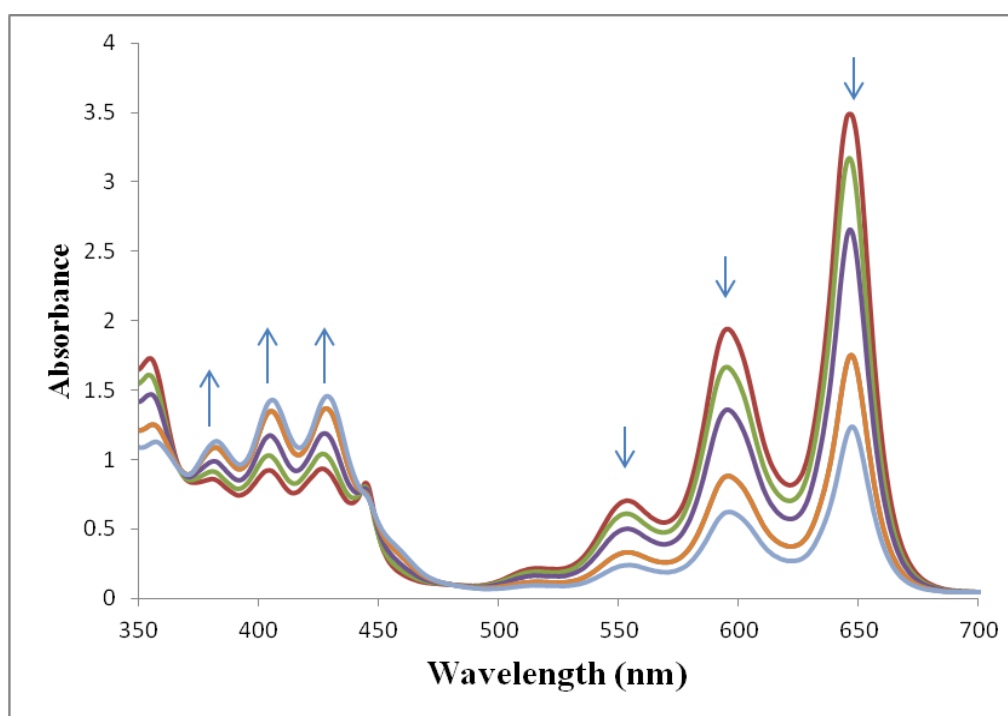


Figure 9.43: UV-visible absorption spectra for the photooxidation of β -di-FTIPS-pentacene 2×10^{-4} M in THF solution in a 10 mm pathlength at 26°C.

Thermal stability of substituted 6,13 trialkylsilylethynylpentacene derivatives

Thermal stability of thin films for TIPS-pentacene

TIPS-pentacene thin films were prepared from solution drop casting and spin coating using a 1 % w/v toluene solution onto glass substrate at room temperature. The thermal properties of TIPS-pentacene thin film drop casting that it exposed to UV light are characterization by TGA and DSC. TGA measurements at heating rate of 10°C/min under nitrogen revealed that the thin film had good thermal stabilities and the onset decomposition temperatures at 360 °C with peak weight loss at around 398 °C. The compound fully decomposed at around 580 °C as shown in figure 98. Different scanning calorimetry (DSC) measurements for TIPS-pentacene showed three peaks at around 119 °C and small peak at around 177 °C in the heating line, and at around 95 °C at the cooling line as shown in figure 99. These result matched the thermal properties of TIPS-pentacene pure [147].

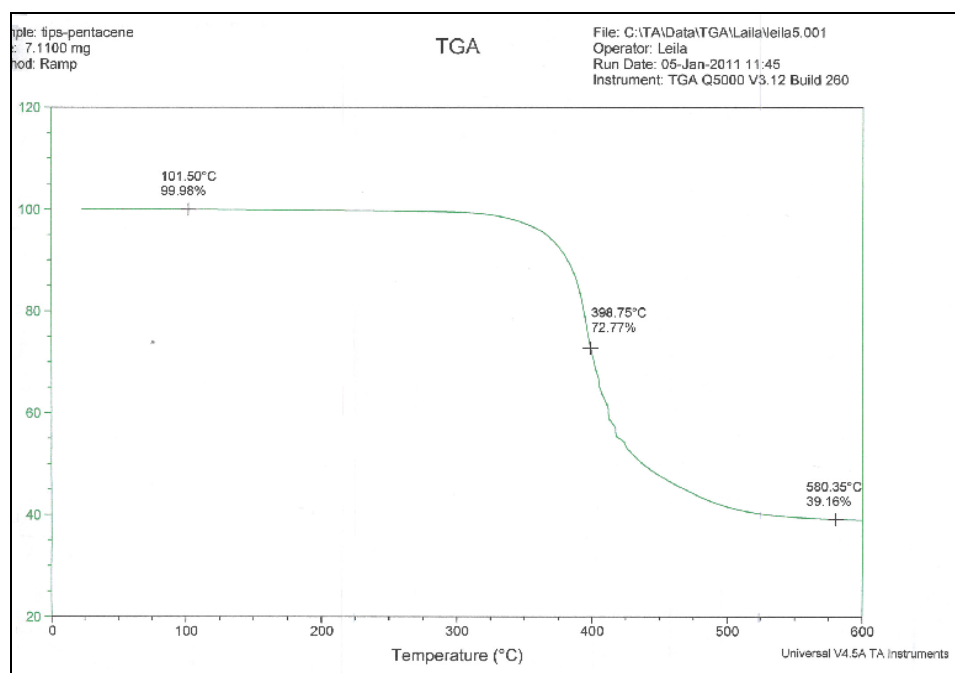


Figure 9.44: TGA plots of TIPS-pentacene thin film drop casting when exposed to UV light.

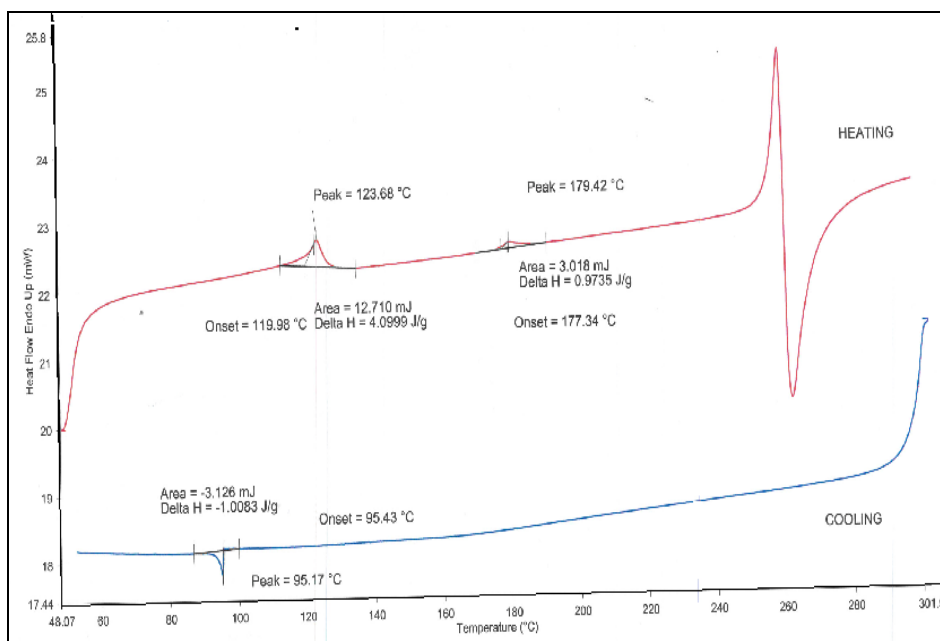


Figure 9.45: Differential scanning calorimetry of TIPS-pentacene thin film drop casting when exposed to UV light.

Thermal stability of thin films for β -di-Flouro-TIPS-pentacene

β -di-Flouro-TIPS-pentacene thin films were deposited by spin coating and drop casting. These films were quite stable (no change). Whine exposed to light and air and when exposed to UV at 20 passes. The thermal properties of the β -DFTIPS-pentacene thin film by a drop casting is characterized by thermal gravimetric analysis (TGA) and differential scanning calorimetry (DSC) to assess thermal stability figure 103 and figure 104 respectively. Thermal stability as assessed by TGA of pentacene had good thermal stabilities and the decomposition process occurred at 272.22 °C due to the molecular structure. Substituted bulky side groups at 6, 13 positions, forms molecular crystals which resulted in decomposition at higher temperature compared to unsubstantiated pentacene. DSC analysis showed small peak was observed (a cooling line) at 130.64°C. The higher thermal stability of β -di-Flouro-TIPS-pentacene compared to the TIPS-pentacene is relapsed to the relative stabilization of difloru function.

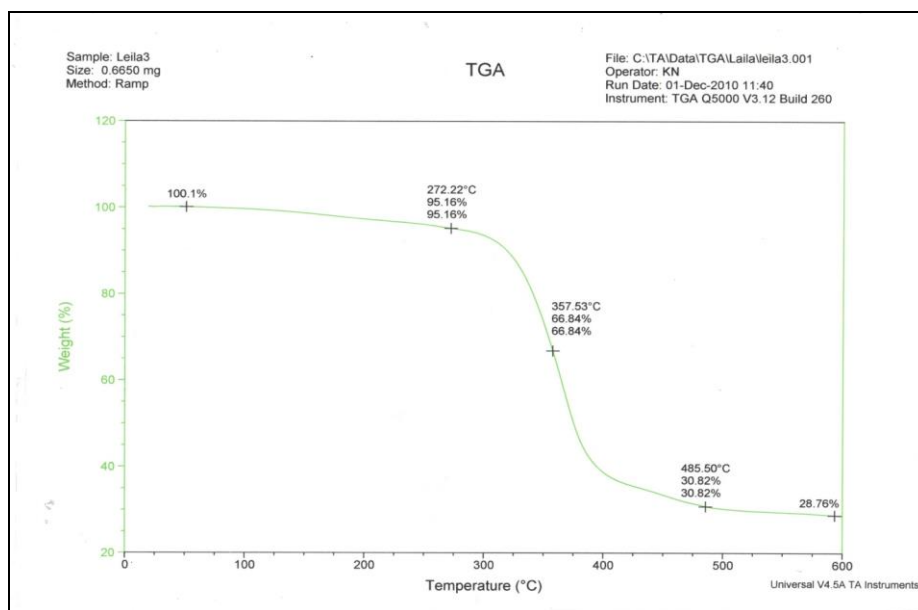


Figure 9.46: TGA plots of thin film drop casting for β -di-Flouro-TIPS-pentacene when exposed to UV light.

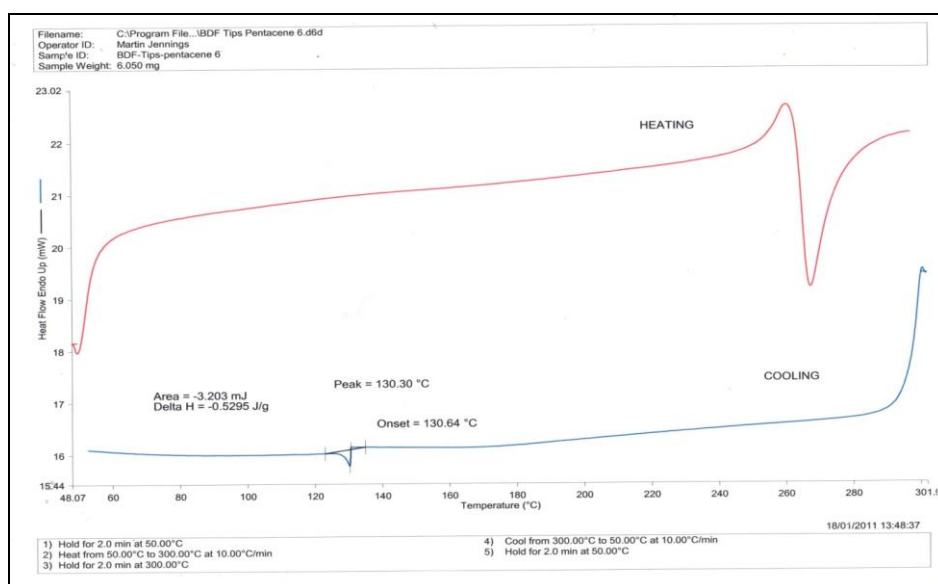


Figure 9.47: The DSC traces of β -di-Flouro-TIPS-pentacene thin film drop casting when exposed to UV light

